Three loop corrections to HQET Sum Rules for the Bag Parameter

DANIEL JAMES KING

Three loop corrections to HQET Sum Rules for the Bag Parameter

Daniel King

A Thesis presented for the degree of
Doctor of Philosophy

Institute for Particle Physics Phenomenology
Department of Physics
Durham University
United Kingdom

June 2022

Three loop corrections to HQET Sum Rules for the Bag Parameter

Daniel King

Submitted for the degree of Doctor of Philosophy

June 2022

Abstract: In this thesis, we compute the bag parameters which parameterise non-perturbative hadronic matrix elements of 4-quark operators. These are required for studies of $B - \overline{B}$ mixing and the inclusive decays of B and D mesons and they represent the largest source of uncertainty in corresponding theory predictions. In this work, the bag parameters are obtained using a HQET sum rule analysis of the 3-point correlator to 3 loops, including $SU(3)$ flavour breaking effects up to m_s^2 corrections. Besides reproducing the known HQET sum rule values for B_d-mixing and the lifetimes of B_d , B^+, D^0 and D^+ mesons, we obtain for the first time results for B_s-mixing and the lifetimes of B_s and D_s^+ mesons. For B_s-mixing, our results are highly competitive, while for the lifetimes no state of the art lattice evaluation is available. Furthermore, we consider the phenomenological implications of our results for mixing observables and the values of the CKM matrix elements. Finally, we give a thorough analysis of inclusive decay widths for charmed mesons, in an attempt to study the viability of the HQE in the charm sector.

Contents

Declaration

The work in this thesis is based on research carried out in the Department of Physics at Durham University. No part of this thesis has been submitted elsewhere for any degree or qualification. This thesis is partly based on joint research, as follows:

- Chapter 3 is partly based on [1], "*B_s mixing observables and $|V_{td}/V_{ts}|$ from sum rules*", published in the Journal of High Energy Physics.
- Chapter 4 is partly based on [2], "*$|V_{cb}|$ and γ from B-mixing - Addendum to B_s mixing observables and $|V_{td}/V_{ts}|$ from sum rules*", published in the Journal of High Energy Physics.
- Chapter 5 is partly based on [3], "*$SU(3)$ breaking effects in B and D meson lifetimes*", currently under review.
- Chapter 6 is partly based on [4], "*Revisiting Inclusive Decay Widths of Charmed Mesons*", currently under review, for which my contribution was the determination of dimension-6 non-perturbative input.

Acknowledgements

Firstly, I would like to thank my supervisor Alex Lenz for the opportunity to work with him and for patiently guiding me throughout my PhD studies. I would also like to thank Valya Khoze who supervised me during my final year. I am also very grateful to Thomas Rauh for sharing his knowledge and time, and to all of my colleagues for the many insightful discussions that have contributed to this work.

I would also like to thank everyone in the IPPP for creating such a lovely community and for making me feel welcome. In particular, I would like to thank all my fellow members of OC118, past and present, for making it the unique work environment that it is. I hope one day that squash-ball-foot-golf gets the official recognition it deserves.

To Vincent and Parisa, thank you for sharing this journey with me. I could not have chosen better people to spend the last 4 years with and I could not have completed it without your support and friendship.

Finally, I want to thank all my family, whose endless encouragement, love and support has made this possible.

Chapter 1

Introduction

The standard model (SM) has proven to be a huge success story for particle physics, culminating in the discovery of the Higgs boson in 2012 [5,6] which cemented our understanding of how fermion and electroweak gauge boson masses are generated [7–9]. Yet colliders continue to run and the prospect of even larger, more capable colliders lies on the horizon [10–12] with many open questions remaining unaccounted for by the SM. One such problem facing particle physicists, is the baryon-asymmetry that the universe exhibits. In order to explain how such an asymmetry could manifest[2], three conditions were put forward by Sakharov [13]: a mechanism for Baryon number violation, C and CP violation, and a departure from thermal equilibrium. The first of these criteria is met by the SM through non-perturbative processes known as Sphalerons [14]. However, although both C and CP violation are present within the SM it is not thought to be enough to explain the amount of asymmetry we observe [15, 16]. Furthermore, a departure from thermal equilibrium would occur during a strong first order phase transition. The electroweak phase transition is a natural candidate, however this too is in contention with the SM since a higgs mass $m_H < 70$ GeV is necessary for it to be strongly first order. Therefore, the baryon-assymetry problem would suggest the need for new physics (NP).

[2]The alternative is that the asymmetry was present from the big bang. However, if this were the case it can be argued that it would be exponentially diluted during inflation of the universe.

Another strong argument for NP comes from cosmological observations that have been found to be inconsistent with the SM and predict that a huge proportion of the matter content of the universe is unaccounted for. Signs of this 'Dark Matter' (DM) were first hinted at as far back as the 1930's [17–20], however no direct observation of its existence has been made to date and even a strong consensus on it's form has yet to be reached [21]. Further evidence supporting the existence of NP, came with the measurement of neutrino oscillations [22, 23] which indicated the non-vanishing neutrino mass. The notion of a neutrino mass categorically requires an extension to the SM due to the lack of a right handed neutrino which has so far not been found in nature.

These are compelling reasons to search for beyond standard model (BSM) physics. The question of how to search for such phenomena, presents us with two options: direct and indirect searches. Direct searches involve scanning for resonances in particle collisions at higher and higher energy scales. However, in the LHC era, other than the discovery of the Higgs boson, this has not proven as fruitful as first hoped[1]. Instead, indirect searches have offered an enlightening source of guidance. This approach focuses our efforts on precision measurements of observables. A comparison with the SM prediction can then highlight missing NP effects if present. Furthermore, this approach has played a crucial role historically in the development of the SM. The discovery of the charm quark is typically accredited to the development of the Glashow, Iliopoulos and Maiani (GIM) mechanism [24] which introduced a 4th quark to the already established u, d and s, in order to remove divergences in K-mixing transitions. Similarly, first measurements of the mass difference ΔM_d in B-mixing by ARGUS in 1987 [25] placed a lower bound on the top quark mass of $m_t > 50\text{GeV}$. This was against consensus at the time and in fact contradicted a supposed 'clear signal' 3 years earlier suggesting $m_t \simeq 40\text{GeV}$ [26], which was later discounted [27]. Both K and B-mixing are examples of a rare set of processes studied in flavour physics known as flavour changing neutral currents (FCNC). Since tree level quark

[1] SUSY didn't show up.

interactions with neutral gauge bosons are flavour diagonal in the SM, FCNC are loop suppressed and appear as the so called box and penguin diagrams. The same loop suppression does not in principle have to be found in BSM physics and therefore FCNC can be highly sensitive to NP contributions. These form a testing ground for potential BSM models, scrutinising their viability by placing constraints on their parameter space [28].

Furthermore, whilst predictions for SM phenomenology continue to demonstrate astounding levels of agreement with experiment, the field of flavour physics has drawn increasing interest by becoming one of the few persisting sources of anomalies. Current data suggests promising flavour anomalies in $b \to s\bar{l}l$ transitions, specifically in the branching fraction ratios $\mathcal{R}(K^{(*)}) = \mathcal{B}(B \to K^{(*)}\ \overline{\mu}\mu)/\mathcal{B}(B \to K^{(*)}\ \overline{e}e)$. These are theoretically clean observables since the uncertainty due to potentially large hadronic matrix elements cancels in the ratio. They can therefore be precisely determined in the SM [29], for which the ratio $\mathcal{R}(K)$ is equal to 1 due to lepton flavour universality (LFU) up to $\mathcal{O}(1\%)$ corrections. Any pronounced shift from unity would therefore be a sign of lepton flavour violating (LFV) effects and suggest the presence of NP. Such a disparity has been found [30], in the form of a deficit in the muon mode and a recent update on $\mathcal{R}(K)$ by LHCb predicts a disagreement with the SM of 3.1σ [31]. The branching ratio of the pure leptonic decay $\mathcal{B}(B \to \overline{\mu}\mu)$ also offers a clean observable to test LFU since the hadronic input only enters as the decay constant f_B, and is precisely determined by lattice QCD [32]. The LHCb update in [33] (see [34, 35] for the previous findings by ATLAS and CMS respectively) found a 1σ deviation from the SM. A combined analysis [36, 37] of $\mathcal{R}(K^{(*)})$ and $\mathcal{B}(K \to \overline{\mu}\mu)$ however uncovers a disagreement with the SM between $4 \sim 4.7\sigma$, indicating a promising area to probe NP[1]. Further hints towards LFV comes from the anomalous magnetic moments of the muon and the electron where we observe 4.2σ [38–40] and 2.4σ [41–43] deviations from the SM respectively. These appear

[1]The global fits in [36] also explore combined analyses including the theoretically less clean angular observables.

with opposing signs, which naturally makes it a challenge to satisfy both with BSM models that don't incorporate LFV.

In order to capitalise on the rich phenomenology that flavour physics offers, we require high precision from both experiment and theory. From the theory perspective, the challenge comes from higher order perturbative corrections and long distance QCD effects. In heavy quark physics, the latter is usually the dominant source of uncertainty and arise in the form of hadronic matrix elements. Undeterred by the obstacle, a concerted effort has spawned the development of several theoretical tools to assist in this struggle and advanced our theoretical understanding of flavour physics considerably. In this regard, the impact of both the Heavy Quark Expansion (HQE) [44] and the Heavy Quark Effective Theory (HQET) [45] cannot be overstated. For processes involving hadrons containing a heavy quark, these disentangle the high and low energy physics contributions and provide frameworks by which the calculation can be expanded in inverse powers of the heavy quark mass. This substantially simplifies the problem and in the case of the latter can also reveal symmetries of the low energy theorem that we can exploit. In the direct computation of hadronic matrix elements, perturbation theory breaks down and non-perturbative methods are unavoidable. For this purpose, the method of QCD sum rules was established by Shifman, Vainshtein and Zakharov (SVZ) [46] and it has since proven itself effective in the determination of these parameters, becoming the standard analytical approach. More recently, the development of lattice QCD [47] has overshadowed the latter method in some cases, benefiting from the tremendous growth in computational power to provide precision numerical determinations. The two methods each have their own strengths however and often are complementary to one another. For example, light cone sum rules (LCSR)[1] [48] and lattice calculations are typically both required for a complete analysis of the form factors entering semi-leptonic decays

[1] A variation on SVZ sum rules, sharing the same notions of quark-hadron duality and dispersion representations but employing a light cone expansion as opposed to the short distance expansion which characterises SVZ sum rules. The details of the LCSR method however are beyond the scope of this work and will not be discussed further.

where they are applicable in separate kinematic regimes [49–53].

Aside from this example, there remain other instances where sum rules have been found to be competitive with lattice. In recent years, this was found to be the case for the bag parameter B [1,3,54,55] which, along with a decay constant, parameterise the hadronic matrix elements of 4-quark operators. In this case, a sum rule can be constructed for the deviation of the bag parameter from the vacuum insertion approximation (VIA) $\Delta B = B - 1$. Since numerically the bag parameter is found to be very close to one [32], even uncertainties of order $\sim 20\%$ for ΔB translate to a precision of order $\sim 2\%$ for the whole bag parameter. This has important phenomenological implications in the study of B-mixing where in the SM prediction of the mass difference $\Delta M_{d/s}$ the bag parameter is the largest contributor to the overall uncertainty. Furthermore, it has been shown [28] that popular BSM models aimed at resolving the $b \to s\bar{l}l$ anomolies, can be strongly constrained by ΔM_s. Therefore the improved understanding of these non-perturbative parameters can have a direct effect on NP searches.

The main purpose of this work is the study of hadronic matrix elements of 4-quark operators involved in B_s mixing and those required for an analysis of B_s and D_s^+ lifetimes. To complement this, we also explore some of the implications of our results to B-mixing and the CKM matrix and include a full analysis of the D_s^+ lifetime.

The rest of the thesis is arranged as follows:

In Chapter 2 we provide an introduction to some theoretical concepts which are used in the latter parts of the thesis. The ideas behind the HQE and the HQET are discussed and a brief overview into B_s-mixing is presented, before outlining the sum rule method in the context of the HQET decay constant. Following this we introduce some useful techniques for the calculation of loop integrals, namely Integration by Parts identities and the concept of master integrals, and methods for expanding loop integrals in some small parameter, specifically the Mellin Barnes representation and the Expansion by Regions method. We end this section by reviewing the Fock-Schwinger gauge, in which we expand the quark propagator in the background field

technique and then demonstrate the computation of condensate corrections through some simple example calculations.

In Chapter 3 we determine the values of the bag parameters for the B_s meson in the full dimension-6 4-quark operator basis relevant for SM and BSM predictions of the mass difference ΔM_s and SM predictions of the decay rate difference $\Delta\Gamma_s$. This is done first in the HQET at NLO in α_s, including $SU(3)$ flavour breaking effects up to quadratic corrections of the strange quark mass, before matching onto QCD. We discuss the effect of these results on the SM predictions for ΔM_s and $\Delta\Gamma_s$ and then extract values for the top quark $\overline{\text{MS}}$ mass and for the leptonic branching fraction $\mathcal{B}(B_{s/d} \to \bar{l}l)$ from these findings.

In Chapter 4 we make a short detour from our sum rule analysis to briefly explore some of the implications of our findings in Chapter 3 for the values of CKM matrix elements. This includes predictions for $|V_{ts}V_{tb}|$, the ratio $|V_{td}/V_{ts}|$, V_{cb} and the angle γ of the unitarity triangle.

In Chapter 5 we return to the topic of sum rules and provide an analysis of the HQET bag parameters for 4-quark operators entering the calculation of B_s and D_s^+ lifetimes. Here we compute for the first time the effect of non-valence contributions and again take into account the effect of $SU(3)$ flavour breaking.

In Chapter 6 we carry out an in depth analysis of inclusive decay widths in charmed mesons. We calculate the total decay rate of the D^0, D^+ and D_s^+ mesons, along with the lifetime ratios $\tau(D^+)/\tau(D^0)$ and $\tau(D_s^+)/\tau(D^0)$, and determine the semileptonic branching fractions $\text{Br}(D_q \to Xe^+\nu_e)$. In doing so, we bring together for the first time in the charm sector, state of the art 4-quark operator matrix elements, and the non-leptonic contribution to the coefficient of the Darwin operator.

Finally, in Chapter 7 we conclude by summarising our findings and discuss their impact on the field of heavy quark physics.

Chapter 2

Theoretical Background

2.1 Heavy Quark Expansion

Whether our aim is to test the validity of the SM, extract a parameter of our theory or probe for New Physics effects, finding an appropriate observable for our purposes generally involves a compromise between what is easier to calculate theoretically and what can be more precisely measured in experiment. In heavy quark physics we study decays of heavy hadrons. If we consider exclusive decays (e.g $\Gamma(B_d \to \pi l^+ \nu)$), where the final outgoing decay channel is singled out, then experimentally this can be determined relatively easily whereas theoretically we have great difficulty due to the non-perturbative effects of the bound states involved. Alternatively, if we consider inclusive decays (e.g $\Gamma(B_d \to X)$) then all possible final states are included. This is obviously a greater undertaking for those in experiment who have to sum up all the contributing decay modes. However, from a theory perspective it allows for a powerful simplification of the calculation through the Heavy Quark Expansion (HQE). For hadrons with a heavy quark the HQE permits us to express inclusive decay rates as an operator expansion in the inverse of the heavy quark mass. For the early development of the HQE, see [56–64] and for a modern review see [44]. Here we summarise some of the key points, taking as an example the total decay rate of

a B meson of mass M_B which can be expressed as,

$$\Gamma(B) = \frac{1}{2M_B} \sum_X \int_{PS} (2\pi)^4 \, \delta^{(4)}(p_B - p_X) | \, \langle X(p_X) | \mathcal{H}_{eff} | B(p_B) \rangle \, |^2, \tag{2.1.1}$$

where $\mathcal{H}_{eff}$ is the effective weak Hamiltonian [65], the delta function enforces momentum conservation between the B meson momentum p_B and the sum of the out going state momenta p_X, we sum over all possible final states X and we integrate over phase space. Through the optical theorem[1] the total decay rate in Eq.(2.1.1) can be expressed in the form,

$$\Gamma(B) = \frac{1}{2M_B} \langle B | \mathcal{T} | B \rangle \, , \tag{2.1.2}$$

for which the transition operator $\mathcal{T}$ is defined by

$$\mathcal{T} \equiv \mathrm{Im}\, i \int d^4x \, \mathrm{T}\{\mathcal{H}_{eff}(x) \mathcal{H}_{eff}(0)\}. \tag{2.1.3}$$

Therefore the total decay rate is proportional to the discontinuity of a forward scattering amplitude of the B meson with a double insertion of the effective Hamiltonian. An additional operator product expansion under the assumption that the b quark mass m_b is large leads to an expansion of Eq.(2.1.3) in $1/m_b$ consisting of local operators[2]. The total decay rate in Eq.(2.1.2) then takes the form,

$$\Gamma(B) = \Gamma_3 \langle \mathcal{O}_3 \rangle + \Gamma_5 \frac{\langle \mathcal{O}_5 \rangle}{m_b^2} + \Gamma_6 \frac{\langle \mathcal{O}_6 \rangle}{m_b^3} + ... + 16\pi^2 \left[\tilde{\Gamma}_6 \frac{\langle \tilde{\mathcal{O}}_6 \rangle}{m_b^3} + \tilde{\Gamma}_7 \frac{\langle \tilde{\mathcal{O}}_7 \rangle}{m_b^4} + ... \right] , \tag{2.1.4}$$

for which Γ_i denote perturbative contributions and the matrix elements $\langle \mathcal{O}_d \rangle$ of mass dimension d represent the non-perturbative input which we expect to be numerically of order $\sim \Lambda_{QCD}$ but must be calculated either through sum rule methods or on the lattice. The tilde on $\langle \tilde{\mathcal{O}}_6 \rangle$ and $\langle \tilde{\mathcal{O}}_7 \rangle$ is to distinguish them as matrix elements of 4-quark operators whereas those without contain 2-quark operators. The form of the operators which are generated by the expansion are as follows:

- At dimension 3 we have the 2-quark operator $\bar{b}b$ and it is worth noting that

[1] The optical theorem follows as a result of conservation of probability (see [66] for proof).

[2] In the B system we find $\Lambda_{QCD}/m_b \ll 1$ and so the power series is justified. However, since $m_c/m_b \sim 3$ it is not obvious that the HQE is viable for charmed hadrons (see Chapter 6).

the perturbative coefficient Γ_3 describes the decay of a free b quark.

- The next independent operators arise at dimension 5 in the form of the kinetic and chromomagnetic operators $\bar{b}D^2b$ and $\bar{b}\sigma^{\mu\nu}G_{\mu\nu}b$ respectively. No independent dimension 4 operator appears in Eq.(2.1.4) since equations of motion relate these back to $\bar{b}b$. This is a significant result in itself since as a consequence the first correction to the free quark decay calculation at dimension 3 comes with a suppression of $1/m_b^2$.

- For dimension 6 the Darwin operator $\bar{b}D_\mu(v\cdot D)D^\mu b$ emerges as the 2 quark operator contribution whilst at this order we also get 4 quark operators contributing of the form $(\bar{b}\Gamma q)(\bar{q}\Gamma b)$ (we also note that the forward scattering matrix elements of the Darwin operator and the 4-quark operators are related via equations of motion). The 4-quark contributions are the first to include effects of the spectator quark q. It therefore has particular importance for studies into $SU(3)$ flavour breaking effects. The factor of $1/(16\pi^2)$ has been pulled out in Eq.(2.1.4) in order to highlight the phase space enhancement of 4 quark operator contributions. Whilst Γ_i is a 2-loop calculation at leading order in α_s, $\tilde{\Gamma}_i$ has non vanishing contributions already at 1-loop.

- At dimension 7 we see 4 quark operators with an additional covariant derivative.

We will return later to explore these contributions in further detail. In particular, analysis of 4 quark operator matrix elements using HQET sum rules are presented in Chapters 3 and 5. Furthermore, in Chapter 6 a full analysis of the charm meson lifetime is discussed.

2.2 Heavy Quark Effective Theory

The guiding principle behind the use of effective field theories is to choose an appropriately detailed physical description for the problem at hand. When considering

processes at low energy scales, we cannot resolve and therefore do not need a full description of high energy degrees of freedom. For example, the W boson mediates flavour changing processes of the SM but at low energies $\mu \approx m_b$, the large mass of the W boson $M_W \gg m_b$ effectively shrinks the W boson propagator down to a point so that the processes can be sufficiently approximated through 4-fermion operators [67, 68]. The weak effective theory (WET) formalises this picture by integrating out degrees of freedom of mass $\geq M_W$ from the generating functional and introducing a Wilsonian operator product expansion (OPE) to form a clear separation of scales. The final element to the procedure is the process of matching the SM and WET at the high scale M_W and running down the couplings of the WET to the low scale m_b using renoralisation group (RG) equations. This sums up large logarithms of the form $\alpha_s(\mu)\log(\mu/M_W)$ that otherwise spoil the perturbative expansion at $\mu = m_b$.

The heavy quark effective theory (HQET) has similar motivations. The purpose of HQET is to describe the physics involved in hadrons containing a heavy quark of mass m_Q. In this case, the high scale is m_Q whereas the low scale is set by Λ_{QCD} and heavy quark refers to a c or b quark[1] since both have masses that are considerably larger than characteristic scale of the hadron $\Lambda_{QCD} \ll m_Q$. In this context, a heavy quark is considered to move with the hadron four-velocity v and be almost on shell. It is therefore appropriate to parameterise the heavy quark momentum as,

$$p_Q^\mu = p^\mu + m_Q\, v^\mu, \tag{2.2.1}$$

where the 'residual' momentum p of the heavy quark is of the order $p \sim \Lambda_{QCD}$. Using this definition, it is easy to see what the form of the heavy quark propagator will be

[1] Obviously the top quark fits the criteria but since it decays too quickly to form bound states it has been neglected here.

by expanding the QCD free quark propagator in the heavy quark limit $m_Q \to \infty$:

$$\begin{aligned} i\frac{\not{p}_Q + m_Q}{p_Q^2 - m_Q^2} &= i\frac{\not{p} + m_Q(1+\not{v})}{p^2 + 2m_Q p\cdot v}, \\ &= i\frac{(1+\not{v})}{2\omega} + \mathcal{O}\left(\frac{1}{m_Q}\right). \end{aligned} \tag{2.2.2}$$

where $\omega = p \cdot v$ denotes the 'residual energy' and determines how far off-shell the heavy quark is, and we have used $v^2 = 1$ (see Table 2.1 for the leading order HQET Feynman rules).

The quark field is then also reparameterised,

$$Q(x) = e^{-im_Q v\cdot x} h(x) + \mathcal{O}\left(\frac{1}{m_Q}\right), \tag{2.2.3}$$

such that the field h, which describes the massless degrees of freedom, is defined by,

$$h(x) = e^{im_Q v\cdot x}\frac{(1+\not{v})}{2} Q(x). \tag{2.2.4}$$

which implies the relation $\not{v} h = h$. If we consider the heavy quark in the hadron rest frame $v^\mu = (1,0,0,0)$, then from Eq.(2.2.4) it's apparent that the field h corresponds to the upper two elements of Q. Using these definitions, it follows that the HQET Lagrangian in the heavy quark limit takes the form [69],

$$\mathcal{L}_h = \overline{h} i\,(v\cdot D)\, h. \tag{2.2.5}$$

This has some important consequences. Firstly, although h annihilates heavy quarks it does not create heavy anti quarks and therefore there are no heavy anti quarks in the strict HQET description of the hadron. These only arise when including $1/m_Q$ corrections to Eq.(2.2.5). Secondly, Eq.(2.2.5) is independent of m_Q and therefore in the heavy quark limit the surrounding light degrees of freedom are insensitive to the mass of the heavy quark. This leads to a flavour symmetry between a system of N_f heavy quarks all moving with the same velocity v. Furthermore, since no gamma matrices appear in Eq.(2.2.5), interactions with gluons have no effect on the spin state of the heavy quark. As a result, the system exhibts an $SU(2N_f)$ spin-flavour symmetry [70–72] which allows for non-trivial relations between the matrix elements

of hadrons with different heavy quark flavours and allows hadrons to be identified by the quantum numbers of their light degrees of freedom [73]. Symmetry breaking effects can then be calculated by introducing $1/m_Q$ corrections.

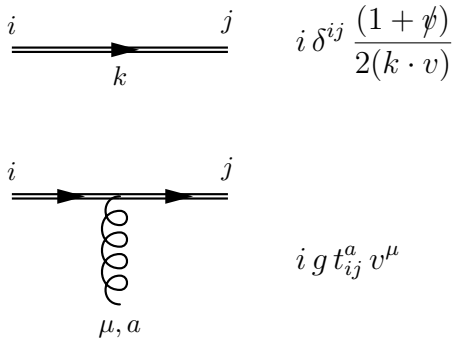

Table 2.1: HQET Feynman rules at leading order in $1/m_Q$.

2.3 B_s-mixing

In this section we give a brief introduction to B_s-mixing. Many reviews on this subject are already available in the literature, in particular, see chapter 1.3 of [74] for a thorough introduction and also the excellent discussions in [68, 75–77].

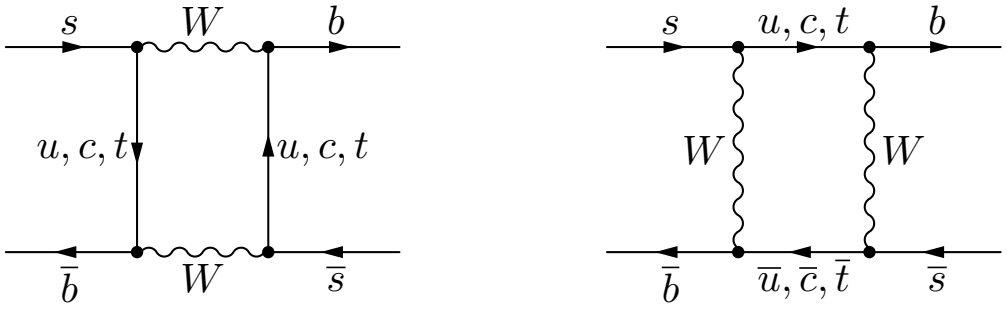

Figure 2.1: Box diagrams that mediate $B_s - \overline{B}_s$ transitions. Both apply to M^s_{12} for which an internal t quark gives the dominant contribution. For Γ^s_{12} only the diagram on the right with internal u and c quarks enter the calculation.

The phenomena of neutral meson mixing can be described through a quantum mechanical picture. Taking a 2 state system at time t consisting of a superposition

of the flavour state $|B_s\rangle$ and the anti flavour state $|\overline{B}_s\rangle$, its time evolution can be expressed through the differential equation,

$$i\frac{d}{dt}\begin{pmatrix}|B_s(t)\rangle\\|\overline{B}_s(t)\rangle\end{pmatrix} = \left(\hat{M}^s - \frac{i}{2}\hat{\Gamma}^s\right)\begin{pmatrix}|B_s(t)\rangle\\|\overline{B}_s(t)\rangle\end{pmatrix}, \tag{2.3.1}$$

where $\hat{M}^s$ and $\hat{\Gamma}^s$ are 2×2 Hermitian matrices. In a system without mixing, the diagonal terms of $\hat{M}^s$ correspond to the B_s mass M_{B_s} and the diagonal terms of $\hat{\Gamma}^s$ correspond to its decay rate Γ_{B_s}, while the off-diagonal terms of both disappear. However, weak interactions in the SM generate nonvanishing off-diagonal terms M^s_{12} and Γ^s_{12} through the box diagrams shown in Figure 2.1.

Contributions to M^s_{12} come from the dispersive part of these diagrams where intermediate states are off-shell, while the absorptive part contributes to Γ^s_{12} where intermediate states are on-shell. For this reason, only the diagram on the right of Figure 2.1 contributes to Γ^s_{12} and unlike M^s_{12} only u and c quarks play a role.

Diagonalising $\hat{M}^s$ and $\hat{\Gamma}^s$ we find the mass eigenstates of the system for which we label the heavy state $|B_H\rangle$ and the light state $|B_L\rangle$. The eigenvalues of $\hat{M}^s$ and $\hat{\Gamma}^s$ then correspond to the mass $M^s_{H/L}$ and the decay rate $\Gamma^s_{H/L}$ of $|B_{H/L}\rangle$. In the B system, we can expand the mass difference ΔM^s and decay rate difference $\Delta\Gamma^s$, using $|\Gamma^s_{12}/M^s_{12}| \ll 1$[1], which leads to the expressions,

$$\begin{aligned}\Delta M_s &\equiv M^s_H - M^s_L\\ &= 2|M^s_{12}|\left(1 - \frac{|\Gamma^s_{12}|\sin^2\phi^s_{12}}{8|M^s_{12}|^2} + ...\right)\\ &\approx 2|M^s_{12}|,\end{aligned} \tag{2.3.2}$$

$$\begin{aligned}\Delta\Gamma_s &\equiv \Gamma^s_H - \Gamma^s_L\\ &= 2|\Gamma^s_{12}|\cos\phi^s_{12}\left(1 - \frac{|\Gamma^s_{12}|\sin^2\phi^s_{12}}{8|M^s_{12}|^2} + ...\right)\\ &\approx 2|\Gamma^s_{12}|\cos\phi^s_{12},\end{aligned} \tag{2.3.3}$$

[1] In D-mixing, a similar treatment is not appropriate. See discussions in [78] on the complications that arise in D-mixing.

where the mixing phase ϕ_{12}^s is defined as,

$$\phi_{12}^s \equiv \left(-\frac{M_{12}^s}{\Gamma_{12}^s}\right). \tag{2.3.4}$$

Calculating M_{12}^s therefore allows us to determine the mass difference ΔM_s. For this we use an effective Hamiltonian with degrees of freedom above the scale m_b integrated out of the theory,

$$M_{12}^s = \frac{\langle \bar{B}_s | \mathcal{H}_{eff}^{\Delta B=2} | B_s \rangle}{2M_{B_s}}. \tag{2.3.5}$$

Here our effective Hamiltonian $\mathcal{H}_{eff}^{\Delta B=2}$ is given in the SM by,

$$\mathcal{H}_{eff}^{\Delta B=2} = C_1 \; Q_1 + h.c. \tag{2.3.6}$$

with the Wilson coefficient C_1 containing all dependence on the heavy degrees of freedom and Q_1 is the only 4-quark operator appearing,

$$Q_1 \;\; = \;\; \bar{b}_i \gamma_\mu (1-\gamma^5) s_i \; \bar{b}_j \gamma^\mu (1-\gamma^5) s_j, \tag{2.3.7}$$

where i, j denote the colour indices in the fundamental representation. With only one operator appearing[1], the procedure is straightforward. To determine the Wilson coefficient we calculate the quark level processes in Figure 2.1 and equate to the calculation done in the effective theory.

Combining all contributions from both box diagrams we find the following structure,

$$\begin{aligned} M_{12}^s \propto\; & \lambda_u^2 F(x_u, x_u) + \lambda_u \lambda_c F(x_u, x_c) + \lambda_u \lambda_t F(x_u, x_t) \\ & + \lambda_c \lambda_u F(x_c, x_u) + \lambda_c^2 F(x_c, x_c) + \lambda_c \lambda_t F(x_c, x_t) \\ & + \lambda_t \lambda_u F(x_t, x_u) + \lambda_t \lambda_c F(x_t, x_c) + \lambda_t^2 F(x_t, x_t), \end{aligned} \tag{2.3.8}$$

where the CKM inputs are represented by $\lambda_i = V_{ib} V_{is}^*$ and the box diagrams are functions of $x_q = m_q^2 / M_W^2$. From this we use CKM unitarity, $\sum_i V_{ij} V_{ik}^* = \delta_{jk}$, specifically $\lambda_u + \lambda_c + \lambda_t = 0$, to remove λ_u. As a result, Eq.(2.3.8) can be expressed

[1] This turns out to be the case even when NLO QCD corrections are considered.

as,

$$\begin{aligned} M_{12}^s \propto & \lambda_c^2 \left[F(x_c, x_c) - 2F(x_u, x_c) + F(x_u, x_u)\right] \\ & + \lambda_c \lambda_t \left[F(x_c, x_t) - F(x_u, x_t) - F(x_u, x_c) + F(x_u, x_u)\right] \\ & + \lambda_t^2 \left[F(x_t, x_t) - 2F(x_u, x_t) + F(x_u, x_u)\right]. \end{aligned} \tag{2.3.9}$$

In this form, the GIM suppression becomes evident [24]. We see that any constant terms arising from the loop integrals cancel in the square brackets and, more significantly, if all masses were equal then each line in Eq.(2.3.9) would independently cancel entirely. Each term is subjected to the same order of CKM suppression and so, setting $m_u = m_c = 0$, we can approximate M_{12}^s by the top contribution alone[1],

$$\begin{aligned} M_{12}^s &\propto \lambda_t^2 \left[F(x_t, x_t) - 2F(0, x_t) + F(0, 0)\right] \\ &\propto \lambda_t^2 S_0(x_t), \end{aligned} \tag{2.3.10}$$

where $S_0(x_t)$ denotes the Inami-Lim function [79],

$$S_0(x) = \frac{4x - 11x^2 + x^3}{4(1-x)^2} - \frac{3x^3 \log x}{2(1-x)^3}, \tag{2.3.11}$$

The result of the full calculation reads,

$$M_{12}^s = \frac{G_F^2}{12\pi^2} \lambda_t^2 M_W^2 S_0(x_t) \hat{\eta}_B B f_{B_s}^2 M_{B_s}, \tag{2.3.12}$$

where the factor $\hat{\eta}_B$ [65] encapsulates higher order QCD corrections, M_W denotes the W boson mass and G_F is the Fermi constant. The hadronic matrix element enters through,

$$\langle \bar{B}_s | Q_1 | B_s \rangle = \left(2 + \frac{2}{N_c}\right) M_{B_s}^2 f_{B_s}^2 B_1(\mu), \tag{2.3.13}$$

where it is parameterised by the decay constant f_{B_s} and the bag parameter $B_1(\mu)$ which determines the deviation from the vacuum insertion approximation (VIA)[2] and is also dependent on the renormalisation scale μ. The bag parameter is by

[1] This is justified since $x_u \sim x_c \ll 1$ while $x_t > 1$.

[2] A full set of states is inserted into Q_1 in Eq.(2.3.13) and the ground state isolated. This is assumed to give the dominant contribution and so all others are dropped. The bag parameter is then a way of quantifying the neglected terms. Numerically, the VIA is in fact found to be a very good approximation (see [28]).

far the largest source of uncertainty in predictions of ΔM_s. Whilst modern lattice groups can achieve precise results for decay constants, the matrix elements of 4-quark operators presents a much greater challenge (see Chapters 3 and 5).

The calculation of Γ_{12}^s is more technically challenging than that of ΔM_s since the intermediate u and c states go on-shell. After integrating out the W boson, we are left with a bi-local object. In order to get a series of local operators a second OPE is applied. This is done through the formalism of the HQE already described in Section 2.1. We therefore get an expression for Γ_{12}^s as a power series in (Λ_{QCD}/m_b) which reads [76],

$$\Gamma_{12}^s = \frac{\Lambda^3}{m_b^3}\left[\Gamma_3^{s(0)} + \frac{\alpha_s}{4\pi}\Gamma_3^{s(1)} + ...\right] + \frac{\Lambda^4}{m_b^4}\left[\Gamma_4^{s(0)} + ...\right] + ... \tag{2.3.14}$$

where the Γ_i^s each contain a product of Wilson coefficients and matrix elements of local operators and we have expanded each contribution in α_s. In addition to the operator Q_1 appearing in ΔM_s, two new operators also contribute to Γ_3^s:

$$Q_2 = \bar{b}_i(1-\gamma^5)s_i\ \bar{b}_j(1-\gamma^5)s_j, \tag{2.3.15}$$

$$Q_3 = \bar{b}_i(1-\gamma^5)s_j\ \bar{b}_j(1-\gamma^5)s_i, \tag{2.3.16}$$

for which their corresponding matrix elements read,

$$\langle \bar{B}_s|Q_2|B_s\rangle = \frac{M_{B_s}^2}{(m_b+m_s)^2}\left(-2+\frac{1}{N_c}\right)M_{B_s}^2 f_{B_s}^2 B_2, \tag{2.3.17}$$

$$\langle \bar{B}_s|Q_3|B_s\rangle = \frac{M_{B_s}^2}{(m_b+m_s)^2}\left(1-\frac{2}{N_c}\right)M_{B_s}^2 f_{B_s}^2 B_3, \tag{2.3.18}$$

where the masses m_b and m_s are evaluated in the $\overline{\text{MS}}$ scheme. The term Γ_4^s in Eq.(2.3.14) is suppressed by an additional power of Λ/m_b and here we find two more 4-quark operators arising,

$$Q_4 = \bar{b}_i(1-\gamma^5)s_i\ \bar{b}_j(1+\gamma^5)s_j, \tag{2.3.19}$$

$$Q_5 = \bar{b}_i(1-\gamma^5)s_j\ \bar{b}_j(1+\gamma^5)s_i, \tag{2.3.20}$$

with the corresponding matrix elements parameterised by,

$$\langle \bar{B}_s|Q_4|B_s\rangle = \left(\frac{2M_{B_s}^2}{(m_b+m_s)^2}+\frac{1}{N_c}\right) M_{B_s}^2 f_{B_s}^2 B_4, \tag{2.3.21}$$

$$\langle \bar{B}_s|Q_5|B_s\rangle = \left(\frac{2M_{B_s}^2}{N_c(m_b+m_s)^2}+1\right) M_{B_s}^2 f_{B_s}^2 B_5, \tag{2.3.22}$$

In Chapter 3, we determine all of the above mentioned bag parameters for the 4-quark operators necessary for calculating ΔM_s in the SM and BSM and $\Delta\Gamma_s$ in the SM with HQET sum rules. Also appearing in Γ_4^s are contributions from dimension-7 operators (4-quark operators with an inserted covariant derivative). First non-perturbative determinations of their matrix elements were carried out very recently [80] on the lattice where before the VIA had to be relied upon. Taking into consideration the recent developments of the non-perturbative inputs to both ΔM_s and $\Delta\Gamma_s$ we discuss the current status of both in Chapter 3.

2.4 QCD Sum Rules

In this section we give an overview of the method of QCD sum rules (for enlightening reviews and early development see [46,81–86]). The approach allows for an analytical computation of hadronic amplitudes using perturbative QCD. Given an ansatz on the hadronic spectral function, it has been successfully applied to extract non-perturbative hadronic parameters in a model independent way. The typical starting point of such calculations are time ordered correlation functions of currents that satisfy the quantum numbers of the hadrons we wish to study. Motivated by the work presented in Chapters 3 and 5 we will restrict our discussion to HQET sum rules for a heavy-light meson H containing heavy-quark Q in this section. The principles of the sum rule set up are no different in this context and it should serve to familiarise the reader with the notation used in the latter half of the thesis.

2.4.1 2 point correlator

Consider the two point correlator,

$$\Pi(\omega) = i \int d^d x \, e^{ip\cdot x} \, \langle 0|\mathrm{T}\left[\tilde{j}_q^\dagger(0)\tilde{j}_q(x)\right]|0\rangle \,, \tag{2.4.1}$$

where the currents are defined by $\tilde{j}_q \equiv \overline{q}\gamma^5 h$ with light quark field q and HQET field h for heavy quark Q, where p is the residual momenta of the heavy quark (as defined in Eq.(2.2.1)) and ω is the corresponding residual energy $\omega = p \cdot v$, and we have used dimensional regularisation with $d = 4 - 2\epsilon$. For large negative residual energy, the quarks in the interpolating current are highly virtual and in the limit $\omega \to -\infty$ can be described through perturbative QCD. However, for values of $\omega > 0$ the correlator can form bound states. These manifest as resonances for single particle meson states and a 'continuum' of multiparticle states along the positive real axis.

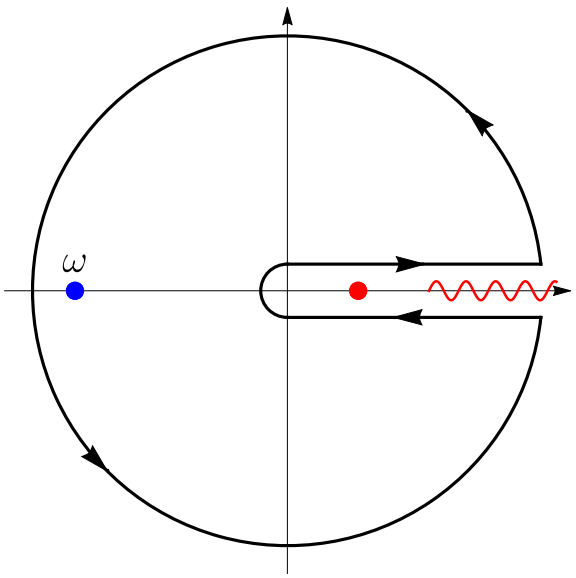

Figure 2.2: Contour chosen to isolate the pole at ω. The red marker indicates the lowest single state hadronic resonance. The squiggly line shows the continuum of multi-particle and excited states.

Since the correlator is analytic away from the positive real axis, these two regimes can be related to one another by means of a dispersion relation:

$$\begin{aligned}\Pi(\omega) &= \frac{1}{2\pi i}\oint_C ds\ \frac{\Pi(s)}{(s-\omega)} \\ &= \frac{1}{2\pi i}\lim_{\epsilon\to 0}\int_0^\infty ds\ \frac{\Pi(s+i\epsilon)-\Pi(s-i\epsilon)}{(s-\omega)} + \frac{1}{2\pi i}\int_R ds\ \frac{\Pi(s)}{(s-\omega)} \\ &= \int_0^\infty ds\ \frac{\rho(s)}{(s-\omega)},\end{aligned} \tag{2.4.2}$$

where $\rho(s) = \lim_{\epsilon\to 0}(\Pi(s+i\epsilon)-\Pi(s-i\epsilon))/2\pi i$ denotes the discontinuity in $\Pi(s)$ along the positive axis. Both the contour C and the discontinuity are indicated by the plot in Figure 2.2. In the last step of Eq.(2.4.2), we have assumed that the radial section vanishes in the limit $R \to \infty$. This is not always the case however and to account for possible divergent behaviour we can instead use the following form,

$$\Pi^n(\omega) = \omega^n \int_0^\infty ds \frac{\rho(s)}{s^n(s-\omega)} + \sum_{i=0}^{n-1} a_i\,\omega^i, \tag{2.4.3}$$

where n is chosen to ensure the radial portion of the integration disappears. In its stead, we have polynomial corrections with coefficients a_i. These can be discarded however by taking the appropriate number of derivatives. This observation will be one of the motivations behind a key alteration to the sum rule that we discuss in Section 2.4.3. With this in mind, we will revert back to the form of the dispersion relation shown in Eq.(2.4.2) for the remainder of this discussion.

For $\omega > 0$ we can express the discontinuity of the 2-point function in terms of hadronic parameters using an ansatz for the hadronic spectral function,

$$\rho^{had}(\omega) = F^2\delta(\omega-\overline{\Lambda}) + \rho^{cont}(\omega), \tag{2.4.4}$$

with $\overline{\Lambda} \equiv M_H - m_Q$ denoting the mass difference [87] between the ground state meson and heavy quark. In Eq.(2.4.4) the delta function determines the ground state resonance while $\rho^{cont}(\omega)$ is defined as the continuum spectral density which contains all of the complications of multi-particle and excited state resonances in one deceptively simple looking term. The HQET variation of the decay constant F

determines the coupling strength of the ground state resonance and is defined by the HQET matrix element[1],

$$\langle 0|\overline{q}\gamma^{\mu}\gamma^{5}h|\mathbf{H}(v)\rangle = -iF_{q}v^{\mu}, \tag{2.4.5}$$

where the HQET state appearing is non-relativistically normalised such that,

$$|H(p)\rangle = \sqrt{2M_{H}}|\mathbf{H}(v)\rangle + \mathcal{O}(1/m_{Q}). \tag{2.4.6}$$

Substituting Eq.(2.4.4) back into our dispersion relation Eq.(2.4.2) we get,

$$\Pi(\omega) = \frac{F_{q}^{2}}{(\overline{\Lambda}-\omega)} + \int_{\omega_{0}}^{\infty} ds\, \frac{\rho^{cont}(s)}{(s-\omega)}, \tag{2.4.7}$$

where we have introduced a threshold parameter ω_0 which indicates the energy at which continuum contributions begin.

If we consider again the limit $\omega \to -\infty$, the correlation function can be described through perturbation theory since the process is predominantly short distance. However, taking some intermediate value of $\omega < 0$, we are sensitive to long distance non-perturbative effects from the QCD vacuum. Fortunately a procedure for separating out long and short distance effects is available to us in the form of the operator product expansion (OPE).

2.4.2 Operator Product Expansion

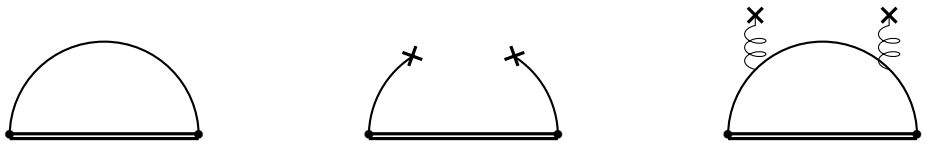

Figure 2.3: Contributions to Eq.(2.4.1) corresponding to LO perturbative (left), quark condensate (middle) and gluon condensate (right).

At large momenta, as the quark-heavy quark pair travel over the short distance

[1]The meson state here contains a heavy particle. In later sections of this work concerned with B mesons the convention in the literature is that B mesons contain $\overline{b}$ quarks while $\overline{B}$ mesons contain b quarks.

x they interact with the non-trivial QCD vacuum fields. Since the vacuum fields generally fluctuate over long distances, it can be argued that to the fields generated by our current j_q they are experienced as static fields. Quantitatively, this idea is formalised through the use of the operator product expansion,

$$\int d^dx\, e^{ip\cdot x}\, \mathrm{T}\left[\tilde{j}_q^\dagger(0)\tilde{j}_q(x)\right] = C_0\mathbb{1} + \sum_{d=1} C_d O^d, \tag{2.4.8}$$

where C_d are Wilson coefficients containing short distance information. Long distance effects are described by operators O^d of mass dimension d which are constructed from gauge invariant combinations of quark and gluon fields. Higher order terms in the expansion generate power corrections $\propto \omega^{-d}$. For the 2-point correlator, the expansion in Eq.(2.4.8) is sandwiched between the initial and final vacuum states and so described by a series of Wilson coefficients and vacuum expectation values (VEV) $\langle O^d\rangle$ known as the QCD condensates. At $d = 0$ we have the identity operator $\mathbb{1}$ and its coefficient C_0 which corresponds to the result calculated in full perturbation theory (since within that framework the VEV of higher dimensional operators vanish). We show some of the leading non-perturbative corrections in Figure 2.3, specifically quark condensate $\langle\overline{q}q\rangle$ and gluon condensate $\langle GG\rangle$ contributions along with the perturbative result at leading order in α_s. We will discuss methods for extracting the coefficients of condensates in Section 2.6. The tools used in this case are the tools of perturbation theory. To determine the condensates themselves however is beyond these methods. Instead, we have three options [85]: simulate them using lattice QCD, construct a model to describe the vacuum (e.g. liquid instanton model [88,89]), or fit them by comparing to other sum rules of measurable quantities. In the latter case, we rely on the the validity of the OPE, by which we mean that there is a clear separation of scales between the Wilson coefficients and the condensates. Under this assumption however, the condensates are universal and can be treated as phenomenological parameters of the theory. This method has proven successful, a clear example being the estimation of the gluon condensate $\langle\frac{\alpha}{\pi}GG\rangle \simeq (0.012\mathrm{GeV})^4$ in the original SVZ sum rule studies [90]. Determined by

fitting moment sum rules to experimental data for charmonium states, this value for the gluon condensate is still in use today.

Though the OPE has been proven to be valid in full perturbation theory, its application in QCD introduces non-perturbative effects which bring this into question. The nontrivial character of the QCD vacuum has two main consequences for the OPE [46]:

1. Non-vanishing condensates, $\langle O^d \rangle \neq 0$
2. The breakdown of the OPE, beginning at critical dimension d_{crit}

The latter of these points can be understood as a breakdown of the separation of scales principle that the OPE assumes. At some d_{crit} the VEVs become sensitive to non-perturbative effects from short distance fluctuations and the validity of the OPE is lost. Importantly, these effects typically only come into play at high orders in the expansion[1], beyond the order at which we need to truncate. We note that truncation in this context is not solely due to our computational limitations. The operator expansion, as with our perturbative expansion in α_s, is divergent (see discussion in [91]). An optimal truncation still leaves a gap between our OPE description of the correlator and its exact theoretical solution. In fact, the effect of neglected terms at $\omega < 0$ may be magnified after analytical continuation to the positive real axis[2]. There is therefore an inherent limitation on the accuracy of the OPE. These effects are referred to as a violation of quark hadron duality (QHD) where QHD is the assumption that the quark level picture of the OPE can be considered 'dual' to the hadronic picture for $\omega > 0$ (for an in depth discussion into QHD read the excellent review by Shifman [91]).

Helpful discussions into how we can estimate the value of d_{crit} through instanton models can be found in [46, 85, 91]. The topic of short distance non-perturbative physics is beyond the scope of this work so we end this discussion here and put together the pieces of our sum rule. Below d_{crit}, the OPE allows us to calculate the

[1] See e.g. [46] for one-instanton solution in the dilute gas approximation showing $d_{crit} = 12$.

[2] The correlation function may exhibit oscillatory behaviour for $\omega > 0$ that the OPE is not sensitive to.

2 point correlator with the methods of perturbation theory supplemented with the condensates. Equating this picture with our hadronic description gives us our 'sum rule',

$$\frac{F^2}{(\overline{\Lambda}-\omega)}+\int_{\omega_0}^{\infty} ds\ \frac{\rho^{cont}(s)}{(s-\omega)}=\int_{0}^{\infty} ds\ \frac{\rho^{OPE}(s)}{(s-\omega)}. \tag{2.4.9}$$

For the 2-point case, the object of interest is the decay constant, as can be seen from how we have isolated its contribution in Eq.(2.4.7). However, standing in our way of directly calculating it is the remaining contribution from the continuum spectral density. A useful alteration to the sum rule which helps to deal with this issue and also with the problem of potential subtraction terms in our dispersion relation is the Borel transform.

2.4.3 Borel Transform

The Borel transformed correlator is defined by [46],

$$\Pi(t)\equiv\mathcal{B}_t\Pi(\omega)=\lim_{\substack{-\omega,n\to\infty\\ -\omega/n\to t}}\frac{(-\omega)^{n+1}}{n!}\left[\frac{d}{d\omega}\right]^n\Pi(\omega), \tag{2.4.10}$$

for which there are three main consequences that are apparent from the following identities for the operator $\mathcal{B}_t$. The first,

$$\mathcal{B}_t[\omega^i]=0, \tag{2.4.11}$$

is immediately obvious since in the limit Eq.(2.4.10) applies infinite derivatives which removes any polynomial terms. Importantly this removes the need for subtraction terms from our dispersion relation.

Secondly we have,

$$\begin{aligned}\mathcal{B}_t\left[\frac{1}{(s-\omega)^i}\right]&=\lim_{\substack{-\omega,n\to\infty\\ -\omega/n\to t}}\frac{(-\omega)^{n+1}}{n!}\left[\frac{d}{d\omega}\right]^n(s-\omega)^{-i}\\ &=\lim_{n\to\infty}\frac{1}{(i-1)!\ t^{(i-1)}}\frac{(i+n-1)!}{(n-1)!\ n^i}\left(1+\frac{s}{nt}\right)^{-(i+n)}\\ &=\frac{e^{\frac{-s}{t}}}{(i-1)!\ t^{(i-1)}},\end{aligned} \tag{2.4.12}$$

which has a two fold effect. On the hadronic side of our sum rule, this introduces an exponential weight function to our integral and therefore reduces our sensitivity to ρ_{cont}. On the theory side, convergence of the OPE is improved since higher order terms in the series become factorially suppressed. The downside is that choosing t to optimise either of these effects worsens the other. Choosing a low value for t isolates the ground state contribution further but increases the significance of the higher order terms in our expansion. This is not ideal, since we are already aware that our expansion must breakdown for some d_{crit}. Alternatively, choosing a higher t suppresses higher order contributions and allows us to safely truncate after the first few terms, but increases our sensitivity to higher energy resonances. Avoiding these scenarios places conditions on our choice of t leading to upper and lower limits which define the range $t \in \{t_{min}, t_{max}\}$ in which the sum rule is stable. This is known as the 'Borel window' [81]. It is worth noting that the existence of such a 'Borel window' for any sum rule is not guaranteed since t_{min} may be found to be higher than t_{max}. This can occur if the OPE is found to converge poorly or is affected by short distance non-perturbative effects at relatively low orders.

The Borel transformed sum rule is by no means the only variation at our disposal. Other alternatives to be used include moment sum rules and Gaussian weight functions methods. Discussions on these as well as a thorough review of all aspects to QCD sum rules can be found in [82].

In order to create a sum rule for the decay constant, we use QHD [81, 91–93] which allows us to approximate[1],

$$\int_{\omega_0}^{\infty} ds\, \frac{\rho^{cont}(s)}{(s-\omega)} = \int_{\omega_c}^{\infty} ds\, \frac{\rho^{OPE}(s)}{(s-\omega)}, \tag{2.4.13}$$

where ω_c is some cut-off which does not necessarily coincide with ω_0 and needs to be fixed. As we have discussed, the Borel transformation suppresses the contribution from $\rho^{cont}(s)$ and therefore reduces our sensitivity to violations of this approximation.

[1] This is an example of 'global' duality. Alternatively 'local' duality considers the approximation that $\rho^{OPE}(\omega) = \rho^{had}(\omega)$ for $\omega \to \infty$ (see discussion in [81]).

Using Eq.(2.4.13) we arrive at our final Borel HQET sum rule for the decay constant (see [94–96] for early works),

$$F^2(\mu) = \int_0^{\omega_c} d\omega \; e^{\frac{\overline{\Lambda}-\omega}{t}} \rho^{OPE}(\omega). \tag{2.4.14}$$

We now have a direct route to calculating a non-perturbative hadronic parameter which, for the most part, can be done using standard Feynman diagram techniques with the additional input of the condensates. In Section 2.6 we will return to this matter and explore how the coefficients of the condensates may be determined.

2.5 Technical Toolbox

In this section we provide an introduction to some useful methods widely used in modern loop calculations. For illustrative purposes we also include simple example calculations with the intention to familiarise the reader with the underlying principles and terminology. This is done in preparation for Chapters 3 and 5, where some of the methods discussed here will be employed in a more advanced setting.

2.5.1 Integration by Parts Identities

When faced with multi-loop processes, we encounter a large number of Feynman diagrams. Each of these correspond to Feynman integrals which after a manipulation of the Dirac algebra and a tensor reduction, in turn generate a large number of scalar integrals. Since the prospect of calculating each of these individually is not a pleasant one[1], it is in our interest to find relations between them that might reduce the amount of human input required. These scalar integrals can be categorised into 'families' which are defined by a distinct set of propagators to arbitrary power[2].

[1] Or feasible, in most modern calculations.

[2] This includes to the power 0 and therefore multiple families can share subsets where the propagators which distinguish them from each other vanish.

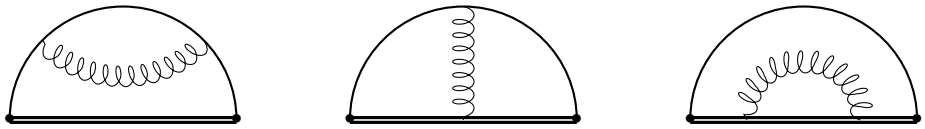

Figure 2.4: NLO correction to two point correlator.

First developed by Chetyrkin and Tkachov [97], integration by parts (IBP) identities allow us to build a system of linear relations between integrals in a family through differential operators (see [98] for an excellent review). A sufficient set of IBP relations allows integrals to be expressed as a linear combination of integrals for which the total sum of propagator powers is reduced and with it also the complexity of the integrals that we are required to directly compute[1]. A profound outcome of this procedure is that recursive applications reduces any integral in the family to a finite set of integrals [99], commonly referred to as 'master integrals', forming a basis. Once the exact form of these are known the entire family of integrals are solved for as well. It is worth highlighting that the freedom in our choice of IBP relations reflects a freedom in the set of master integrals, too. This observation is an important aspect in the differential equations method of solving master integrals [100, 101] which rests on finding a choice of basis for which the system of differential equations of the master integrals takes on a 'canonical form'[2].

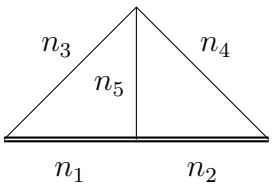

Figure 2.5: HQET 2 loop scalar integral.

To illustrate how IBPs are constructed, we consider the NLO contribution to the perturbative part of the two point correlator Eq.(2.4.1). The Feynman diagrams this corresponds to are found in Figure 2.4. The processes on the left and right contain recursively 1 loop integrals. However, the middle diagram generates genuine 2 loop

[1]There is a freedom in our choice of IBP's to generate and it is not always intuitive which combinations will be most beneficial.

[2]This is used specifically for finding the analytical form of master integrals as an expansion in ϵ.

scalar integrals of the form found in Figure 2.5 which corresponds to the expression,

$$\begin{aligned} I(n_1,n_2,n_3,n_4,n_5) &\equiv \int \frac{d^dk_1}{(2\pi)^d}\,\frac{d^dk_2}{(2\pi)^d}\frac{1}{D_1^{n_1}D_2^{n_2}D_3^{n_3}D_4^{n_4}D_5^{n_5}} \\ &\equiv \int [dk]\; f(n_1,n_2,n_3,n_4,n_5), \end{aligned} \tag{2.5.1}$$

where we have assigned arbitrary powers n_i to the propagators and in the second line denoted the integrand by the function $f(n_1,...)$ and used the shorthand $[dk] \equiv d^dk_1\, d^dk_2/(2\pi)^{2d}$ to make things compact. The set of propagators in Eq.(2.5.1) are defined by,

$$\begin{aligned} D_1 &= 2(k_1\cdot v+\omega), & D_2 &= 2(k_2\cdot v+\omega), \\ D_3 &= k_1^2, & D_4 &= k_2^2, \\ D_5 &= (k_1-k_2)^2, \end{aligned} \tag{2.5.2}$$

where we have taken the light quark to be massless. The IBP relations between different integrals of the family defined through Eq.(2.5.1) are generated by,

$$\int [dk]\,\frac{\partial}{\partial k_j}\cdot(k_i f) = 0, \tag{2.5.3}$$

which equates to zero since surface terms vanish in dimensional regularisation, though the fact that we get zero on the r.h.s of Eq.(2.5.3) is not actually essential to the construction of IBPs. Choosing $i=1$ and $j=1$, and using the relations,

$$\begin{aligned} k_1\cdot\partial_1\; D1^{-n_1} &= -n_1(D_1^{-n_1}-2\omega D_1^{-n_1-1}), \\ k_1\cdot\partial_1\; D3^{-n_3} &= -n_3 2D_3^{-n_3}, \\ k_1\cdot\partial_1\; D5^{-n_5} &= -n_5(D_3-D_4)D_5^{-n5-1}-n_5D_5^{-n_5}, \end{aligned} \tag{2.5.4}$$

we derive a linear relation between integrals of different propagator powers:

$$[(d-n_1-2n_3-n_5)+2\omega n_1\mathbf{1}^+ - n_5(\mathbf{3}^-\mathbf{5}^+-\mathbf{4}^-\mathbf{5}^+)]I(n_1,n_2,n_3,n_4,n_5)=0, \tag{2.5.5}$$

where we use the operator notation for which $\mathbf{1}^+I(n_1,...) = I(n_1+1,...)$. Choosing instead $i=2$ and $j=1$, we create a second IBP identity,

$$[(-n_3+n_5)-n_3(\mathbf{4}^-\mathbf{3}^+-\mathbf{5}^-\mathbf{3}^+)-n_1\mathbf{1}^+\mathbf{2}^-+2\omega n_1\mathbf{1}^+ \\ +n_5(\mathbf{4}^-\mathbf{5}^+-\mathbf{3}^-\mathbf{5}^+)]I(n_1,n_2,n_3,n_4,n_5)=0. \quad (2.5.6)$$

Substituting Eq.(2.5.6) back into Eq.(2.5.5)we arrive at,

$$I(n_1,n_2,n_3,n_4,n_5)=\frac{[n_3\mathbf{5}^-\mathbf{3}^+-n_3\mathbf{4}^-\mathbf{3}^+-n_1\mathbf{2}^-\mathbf{1}^+]}{(d-n_1-n_3-2n_5)}I(n_1,n_2,n_3,n_4,n_5). \quad (2.5.7)$$

This relation removes the only non-trivial integral from the NLO calculation and in fact for any integral with all $n_i > 0$ it can be repeatedly used to express it as a combination of integrals which all have one $n_i = 0$. Setting all $n_i = 1$, Eq.(2.5.7) expresses our integral as a linear combination of 3 integrals, each with one propagator raised and one propagator removed. Diagrammatically, this corresponds to,

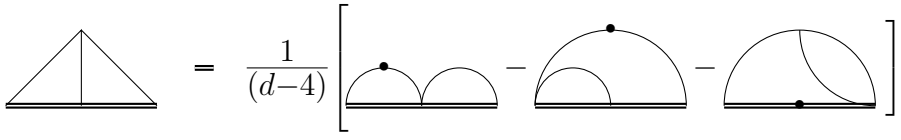

where the dotted propagators appear twice in the integrand. The first diagram appearing on the r.h.s is obviously factorised for us already whilst the second two are recursively 1-loop integrals and therefore all three are easily expressible in terms of gamma functions.

To completely solve the system, from this one could continue applying more combinations of IBPs until we reach the irreducible master integrals, however realistically this is not how such calculations are carried out. Instead of solving recurrence relations for master integrals by hand on a case by case basis, it is common practice to automate the process through dedicated computer programs. In the absence of a general solution, the most popular alternative is to use the Laporta Algorithm [102]. This approach instead takes integrals with fixed integer powers and yields a large system of IBPs. Predetermined rules for the ordering of integrals[1] are then used with Gauss elimination to replace complex integrals with simpler ones until a set of master

[1]For example, total number of positive indices, sum of positive indices, value of highest propagator power etc..

integrals is reached. The downside to the Laporta approach however, is that the large and highly redundant system of linear equations it generates comes at the cost of substantial computation times if left unaided. To counteract this effect, symmetries are often used to remove some of the redundancies. This includes symmetries under the permutation of propagator indices, Lorentz invariance identities [103], boundary conditions[1] and the Lie algebra [104] of the IBPs themselves. This brute force method has proven very effective in the calculation of multiloop processes and many implementations are publicly available (see FIRE [105], KIRA [106], AIR [107], REDUZE [108]).

2.5.2 Mass Expansion methods

Motivated by the discussions in Chapters 3 and 5, here we introduce some methods for calculating mass corrections to Feynman integrals.

Mellin-Barnes Integrals

First, we will outline how this can be achieved through Mellin Barnes integral representations (see [109] for an introduction and [110–112] for the development of its application to Feynman integrals). To begin with, let us consider the leading order perturbative contribution to the correlator in Eq.(2.4.1), where we now take the light quark to have mass m. This corresponds to the 1-loop diagram shown on the left of Figure 2.3.

After wick contracting all of the fields,

$$\begin{aligned}\Pi(\omega) &= i\int d^dx\, e^{ipx}\,\langle 0|\mathrm{T}\left[\tilde{j}_q^\dagger(0)\tilde{j}_q(x)\right]|0\rangle \\ &= i\int d^dx\, e^{ipx}\,\langle 0|\overbrace{h_{i\delta}(x)\,\overline{h}}_{j\alpha}(0)\gamma^5_{\alpha\beta}\overbrace{q_{j\beta}(0)\,\overline{q}}_{i\gamma}(x)\gamma^5_{\gamma\delta}|0\rangle\end{aligned}$$

[1] For example, if for some subset of propagators, when $n_i = 0$ the integral vanishes.

and substituting in the form of the propagators we find,

$$\begin{aligned}\Pi(\omega) &= i\int d^dx\, e^{ipx}\,\mathrm{Tr}\left[S^h_{ij}(x)\,\gamma^5\,S^{(0)}_{ji}(-x)\,\gamma^5\right]\\ &= i\int \frac{d^dk}{(2\pi)^d}\,\mathrm{Tr}\left[S^h_{ij}(p+k)\,\gamma^5\,S^{(0)}_{ji}(k)\,\gamma^5\right]\\ &= i\int \frac{d^dk}{(2\pi)^d}\,\frac{4N_c(m-k\cdot v)}{2(k\cdot v+\omega)\,(k^2-m^2)},\end{aligned} \tag{2.5.8}$$

where $S^h(x)$ denotes the HQET propagator and $S^{(0)}(x)$ denotes the free light quark propagator which we define as,

$$iS^h_{ij}(x) = i\int \frac{d^dp}{(2\pi)^d}e^{-ip\cdot x}S^h_{ij}(p), \qquad iS^{(0)}_{ij}(x) = i\int \frac{d^dp}{(2\pi)^d}e^{-ip\cdot x}S^{(0)}_{ij}(p), \tag{2.5.9}$$

with their momentum space representations given by,

$$S^h_{ij}(p) \equiv \delta_{ij}\,\frac{(1+\not{v})}{2(p\cdot v)}, \qquad S^{(0)}_{ij}(p) \equiv \delta_{ij}\,\frac{\not{p}+m}{p^2-m^2}. \tag{2.5.10}$$

Denominators of HQET propagators are linear in their momentum dependence[1] and instead of using the usual Feynman parameterisation, a more appropriate alternative is found to be,

$$\frac{1}{A^\alpha\,B^\beta} = \frac{\Gamma(\alpha+\beta)}{\Gamma(\alpha)\Gamma(\beta)}\int_0^\infty dy\,\frac{y^{\beta-1}}{[A+By]^{\alpha+\beta}}, \tag{2.5.11}$$

which after applying to Eq.(2.5.8) and carrying out the loop integration leaves us with,

$$\Pi(\omega) = \frac{-4N_c\Gamma(\epsilon)}{(4\pi)^{\frac{d}{2}}}\int_0^\infty dy\,(m+y)[y(y-2\omega)+m^2]^{-\epsilon}, \tag{2.5.12}$$

At this point, we can replace the term from Eq.(2.5.12) in the square brackets with a Mellin Barnes integral representation defined by,

$$\frac{1}{(X+Y)^\lambda} = \frac{1}{\Gamma(\lambda)}\frac{1}{2\pi i}\int_{-i\infty}^{i\infty} dz\,\Gamma(\lambda+z)\Gamma(-z)\frac{Y^z}{X^{\lambda+z}}, \tag{2.5.13}$$

for which poles from terms of the form $\Gamma(a+bz)$ must appear on the left side of the integration contour whereas those from $\Gamma(a-bz)$ must appear on the right for the relation to hold. This prescription continues through the calculation and should be

[1] A useful consequence of this fact is that if the number of loops is less than the number of HQET propagators then the propagators are not linearly independent and partial fraction decomposition can be used to remove some of the propagators.

held even for Gamma functions that arise after carrying out the Feynman parameter integral in the subsequent step.

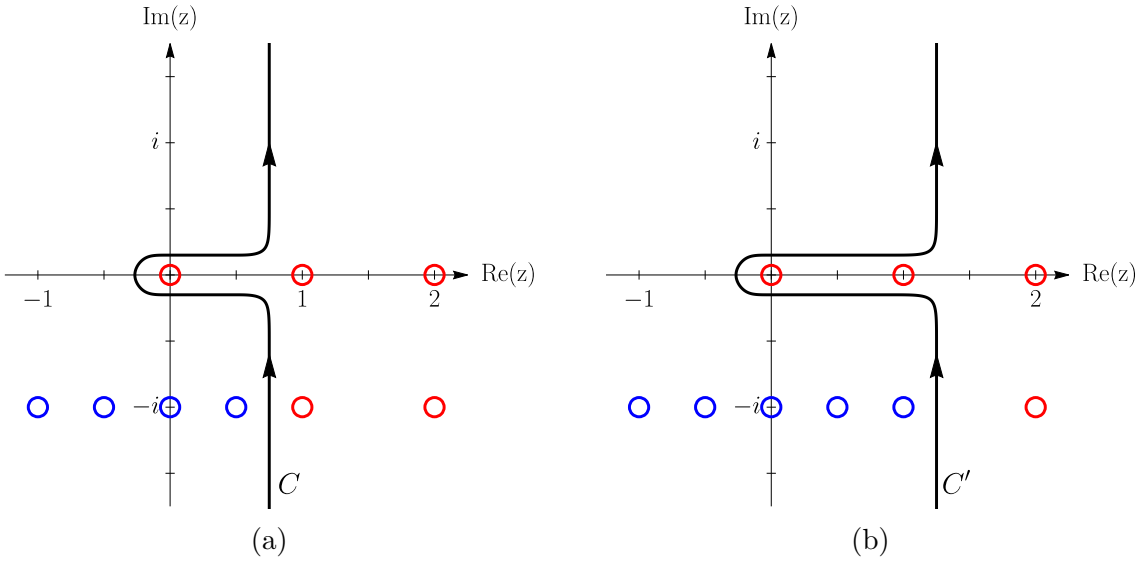

Figure 2.6: Potential contour choices, keeping to the left/right (blue/red) prescription for the poles.

Applying Eq.(2.5.13) with the choice $X = y(y-2\omega)$, $Y = m^2$ for $\lambda = \epsilon$, we can separate out the mass dependence,

$$\Pi(\omega) = \frac{-4N_c}{(4\pi)^{d/2}} \frac{1}{2\pi i} \int_{-i\infty}^{i\infty} dz\, \Gamma(\epsilon+z)\Gamma(-z) \int_0^\infty dy\, (m+y)[y(y-2\omega)]^{-\epsilon-z} m^{2z}. \tag{2.5.14}$$

Using the change of variables,

$$y \to \frac{\frac{y}{(-2\omega)}}{\frac{y}{(-2\omega)}+1}, \tag{2.5.15}$$

we find that the integral over the loop momenta is expressable in terms of Gamma functions leaving us with,

$$\Pi(\omega) = \frac{-4N_c}{(4\pi)^{\frac{d}{2}}} \frac{(-2\omega)^{2-2\epsilon}}{2\pi i} \int_{-i\infty}^{i\infty} dz \left\{ \left(\frac{m}{-2\omega}\right)^{2z} \Gamma(-z)\Gamma(2-\epsilon-z)\Gamma(-2+2\epsilon+2z) + \left(\frac{m}{-2\omega}\right)^{2z+1} \Gamma(-z)\Gamma(1-\epsilon-z)\Gamma(-1+2\epsilon+2z) \right\}. \tag{2.5.16}$$

In Figure 2.6, the plot on the left shows a potential choice of contour C for the

integration of the second term in Eq.(2.5.16) whereas the plot on the right shows a contour C' for integrating over the first term. The disparity between the two contours arises due to a different left/right prescription of the pole positioned at $z = 1 - \epsilon$. It is important to be careful with any manipulation of the Gamma functions aimed to 'tidy up' this expression since this can confuse the original left/right prescription of the poles and lead to incorrect results. For example, using $x\Gamma(x) = \Gamma(x+1)$, we might be tempted to recast the first term of Eq.(2.5.16) so as to have a common set of Gamma functions between the two:

$$\Gamma(2-\epsilon-z)\Gamma(-2+2\epsilon+2z) = -\frac{1}{2}\Gamma(1-\epsilon-z)\Gamma(-1+2\epsilon+2z). \tag{2.5.17}$$

However, in doing so the pole at $z = 1 - \epsilon$ now seems to require to sit on the right of the integration contour, which contradicts the original determination. In general, it is best to leave the expression in Eq.(2.5.16) as it stands to avoid this confusion. At this point, we can choose to close the contour to the right(left) and our integration equates to an infinite sum over the residues of the poles lying to the right(left) of the contour. The full form of integrals can be found this way by comparing the sum of residues to known series representations of functions. In our case, we instead consider the limit $m \ll \omega$. In this kinematic regime, we see from Eq.(2.5.16) that by closing the contour to the right we achieve a power series in $m/(-2\omega)$ which we can truncate by picking up only the residues of the poles closest to $z = 0$. To $\mathcal{O}(m^3)$ we arrive at,

$$\Pi(\omega) \simeq \frac{4N_c}{(4\pi)^{\frac{d}{2}}}(-2\omega)^{2-2\epsilon}\Gamma(1-\epsilon)\Gamma(2\epsilon-1)\left[\frac{1}{2} - \left(\frac{m}{-2\omega}\right) + (2\epsilon-1)\left(\frac{m}{-2\omega}\right)^2 \right.$$
$$\left. -2(2\epsilon-1)\left(\frac{m}{-2\omega}\right)^3 - \frac{\Gamma(\epsilon-1)}{\Gamma(1-\epsilon)\Gamma(2\epsilon-1)}\left(\frac{m}{-2\omega}\right)^{3-2\epsilon}\right]. \tag{2.5.18}$$

The last term of Eq.(2.5.18) clearly would not have been found by a Taylor expansion in the small mass m of the integrand in Eq.(2.5.8). This approach would hold to $\mathcal{O}(m^2)$ but misses this contribution that we are sensitive to at $\mathcal{O}(m^3)$ and which the use of Mellin-Barnes integrals has allowed us to find. This is an incredibly useful tool

to have when encountering integrals for which the massless case is known but the full mass dependence is not. However, the cost of finding our expansion using this method is the introduction of another integral and a procedure of taking residues, which becomes increasingly computationally difficult as we consider more complex processes at higher loop orders.

Expansion by Regions

As we saw from the previous section, though effective, the Mellin Barnes procedure of acquiring an expansion in the small mass limit grew relatively involved for what is a basic example. Clearly, an alternative with more scalabilty would be greatly appreciated before we want to attempt higher order perturbative corrections. Fortunately, such a method is available to us. The 'Expansion by Regions' technique, first put forward by Beneke and Smirnov [113] and later developed further by Jantzen [114][1], allows us to expand on the integrand level. If we consider again the 1-loop example in Section 2.5.2, a naive Taylor expansion of the integrand in m will not reproduce the expansion of the full integral to all orders since the domain of the loop integral k includes regions for which $k \sim m$. The validity of the expansion breaks down in these regions and we lose contributions to the full expanded result. Instead, the Expansion by Regions tells us to proceed as follows:

1. Identify and separate regions of the loop momenta domain for which external parameters may be considered large/small and Taylor expand the integrand accordingly.
2. For each distinct region, integrate the expanded integrand over the full domain of the loop momenta.

For our 1-loop example, we identify two regions: a hard region characterised by $k \sim \omega$, and a soft region associated with $k \sim m$. In the hard region it holds that

[1] See the paper by Janzten for general proofs and examples.

$|k^2| \gg m^2$ and therefore we can expand the light quark propagator in the small mass whereas in the soft region we expand the heavy quark propagator in inverse powers of the large residual energy. Applying the above to Eq.(2.5.8) we arrive at:

$$\begin{aligned}\mathcal{T}_{\frac{m}{\omega}}\left[\Pi(\omega)\right] = i\int \frac{d^dk}{(2\pi)^d}\frac{4N_c(m-k\cdot v)}{2(k\cdot v+\omega)}\mathcal{T}_h\left[\frac{1}{(k^2-m^2)}\right] \\ + i\int \frac{d^dk}{(2\pi)^d}\frac{4N_c(m-k\cdot v)}{(k^2-m^2)}\mathcal{T}_s\left[\frac{1}{2(k\cdot v+\omega)}\right],\end{aligned} \tag{2.5.19}$$

where $\mathcal{T}_{\frac{m}{\omega}}[\Pi(\omega)]$ denotes the Taylor expansion of the correlator and the expansion operators $\mathcal{T}_h$ and $\mathcal{T}_s$ act as,

$$\mathcal{T}_h\left[\frac{1}{(k^2-m^2)}\right] = \frac{1}{k^2}\sum_{a=0}\left(\frac{m^2}{k^2}\right)^a \tag{2.5.20}$$

$$\mathcal{T}_s\left[\frac{1}{2(k\cdot v+\omega)}\right] = \frac{1}{2\omega}\sum_{b=0}(-1)^b\left(\frac{k\cdot v}{\omega}\right)^b. \tag{2.5.21}$$

To calculate our expansion up to m^3 it is sufficient to take terms up to $a=1$ and $b=0$. Carrying out the integration is then straightforward and we find that the hard region generates the first 3 terms of Eq.(2.5.18) while the last term originates from the soft region[1].

At this point, having blindly followed the two step plan above, it might seem surprising that we have arrived at the same expression as Eq.(2.5.18) since it would not be unreasonable to expect a fair amount of double counting going on by integrating over the whole loop momenta domain for each expansion. To explain why this is not the case, we consider an intermediate scale Λ which obeys $m \ll \Lambda \ll \omega$, and use it to split the integration domain D into $D_s = \{k \in \mathbb{R}^d : |k^2| < \Lambda^2\}$ and $D_h = \{k \in \mathbb{R}^d : |k^2| \geq \Lambda^2\}$ such that $D = D_s \cup D_h$ and $D_s \cap D_h = \emptyset$. Using these

[1]Note that this confirms our previous statement that a naive Taylor expansion in m of the integrand holds to quadratic order.

definitions we can write,

$$\begin{aligned}\int_D I &= \int_{D_s} I + \int_{D_h} I \\ &= \int_{D_s} \mathcal{T}_s I + \int_{D_h} \mathcal{T}_h I,\end{aligned} \tag{2.5.22}$$

where to keep things compact we denote the integrand by I and in the the second line we have acknowledged the fact that soft and hard expansions to I are valid in D_s and D_h respectively by their definition[1]. Next we take the first term in Eq.(2.5.22) and express the integral of $\mathcal{T}_s I$ over D_s as an integral over the full domain D and substract the integral over the hard region D_h,

$$\begin{aligned}\int_{D_s} \mathcal{T}_s I &= \int_D \mathcal{T}_s I - \int_{D_h} \mathcal{T}_s I \\ &= \int_D \mathcal{T}_s I - \int_{D_h} \mathcal{T}_{hs} I,\end{aligned} \tag{2.5.23}$$

where the notation $\mathcal{T}_{hs} I$ represents the application of the soft expansion operator $\mathcal{T}_s$ followed by $\mathcal{T}_h$ which we are now free to apply since the integral is over D_h. Likewise, a similar expression for the second term in Eq.(2.5.22) can be found,

$$\int_{D_h} \mathcal{T}_h I = \int_D \mathcal{T}_h I - \int_{D_s} \mathcal{T}_{sh} I. \tag{2.5.24}$$

Using,

$$\int_{D_s} \mathcal{T}_{sh} I + \int_{D_h} \mathcal{T}_{hs} I = \int_D \mathcal{T}_{sh} I, \tag{2.5.25}$$

where we have used the commutability between the operators $\mathcal{T}_h$ and $\mathcal{T}_s$, substituting Eqs.(2.5.23) and (2.5.24) back into Eq.(2.5.22) we arrive at,

$$\int_D I = \int_D \mathcal{T}_s I + \int_D \mathcal{T}_h I - \int_D \mathcal{T}_{sh} I. \tag{2.5.26}$$

All of the integrals in Eq.(2.5.26) are over the whole domain and all dependence on our intermediate scale Λ through the definitions of D_s and D_h has therefore dropped out too. A closer look at the third term reveals one last interesting feature.

[1] While it is not strictly true that $|k \cdot v| \ll \Lambda$ in D_s, under integration only terms of even powers of $|k \cdot v|$ are non-vanishing, and tensor reduction allows us to exchange terms $(k \cdot v)^2$ with terms proportional to k^2. Therefore this treatment is valid under integration.

Explicitly we find,

$$\begin{aligned}\int_D \mathcal{T}_{sh} I &= i \int \frac{d^d k}{(2\pi)^d} \frac{4N_c(m - k\cdot v)}{2\omega\ k^2} \sum_{a=0} \left(\frac{m^2}{k^2}\right)^a \sum_{b=0} (-1)^b \left(\frac{k\cdot v}{\omega}\right)^b \\ &= 0,\end{aligned} \tag{2.5.27}$$

since the double expansion generates scaleless integrals which vanish in dimensional regularisation. As a result, Eq.(2.5.26) becomes,

$$\int_D I = \int_D \mathcal{T}_s I + \int_D \mathcal{T}_h I, \tag{2.5.28}$$

which matches the form of Eq.(2.5.19).

2.6 QCD Condensates

Here we discuss the treatment of higher dimension terms in the OPE, namely the condensates[1]. The standard approach is to use the background field technique. In the context of our 2-point corelator, the vacuum that the quark-antiquark pair propagates through is considered to be populated by soft external background fields which oscillate over scales much larger than the distance the pair travels between creation and annihilation. Closely related to the operator method first developed by Schwinger for use in QED [115], the advantages of it's application to QCD was first made apparent in the early 80's (see [116–119]). A key element of it's effectiveness is through the choice of the Fock-Schwinger (FS) gauge [115, 120, 121]. Also referred to as the fixed-point gauge, this proves to be a powerful tool in the context of the background field technique as it allows for a fully covariant expansion of the external gluon 4-potential. A thorough introduction to the methods used in this section can be found in [122] which discusses in detail the background field technique and presents many example calculations relevant to those working in sum rules. Other useful sources include the lecture notes by Pascual [123] and the review by Reinders,

[1] Our focus is on calculating the coefficients of the condensates in the OPE and not the condensates themselves which is beyond the scope of this work.

Rubenstein and Yazaki [85], both of which serve as helpful practical guides. In Section 2.6.1 we first define the FS gauge and then present the expansions of the external quarks and gluons. Then in Section.2.6.2 we derive the expansion of the light quark propagator in the presence of a background gluon field. Following on from this, in Section 2.6.3 we put these results to use by calculating the leading condensate contributions to Eq.(2.4.1).

2.6.1 Fock-Schwinger Gauge

The Fock-Schwinger gauge is defined by:

$$(x - x_0)^\mu A^a_\mu = 0 \tag{2.6.1}$$

for which the coordinate point x^μ_0 represents a gauge freedom that we fix in the following by setting $x_0 = 0$. This is not a necessary step since for any amplitude the dependency on x_0 drops out and in doing so can even provide a useful way to check our final result. Nevertheless, to keep our expressions compact we will place x_0 at the origin.

Now consider the following relation for the 4-potential $A_\mu(x)$,

$$\begin{aligned} A_\mu(x) &= \frac{\partial}{\partial x_\mu}\left(A_\rho(x)x^\rho\right) - x^\rho\frac{\partial A_\rho(x)}{\partial x_\mu} \\ &= \frac{\partial}{\partial x_\mu}(A_\rho(x)x^\rho) - x^\rho\frac{\partial A_\mu(x)}{\partial x_\rho} - x^\rho G_{\mu\rho}(x) + ig\,x^\rho\left[A_\rho(x), A_\mu(x)\right] \\ &= -x^\rho\frac{\partial A_\mu(x)}{\partial x_\rho} - x^\rho G_{\mu\rho}(x) \end{aligned} \tag{2.6.2}$$

where in the second line we have used the definition of the field strength tensor $G_{\mu\rho} = \frac{i}{g}[D_\mu, D_\rho]$ with covariant derivative $D_\mu = \partial_\mu - igA_\mu$ for $A_\mu = t^a_{ij}A^a_\mu$ (with t^a a colour generator in the fundamental representation) and in the third line we have removed the terms which vanish as a result of the gauge condition in Eq.(2.6.1). Moving the first term of the r.h.s. over to the l.h.s to join $A_\mu(x)$ and changing

variables $x = x'\alpha$ we arrive at,

$$\frac{d(\alpha A_\mu(\alpha x))}{d\alpha} = \alpha x^\rho G_{\rho\mu}(\alpha x). \tag{2.6.3}$$

Integrating over the full derivative in α from 0 to 1, we get a new expression for the 4 potential that will prove useful to us in later calculations,

$$A_\mu(x) = \int_0^1 d\alpha\, \alpha x^\rho G_{\rho\mu}(\alpha x) \tag{2.6.4}$$

Next we recall the kinematic conditions under which we always work within the OPE, specifically that our vacuum fields vary slowly with x. Therefore we expand $A_\mu(x)$ in x about the origin. Consequently, expanding Eq.(2.6.1) gives us,

$$x^\mu A_\mu(0) + x^\mu x^{\nu_1}\partial_{\nu_1} A_\mu(0) + \frac{1}{2}x^\mu x^{\nu_1} x^{\nu_2}\partial_{\nu_1}\partial_{\nu_2} A_\mu(0) + ... = 0. \tag{2.6.5}$$

For the gauge condition to hold for all x then each individual term of the expansion in Eq.(2.6.5) must also equate to zero. As a result, if we similarly expand the field strength tensor in Eq.(2.6.4) we see that we can replace each partial derivative with a covariant derivative,

$$\begin{aligned} A^a_\mu(x) &= \int_0^1 d\alpha\, \alpha x^\rho (G^a_{\mu\rho}(0) + \alpha x^{\nu_1}\partial_{\nu_1} G^a_{\mu\rho}(0) + \frac{1}{2!}\alpha^2 x^{\nu_1} x^{\nu_2}\partial_{\nu_1}\partial_{\nu_2} G^a_{\mu\rho}(0) + ...) \\ &= \int_0^1 d\alpha\, \alpha x^\rho (G^a_{\mu\rho}(0) + \alpha x^{\nu_1} D_{\nu_1} G^a_{\mu\rho}(0) + \frac{1}{2!}\alpha^2 x^{\nu_1} x^{\nu_2} D_{\nu_1} D_{\nu_2} G^a_{\mu\rho}(0) + ...) \end{aligned} \tag{2.6.6}$$

After carrying out the integration we are left with an expression for $A_\mu(x)$ in terms of the field strength tensor and covariant derivatives evaluated at the origin,

$$A^a_\mu(x) = \frac{1}{2}x^\rho G^a_{\rho\mu}(0) + \frac{1}{3}x^\nu x^\rho D_\nu G^a_{\rho\mu}(0) + ... \tag{2.6.7}$$

The same principles also give us an expansion of the external quark fields in terms of covariant derivatives,

$$q_\alpha(x) = q_\alpha(0) + x^\rho D_\rho q_\alpha(0) + \frac{1}{2!}x^\rho x^\sigma D_\rho D_\sigma q_\alpha(0) + ... \tag{2.6.8}$$

These expansions of the quark and gluon fields allow the condensates to arise naturally when evaluating Eq.(2.4.1). We will see later that for the quark condensate $\langle\overline{q}q\rangle \equiv \langle 0|\overline{q}_{i\alpha}(0)q_{i\alpha}(0)|0\rangle$ the effect immediately follows after applying wicks theorem to the time ordered correlator. For the gluon condensate $\langle GG\rangle \equiv \langle 0|G^a_{\mu\nu}(0)G^a_{\mu\nu}(0)|0\rangle$ we first need to expand the quark propagator in the background field.

2.6.2 Quark propagator

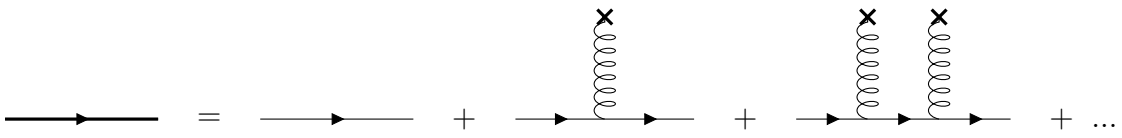

Figure 2.7: Vacuum gluon corrections to the quark propagator.

In the fixed point gauge and in the strict HQET limit, interactions between the heavy quark and gluons in the vacuum vanish. Therefore, to find the coefficient of the gluon condensate we will only consider contributions from the light quark. In the presence of a background gluon field the light quark propagator admits the expansion,

$$iS(x,y) = iS^0(x-y) + iS^{(1)}(x,y) + iS^{(2)}(x,y) + ... \tag{2.6.9}$$

defined by [122],

$$\begin{aligned} iS(x,y) = iS^{(0)}(x-y) &+ g\int d^4z\, iS^{(0)}(x-z)\, i\not{A}(z)\, iS^{(0)}(z-y) \\ &+ g^2\int d^4z\, d^4z'\, iS^{(0)}(x-z')\, i\not{A}(z')\, iS^{(0)}(z'-z)\, i\not{A}(z)\, iS^{(0)}(z-y) \\ &+ ... \end{aligned} \tag{2.6.10}$$

where $S^{(0)}(x-y)$ denotes the free light quark propagator. Schematically, this expansion is depicted in Figure 2.7. If we wish to work in momentum space then

the Fourier transformed propagator is defined as usual by,

$$S(p) = \int d^4x e^{ipx} S(x,0). \tag{2.6.11}$$

However, before continuing to derive the higher order corrections to the propagator, we should pay closer attention to the notation in our definition of $S(p)$ and make the reader aware of a drawback of the Fock-Schwinger gauge. As a result of choosing a fixed point x_0 in our gauge condition, we lost translation invariance in our propagator. Specifically, $S(0,x) \neq S(-x)$ and as a result,

$$S(0,x) = \int \frac{d^4p}{(2\pi)^4} e^{ipx} \tilde{S}(p), \tag{2.6.12}$$

for which $\tilde{S}(p) \neq S(p)$. Therefore we should be careful when switching to momentum space in our calculation of the correlator. We will return to this issue when it arises and continue with our derivation of the propagator corrections. In momentum space, using Eq.(2.6.10) and Eq.(2.6.11) and taking only the leading term from Eq.(2.6.7) the first correction takes the form,

$$\begin{aligned} iS^{(1)}(p) &= -ig \int d^4z\, e^{ipz} \left[\int d^4x\, e^{ip(x-z)} S^{(0)}(x-z) \right] \not{A}(z) S^{(0)}(z) \\ &= -ig\, S^{(0)}(p) \frac{\gamma^\mu G_{\rho\mu}}{2} \int d^4z\, z^\rho\, e^{ipz} S^{(0)}(z) \\ &= -ig\, S^{(0)}(p) \frac{\gamma^\mu G_{\rho\mu}}{2} \left(-i \frac{\partial}{\partial p^\rho} \right) S^{(0)}(p), \end{aligned} \tag{2.6.13}$$

where on the third line we have used $z^\rho e^{ipz} = -i\frac{\partial}{\partial p^\rho} e^{ipz}$ to remove z^ρ from the integral which then takes the form of $S^{(0)}(p)$. Applying the partial derivative we find,

$$\begin{aligned} iS^{(1)}(p) &= -ig\, G_{\rho\mu} \left(\frac{\not{p} + m}{\left(p^2 - m^2\right)} \right) \gamma^\mu \left(\frac{\gamma^\rho}{\left(p^2 - m^2\right)} - \frac{2p^\rho(\not{p} + m)}{\left(p^2 - m^2\right)^2} \right) \\ &= -ig \frac{t^a G^a_{\mu\rho}}{4(p^2 - m^2)^2} \left((\not{p} + m)\sigma_{\mu\rho} + \sigma_{\mu\rho}(\not{p} + m) \right), \end{aligned} \tag{2.6.14}$$

where we have pulled out the colour generator from the field strength tensor and skipped some tedious Dirac algebra to arrive at the final form. For the purposes of extracting the gluon condensate however, the first order correction is not sufficient

and we must calculate $S^{(2)}(p)$. The process is in principle the same as for the $S^{(1)}(p)$, but for completeness we will illustrate the steps to get there. We begin with,

$$\begin{aligned} iS^{(2)}(p) &= \int d^4x e^{ipx} iS^{(2)}(x,0) \\ &= ig^2 \int d^4z d^4z' d^4x e^{ipx} S^{(0)}(x-z') \not{A}(z') S^{(0)}(z'-z) \not{A}(z) S^{(0)}(z) \\ &= ig^2 \int d^4z d^4z' e^{ipz'} \left[\int d^4x e^{ip(x-z')} S^{(0)}(x-z') \right] \not{A}(z') S^{(0)}(z'-z) \not{A}(z) S^{(0)}(z) \\ &= ig^2 S^{(0)}(p) \int d^dz d^dz' e^{ipz'} \not{A}(z') S^{(0)}(z'-z) \not{A}(z) S^{(0)}(p), \end{aligned} \tag{2.6.15}$$

where again we use a change of variables in the final line to remove integration over x and pull out the free quark momentum space propagator $S^{(0)}(p)$. We then substitute in the expanded 4-potential in Eq.(2.6.7) keeping only the leading order term and successively replace factors of z and z' with derivatives,

$$\begin{aligned} iS^{(2)}(p) &= ig^2 S^{(0)}(p) \int d^4z d^4z' e^{ipz'} \frac{1}{2} G_{\rho\mu} \gamma^\mu z'^\rho S^{(0)}(z'-z) \frac{1}{2} G_{\sigma\nu} \gamma^\nu z^\sigma S^{(0)}(z) \\ &= i\frac{g^2}{4} S^{(0)}(p)\, G_{\rho\mu}\gamma^\mu \left(-i\frac{\partial}{\partial p_\rho} \right) S^{(0)}(p)\, G_{\sigma\nu}\gamma^\nu \left(-i\frac{\partial}{\partial p_\sigma} \right) S^{(0)}(p). \end{aligned} \tag{2.6.16}$$

From this we can predict how additional soft gluon insertions will affect the propagator. In the momentum space representation, the quark travels freely between each interaction with a gluon from the vacuum and each time it interacts we pick up an insertion of the field strength tensor, a gamma matrix and a partial derivative which acts on all preceding free propagators. Applying the first partial derivative gives us,

$$\begin{aligned} iS^{(2)}_{ij}(p) &= -i\frac{g^2}{4} \left[t^a t^b \right]_{ij} G^a_{\rho\mu} G^b_{\sigma\nu} \frac{(\not{p}+m)}{(p^2-m^2)} \frac{\partial}{\partial p_\rho} \gamma^\mu \frac{(\not{p}+m)}{(p^2-m^2)} \frac{\partial}{\partial p^\sigma} \gamma^\nu \frac{(\not{p}+m)}{(p^2-m^2)} \\ &= -i\frac{g^2}{4} \left[t^a t^b \right]_{ij} G^a_{\rho\mu} G^b_{\sigma\nu} \frac{(\not{p}+m)}{(p^2-m^2)} \\ &\qquad \times \frac{\partial}{\partial p_\rho} \left[\frac{\gamma^\mu (\not{p}+m) \gamma^\nu \gamma^\sigma}{(p^2-m^2)^2} - \frac{2\gamma^\mu (\not{p}+m) \gamma^\nu (\not{p}+m) p^\sigma}{(p^2-m^2)^3} \right], \end{aligned} \tag{2.6.17}$$

where we have pulled out the colour generators from factors of the field strength tensor. Following this we note that the term within the square brackets can be

simplified using the anti-symmetric properties of $G^b_{\sigma\nu}$ which leads to,

$$iS^{(2)}_{ij}(p) = -i\frac{g^2}{4}\left[t^a t^b\right]_{ij} G^a_{\rho\mu} G^b_{\sigma\nu} \frac{(\not{p}+m)}{(p^2-m^2)} \times \frac{\partial}{\partial p_\rho}\left[\frac{\left(\gamma^\mu(\not{p}+m)\gamma^\nu\gamma^\sigma + 2\gamma^\mu\gamma^\nu p^\sigma\right)}{(p^2-m^2)^2}\right]. \tag{2.6.18}$$

With our intention being to extract the gluon condensate from Eq.(2.4.1) it is helpful to already have in mind the relation [85],

$$\langle 0|G^a_{\mu\rho}(0)G^b_{\nu\sigma}(0)|0\rangle = \delta^{ab}\frac{(g_{\mu\nu}g_{\rho\sigma} - g_{\mu\sigma}g_{\rho\nu})}{d(d-1)(N_c^2-1)}\langle GG\rangle\,. \tag{2.6.19}$$

Using Eq.(2.6.19), the partial derivative of the term in round brackets in Eq.(2.6.18) vanishes. Therefore after applying the final derivative we arrive at,

$$iS^{(2)}_{ij}(p) = ig^2\left[t^a t^a\right]_{ij}\frac{(\not{p}+m)}{(p^2-m^2)^4}\left[\gamma^\mu(\not{p}+m)\gamma^\nu\gamma^\sigma p^\rho + 2\gamma^\mu\gamma^\nu p^\sigma p^\rho\right] \times \frac{(g_{\rho\sigma}g_{\mu\nu} - g_{\rho\nu}g_{\mu\sigma})}{d(d-1)(N_c^2-1)}GG, \tag{2.6.20}$$

where summation over the indices of GG is implied. Contracting the Lorentz indices, the gamma matrices reduce to a much less cumbersome form,

$$\left(\gamma^\mu(\not{p}+m)\gamma^\nu\gamma^\sigma p^\rho + 2\gamma^\mu\gamma^\nu p^\sigma p^\rho\right)(g_{\rho\sigma}g_{\mu\nu} - g_{\rho\nu}g_{\mu\sigma}) = 2(d-1)m\not{p}, \tag{2.6.21}$$

and after substituting Eq.(2.6.21) back into Eq.(2.6.20) we find a conveniently compact form for $S^{(2)}(p)$:

$$iS^{(2)}_{ij}(p) = ig^2\frac{\delta_{ij}\,GG}{d\,N}\frac{m(p^2+m\not{p})}{(p^2-m^2)^4}. \tag{2.6.22}$$

The final results in Eq.(2.6.14) and Eq.(2.6.22) can be found in [85]. For a full derivation of the first correction to the quark propagator with a non-zero mass including terms up to a covariant derivative of the field strength tensor in both momentum and position space representations, see [124, 125]. Additional higher order corrections can be found in [126].

2.6.3 Example Calculations

To calculate the condensate contribution to the correlator Eq.(2.4.1) stemming from soft quark interactions at the spacetime points x and 0 (see Figure 2.3), we wick contract only the 2 heavy quark fields, treating light quarks as soft external states,

$$\begin{aligned}\Pi^q(\omega) &= i\int d^dx\, e^{ipx}\,\langle 0|-\overbrace{\overline{h}_{i\alpha}(0)\gamma^5_{\alpha\beta}q_{i\beta}(0)\overline{q}_{j\gamma}(x)\gamma^5_{\gamma\delta}}h_{j\delta}(x)|0\rangle \\ &= \int d^dx\, e^{ipx}\left[\gamma^5 S^h_{ij}(x)\gamma^5\right]_{\gamma\beta}\langle 0|\overline{q}_{j\gamma}(x)q_{i\beta}(0)|0\rangle\end{aligned} \tag{2.6.23}$$

We can now use Eq.(2.6.8) to expand the field $\overline{q}_{j\gamma}(x)$ about x. Taking the leading term only, we find the quark condensate:

$$\begin{aligned}\langle 0|\overline{q}_{j\gamma}(x)q_{i\beta}(0)|0\rangle &= \langle 0|\overline{q}_{j\gamma}(0)q_{i\beta}(0)|0\rangle + ... \\ &= \frac{1}{4N_c}\langle\overline{q}q\rangle ...\end{aligned} \tag{2.6.24}$$

where on the second line we have used $\langle 0|\overline{q}_{j\gamma}(0)q_{i\beta}(0)|0\rangle = A\delta_{ji}\delta_{\gamma\beta}$ and taken traces over the colour and spinor indices to solve for A. Higher order terms in Eq.(2.6.24) can also be manipulated into the form of condensates by using equations of motion [81, 123]. After a few pages of algebra, we find to dimension-5 [123]:

$$\begin{aligned}\langle 0|\overline{q}_{j\gamma}(x)\,q_{i\beta}(0)|0\rangle = \frac{\delta_{ji}}{4N_c}\Bigg[&\left(\delta_{\gamma\beta}\left(1-\frac{m^2x^2}{8}\right)+\frac{i}{4}m\not{x}_{\beta\gamma}\right)\langle\overline{q}q\rangle \\ &+\delta_{\gamma\beta}\frac{x^2}{16}\langle\overline{q}g\sigma Gq\rangle\Bigg]\end{aligned} \tag{2.6.25}$$

where the mixed quark-gluon condensate $\langle\overline{q}g\sigma Gq\rangle \equiv \langle 0|\overline{q}_{i\alpha}\; g\sigma^{\mu\nu}_{\alpha\beta}t^a_{ij}G^a_{\mu\nu}\; q_{j\beta}|0\rangle$ appears after the insertion of 2 covariant derivates from Eq.(2.6.8) and we use the convention $\sigma^{\mu\nu} \equiv \frac{i}{2}\left[\gamma^\mu,\gamma^\nu\right]$. Substituting Eq.(2.6.25) back into Eq.(2.6.23) gives us,

$$\begin{aligned}\Pi^q(\omega) = \int d^dx\frac{d^dk}{(2\pi)^d}\frac{e^{i(p-k)x}}{4N_c}\Bigg\{&\mathrm{Tr}\left[\gamma^5 S^h_{ii}(k)\gamma^5\right]\left[\left(1-\frac{m^2x^2}{8}\right)\langle\overline{q}q\rangle+\frac{x^2}{16}\langle\overline{q}g\sigma Gq\rangle\right] \\ &+\mathrm{Tr}\left[\gamma^5 S^h_{ii}(k)\gamma^5\not{x}\right]\left[\frac{i}{4}m\langle\overline{q}q\rangle\right]\Bigg\}\end{aligned} \tag{2.6.26}$$

where we have switched to a momentum representation of the heavy quark propagators. Evaluating the traces, using the HQET Feynman rule for $S^h(k)$ from Eq.(2.5.10)

gives us,

$$\mathrm{Tr}\left[\gamma^5 S^h_{ii}(k)\gamma^5\right] = \frac{4N_c}{2(k\cdot v)} \qquad \mathrm{Tr}\left[\gamma^5 S^h_{ii}(k)\gamma^5 \not{x}\right] = \frac{-4N_c(v\cdot x)}{2(k\cdot v)} \tag{2.6.27}$$

In order to carry out the integration over x we make use of the relation,

$$\int \frac{d^d x}{(2\pi)^d}\left(x_{\mu_1}x_{\mu_2}...x_{\mu_n}\right)e^{i(p-k)x} = (i)^n \frac{\partial}{\partial k_{\mu_1}\partial k_{\mu_2}...\partial k_{\mu_n}}\delta^{(d)}(p-k), \tag{2.6.28}$$

which allows us to express Eq.(2.6.26) as,

$$\begin{aligned}\Pi^q(\omega) = \int d^d k\, \frac{1}{2(k\cdot v)}\Bigg[\Bigg(1 + \frac{m}{4}v^\mu\frac{\partial}{\partial k_\mu} + \frac{m^2}{8}\frac{\partial}{\partial k_\mu \partial k^\mu}\Bigg)\langle\bar{q}q\rangle \\ -\frac{1}{16}\frac{\partial}{\partial k_\mu \partial k^\mu}\langle\bar{q}g\sigma Gq\rangle\Bigg]\delta^{(d)}(p-k),\end{aligned} \tag{2.6.29}$$

for which the partial derivatives act on the delta function on the far right of the expression. We can then use integration by parts,

$$\int d^d k\, f(k)\frac{\partial}{\partial k_{\mu_1}\partial k_{\mu_2}...\partial k_{\mu_n}}\delta^{(d)}(p-k) = (-1)^n \left.\frac{\partial f(k)}{\partial k_{\mu_1}\partial k_{\mu_2}...\partial k_{\mu_n}}\right|_{k=p} \tag{2.6.30}$$

to instead apply the derivatives to the heavy quark propagator, leaving us with the final step of simply integrating over the delta function. As a result, we are left with,

$$\Pi^q(\omega) = \frac{\langle\bar{q}q\rangle}{2\omega}\left(1 + \frac{m}{4\omega} + \frac{m^2}{4\omega^2} + ...\right) - \frac{\langle\bar{q}g\sigma Gq\rangle}{16\omega^3}(1 + ...) \tag{2.6.31}$$

where we have substituted in the residual energy $\omega = p\cdot v$ and the ellipsis' denote the higher dimension contributions that we have neglected. In the massless light quark limit $m \to 0$, the expression in Eq.(2.6.31) matches the leading order result found by [94] up to dimension-5.

Next we wish to find the coefficient of the gluon condensate $\langle GG\rangle$ for $\Pi(\omega)$. In the Fock-Schwinger gauge, we do not have interactions between the static quark and the background gluons. Therefore the only contribution comes from a double insertion of the gluon field to the light quark propagator. Before factorising out this term

from the correlator we first wick contract both heavy fields and both light quarks,

$$\begin{aligned}\Pi(\omega) &= i\int d^dx\, e^{ipx}\,\langle 0| -\overline{h_{i\alpha}(0)\gamma^5_{\alpha\beta}q_{i\beta}(0)\bar{q}_{j\gamma}(x)\gamma^5_{\gamma\delta}h_{j\delta}(x)}|0\rangle \\ &= i\int d^dx\, e^{ipx}\,\langle 0|\gamma^5_{\alpha\beta}\overline{q_{i\beta}(0)\bar{q}_{j\gamma}(x)}\gamma^5_{\gamma\delta}\overline{h_{j\delta}(x)\bar{h}_{i\alpha}(0)}|0\rangle \\ &= -i\int d^dx\, e^{ipx}\mathrm{Tr}\left[\gamma^5 S_{ij}(0,x)\gamma^5 S^h_{ji}(x)\right].\end{aligned} \tag{2.6.32}$$

At this point, we are presented with $S(0,x)$ and if we wish to switch to a momentum space description we should remind ourselves that since we have lost translation invariance by using the FS gauge, that $\tilde{S}(p) \neq S(p)$. In their expanded forms however, the differences between the two arise when we consider terms higher than leading order in our expression for the 4-potential in Eq.(2.6.7), which come with covariant derivatives. We do not consider these contributions here and a check of the calculation for the fourier transform of $S^{(2)}(0,x)$ reveals $\tilde{S}^{(2)}(p) = S^{(2)}(p)$. Isolating the second order correction $S^{(2)}(p)$ and using the result from Eq.(2.6.22) we find,

$$\begin{aligned}\Pi^{gg}(\omega) &= -i\int \frac{d^dk}{(2\pi)^d}\frac{\mathrm{Tr}\left[\gamma^5 S^{(2)}_{ij}(k)\gamma^5(1+\not{v})\delta_{ij}\right]}{2(k\cdot v+\omega)} \\ &= -i\int \frac{d^dk}{(2\pi)^d}\frac{g^2\langle GG\rangle\, m}{d}\frac{\mathrm{Tr}\left[(k^2+m\not{k})(1-\not{v})\right]}{2(k\cdot v+\omega)(k^2-m^2)^4} \\ &= -i\int \frac{d^dk}{(2\pi)^d}\frac{g^2\langle GG\rangle\,(m+...)}{d\,2(k\cdot v+\omega)(k^2)^3}\end{aligned} \tag{2.6.33}$$

where we have kept only the leading term in the light quark mass m. The integral is then easily solvable using,

$$\int \frac{d^dk}{(2\pi)^d}\frac{1}{2(k\cdot v+\omega)(k^2)^a} = \frac{i}{(4\pi)^{d/2}}\frac{\Gamma(2-a-\epsilon)\Gamma(2a+2\epsilon-3)}{\Gamma(a)}(-2\omega)^{3-2a-2\epsilon} \tag{2.6.34}$$

and we reach our expression for the $\langle GG\rangle$ condensate,

$$\Pi^{gg}(\omega) = \frac{\langle\frac{\alpha}{\pi}GG\rangle}{8d(4\pi)^{-\epsilon}}\Gamma(-1-\epsilon)\Gamma(3+2\epsilon)(-2\omega)^{-3-2\epsilon}(m+...). \tag{2.6.35}$$

Note that this whole contribution vanishes in the massless light quark limit.

Chapter 3

Mixing Bag Parameter

3.1 Introduction

In Section 2.3 we discussed the theory behind the mixing of B_s mesons. Experimentally, this phenomena is well studied [76] and the mass difference $\Delta M_s = 2|M_{12}^s|$ is known to a high precision, with the current world average by HFLAV [127] (based on the individual measurements [128–133]) placing the experimental value at,

$$\Delta M_s^{\text{Exp.}} = (17.741 \pm 0.020)\,\text{ps}^{-1}\,. \tag{3.1.1}$$

Note that this average does not yet include the most recent measurement by LHCb [134] where a substantial reduction in their uncertainties was achieved.

As already mentioned, the hadronic contribution to B-mixing comes in the form of the bag parameter $B \equiv \overline{B}^s_{Q_1}$ and the decay constant f_{B_s} and the uncertainties of their numerical values make up the largest contribution by far to the uncertainty of the mass difference in the SM prediction. These parameters have been determined by lattice simulations [135–137][2] and for the case of B_d mesons with HQET sum rules [54, 55, 139, 140]. There is also a recent lattice determination of the SU(3) breaking ratios [141].

[2]Work is currently ongoing to extract the B_s and B_d mixing bag parameters by JLQCD and RBC/UKQCD [138].

In this chapter we extend the analysis of [55] with the inclusion of $SU(3)$ breaking effects corresponding to a non-vanishing strange-quark mass, thus getting for the first time a HQET sum rule prediction for the mixing Bag parameter of B_s mesons. Lattice simulations typically achieve a much higher precision than sum rule calculations, but in our case a sum rule for $B-1$ is formed. Since the value of the Bag parameter B is close to 1, even a moderate precision of the sum rule of the order of 20 % for $B-1$, translates into a precision of the order of 2% for the Bag parameter as a whole, which is highly competitive. The determination we present here therefore stands as an independent cross-check of the findings from the lattice. Additionally, we find that by taking a ratio of ΔM_s and the rare branching ratio $Br(B_s \to \mu^+\mu^-)$ the decay constant and the CKM dependence cancel and the Bag parameter will be the only relevant input parameter.

The rest of this chapter is arranged as follows: in Section 3.2 we set up the sum rule for the Bag parameter and determine the m_s corrections, in Section 3.3 we present a numerical analysis of the Bag parameters and study some of the phenomenological implications. Finally, in Section 3.4 we summarise our findings and make some concluding remarks.

3.2 Sum rules in HQET

3.2.1 Operator basis and definition of bag parameters

In this chapter we use the full dimension-six $\Delta B = 2$ operator basis required for a calculation of ΔM_s in the SM[1] and BSM theories and for a SM prediction of $\Delta\Gamma_s$. The QCD operators involved are

$$
\begin{aligned}
Q_1 &= \bar{b}_i\gamma_\mu(1-\gamma^5)s_i\ \bar{b}_j\gamma^\mu(1-\gamma^5)s_j, \\
Q_2 &= \bar{b}_i(1-\gamma^5)s_i\ \bar{b}_j(1-\gamma^5)s_j, \qquad Q_3 = \bar{b}_i(1-\gamma^5)s_j\ \bar{b}_j(1-\gamma^5)s_i, \\
Q_4 &= \bar{b}_i(1-\gamma^5)s_i\ \bar{b}_j(1+\gamma^5)s_j, \qquad Q_5 = \bar{b}_i(1-\gamma^5)s_j\ \bar{b}_j(1+\gamma^5)s_i. \quad (3.2.1)
\end{aligned}
$$

[1] The operator Q_1 corresponds to the SM contribution to ΔM_s.

while our HQET basis is defined as

$$\begin{aligned}
\tilde{Q}_1 &= \bar{h}_i^{\{(+)}\gamma_\mu(1-\gamma^5)s_i\ \bar{h}_j^{(-)\}}\gamma^\mu(1-\gamma^5)s_j, \quad & \tilde{Q}_2 &= \bar{h}_i^{\{(+)}(1-\gamma^5)s_i\ \bar{h}_j^{(-)\}}(1-\gamma^5)s_j, \\
\tilde{Q}_4 &= \bar{h}_i^{\{(+)}(1-\gamma^5)s_i\ \bar{h}_j^{(-)\}}(1+\gamma^5)s_j, & \tilde{Q}_5 &= \bar{h}_i^{\{(+)}(1-\gamma^5)s_j\ \bar{h}_j^{(-)\}}(1+\gamma^5)s_i,
\end{aligned} \tag{3.2.2}$$

where $h^{(+/-)}(x)$ is the HQET bottom/anti-bottom field[1] and we use the notation

$$\bar{h}^{\{(+)}\Gamma_A s\ \bar{h}^{(-)\}}\Gamma_B s = \bar{h}^{(+)}\Gamma_A s\ \bar{h}^{(-)}\Gamma_B s + \bar{h}^{(-)}\Gamma_A s\ \bar{h}^{(+)}\Gamma_B s. \tag{3.2.3}$$

The matching condition is given by

$$\langle Q_i\rangle(\mu) = \sum C_{Q_i\tilde{Q}_j}\langle\tilde{Q}_j\rangle + \mathcal{O}(1/m_b), \tag{3.2.4}$$

for which the NLO HQET-QCD matching coefficients $C_{Q\tilde{Q}}$ were presented in [55]. We also use the same basis of evanescent operators. As mentioned in [55], the HQET evanescent operators are defined up to 3 constants a_i with $i = 1, 2, 3$ in order to gauge the scheme dependence. In the following we always work within the NDR scheme and in dimensional regularisation with $d = 4 - 2\epsilon$ dimensions.
The QCD bag parameters B_Q^s are defined through [142]

$$\langle Q(\mu)\rangle = A_Q\, f_{B_s}^2 M_{B_s}^2\, B_Q^s(\mu) = \overline{A}_Q(\mu)\, f_{B_s}^2 M_{B_s}^2\, \overline{B}_Q^s(\mu), \tag{3.2.5}$$

with the coefficients A_Q given by

$$\begin{aligned}
A_{Q_1} &= 2 + \tfrac{2}{N_c}, \\
A_{Q_2} &= \tfrac{M_{B_s}^2}{(m_b+m_s)^2}\left(-2+\tfrac{1}{N_c}\right),\ A_{Q_3} = \tfrac{M_{B_s}^2}{(m_b+m_s)^2}\left(1-\tfrac{2}{N_c}\right), \\
A_{Q_4} &= \tfrac{2M_{B_s}^2}{(m_b+m_s)^2} + \tfrac{1}{N_c}, \qquad A_{Q_5} = 1 + \tfrac{2M_{B_s}^2}{N_c(m_b+m_s)^2},
\end{aligned} \tag{3.2.6}$$

where M_{B_s} denotes the B_s meson mass, m_q corresponds to quark pole masses and the B_s meson decay constant f_{B_s} is defined by

$$\langle 0|\bar{b}\gamma^\mu\gamma^5 s|B_s(p)\rangle = -if_{B_s}p^\mu. \tag{3.2.7}$$

[1] The definition of the anti-bottom field in the HQET limit can be derived from Eq.(2.2.4) by changing $v \to -v$

The barred terms in the far right expression of (3.2.5) indicate that the quark masses used there are in the $\overline{\rm MS}$ scheme. We use the pole masses for our analysis and convert to this form at the end. Similarly, the HQET bag parameters are defined through

$$\langle\!\langle \tilde{Q}(\mu) \rangle\!\rangle = A_{\tilde{Q}}\, F_s^2(\mu)\, B_{\tilde{Q}}^s(\mu), \tag{3.2.8}$$

with the coefficients $A_{\tilde{Q}}$ given by

$$A_{\tilde{Q}_1} = 2 + \frac{2}{N_c}, \quad A_{\tilde{Q}_2} = -2 + \frac{1}{N_c}, \quad A_{\tilde{Q}_4} = 2 + \frac{1}{N_c}, \quad A_{\tilde{Q}_5} = 1 + \frac{2}{N_c}, \tag{3.2.9}$$

and where the matrix elements are taken between non-relativistically normalised states $\langle\!\langle \tilde{Q}(\mu) \rangle\!\rangle \equiv \langle \overline{\mathbf{B}}_s | \tilde{Q}(\mu) | \mathbf{B}_s \rangle$ with

$$|B_s(p)\rangle = \sqrt{2M_{B_s}} |\mathbf{B}_s(v)\rangle + \mathcal{O}(1/m_b). \tag{3.2.10}$$

The HQET decay constant $F_s(\mu)$ follows from the definition in Eq.(2.4.5) and is defined by,

$$\langle 0 | \bar{h}^{(-)} \gamma^\mu \gamma^5 s | \mathbf{B}_s(v) \rangle = -i F_s(\mu) v^\mu, \tag{3.2.11}$$

which can then be related to the full QCD decay constant f_{B_s} via

$$f_{B_s} = \sqrt{\frac{2}{M_{B_s}}} C(\mu) F_s(\mu) + \mathcal{O}\left(1/m_b\right), \tag{3.2.12}$$

where $C(\mu)$ is found to be [143],

$$C(\mu) = 1 - 2C_F \frac{\alpha_s(\mu)}{4\pi} + \mathcal{O}(\alpha_s^2). \tag{3.2.13}$$

From our sum rule analysis we determine the HQET bag parameters $B_{\tilde{Q}}^s$. After using Eq.(3.2.4), Eq.(3.2.5), Eq.(3.2.8), and Eq.(3.2.12) we construct relation,

$$B_{Q_i}^s(\mu) = \sum_j \frac{A_{\tilde{Q}_j}}{A_{Q_i}} \frac{C_{Q_i \tilde{Q}_j}(\mu)}{C^2(\mu)} B_{\tilde{Q}_j}^s(\mu) + \mathcal{O}(1/m_b), \tag{3.2.14}$$

which allows us to then match the values of $B_{\tilde{Q}}^s$ onto their QCD counterparts.

3.2.2 Finite m_s effects in the HQET decay constant

In order to demonstrate our method for the treatment of finite m_s effects, we first consider the Borel sum rule for the HQET decay constant F_s (as discussed in Chapter 2 and presented in Eq.(2.4.14)). For the B_s system it takes the form,

$$F_s^2(\mu_\rho)e^{-\frac{\overline{\Lambda}+m_s}{t}} = \int_0^{\omega_c} d\omega\, e^{-\frac{\omega}{t}}\rho_\Pi(\omega)\,, \tag{3.2.15}$$

where ρ_Π is the discontinuity[1] of the two-point correlator

$$\Pi(\omega) = i\int d^dx e^{ipx}\,\langle 0|\mathrm{T}\left[\tilde{j}_+^\dagger(0)\tilde{j}_+(x)\right]|0\rangle\,, \tag{3.2.16}$$

with $\omega = p\cdot v$ and the interpolating current $\tilde{j}_+ = \bar{s}\gamma^5 h^{(+)}$. The leading perturbative part of the discontinuity is given by

$$\rho_\Pi^{\mathrm{pert}}(\omega) = \frac{N_c}{2\pi^2}\left[(\omega+m_s)\sqrt{\omega^2-m_s^2}\,\theta(\omega-m_s)+\mathcal{O}(\alpha_s)\right]. \tag{3.2.17}$$

For the remainder of this subsection we will consider the finite-energy (FESR) version of the sum rule in Eq.(3.2.15) which is constructed by taking the limit $t\to\infty$ and allows for concise analytic expressions. We obtain

$$\begin{aligned} F_s^2(\mu_\rho)|_{\mathrm{FESR}} &= \frac{N_c}{6\pi^2}\Bigg[\left(\omega_c-\frac{m_s}{2}\right)(\omega_c+2m_s)\sqrt{\omega_c^2-m_s^2} \\ &\quad +\frac{3m_s^3}{2}\ln\left(\frac{m_s}{\omega_c+\sqrt{\omega_c^2-m_s^2}}\right)+\mathcal{O}(\alpha_s)+[\text{condensates}]\Bigg] \\ &= \frac{N_c\omega_c^3}{6\pi^2}\left[1+\frac{3m_s}{2\omega_c}-\frac{3m_s^2}{2\omega_c^2}-\frac{3m_s^3}{4\omega_c^3}\left(1-\ln\frac{m_s^2}{4\omega_c^2}\right)+\ldots\right]. \end{aligned} \tag{3.2.18}$$

In the last step we have expanded the result in the small ratio $m_s/\omega_c\sim 0.1$. The appearance of a $m_s^3\ln(m_s)$ term in the expansion indicates that energies ω of the order m_s contribute at order m_s^3. These logarithms can be absorbed into the quark condensate [94, 144]. In the following we show how the terms up to order m_s^2 can be determined without knowing the full m_s dependence of the discontinuity

[1] This is equivalent to the imaginary part of the two-point correlator but we change notation here to be consistent with our discussion of the 3-point correlator where the double discontinuity is taken.

Eq.(3.2.17). This property is necessary for our determination of the m_s effects to the bag parameters. Without this being the case, the calculation with the inclusion of full m_s dependence involves very challenging Feynman integrals consisting of 3 loops and 3 scales. To begin with, we split the integration at an arbitrary scale ν with $m_s \ll \nu \ll \omega_c$. Above ν we are permitted to expand the integrand in m_s/ω, yielding the identity

$$\mathcal{T}_{\frac{m_s}{\omega_c}}[F_s^2(\mu_\rho)]e^{-\frac{\bar{\Lambda}+m_s}{t}} = \mathcal{T}_{\{\frac{m_s}{\omega_c},\frac{m_s}{\nu},\frac{\nu}{\omega_c}\}}\left[\int_{m_s}^{\nu} d\omega\, e^{-\frac{\omega}{t}}\rho_\Pi(\omega) + \int_{\nu}^{\omega_c} d\omega\, e^{-\frac{\omega}{t}}\mathcal{T}_{\frac{m_s}{\omega}}[\rho_\Pi(\omega)]\right], \tag{3.2.19}$$

where $\mathcal{T}_x[\dots]$ follows from the notation in Section 2.5.2 of the Chapter 2. The dependence on the scale ν has to cancel in the expanded result. We can therefore take the limit $\nu \to m_s$ *after* expanding the result according to the scaling $m_s \ll \nu \ll \omega_c$. We note that the contribution from the integration of the full integrand between m_s and ν does not vanish for $\nu \to m_s$, because the limit has to be taken after the expansion in m_s and the two operations do not commute. It is however clear from dimensional analysis that this contribution must be polynomial in m_s starting at m_s^3 since the exponential can be Taylor expanded. This demonstrates that it is sufficient to compute the discontinuity in Eq.(3.2.17) as an expansion in m_s/ω if we restrict the analysis to the linear and quadratic terms which is clearly sufficient due to the small expansion parameter. In the FESR limit considered above we find[1]

$$\mathcal{T}_{\frac{m_s}{\omega_c}}\left[\int_{m_s}^{\omega_c} d\omega\, \mathcal{T}_{\frac{m_s}{\omega}}[\rho_\Pi(\omega)]\right] = \frac{N_c\omega_c^3}{6\pi^2}\left[1+\frac{3m_s}{2\omega_c}-\frac{3m_s^2}{2\omega_c^2}-\frac{m_s^3}{\omega_c^3}\left(1-\frac{3}{4}\ln\frac{m_s^2}{\omega_c^2}\right)+\dots\right]. \tag{3.2.20}$$

The difference between Eq.(3.2.18) and Eq.(3.2.20) is indeed of order m_s^3 and is compensated by the contribution from the first term on the right-hand side of Eq.(3.2.19).

At NLO we therefore only compute the expanded result by using the method of regions(see our discussion in Section 2.5.2 of Chapter 2). The light degrees of freedom

[1] Here the limit $\nu \to m_s$ and the Taylor expansion commute, because the integrand is polynomial in m_s.

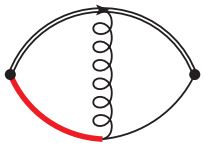

Figure 3.1: Sample diagram involving a soft light-quark propagator (red thick line).

can be either hard with momentum $k \sim \omega$ or soft with momentum $k \sim m_s$ whereas the heavy quark field is always hard. Up to and including the order m_s^2 there are however only contributions from diagrams where all lines are hard. An example diagram involving a soft line is shown in Figure 3.1. The integral measure scales as m_s^4 and the soft light-quark propagator scales as m_s^{-1}, yielding an overall scaling of m_s^3. Diagrams where only the gluon is soft are scaleless and vanish in dimensional regularization. Contributions where both loop momenta are soft are of the order m_s^4. Therefore, we only need to consider the fully hard momentum region where the integrand can be naively Taylor expanded in m_s. We obtain

$$\begin{aligned}\rho_\Pi(\omega) &\equiv \frac{\Pi(\omega+i0)-\Pi(\omega-i0)}{2\pi i} \\ &= \frac{N_c\omega^2}{2\pi^2}\,\theta(\omega-m_s)\Bigg\{1+\frac{m_s}{\omega}-\frac{1}{2}\left(\frac{m_s}{\omega}\right)^2+\dots \\ &\quad+\frac{\alpha_s C_F}{4\pi}\left[17+\frac{4\pi^2}{3}+3\ln\frac{\mu_\rho^2}{4\omega^2}+\left(20+\frac{4\pi^2}{3}+6\ln\frac{\mu_\rho^2}{4\omega^2}-3\ln\frac{\mu_\rho^2}{m_s^2}\right)\frac{m_s}{\omega}\right. \\ &\quad\left.+\left(1-\frac{9}{2}\ln\frac{\mu_\rho^2}{4\omega^2}+3\ln\frac{\mu_\rho^2}{m_s^2}\right)\left(\frac{m_s}{\omega}\right)^2+\dots\right]+\mathcal{O}(\alpha_s^2)\Bigg\}+[\text{condensates}],\end{aligned} \tag{3.2.21}$$

in agreement with [94].

3.2.3 Finite m_s effects in the Bag parameters

Whereas the central object for the decay constant sum rule was the two-point correlator, for the Bag parameters our sum rule is based on the three-point correlator defined by,

$$K_{\tilde{Q}}(\omega_1,\omega_2)=\int d^dx_1 d^dx_2 e^{ip_1\cdot x_1-ip_2\cdot x_2}\,\langle 0|\mathrm{T}\left[\tilde{j}_+(x_2)\tilde{Q}(0)\tilde{j}_-(x_1)\right]|0\rangle\,, \tag{3.2.22}$$

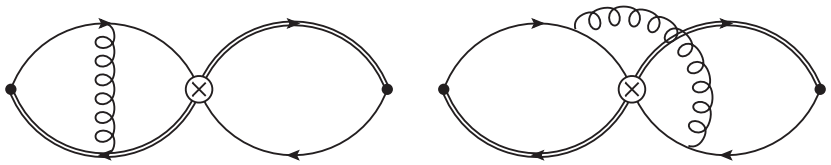

Figure 3.2: Examples for factorizing (left) and non-factorizing (right) contributions to the three-point correlator Eq.(3.2.22) at NLO in α_s.

where $\omega_{1,2} = p_{1,2} \cdot v$ and the interpolating currents for the $\overline{B}_s$ and B_s mesons read

$$\tilde{j}_+ = \bar{s}\gamma^5 h^{(+)}, \qquad \tilde{j}_- = \bar{s}\gamma^5 h^{(-)}. \tag{3.2.23}$$

The accuracy of the sum rule approach crucially depends on the observation that the contributions to the correlator can be split into factorizable and non-factorizable ones, examples of which are given in Figure 3.2. Factorizable diagrams consist of the LO contributions and α_s corrections for which the gluon exchange is confined either to the left or right loop separately. In these cases, the correlator factorises into two 2-point functions. The remaining diagrams do not exhibit this behaviour and are therefore classed as non-factorizable contributions which consist of gluon exchange between the left and right loops. The full set of factorizable contributions amounts to $B^s_{\tilde{Q}} = 1$ which allows us to formulate a sum rule for the deviation $\Delta B^s_{\tilde{Q}} = B^s_{\tilde{Q}} - 1$ based only on the non-factorizable contributions [54, 55, 145, 146]

$$\Delta B^s_{\tilde{Q}_i}(\mu_\rho) = \frac{1}{A_{\tilde{Q}_i} F_s(\mu_\rho)^4} \int_0^{\omega_c} d\omega_1 d\omega_2 e^{\frac{\overline{\Lambda}+m_s-\omega_1}{t_1}+\frac{\overline{\Lambda}+m_s-\omega_2}{t_2}} \Delta\rho_{\tilde{Q}_i}(\omega_1,\omega_2) \tag{3.2.24}$$

$$= \frac{1}{A_{\tilde{Q}_i}} \frac{\int_0^{\omega_c} d\omega_1 d\omega_2 e^{-\frac{\omega_1}{t_1}-\frac{\omega_2}{t_2}} \Delta\rho_{\tilde{Q}_i}(\omega_1,\omega_2)}{\left(\int_0^{\omega_c} d\omega_1 e^{-\frac{\omega_1}{t_1}} \rho_\Pi(\omega_1)\right)\left(\int_0^{\omega_c} d\omega_2 e^{-\frac{\omega_2}{t_2}} \rho_\Pi(\omega_2)\right)}. \tag{3.2.25}$$

where the second equation makes use of Eq.(3.2.15). The quantity $\Delta\rho_{\tilde{Q}_i}$ is the non-factorizable part of the double discontinuity

$$\rho_{\tilde{Q}_i}(\omega_1,\omega_2) = A_{\tilde{Q}_i}\rho_\Pi(\omega_1)\rho_\Pi(\omega_2) + \Delta\rho_{\tilde{Q}_i}\,. \tag{3.2.26}$$

In [55] a simple analytical result for the HQET bag parameters was derived by comparing Eq.(3.2.24) to the square of the sum rule for the decay constant Eq.(3.2.15) with an appropriately chosen weight function

$$w_{\tilde{Q}_i}(\omega_1,\omega_2)=\frac{\Delta\rho^{\rm pert}_{\tilde{Q}_i}(\omega_1,\omega_2)}{\rho^{\rm pert}_{\Pi}(\omega_1)\rho^{\rm pert}_{\Pi}(\omega_2)}\,. \tag{3.2.27}$$

The generalization of this approach to the m_s corrections is straightforward. Expanding the double discontinuity in m_s, we obtain

$$\begin{aligned}\Delta\rho^{\rm pert}_{\tilde{Q}_i}(\omega_1,\omega_2)\equiv\frac{N_cC_F}{4}\frac{\omega_1^2\omega_2^2}{\pi^4}\frac{\alpha_s}{4\pi}\Bigg[&r^{(0)}_{\tilde{Q}_i}(x,L_\omega)+\left(\frac{m_s}{\omega_1}+\frac{m_s}{\omega_2}\right)r^{(1)}_{\tilde{Q}_i}(x,L_\omega)\\&+\left(\frac{m_s^2}{\omega_1^2}+\frac{m_s^2}{\omega_2^2}\right)r^{(2)}_{\tilde{Q}_i}(x,L_\omega)+\ldots\Bigg]\theta(\omega_1-m_s)\theta(\omega_2-m_s),\end{aligned} \tag{3.2.28}$$

where $x=\omega_2/\omega_1$ and $L_\omega=\ln(\mu_\rho^2/(4\omega_1\omega_2))$. With this parametrization, the symmetry of the three-point correlator under exchange of ω_1 and ω_2 manifests as a symmetry under $x\leftrightarrow 1/x$ of the $r^{(j)}_{\tilde{Q}_i}$. The result for the deviation of the Bag parameters from the VSA reads

$$\begin{aligned}&\Delta B^{s,\rm pert}_{\tilde{Q}_i}(\mu_\rho)=\frac{w_{\tilde{Q}_i}(\overline{\Lambda}+m_s,\overline{\Lambda}+m_s)}{A_{\tilde{Q}_i}}=\\&\frac{C_F}{N_cA_{\tilde{Q}_i}}\frac{\alpha_s(\mu_\rho)}{4\pi}\Bigg\{r^{(0)}_{\tilde{Q}_i}\left(1,L_{\overline{\Lambda}+m_s}\right)+\frac{2m_s}{\overline{\Lambda}+m_s}\left[r^{(1)}_{\tilde{Q}_i}\left(1,L_{\overline{\Lambda}+m_s}\right)-r^{(0)}_{\tilde{Q}_i}\left(1,L_{\overline{\Lambda}+m_s}\right)\right]\\&+\frac{2m_s^2}{(\overline{\Lambda}+m_s)^2}\left[r^{(2)}_{\tilde{Q}_i}\left(1,L_{\overline{\Lambda}+m_s}\right)-2r^{(1)}_{\tilde{Q}_i}\left(1,L_{\overline{\Lambda}+m_s}\right)+2r^{(0)}_{\tilde{Q}_i}\left(1,L_{\overline{\Lambda}+m_s}\right)\right]+\ldots\Bigg\},\end{aligned} \tag{3.2.29}$$

where $L_{\overline{\Lambda}+m_s}=\ln(\mu_\rho^2/(4(\overline{\Lambda}+m_s)^2))$. We find that the result only depends on the value of the double discontinuity at $\omega_1=\omega_2=\overline{\Lambda}+m_s$. Thus, the knowledge of the m_s-expanded double discontinuity is sufficient to determine the m_s effects for the Bag parameters in B_s mixing. However, the use of this weight function approach relies on the expanded version of the sum rule Eq.(3.2.15) for the decay constant. As discussed in the previous subsection, this approach gives an incorrect result at the order m_s^3 and the result Eq.(3.2.29) is therefore limited to the quadratic order in m_s.

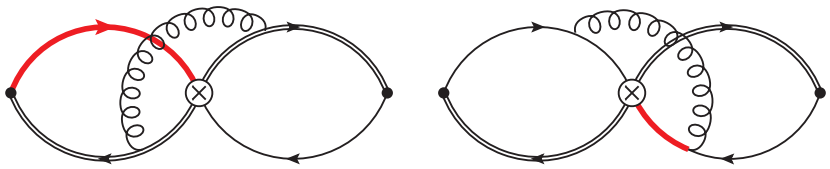

Figure 3.3: Examples for soft corrections to the non-factorizable part of the three-point correlator Eq.(3.2.22). The red, thick light-quark line carries momentum of the order of $m_s \ll \omega \sim \overline{\Lambda}$.

3.2.4 Non-zero m_s corrections to the non-factorizable part

We compute the m_s-expanded result for the leading non-factorizable part of the three-point correlators using the expansion by regions [113, 114]. As in the case of the two-point correlator, contributions involving soft propagators like the ones shown in Figure 3.3 first contribute at order m_s^3. Therefore, only the fully hard momentum region for which all loop momenta admit the scaling $l \sim \omega_i \gg m_s$ are considered in our calculation. This corresponds to a naive Taylor expansion in m_s of the loop integrands. The amplitudes were generated manually and also using `QGRAF` [147] with further processing in `Mathematica`. Manipulation of the Dirac algebra was done with `TRACER` [148]. The scalar loop integrals were reduced to a set of master integrals through IBP relations generated by `FIRE` [105] using the Laporta algorithm [102]. The analytical form of these master integrals have been computed to all orders in ϵ in [149]. Using `HypExp` [150], they were then expanded in ϵ up to the necessary order. For completeness we state the results $r^{(0)}_{\tilde{Q}_i} = r^{(0)}_{\tilde{Q}_i}(x, L_\omega)$ for $m_s = 0$ previously presented in [55]

$$
\begin{aligned}
r^{(0)}_{\tilde{Q}_1} &= 8 - \frac{a_2}{2} - \frac{8\pi^2}{3}, \\
r^{(0)}_{\tilde{Q}_2} &= 25 + \frac{a_1}{2} - \frac{4\pi^2}{3} + 6L_\omega + \phi(x), \\
r^{(0)}_{\tilde{Q}_4} &= 16 - \frac{a_3}{4} - \frac{4\pi^2}{3} + 3L_\omega + \frac{\phi(x)}{2}, \\
r^{(0)}_{\tilde{Q}_5} &= 29 - \frac{a_3}{2} - \frac{8\pi^2}{3} + 6L_\omega + \phi(x),
\end{aligned}
\tag{3.2.30}
$$

with

$$\phi(x) = \begin{cases} x^2 - 8x + 6\ln(x), & x \le 1, \\ \frac{1}{x^2} - \frac{8}{x} - 6\ln(x), & x > 1. \end{cases} \tag{3.2.31}$$

For the linear terms $r^{(1)}_{\tilde{Q}_i} = r^{(1)}_{\tilde{Q}_i}(x, L_\omega)$ we obtain

$$\begin{aligned}
r^{(1)}_{\tilde{Q}_1} &= -\frac{a_2}{2} - \frac{8\pi^2}{3} - 2\psi(x) + \begin{cases} \frac{2(18-63x+23x^2)}{9(1+x)} + \left(2 - \frac{2(3+x^3)}{3x(1+x)}\right)\ln(x), & x \le 1, \\ \frac{2(23-63x+18x^2)}{9x(1+x)} - \left(2 - \frac{2(1+3x^3)}{3x(1+x)}\right)\ln(x), & x > 1, \end{cases} \\
r^{(1)}_{\tilde{Q}_2} &= \frac{a_1}{2} - \frac{4\pi^2}{3} + 6L_\omega + \psi(x) + \begin{cases} \frac{243+162x-41x^2}{9(1+x)} + \left(5 + \frac{3+x^3}{3x(1+x)}\right)\ln(x), & x \le 1, \\ \frac{243x^2+162x-41}{9x(1+x)} - \left(5 + \frac{1+3x^3}{3x(1+x)}\right)\ln(x), & x > 1, \end{cases} \\
r^{(1)}_{\tilde{Q}_4} &= -\frac{a_3}{4} - \frac{4\pi^2}{3} + 3L_\omega + \begin{cases} \frac{4(36+9x+x^2)}{9(1+x)} + \left(3 - \frac{2x^2}{3(1+x)}\right)\ln(x), & x \le 1, \\ \frac{4(1+9x+36x^2)}{9x(1+x)} - \left(3 - \frac{2}{3x(1+x)}\right)\ln(x), & x > 1, \end{cases} \\
r^{(1)}_{\tilde{Q}_5} &= -\frac{a_3}{2} - \frac{8\pi^2}{3} + 6L_\omega + \begin{cases} \frac{29+11x-2x^2}{1+x} + 6\ln(x), & x \le 1, \\ \frac{29x^2+11x-2}{x(1+x)} - 6\ln(x), & x > 1, \end{cases}
\end{aligned} \tag{3.2.32}$$

with

$$\psi(x) = \begin{cases} \frac{(1-x)^2}{x}\left[2\ln(1-x) - \ln(x)\right], & x \le 1, \\ \frac{(1-x)^2}{x}\left[2\ln(x-1) - \ln(x)\right], & x > 1. \end{cases} \tag{3.2.33}$$

Last but not least, our results for the quadratic terms $r^{(2)}_{\tilde{Q}_i} = r^{(2)}_{\tilde{Q}_i}(x, L_\omega)$ are

$$\begin{aligned}
r^{(2)}_{\tilde{Q}_1} &= \frac{1}{1+x^2}\left[\frac{(1-x)^2 a_2}{4} + \frac{2\pi^2(1-4x+x^2)}{3} + 2x\psi(x)\left(2 + \frac{1+x}{1-x}\ln(x)\right)\right. \\
&\quad \left. + \begin{cases} -\frac{2(6+6x-x^2+2x^3)}{3} + 2(2-4x+x^2)\ln(x) - 4(1-x^2)\mathrm{Li}_2(1-1/x), & x \le 1, \\ -\frac{2(2-x+6x^2+6x^3)}{3x} - 2(1-4x+2x^2)\ln(x) + 4(1-x^2)\mathrm{Li}_2(1-x), & x > 1, \end{cases}\right], \\
r^{(2)}_{\tilde{Q}_2} &= \frac{1}{1+x^2}\left[\frac{-(1-x)^2 a_1}{4} - 3(1-x)^2 L_\omega + \frac{\pi^2(1-4x+x^2)}{3} + \frac{x(1+x)}{1-x}\ln(x)\psi(x)\right. \\
&\quad \left. + \begin{cases} -\frac{75-198x+89x^2-4x^3}{6} - (3-6x+2x^2)\ln(x) - 2(1-x^2)\mathrm{Li}_2(1-1/x), & x \le 1, \\ +\frac{4-89x+198x^2-75x^3}{6x} + (2-6x+3x^2)\ln(x) + 2(1-x^2)\mathrm{Li}_2(1-x), & x > 1, \end{cases}\right],
\end{aligned}$$

$$
\begin{aligned}
r^{(2)}_{\tilde{Q}_4} &= \frac{1}{1+x^2}\left[\frac{(1-x)^2 a_3}{8} - \frac{3(1-x)^2}{2}L_\omega + \frac{x\psi(x)}{2}\left(1+\frac{3(1+x)}{1-x}\ln(x)\right)\right.\\
&\quad \left. + \begin{cases} -(1+8x-5x^2)\frac{\pi^2}{6} - \frac{24-48x+16x^2+x^3}{3} - (1+x^2)\ln(x) & \\ -(1-x^2)\ln^2(x) - 5(1-x^2)\mathrm{Li}_2(1-1/x), & x\le 1, \\ +(5-8x-x^2)\frac{\pi^2}{6} - \frac{1+16x-48x^2+24x^3}{3x} + (1+x^2)\ln(x) & \\ +(1-x^2)\ln^2(x) + 5(1-x^2)\mathrm{Li}_2(1-x), & x>1, \end{cases}\right],\\
r^{(2)}_{\tilde{Q}_5} &= \frac{1}{1+x^2}\left[\frac{(1-x)^2 a_3}{4} - 3(1-x)^2 L_\omega + \frac{2\pi^2(1-4x+x^2)}{3}\right.\\
&\quad +2x\psi(x)\left(1+\frac{1+x}{1-x}\ln(x)\right) - \frac{29-62x+29x^2}{2}\\
&\quad \left. + \begin{cases} -(1-x)^2\ln(x) - 4(1-x^2)\mathrm{Li}_2(1-1/x), & x\le 1, \\ +(1-x)^2\ln(x) + 4(1-x^2)\mathrm{Li}_2(1-x), & x>1, \end{cases}\right].
\end{aligned}
\tag{3.2.34}
$$

3.3 Results and phenomenology

Here we present a numerical analysis using the analytic results derived in the previous section. To begin with we give a determination of the Bag parameters in Section 3.3.1. We subsequently discuss the impact of these results for B_s mixing observables in Section 3.3.2. We use the results of our mixing studies to extract a value for the top-quark $\overline{\mathrm{MS}}$ mass in Section 3.3.3. Finally, we then present an alternative prediction of the branching ratios $\mathcal{B}(B_q \to l^+l^-)$ derived from the ratios $\mathcal{B}(B_q \to l^+l^-)/\Delta M_q$ in Section 3.3.4.

3.3.1 Bag parameters

We determine the HQET Bag parameters at the scale $\mu_\rho = 1.5$ GeV using the weight function approach Eq.(3.2.29). The strange-quark mass scheme in Eq.(3.2.29) is undetermined since any scheme change would only affect the expressions at

higher orders which are not taken into account. We use the value in the $\overline{\text{MS}}$ scheme at the scale μ_ρ which is determined from the central value of the average $\overline{m}_s(2\,\text{GeV}) = (95^{+9}_{-3})\,\text{MeV}$ [151]. To account for the uncertainties related to the scheme choice and the truncation of the expansion in m_s we increase the parametric uncertainty and use $\overline{m}_s(2\,\text{GeV}) = (95 \pm 30)\,\text{MeV}$. To the perturbative part we add the condensate contributions [152, 153]. The lattice simulation [154] shows that light and strange quark condensates agree within uncertainties and their result for the strange-quark condensate has since been confirmed with a different method [155]. With the factorization hypothesis $\langle\bar{q}Gq\rangle = m_0^2\langle\bar{q}q\rangle$ the same holds for the quark-gluon condensate. We therefore assume the condensate corrections to be the same in the B^0 and B_s^0 systems. We obtain

$$\begin{aligned}
B^s_{\tilde{Q}_1}(1.5\text{ GeV}) &= (0.910 - 0.016_{m_s} + 0.003_{m_s^2})^{+0.025}_{-0.036} \\
&= 0.897^{+0.002}_{-0.002}(\overline{\Lambda})^{+0.020}_{-0.020}(\text{intr.})^{+0.005}_{-0.005}(\text{cond.})^{+0.014}_{-0.029}(\mu_\rho)^{+0.003}_{-0.003}(m_s), \\
B^s_{\tilde{Q}_2}(1.5\text{ GeV}) &= (0.939 - 0.006_{m_s} + 0.002_{m_s^2})^{+0.027}_{-0.031} \\
&= 0.936^{+0.014}_{-0.016}(\overline{\Lambda})^{+0.020}_{-0.020}(\text{intr.})^{+0.004}_{-0.004}(\text{cond.})^{+0.011}_{-0.016}(\mu_\rho)^{+0.004}_{-0.004}(m_s), \\
B^s_{\tilde{Q}_4}(1.5\text{ GeV}) &= (1.003 - 0.004_{m_s} + 0.001_{m_s^2})^{+0.023}_{-0.023} \\
&= 1.000^{+0.005}_{-0.004}(\overline{\Lambda})^{+0.020}_{-0.020}(\text{intr.})^{+0.010}_{-0.010}(\text{cond.})^{+0.000}_{-0.002}(\mu_\rho)^{+0.003}_{-0.002}(m_s), \\
B^s_{\tilde{Q}_5}(1.5\text{ GeV}) &= (0.988 - 0.008_{m_s} + 0.000_{m_s^2})^{+0.028}_{-0.027} \\
&= 0.980^{+0.015}_{-0.012}(\overline{\Lambda})^{+0.020}_{-0.020}(\text{intr.})^{+0.010}_{-0.010}(\text{cond.})^{+0.000}_{-0.007}(\mu_\rho)^{+0.007}_{-0.006}(m_s),
\end{aligned} \tag{3.3.1}$$

where we have indicated the orders in m_s with subscripts and find good convergence of the expansion. The differences in the leading terms with respect to the results for B_d mixing obtained in [55] arise because the logarithms $L_{\overline{\Lambda}}$ are replaced by $L_{\overline{\Lambda}+m_s}$ which we do not expand in $m_s/\overline{\Lambda}$.

The results Eq.(3.3.1) are then evolved to the matching scale $\mu_m = \overline{m}_b(\overline{m}_b)$ where they are converted to QCD Bag parameters B_Q^s using Eq.(3.2.14). We do not consider the effects of a non-zero strange-quark mass in the QCD-HQET matching. The

matching corrections are of the order $\alpha_s(\overline{m}_b(\overline{m}_b))/\pi \times \overline{m}_s(\overline{m}_b)/\overline{m}_b(\overline{m}_b) \sim 0.001$ and therefore subleading compared to the linear terms $\alpha_s(\mu_\rho)/\pi \times \overline{m}_s(\mu_\rho)/(\overline{\Lambda}+\overline{m}_s(\mu_\rho)) \sim 0.019$ and even the quadratic terms $\alpha_s(\mu_\rho)/\pi \times [\overline{m}_s(\mu_\rho)/(\overline{\Lambda}+\overline{m}_s(\mu_\rho))]^2 \sim 0.003$ in the sum rule. We do not include this uncertainty as a separate contribution in our error analysis since it is covered by the conservative variation of the input value for m_s. Lastly, we convert the QCD Bag parameters to the usual convention which we denoted as $\overline{B}^s_Q$ in Eq.(3.2.5). We find

$$\begin{aligned}
\overline{B}^s_{Q_1}(\overline{m}_b(\overline{m}_b)) &= 0.858^{+0.051}_{-0.052} = (0.870 - 0.015_{m_s} + 0.002_{m_s^2})^{+0.022}_{-0.033}(\mathrm{SR})^{+0.046}_{-0.040}(\mathrm{M}),\\
\overline{B}^s_{Q_2}(\overline{m}_b(\overline{m}_b)) &= 0.854^{+0.079}_{-0.072} = (0.857 - 0.005_{m_s} + 0.002_{m_s^2})^{+0.026}_{-0.030}(\mathrm{SR})^{+0.074}_{-0.066}(\mathrm{M}),\\
\overline{B}^s_{Q_3}(\overline{m}_b(\overline{m}_b)) &= 0.907^{+0.164}_{-0.155} = (0.880 + 0.027_{m_s} + 0.000_{m_s^2})^{+0.124}_{-0.125}(\mathrm{SR})^{+0.107}_{-0.091}(\mathrm{M}),\\
\overline{B}^s_{Q_4}(\overline{m}_b(\overline{m}_b)) &= 1.039^{+0.092}_{-0.083} = (1.043 - 0.004_{m_s} + 0.001_{m_s^2})^{+0.024}_{-0.024}(\mathrm{SR})^{+0.088}_{-0.080}(\mathrm{M}),\\
\overline{B}^s_{Q_5}(\overline{m}_b(\overline{m}_b)) &= 1.050^{+0.081}_{-0.074} = (1.058 - 0.007_{m_s} + 0.000_{m_s^2})^{+0.025}_{-0.025}(\mathrm{SR})^{+0.077}_{-0.069}(\mathrm{M}),
\end{aligned} \tag{3.3.2}$$

where we have included the uncertainty from variation of $\overline{m}_s$ in the sum rule (SR) error and M denotes the uncertainty from the QCD-HQET matching. We compare our results to other determinations from lattice simulations [135–137, 156] and sum rules [54] and the FLAG averages [157] in Figure 3.4 and find very good agreement overall with similar uncertainties. We observe that the FNAL/MILC'16 value for $\overline{B}_{Q_1}$ is larger than all the other results – with respect to our value the difference corresponds to 1.1 sigma. More recently HPQCD'19 completed an independent lattice determination with $(N_f = 2+1+1)$ which we find is in good agreement with our own. Our Bag parameters for $Q_{4,5}$ are consistent with both HPQCD'19 and FNAL/MILC'16, while there is a tension of more than two sigma with respect to the results of ETM'14. Similar tensions have been observed in the Kaon system [158] where it was conjectured that a difference in intermediate renormalization schemes might be responsible. We also consider the ratios $\overline{B}^{s/d}_{Q_1} \equiv \overline{B}^s_{Q_1}/\overline{B}^d_{Q_1}$ of the Bag

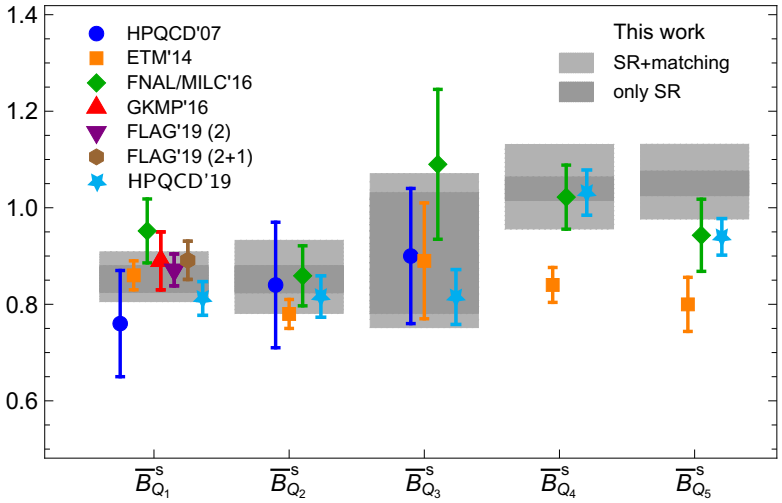

Figure 3.4: Comparison of Bag parameters relevant for B_s mixing. The dark gray regions indicate the ranges spanned only by the sum rule error whereas the light gray regions correspond to the total uncertainties. The sum rule value GKMP'16 corresponds to the result [54] for the B_d system with an uncertainty of ± 0.02 for the m_s effects added in quadrature as suggested by the authors in [139].

parameters in the B_s^0 and B_d^0 system where a large part of the uncertainties cancel

$$\begin{aligned}
\overline{B}^{s/d}_{Q_1}(\overline{m}_b(\overline{m}_b)) &= 0.987^{+0.007}_{-0.009} = (1.001 - 0.017_{m_s} + 0.003_{m_s^2})^{+0.007}_{-0.008}(\mathrm{SR})^{+0.002}_{-0.002}(\mathrm{M}),\\
\overline{B}^{s/d}_{Q_2}(\overline{m}_b(\overline{m}_b)) &= 1.013^{+0.010}_{-0.008} = (1.017 - 0.006_{m_s} + 0.002_{m_s^2})^{+0.009}_{-0.008}(\mathrm{SR})^{+0.002}_{-0.002}(\mathrm{M}),\\
\overline{B}^{s/d}_{Q_3}(\overline{m}_b(\overline{m}_b)) &= 1.108^{+0.068}_{-0.051} = (1.076 + 0.033_{m_s} - 0.001_{m_s^2})^{+0.068}_{-0.051}(\mathrm{SR})^{+0.007}_{-0.007}(\mathrm{M}),\\
\overline{B}^{s/d}_{Q_4}(\overline{m}_b(\overline{m}_b)) &= 0.991^{+0.007}_{-0.008} = (0.994 - 0.004_{m_s} + 0.001_{m_s^2})^{+0.006}_{-0.008}(\mathrm{SR})^{+0.002}_{-0.002}(\mathrm{M}),\\
\overline{B}^{s/d}_{Q_5}(\overline{m}_b(\overline{m}_b)) &= 0.979^{+0.010}_{-0.014} = (0.985 - 0.007_{m_s} + 0.000_{m_s^2})^{+0.010}_{-0.013}(\mathrm{SR})^{+0.002}_{-0.002}(\mathrm{M}).
\end{aligned} \tag{3.3.3}$$

The leading terms in the m_s-expansion differ from unity because we do not expand the logarithms $L_{\overline{\Lambda}+m_s}$ in $m_s/\overline{\Lambda}$. Compared to the absolute Bag parameters we reduce the intrinsic sum rule error to 0.005, the condensate error to 0.002 and the uncertainty due to power corrections to 0.002 since the respective uncertainties cancel to a large extent in the ratios. However, we enhance the intrinsic sum rule and condensate error estimates for the operator Q_3 by a factor of five since the sum rule uncertainties

for this operator are enhanced by large ratios of color factors $A_{Q_{1,2}}/A_{Q_3}$. A detailed overview of the uncertainties is given in Appendix A.1. The ratios Eq.(3.3.3) are in excellent agreement with the parametric estimates 1 ± 0.02 from [55, 139] with the exception of Q_3 where this uncertainty should have been enhanced like the other sum rule uncertainties listed above to account for the large color factors in the QCD-HQET matching relation Eq.(3.2.14) for the Bag parameter.

Taking the FLAG [157][1] value with $N_f = 2+1+1$ for the ratio f_{B_s}/f_B of the decay constants of B_s^0 and B_d^0 we obtain a high level of precision for the ratio

$$\xi \equiv \frac{f_{B_s}}{f_B}\sqrt{\overline{B}_{Q_1}^{s/d}} = 1.2014^{+0.0065}_{-0.0072} = 1.2014 \pm 0.0050 \left(\frac{f_{B_s}}{f_B}\right)^{+0.0043}_{-0.0053} \left(\overline{B}_{Q_1}^{s/d}\right), \quad (3.3.4)$$

where the ratio of decay constants and Bag parameters contributes equally to the error budget.

3.3.2 B_s mixing observables

In this section we present the current status of the B mixing observables: ΔM_s, ΔM_d, the decay rate differences $\Delta\Gamma_s$ and $\Delta\Gamma_d$, and the ratio $\Delta M_s/\Delta M_d$, of which the latter benefits from a reduced uncertainty due to the cancellation of CKM factors and hadronic effects. In doing so we hope to provide the reader with a more up to date picture of the analysis we carried out in [1]. Since that analysis was done, weighted averages of the bag parameter results presented here along with other sum rule [54, 55] and lattice determinations [136, 137, 141, 156, 157] were presented in [28]. The source of uncertainties between sum rules and lattice are independent and therefore the findings of [28] provide a reliable picture. Furthermore, the SM predictions of $\Delta\Gamma_q$ obtained in [161] using the averaged non-perturbative input from [28] are now used as the benchmark SM results by HFLAV [127].

Comparing the SM value for ΔM_s [28] we see an excellent agreement with the

[1] The average is dominated by the HPQCD'17 [159] and FNAL/MILC'17 [160] results.

experimental measurement [127]:

$$\begin{aligned}\Delta M_s^{\rm Exp} &= (17.741 \pm 0.020)\,{\rm ps}^{-1},\\ \Delta M_s^{\rm SM} &= (18.4^{+0.7}_{-1.2})\,{\rm ps}^{-1},\end{aligned} \tag{3.3.5}$$

where the hadronic input for ΔM_s^{12} was composed of the FLAG ($N_f = 2+1+1$) value for the decay constant and the averaged bag parameter $B_{Q_1}^{AV} = 0.849 \pm 0.023$ based on [1, 137, 156] which is in excellent agreement with our sum rule result in Eq.(3.3.2) albeit with a reduced uncertainty. As such, the SM value in Eq.(3.3.5) is very close to our original sum rule prediction [1].

The SM value for $\Delta\Gamma_s$ was updated in [161] and compared to experiment [127] reads as:

$$\begin{aligned}\Delta\Gamma_s^{\rm Exp} &= (0.082 \pm 0.005)\,{\rm ps}^{-1},\\ \Delta\Gamma_s^{\rm SM} &= (0.091 \pm 0.013)\,{\rm ps}^{-1}.\end{aligned} \tag{3.3.6}$$

The theoretical prediction for the decay rate difference includes NLO QCD [75, 162–164] and $1/m_b$ [165, 166] corrections. The SM estimate in Eq.(3.3.6) represents a significant improvement on previous theory predictions, partly due to the increased precision of dimension-6 matrix elements. It also benefits from the inclusion of non-perturbative results for dimension seven matrix elements calculated in [80], where previously only the vacuum insertion approximation for these parameters was available. Further reductions to the uncertainty can be made with a NNLO computation of the HQE matching coefficients (see [167]).

Similarly, for B_d observables, the SM value with averaged hadronic inputs currently agrees well with experiment [127]:

$$\begin{aligned}\Delta M_d^{\rm Exp} &= (0.5065 \pm 0.0019)\,{\rm ps}^{-1},\\ \Delta M_d^{\rm SM} &= (0.533^{+0.022}_{-0.036})\,{\rm ps}^{-1},\end{aligned} \tag{3.3.7}$$

and:

$$\begin{aligned}\Delta\Gamma_d^{\rm exp} &= (\ 0.7 \pm 6.6) \cdot 10^{-3}\,{\rm ps}^{-1},\\ \Delta\Gamma_d^{\rm SM} &= (2.6 \pm 0.4) \cdot 10^{-3}\,{\rm ps}^{-1},\end{aligned} \tag{3.3.8}$$

where $\Delta M_d^{\rm SM}$ was calculated by [28] and $\Delta\Gamma_d^{\rm SM}$ from [124]. Currently there is only an upper bound on $\Delta\Gamma_d^{\rm Exp}$ available and so we estimate its value through [127]:

$$\left(\frac{\Delta\Gamma_d}{\Gamma_d}\right)^{\rm Exp} = 0.001 \pm 0.010, \qquad \tau_{B_d}^{\rm Exp} = (1.519 \pm 0.004)\,{\rm ps}. \tag{3.3.9}$$

Lastly, for the ratio of the mass differences, the current SM value [28] compared to experiment reads as:

$$\begin{aligned}\left(\frac{\Delta M_d}{\Delta M_s}\right)^{\rm Exp} &= 0.0285 \pm 0.0001,\\ \left(\frac{\Delta M_d}{\Delta M_s}\right)^{\rm SM} &= 0.0298^{+0.0005}_{-0.0009} = 0.0297^{+0.0004}_{-0.0003}\,({\rm had.})^{+0.0005}_{-0.0008}\,({\rm CKM}).\end{aligned} \tag{3.3.10}$$

The hadronic input entering the SM prediction is the ratio ξ, taken from a weighted average of Eq.(3.3.4) and lattice determinations from [141, 156, 157]. We find that our value for ξ has a precision almost twice that of the lattice determinations and therefore the value of $(\Delta M_d/\Delta M_s)^{\rm SM}$ is dominated by our sum rule result. We have also broken down the uncertainty contributions in Eq.(3.3.10) to illustrate that CKM is the dominant source in this case. Furthermore, we observe a small deviation from experiment $\sim 1.4\sigma$.

3.3.3 Determination of the top-quark $\overline{\rm MS}$ mass

The parametric error from the top-quark mass currently dominates the uncertainty in the determination of the stability or meta-stability of the electroweak vacuum [168]. Direct measurements quote very precise values $m_t^{\rm MC} = (172.76 \pm 0.3)\,{\rm GeV}$ for the top quark mass [169], but these results correspond to so-called Monte-Carlo (MC) masses and not the top-quark pole mass. One therefore needs to account for additional uncertainties from the scheme conversion [170] when these values are used for

phenomenological predictions. Alternatively one can determine the top-quark mass by fitting observables like the total top-pair production cross section which can be predicted in terms of the top-quark mass in a well-defined scheme like $\overline{\text{MS}}$. Similarly, we can use the mass differences ΔM_q for a theoretically clean determination of $\overline{m}_t(\overline{m}_t)$. Using the CKMfitter values for V_{td} and V_{ts} as input we obtain

$$\begin{aligned}\overline{m}_t(\overline{m}_t) &= (158^{+9}_{-6})\,\text{GeV} = (158^{+7}_{-6}\,(\text{had.})^{+0}_{-1}\,(\mu)^{+6}_{-1}\,(\text{param.}))\,\text{GeV, from } \Delta M_s,\\ \overline{m}_t(\overline{m}_t) &= (155^{+9}_{-6})\,\text{GeV} = (155^{+6}_{-6}\,(\text{had.})^{+0}_{-1}\,(\mu)^{+6}_{-2}\,(\text{param.}))\,\text{GeV, from } \Delta M_d.\end{aligned} \tag{3.3.11}$$

Combining both results we find

$$\overline{m}_t(\overline{m}_t) = (157^{+8}_{-6})\,\text{GeV} = (157^{+7}_{-6}\,(\text{had.})^{+0}_{-1}\,(\mu)^{+4}_{-1}\,(\text{param.}))\,\text{GeV}, \tag{3.3.12}$$

where we have averaged over the hadronic and scale uncertainties, which are correlated, and treated the parametric uncertainties, which are dominated either by V_{td} or V_{ts}, as independent. This is in good agreement with the PDG average [169]

$$\overline{m}_t(\overline{m}_t) = (162.5^{+2.1}_{-1.5})\,\text{GeV}, \tag{3.3.13}$$

of $\overline{\text{MS}}$ mass determinations from cross section measurements, albeit with much larger uncertainties. A very precise measurement of the top-quark PS or $\overline{\text{MS}}$ mass with a total uncertainty of about 50 MeV is possible at a future lepton collider running at the top threshold [171–173].

3.3.4 $\mathcal{B}(B_q \to \mu^+\mu^-)$

The branching ratio $\mathcal{B}(B_q \to l^+l^-)$ is strongly suppressed in the SM and theoretically clean. Thus, it provides a very sensitive probe for new physics. At present it has been computed at NNLO QCD plus NLO EW [174] and the dominant uncertainties are parametric, stemming from the decay constant and the CKM parameters. Both uncertainties cancel out of the ratio [175]

$$\frac{\mathcal{B}(B_q \to l^+l^-)}{\Delta M_q} = \frac{3G_F^2 M_W^2 m_l^2 \tau_{B_q^H}}{\pi^3}\sqrt{1-\frac{4m_l^2}{M_{B_q}^2}}\,\frac{|C_A(\mu)|^2}{S_0(x_t)\hat{\eta}_B \overline{B}^q_{Q_1}(\mu)}\,, \tag{3.3.14}$$

which in turn receives its dominant uncertainty from the Bag parameter $\overline{B}^q_{Q_1}$. Using our result Eq.(3.3.3) and including the power-enhanced QED corrections determined in [176] we predict the branching ratio by multiplying Eq.(3.3.14) with the measured mass differences

$$\begin{aligned}
\mathcal{B}(B_s^0 \to \mu^+\mu^-)_{\rm SM} &= (3.55^{+0.23}_{-0.20}) \cdot 10^{-9}\,, \\
\mathcal{B}(B_d^0 \to \mu^+\mu^-)_{\rm SM} &= (9.40^{+0.58}_{-0.53}) \cdot 10^{-11}\,, \\
\left(\frac{\mathcal{B}(B_d^0 \to \mu^+\mu^-)}{\mathcal{B}(B_s^0 \to \mu^+\mu^-)}\right)_{\rm SM} &= 0.0265 \pm 0.0003 = 0.0265 \pm 0.0002 \left(\overline{B}^{s/d}_{Q_1}\right) \pm 0.0002(\text{exp})\,,
\end{aligned} \tag{3.3.15}$$

where the uncertainties for the branching ratios are completely dominated by the error from $\overline{B}^q_{Q_1}$. The result for $B_s^0 \to \mu^+\mu^-$ is in good agreement with the current experimental average [127]

$$\mathcal{B}(B_s^0 \to \mu^+\mu^-)_{\rm exp} = (3.1 \pm 0.6) \cdot 10^{-9}\,, \tag{3.3.16}$$

while the latest measurements only provide upper bounds at 95% confidence level for $B_d^0 \to \mu^+\mu^-$

$$\mathcal{B}(B_d^0 \to \mu^+\mu^-)_{\rm exp} < \begin{cases} 3.6 \cdot 10^{-10}\,, & (\text{CMS [35]})\,, \\ 2.6 \cdot 10^{-10}\,, & (\text{LHCb [33]})\,, \\ 2.1 \cdot 10^{-10}\,, & (\text{ATLAS [34]})\,. \end{cases} \tag{3.3.17}$$

We compare our prediction Eq.(3.3.15) to the direct predictions from [160, 174, 176] which depend on the decay constants and CKM elements $|V_{tq}|$, the predictions [137, 156] from the ratios $\mathcal{B}(B_q \to l^+l^-)/\Delta M_q$ and the experimental average Eq.(3.3.16) in Figure 3.5. The shaded regions correspond to the overlap of the one-sigma regions for $\mathcal{B}(B_s^0 \to \mu^+\mu^-)$, $\mathcal{B}(B_d^0 \to \mu^+\mu^-)$ and $\mathcal{B}(B_d^0 \to \mu^+\mu^-)/\mathcal{B}(B_s^0 \to \mu^+\mu^-)$ where they were provided. We find good consistency among the various predictions with similar uncertainties for both approaches and good agreement with experiment whose uncertainty currently exceeds the theoretical one by a factor of about 3-4 in $\mathcal{B}(B_s^0 \to \mu^+\mu^-)$. For completeness we provide our predictions for the branching

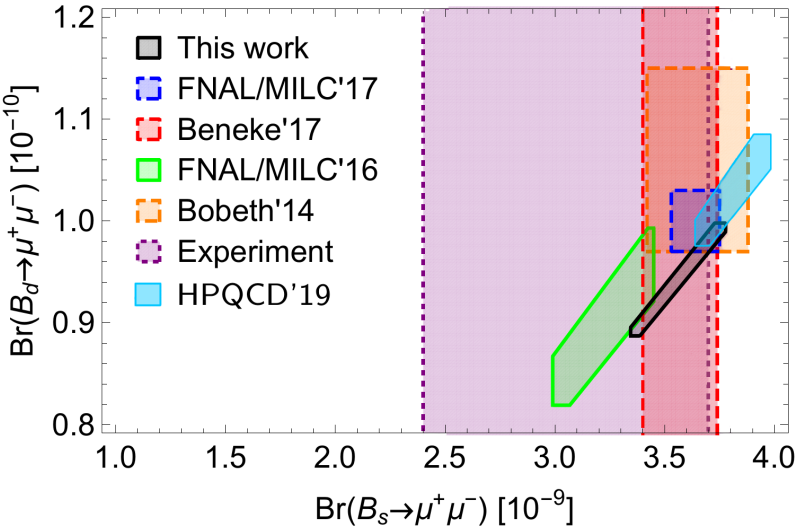

Figure 3.5: We compare our prediction for the branching ratios $\mathcal{B}(B_q^0 \to \mu^+\mu^-)$ with $q = s, d$ to other predictions using either the decay constants [160, 174, 176] (dashed boundaries) or the Bag parameter $\overline{B}_{Q_1}^q$ [137, 156] (solid boundaries) as input. The experimental average for $\mathcal{B}(B_s^0 \to \mu^+\mu^-)$ is indicated by the region with the dotted boundary.

ratios to electrons

$$\mathcal{B}(B_s^0 \to e^+e^-)_{\rm SM} = (8.37^{+0.55}_{-0.48}) \cdot 10^{-14}\,, \tag{3.3.18}$$

$$\mathcal{B}(B_d^0 \to e^+e^-)_{\rm SM} = (2.22^{+0.14}_{-0.13}) \cdot 10^{-15}\,,$$

$$\left(\frac{\mathcal{B}(B_d^0 \to e^+e^-)}{\mathcal{B}(B_s^0 \to e^+e^-)}\right)_{\rm SM} = 0.0265 \pm 0.0003 = 0.0265 \pm 0.0002 \left(\overline{B}_{Q_1}^{s/d}\right) \pm 0.0002(\text{exp})\,,$$

and tau leptons

$$\mathcal{B}(B_s^0 \to \tau^+\tau^-)_{\rm SM} = (7.58^{+0.50}_{-0.44}) \cdot 10^{-7}\,, \tag{3.3.19}$$

$$\mathcal{B}(B_d^0 \to \tau^+\tau^-)_{\rm SM} = (1.98^{+0.12}_{-0.11}) \cdot 10^{-8}\,,$$

$$\left(\frac{\mathcal{B}(B_d^0 \to \tau^+\tau^-)}{\mathcal{B}(B_s^0 \to \tau^+\tau^-)}\right)_{\rm SM} = 0.0262 \pm 0.0003 = 0.0262 \pm 0.0002 \left(\overline{B}_{Q_1}^{s/d}\right) \pm 0.0002(\text{exp})\,.$$

3.4 Summary

In this chapter we have presented a HQET sum rule determination of the five $\Delta B = 2$ Bag parameters describing B_s-mixing in the SM and beyond. In order to achieve

this we had to calculate m_s and m_s^2 corrections to the three-point correlator at the 3-loop level. In doing so, we obtain the most precise values for the ratios of Bag parameters in the B_s and B_d system. Combining these findings with the current FLAG value for f_{B_s}/f_{B_d} [157, 159, 160] we obtain the world's most precise value for the ratio

$$\xi \equiv \frac{f_{B_s}}{f_B}\sqrt{\overline{B}_{Q_1}^{s/d}} = 1.2014^{+0.0065}_{-0.0072}\,, \tag{3.4.1}$$

which represents a reduction of the uncertainty by more than a factor of two compared to the latest lattice results [137, 141, 156]. Our results enable a rich phenomenology: contributing to a significant improvement in the theoretical determination of ΔM_s and $\Delta\Gamma_s$, which are now in agreement with the experimental values. The control we have over the hadronic uncertainties thanks to the efforts of [1, 28, 54, 55, 137, 141, 156] means we are now in a much stronger position to probe for NP effects in B-mixing. Using all CKM elements as inputs we get constraints on the values of the top quark $\overline{\text{MS}}$ mass which are compatible with direct collider determinations. Finally, using our results we were able to give precise SM predictions for the leptonic branching ratios of the rare decays $B_q \to ll$.

Further improvements to the precision of our HQET sum rule results can be obtained through the use of the HQET-QCD matching at NNLO (first steps in that direction have been performed in [140]). Another line of improvement would be the determination of $1/m_b$-corrections to the HQET limit.

Chapter 4

Determination of CKM parameters

4.1 Introduction

In the previous Chapter we determined the hadronic matrix elements for B_s-mixing with HQET sum rules [1, 55] (cf. also [54]) and discussed their impact on the SM predictions of ΔM_d and ΔM_s when used along side the lattice results [137, 141, 156] through the weighted averages presented in [28]. Assuming only SM contributions, these can also be used to obtain a direct determination of $|V_{ts}^* V_{tb}|$ from the experimental value of the mass difference $\Delta M_s^{\text{Exp.}}$. Additionally, by taking instead the ratio of the mass differences in the B_d and the B_s systems we can get a clean handle on $|V_{td}/V_{ts}|$. In this Chapter we investigate the implications of these results for the unitarity triangle angle γ, and use them to extract a value for the CKM element $|V_{cb}|$.

4.2 Analysis

Using the results of [28] we determine the following combinations of CKM elements:

$$\begin{aligned} |V_{ts}V_{tb}| &= \left(40.91^{+0.67}_{-0.64}\right) \cdot 10^{-3} \qquad (1) \\ &= \left(40.91\ ^{+0.65}_{-0.62}\Big|_{f_B^2 B} \pm 0.17|_{m_t} \pm 0.05|_{\alpha_s(M_Z)} \pm 0.02|_{\Delta M_s}\right) \cdot 10^{-3}\,, \end{aligned}$$

$$\left|\frac{V_{td}}{V_{ts}}\right| = 0.2043^{+0.0010}_{-0.0011} \qquad (2)$$
$$= 0.2043\ ^{+0.0009}_{-0.0010}\Big|_{\xi} \pm 0.0003|_{\Delta M_d} \pm 0.0001|_{\Delta M_s}\ ,$$

from the experimental measurements of the mass differences, updating the results in [1]. Motivated by the well-known discrepancy between the direct determination of the CKM elements V_{cb} and V_{ub} from semi-leptonic b-hadron decays (see [177]) we study the impact of these values on CKM unitarity fits.

The effects of B-mixing on CKM unitarity fits can be illustrated with the unitarity triangle shown in Figure 4.1. The combinations of CKM elements (1) and (2) we determined from ΔM_s and ΔM_d appear in the lengths of the two non-trivial sides of the triangle if we expand to leading order in the Wolfenstein parameter $\lambda = |V_{us}|$. Up to reflection with respect to the $\bar{\rho}$ axis the apex of the triangle is exactly fixed with the addition of $|V_{ub}|$ and the precisely measured $|V_{us}|$. Here, we use this information to determine the angle γ. Furthermore, we can extract $|V_{cb}| = |V_{ts}V_{tb}| \times [1 + \mathcal{O}(\lambda^2)]$ with a precision that is competitive with direct measurements.

We perform a minimalistic CKM unitarity fit, first taking only the direct measurements of the CKM element $|V_{us}| = 0.2243 \pm 0.0005$ [151] and the mass differences ΔM_d and ΔM_s into account. This strongly constrains the length of the side R_t. Figure 4.2 shows our results in the $|V_{ub}| - \gamma$ and $|V_{cb}| - \gamma$ planes where the shaded blue regions indicate the parameter space satisfying the inputs within one and two standard deviations. For values of γ larger than about 65° the unitarity triangle does

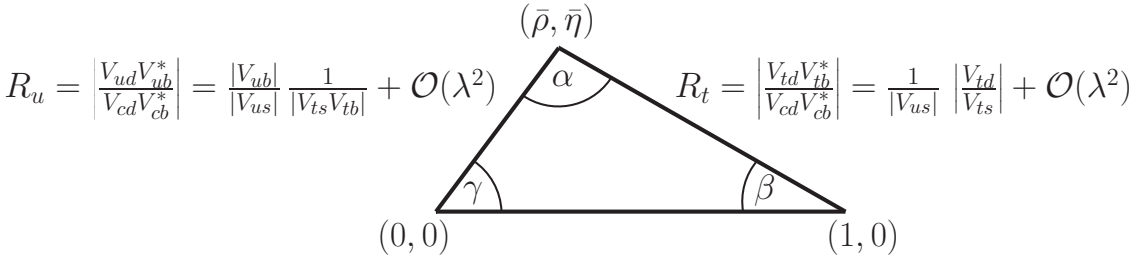

Figure 4.1: Our conventions for the unitarity triangle in the $\bar{\rho} - \bar{\eta}$ plane.

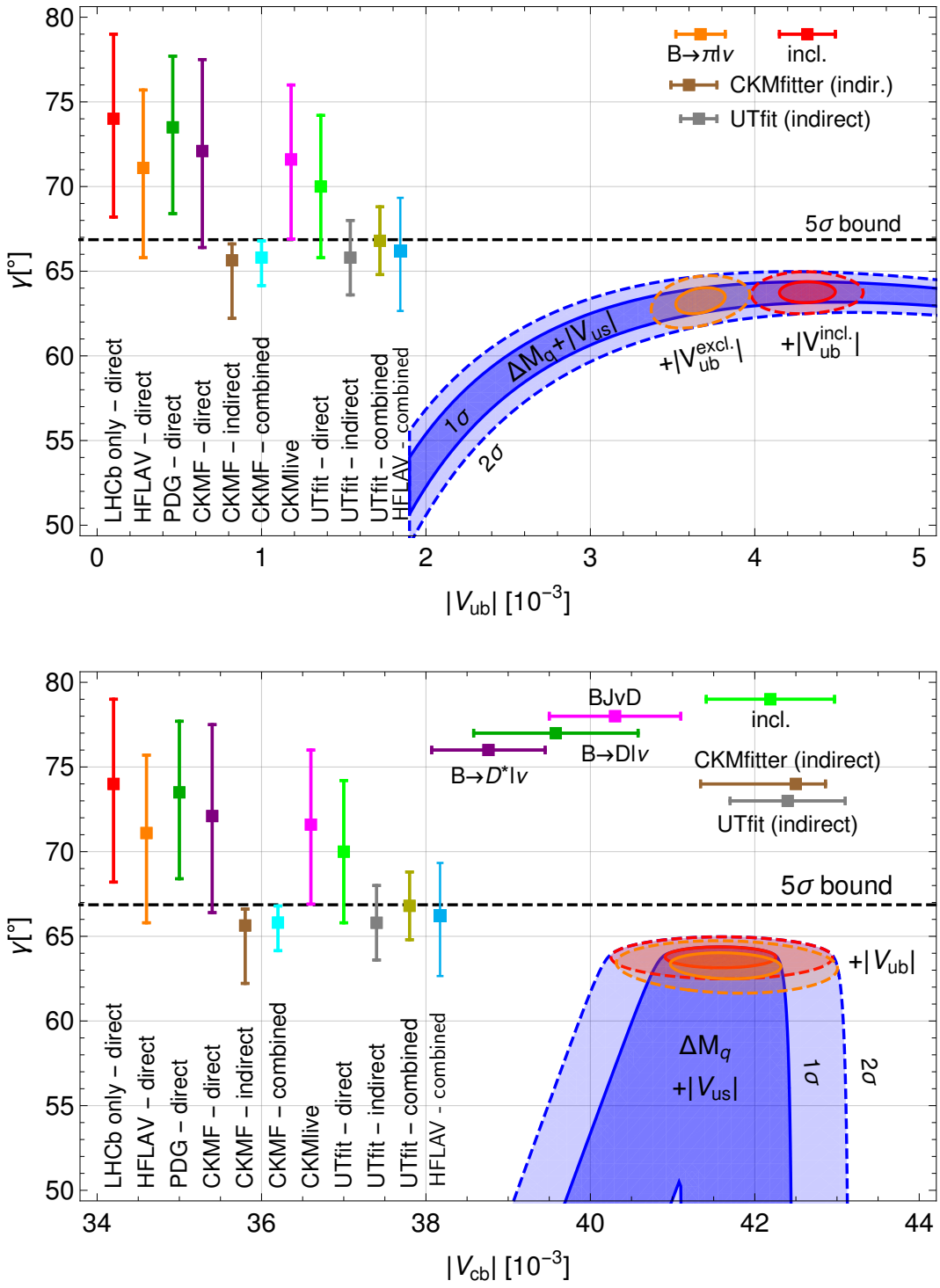

Figure 4.2: Our results for a minimalistic CKM unitarity fit based on direct measurements of $|V_{us}|$ and the mass differences ΔM_d and ΔM_s are given as shaded blue regions. Including the exclusive or inclusive measurements of $|V_{ub}|$ yields the orange and red regions, respectively. See text for details.

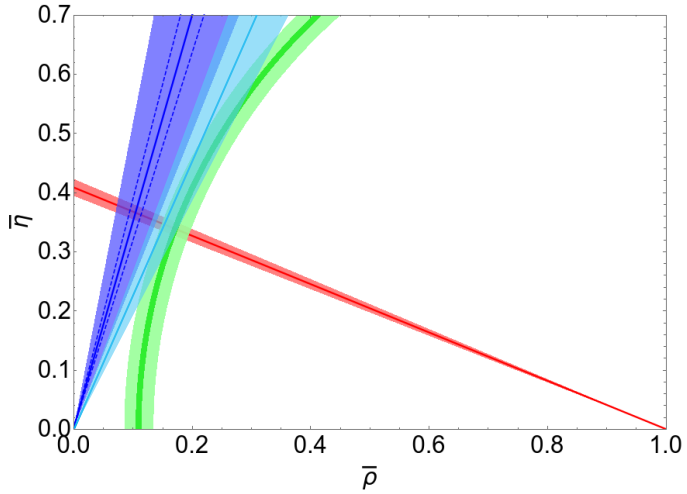

Figure 4.3: We show the updated constraints on the apex of the unitarity triangle. The latest value for γ taken from HFLAV [127] (light blue) is found to be much more consistent with the constraints from B-mixing (green) and the value of β, taken from HFLAV [127] (red) than the previous measurement by LHCb [178] (dark blue). The dark and light green regions indicate the 1σ and 5σ bounds from mixing, while the blue and red regions refer to the 1σ constraints. The dashed blue lines illustrate the future precision of $\pm 1.5^\circ$ on the measurement of γ if the central value had not shifted from its 2019 value.

not close within the two-sigma region[1]. This behaviour is illustrated in Figure 4.3 and allows us to derive a stringent upper limit on γ. At the level of five standard deviations we obtain

$$\gamma \leq 66.9^\circ \qquad [5\sigma]\,, \tag{3}$$

which is indicated by the horizontal dashed line in Figure 4.2. At this point we note that at the time of our original analysis in [2] our results suggested a possible tension with the latest measurements by LHCb [178], indicated on the far left of Figure 4.2 where it sits clearly above our 5σ bound. Recently an update by LHCb [180] brought their measurement down considerably. This is reflected in Figure 4.2 in the result on the far right which was obtained from HFLAV [127] using the new measurements by LHCb and the findings by BaBar [181]. This illustrates that the status of γ is now consistent with mixing constraints at the current level of precision. We note that the

[1] Similar observations were made in e.g. [179].

indirect determinations of γ from the CKMfitter [182] and UTfit [183] collaborations yield values that agree with the updated direct measurements also.

For smaller values of γ there are two intersections between the circle of length R_t around the point (1,0) and the line crossing the origin at angle γ, leading to two degenerate perfect-fit results for $|V_{ub}|$ and $|V_{cb}|$ at a fixed value of γ. This degeneracy can be broken by constraining the length of the side R_u by including the measurements of $|V_{ub}|$ in the fit. Due to the well-known puzzle about different results in exclusive and inclusive measurements (shown by the orange and red horizontal error bars in Figure 4.2, values from HFLAV [127]) this step would normally have to be taken with a grain of salt. However, due to a lucky numerical coincidence the values of $|V_{ub}|$ are very close to the region where the intersection point of the circles of length R_t and R_u lies at the maximal value of γ allowed by R_t as shown by the orange and red ellipses in Figure 4.2 which are the results of the fit when the exclusive or inclusive measurements of $|V_{ub}|$ are included. Thus, the dependence of γ on the exact value of $|V_{ub}|$ is rather small. Indeed we find

$$\gamma = \left(63.3^{+0.7}_{-0.8}\right)^\circ , \qquad \text{from } |V_{ub}^{\text{excl.}}| , \tag{4}$$

$$\gamma = \left(63.8^{+0.6}_{-0.6}\right)^\circ , \qquad \text{from } |V_{ub}^{\text{incl.}}| . \tag{5}$$

We take the envelope of both values

$$\gamma = (63.4 \pm 0.9)^\circ , \tag{6}$$

as our final result to be sufficiently conservative about the uncertainty associated with the direct measurements of $|V_{ub}|$. Eq. (6) represents the most precise determination of γ to date. The result is fairly insensitive to the input value for $|V_{us}|$. If we inflate the error in $|V_{us}|$ by a factor of three we obtain $\gamma = (63.4 \pm 1.3)^\circ$ and the upper five-sigma bound (3) becomes 68.9°, which still poses a very stringent constraint.

The effect of the exclusive or inclusive $|V_{ub}|$ measurements on the fit is also indicated in the $|V_{cb}| - \gamma$ plane by the orange and red ellipses, respectively. The difference in the extracted values of $|V_{cb}|$ is negligible and we again adopt the envelope as our

final result

$$|V_{cb}| = (41.6 \pm 0.7) \cdot 10^{-3} \,. \tag{7}$$

We also show the exclusive and inclusive HFLAV averages [127] and the result of a reanalysis BJvD [184] of exclusive determinations in Figure 4.2. Our result yields a competitive uncertainty and the one-sigma region overlaps with the inclusive and the BJvD results, while there is a 1.7 and 2.9 σ tension with respect to the $B \to D\ell\nu$ and $B \to D^*\ell\nu$ values quoted by HFLAV. The result (7) remains unaffected when we inflate the $|V_{us}|$-uncertainty by a factor of three.

4.3 Summary

To summarise, we have performed here a minimal χ^2 fit of the CKM parameters based on the mass differences in the B system and direct measurements of $|V_{us}|$ and $|V_{ub}|$. We found competitive results for $|V_{cb}|$ which are in good agreement with the inclusive determinations. In addition to this, we also obtained the currently most precise value for the angle γ in the unitarity triangle. We find that the latest direct measurements of γ are consistent with the B-mixing constraints. Furthermore, we look forward to updates of the complete CKM unitarity fits by the CKMfitter and UTfit collaborations where the latest theoretical developments [1, 28, 54, 55, 137, 141, 156] in B-mixing are taken into account.

Chapter 5

Lifetime Bag Parameter

5.1 Introduction

The theoretical predictions for B-meson lifetime ratios currently stand in close agreement with experimental results, see Table 5.1. The measurements of the B_s

Lifetime Ratio	Experiment	Theory
$\frac{\tau(B^+)}{\tau(B_d)}$	1.076 ± 0.004 [127]	$1.078^{+0.021}_{-0.023}$ [55]
$\frac{\tau(B_s)}{\tau(B_d)}$	0.998 ± 0.005 [127]	1.0007 ± 0.0025 [55]

Table 5.1: Experimental values (HFLAV [127]) of the lifetime ratio of B mesons versus theoretical predictions based on the 2017 HQET sum rule prediction for the matrix elements of the four quark operators in the $\overline{MS}$ scheme [55].

lifetime have recently been updated by the LHCb collaboration [132,185], the ATLAS collaboration [186] and by the CMS collaboration [133] and interestingly the value of ATLAS deviates from the other measurements [187]. In future we expect a further improvement of the experimental precision indicated in Table 5.1. On the theory side there has also been significant progress in the last years. As discussed in Section 2.1, according to the heavy quark expansion (HQE) the total decay rate of a hadron H_Q containing a heavy quark Q can be expanded in inverse powers of the heavy quark mass m_Q and each term in the expansion is a product of a perturbative coefficient

Γ_i or $\tilde{\Gamma}_i$ and a non-perturbative matrix element of a $\Delta Q = 0$ operator $\mathcal{O}_D$ or $\tilde{\mathcal{O}}_D$ of dimension D:

$$\Gamma = \Gamma_3\langle\mathcal{O}_3\rangle + \Gamma_5\frac{\langle\mathcal{O}_5\rangle}{m_Q^2} + \Gamma_6\frac{\langle\mathcal{O}_6\rangle}{m_Q^3} + ... + 16\pi^2\left[\tilde{\Gamma}_6\frac{\langle\tilde{\mathcal{O}}_6\rangle}{m_Q^3} + \tilde{\Gamma}_7\frac{\langle\tilde{\mathcal{O}}_7\rangle}{m_Q^4} + ...\right], \quad (5.1.1)$$

with $\langle\mathcal{O}_D\rangle = \langle H_Q|\mathcal{O}_D|H_Q\rangle/(2M_{H_Q})$. We denote with Γ_i contributions related to two quark operators $\mathcal{O}_i$ and with $\tilde{\Gamma}_i$ contributions related to four quark operators $\tilde{\mathcal{O}}_i$. Each perturbative coefficient Γ_i ($\tilde{\Gamma}_i$) can be further expanded in the strong coupling constant

$$\overset{(\sim)}{\Gamma}_i = \overset{(\sim)}{\Gamma}_i^{(0)} + \frac{\alpha_s}{4\pi}\overset{(\sim)}{\Gamma}_i^{(1)} + \left(\frac{\alpha_s}{4\pi}\right)^2\overset{(\sim)}{\Gamma}_i^{(2)} + \dots . \quad (5.1.2)$$

Traditionally the four quark contributions indicated by $\tilde{\Gamma}_6\langle\tilde{\mathcal{O}}_6\rangle$ are considered to give the dominant contributions to lifetimes ratios, because of the phase space enhancement factor $16\pi^2$, see e.g. [188,189]. In these so-called spectator contributions, which are known to NLO-QCD accuracy [190–193], the by far largest source of uncertainty resides in the non-perturbative hadronic matrix elements $\langle\tilde{\mathcal{O}}_6\rangle$. The most recent estimates for these parameters from lattice QCD [194] were carried out in 2001 and only made public in proceedings. Movtivated by the successful findings of our HQET sum rules analysis of B_s-mixing presented in Chapter 3, in this chapter we present the first computation of the dimension-6 matrix elements of $\Delta Q = 0$ four quark operators with a non-zero strange quark mass. Furthermore, for the first time eye contractions of the $\Delta Q = 0$ four quark operators are determined as well as matrix elements of penguin operators.

Very recently the Darwin term $\Gamma_6\langle\mathcal{O}_6\rangle$ was calculated for the first time for non-leptonic decays and found to be very large [124, 195, 196]. For the lifetime ratio $\tau(B^+)/\tau(B_d)$ this contribution will cancel due to isospin symmetry. However, for a precise calculation of the ratio $\tau(B_s)/\tau(B_d)$ the $SU(3)_F$ breaking contribution of the form $\Gamma_6(\langle\mathcal{O}_6\rangle_{B_d} - \langle\mathcal{O}_6\rangle_{B_s})$ has to be determined. The matrix element $\langle\mathcal{O}_6\rangle_{B_d}$ is known quite well from fits of the inclusive semileptonic B meson decays, see e.g. [197, 198], unfortunately a corresponding analysis has not been performed for the B_s meson, thus $\langle\mathcal{O}_6\rangle_{B_s}$ is largely unknown. However, the Darwin operator can be related to

four quark operators via equations of motion (see e.g. [4, 195]) and thus our results can also be used to estimate the size of the matrix element of the Darwin operator for the B_s meson.

Since we work here in the strict HQET limit our results can also be applied to the charm sector, where sizeable lifetime differences have been found experimentally [169, 199]:

$$\frac{\tau(D^+)}{\tau(D_0)} = 2.54 \pm 0.02\,, \qquad \frac{\tau(D_s^+)}{\tau(D_0)} = 1.20 \pm 0.01\,. \tag{5.1.3}$$

As the expansion parameter $\alpha_s(m_c)$ and Λ/m_c where Λ is a hadronic scale are quite sizeable, a study of charm lifetimes can shed light on the convergence radius of the HQE (this is discussed further in Chapter 6).

Our results can of course also be used for an analysis of spectator effects in inclusive semi-leptonic B and D meson decays, where the same matrix elements will appear (see Chapter 6).

The rest of this chapter is organised as follows: The sum rule setup is presented in Section 5.2. We introduce the $\Delta Q = 0$ operator basis and the parameterisation of the matrix elements in Section 5.2.1. After this, Section 5.2.2 covers the sum rule itself. Here there are large similarities with the methodology presented in Chapter 3 but due to the inclusion of non-valence contributions there is some additional notation required. We overview the perturbative part of the calculation in Section 5.2.3 including a brief overview of the obstacles that arise due to eye-contractions. Condensate contributions will be revisited in Section 5.2.4 and in Section 5.2.5 we present analytic results. Lastly, our numerical analysis is discussed in Section 5.3 before we summarise our findings and prospects in Section 5.4.

5.2 Setup and calculation

5.2.1 Operator Basis

We carry out the sum rule in the exact HQET limit in order to avoid mixing between operators of different mass dimensions. The basis we use coincides with that of [191], except for the naming of the colour-octett operators. In the HQET limit (denoted by the tilde) we get

$$\begin{aligned}
\tilde{Q}_1^q &= \bar{h}\gamma_\mu(1-\gamma^5)q\cdot\bar{q}\gamma^\mu(1-\gamma^5)h, & \tilde{T}_1^q &= \bar{h}\gamma_\mu(1-\gamma^5)T^Aq\cdot\bar{q}\gamma^\mu(1-\gamma^5)T^Ah,\\
\tilde{Q}_2^q &= \bar{h}(1-\gamma^5)q\cdot\bar{q}(1+\gamma^5)h, & \tilde{T}_2^q &= \bar{h}(1-\gamma^5)T^Aq\cdot\bar{q}(1+\gamma^5)T^Ah, \qquad (5.2.1)
\end{aligned}$$

where h denotes the HQET field describing the heavy quark Q with mass m_Q, the light quark fields are denoted by q. In addition we use the same evanescent operators as in [55] (choosing $a_1 = a_2 = -8$). A full description of SU(3) flavour-breaking contributions at NLO in QCD also requires us to consider the QCD penguin operators

$$\tilde{Q}_P^q = \bar{h}\gamma_\mu T^A h\cdot\bar{q}\gamma^\mu T^A q\,. \qquad (5.2.2)$$

Note, that differing from the definition in [191] we need the flavour specific contribution of the penguins, thus we are not summing over the light quark flavour q. Inspired by [191, 200] we parametrize the matrix elements of the above operators as,

$$\begin{aligned}
\langle\mathbf{B}_q|\tilde{Q}_i^q(\mu)|\mathbf{B}_q\rangle &= A_{\tilde{Q}_i}F_q^2(\mu)\tilde{B}_i^q(\mu) & \langle\mathbf{B}_q|\tilde{Q}_i^{q'}(\mu)|\mathbf{B}_q\rangle &= A_{\tilde{Q}_i}F_q^2(\mu)\tilde{\delta}_i^{q'q}(\mu)\,,\\
\langle\mathbf{B}_q|\tilde{T}_i^q(\mu)|\mathbf{B}_q\rangle &= A_{\tilde{T}_i}F_q^2(\mu)\tilde{\epsilon}_i^q(\mu) & \langle\mathbf{B}_q|\tilde{T}_i^{q'}(\mu)|\mathbf{B}_q\rangle &= A_{\tilde{T}_i}F_q^2(\mu)\tilde{\delta}_{i+2}^{q'q}(\mu)\,,\\
\langle\mathbf{B}_q|\tilde{Q}_P^q(\mu)|\mathbf{B}_q\rangle &= A_{\tilde{Q}_P}F_q^2(\mu)\tilde{B}_P^q(\mu) & \langle\mathbf{B}_q|\tilde{Q}_P^{q'}(\mu)|\mathbf{B}_q\rangle &= A_{\tilde{Q}_P}F_q^2(\mu)\tilde{\delta}_P^{q'q}(\mu)\,, \qquad (5.2.3)
\end{aligned}$$

for which the colour factors correspond to,

$$A_{\tilde{Q}_i} = A_{\tilde{T}_i} = 1 \qquad A_{\tilde{Q}_P} = -\frac{C_F}{2N_c}\,, \qquad (5.2.4)$$

with the HQET decay constant F_q, the bag parameters $\tilde{B}_i^q$, $\tilde{B}_P^q$ and $\tilde{\epsilon}_i^q$ and the non-valence contribution $\tilde{\delta}_i^{q'q}$, for $q \neq q'$. Note that differing from [191] and [200] we

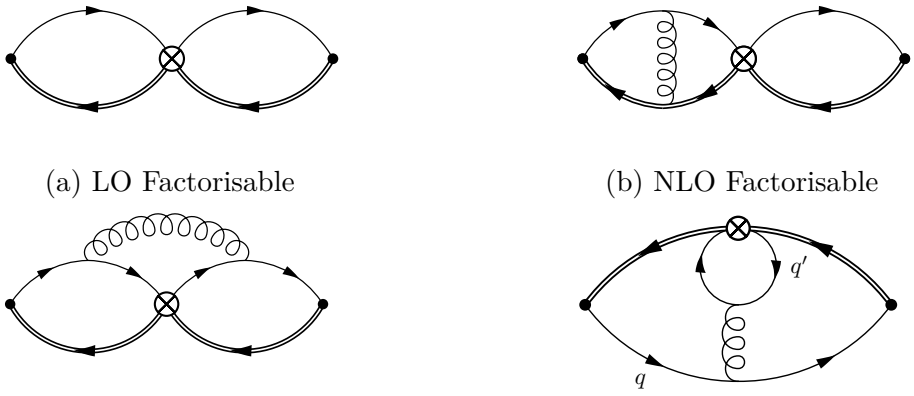

(a) LO Factorisable (b) NLO Factorisable

(c) NLO Nonfactorisable (d) NLO Non-Valence

Figure 5.1: Some of the diagrams contributing to the correletor in Eq.(5.2.5). Non-valence type diagrams like that shown in (d) only appear at NLO.

have included in $\tilde{B}_i^q$, $\tilde{B}_P^q$ and $\tilde{\epsilon}_i^q$ also the non-valence contributions with $q = q'$. As usual μ denotes the renormalisation scale dependence. In addition the heavy $|\mathbf{B}_q\rangle$ meson states (consisting of a heavy anti-quark $\overline{Q}$ and a light quark q) are considered in the strict HQET limit and thus our expressions hold both for B and D mesons.

5.2.2 The Sum Rule

As was the case in our analysis of the B_s-mixing bag parameters, the starting point of our sum rule is the 3-point correlator,

$$K^q_{\tilde{\mathcal{O}}^{q'}}(\omega_1,\omega_2) = \int d^dx_1 d^dx_2 e^{i(p_1\cdot x_1 - p_2\cdot x_2)} \langle 0|\mathrm{T}\left[\tilde{j}_q(x_2)\tilde{\mathcal{O}}^{q'}(0)\tilde{j}_q^\dagger(x_1)\right]|0\rangle\,, \qquad (5.2.5)$$

with the current defined as $j_q = \overline{q}\gamma^5 h$ and the rest of the terms identical to Eq.(3.2.22). Additionally, we have generalised the definition of the 3-point correlator to allow for different light quark flavours between the inserted operators $\tilde{\mathcal{O}}^{q'}$ and the interpolating currents $\tilde{j}_q$.

Following our treatment of the correlator in Chapter 3, we categorise the possible field contractions of Eq.(5.2.5) into factorisable and non-factorisable contributions. Examples of the corresponding Feynman diagrams are found in Fig.5.1. As previously discussed, this separation of contributions allows us to formulate a sum rule for the

deviation of the bag parameter ΔB from its vacuum saturation approximation (VSA) value.

$$\tilde{B}_i^q(\mu) = 1 + \Delta B^q_{\tilde{Q}_i^q}(\mu)\,, \tag{5.2.6}$$

$$\tilde{\epsilon}_i^q(\mu) = 0 + \Delta B^q_{\tilde{T}_i^q}(\mu)\,, \tag{5.2.7}$$

$$\tilde{B}_P^q(\mu) = 1 + \Delta B^q_{\tilde{Q}_P^q}(\mu)\,. \tag{5.2.8}$$

We find the following finite energy Borel sum rules,

$$\Delta B^q_{\tilde{\mathcal{O}}^q}(\mu) = \frac{1}{A_{\mathcal{O}} F_q^4(\mu)} \int_0^{\omega_c} d\omega_1 d\omega_2 e^{\frac{\overline{\Lambda}_q - \omega_1}{t} + \frac{\overline{\Lambda}_q - \omega_2}{t}} \Delta\rho^q_{\tilde{\mathcal{O}}^q}(\omega_1, \omega_2) \tag{5.2.9}$$

in which the term $\Delta\rho^q_{\tilde{\mathcal{O}}^q}(\omega_1, \omega_2)$ corresponds to the non-factorisable part of the double discontinuity of Eq.(5.2.5). Looking at the whole double discontinuity of the 3-point correlator it is useful to separate out the various contributions further as,

$$\begin{aligned} \rho^q_{\tilde{\mathcal{O}}^q}(\omega_1, \omega_2) &= \delta_{\tilde{\mathcal{O}}\tilde{Q}} \rho_\Pi(\omega_1)\rho_\Pi(\omega_2) + \Delta\rho^q_{\tilde{\mathcal{O}}^q}(\omega_1, \omega_2) \\ &= \delta_{\tilde{\mathcal{O}}\tilde{Q}} \rho_\Pi(\omega_1)\rho_\Pi(\omega_2) + \Delta_{\text{tree}}\rho^q_{\tilde{\mathcal{O}}^q}(\omega_1, \omega_2) + \Delta_{\text{peng}}\rho^q_{\tilde{\mathcal{O}}^q}(\omega_1, \omega_2)\,, \end{aligned} \tag{5.2.10}$$

for which $\delta_{\tilde{\mathcal{O}}\tilde{Q}}$ is equal to 1 for the colour singlet and penguin operators and 0 for the colour octet operators. In Eq.(5.2.10), the first term corresponds to factorisable contributions, whilst $\Delta_{\text{tree}}\rho$ corresponds to the first set of non-factorisbale contractions (see Fig.5.1c). The term denoted by $\Delta_{\text{peng}}\rho$, stems from 'eye-contraction' diagrams like that of the example illustrated in Fig.5.1d and was not considered in [55] as these diagrams only become necessary when taking into account SU(3) flavour breaking effects. Note also, that these contributions first appear at NLO in QCD. The presence of the non-valence terms also forces us to expand our basis of operators to include the penguin operator defined in Eq.(5.2.2), which arises in renormalisation and thus mixes with the original basis under renormalisation group (RG) running. Details of the correlator renormalisation and the resulting structure of the renormalisation group equations (RGE) are presented in Appendix B.1. For the matrix elements of operators with a different light-quark flavour to that of the external meson state,

only these 'eye-contraction' diagrams contribute and so the sum-rule has the form,

$$\delta^{q'q}_{\tilde{\mathcal{O}}^{q'}}(\mu) = \frac{1}{A_{\mathcal{O}} F_q^4(\mu)} \int_0^{\omega_c} d\omega_1 d\omega_2 e^{\frac{\overline{\Lambda}_q - \omega_1}{t} + \frac{\overline{\Lambda}_q - \omega_2}{t}} \Delta_{\text{peng}} \rho^q_{\tilde{\mathcal{O}}^{q'}}(\omega_1, \omega_2) \tag{5.2.11}$$

In our analysis of the Bag parameters in B_s-mixing, the condensate contributions were taken from [152, 153]. However, for the analysis in this chapter we also present analytic results of our calculation of the non-factorisable condensate discontinuites. To distinguish these from the perturbative contribution, we therefore use the following notation,

$$\Delta_{\text{tree/peng}} \rho^q_{\tilde{\mathcal{O}}^{q'}}(\omega_1, \omega_2) = \Delta^{\text{pert}}_{\text{tree/peng}} \rho^q_{\tilde{\mathcal{O}}^{q'}}(\omega_1, \omega_2) + \Delta^{\text{cond}}_{\text{tree/peng}} \rho^q_{\tilde{\mathcal{O}}^{q'}}(\omega_1, \omega_2)\,, \tag{5.2.12}$$

where the tree contribution vanishes if $q \neq q'$. These are discussed in Section 5.2.3 and Section 5.2.4 respectively and we show the results of our calculations in Section 5.2.5.

5.2.3 Perturbative contributions

As already mentioned, the eye-contraction diagrams represent a new contribution, not previously calculated, to the sum rule analysis of the B_s lifetime matrix elements. However the procedure for calculating them is no different than for the standard tree-contraction terms and both are completely analogous to the calculation in B_s-mixing from Chapter 3. Therefore here we will only briefly summarise the approach and highlight the points where the two cases differ.

The amplitudes of the 3-loop processes were generated manually and the Dirac algebra was computed using `Tracer` [148], treating γ^5 in accordance with the Larin scheme [201]. Alternatively, the amplitudes were also generated using `QGRAF` [147] and the Dirac algebra computed using a private implementation in the 'NDR' scheme. We found full agreement between both computations. An IBP reduction with `FIRE5` [105] leads the same set of master integrals as found in B_s.

It became apparent in this work that when considering m_s corrections to eye-contractions terms, these contributions could only be treated consistently within the traditional sum rule approach and not with the weight function method. Therefore

in this analysis we explicitly evaluate the integral in Eq.(5.2.9) and Eq.(5.2.11). However, when applicable we compare the results of both methods and show that we find them to be consistent. This will be discussed further in Sections 5.2.5 and 5.3. Two notable consequences for our analysis result from the change to a traditional sum rule approach. The first is that when also using the HQET sum rule for the decay constant, the $\overline{\Lambda}_q$ dependence of the bag parameter drops out. Secondly, we gain an explicit dependence of the bag parameter on both the cut-off ω_c and the Borel parameter t. As discussed in Section 2.4, these parameters need to be fixed. In our implementation, this was done by comparing the HQET sum rules for F_q and $\overline{\Lambda}_q$ to values found in the literature (see Appendix B.3 for the details of this fit).

5.2.4 Condensate contributions

We also carried out an independent analysis of the condensate contributions, that have previously been determined for the massless case in [202, 203][1] for the Q_i and T_i operators, but not for Q_P. Whenever appropriate we compare our results with the literature in Section 5.2.5.

We use the standard approach of the background field technique in the Fock-Schwinger gauge (see Section 2.6). Since, in calculating the deviation of the bag parameters from their VSA values, we are only concerned with non-factorisable contributions, the only diagrams that need to be considered are those found in Fig. 5.2 along with their symmetric counterparts. These represent the only condensate corrections up to dimension-6 and leading order in α_s, assuming that the quark condensate factorises and thus leads to no correction to the non-factorisable contribution.

With regards to the non-valence terms, there is no dimension three quark condensate contribution at the leading order in α_s from the diagrams in Fig. 5.3. The left diagram vanishes because the quark condensate flips the chirality and the Dirac struc-

[1] In the paper by Baek *et al.* [203], Eq.(20) yields an additional factor of 4 for ϵ_1 compared to the expression found in Eq.(11) of the same paper.

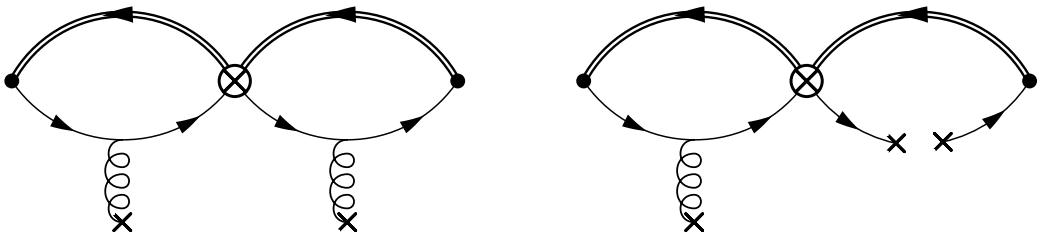

Figure 5.2: Condensate corrections corresponding to $\langle \frac{\alpha_s}{4\pi} GG \rangle$ and $\langle g_s \bar{q} \sigma_{\mu\nu} G^{\mu\nu} q \rangle$ respectively.

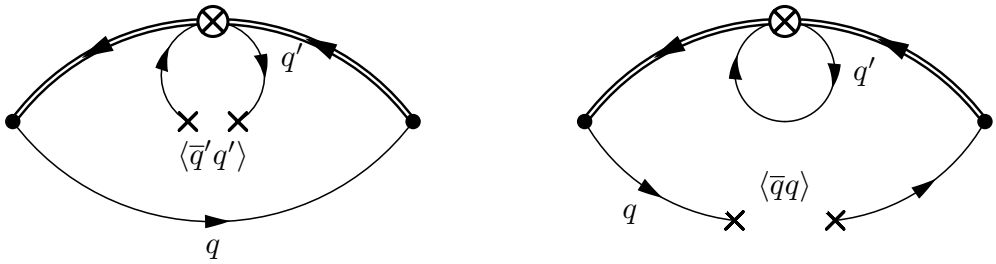

Figure 5.3: Quark condensate contributions to the eye contractions at leading order in α_s.

ture $\Gamma_1 \langle \bar{q}' q' \rangle \Gamma_2$ vanishes for all the combinations of currents $\Gamma_{1,2}$ appearing in the considered operators. The $\langle \bar{q}' q' \rangle$ condensate is therefore suppressed by an additional $\alpha_s m_{q'} / \overline{\Lambda}$. The right diagram is scaleless. The $\langle \bar{q} q \rangle$ condensate is therefore suppressed by at least an extra α_s. There is also no dimension four gluon condensate $\langle \alpha_s G^2 \rangle$ contribution at leading order in α_s because the penguin loop is scaleless without an extra gluon. Similar arguments lead us to conclude that the dimension five quark gluon condensate $\langle \bar{q}^{(')} \sigma_{\mu\nu} G^{\mu\nu} q^{(')} \rangle$ and the dimension six quark condensate $\langle \bar{q}' q' \bar{q} q \rangle$[1] do not contribute at leading order in α_s. Therefore, condensate contributions to the eye-contractions are suppressed with respect to the perturbative contribution at first order in the strong coupling and are not taken into account.

[1] If $q' = q$ this does not vanish, but is part of the factorisable contribution.

5.2.5 Analytic results

In this section we present the analytic expressions of our calculation. Beginning with the perturbative contribution, the double discontinuities defined in Eq.(5.2.10) can be expressed in terms of their m_s (generally denoted as m_q below) expansion as,

$$\Delta^{\rm pert}_{\rm tree}\rho^{q}_{\tilde{\mathcal{O}}^q}(\omega_1,\omega_2) \equiv \frac{N_c C_F}{4}\frac{\omega_1^2\omega_2^2}{\pi^4}\frac{\alpha_s}{4\pi}\Bigg[r^{(0)}_{\tilde{\mathcal{O}}}(x,L_\omega) + \left(\frac{m_q}{\omega_1}+\frac{m_q}{\omega_2}\right) r^{(1)}_{\tilde{\mathcal{O}}}(x,L_\omega) + \left(\frac{m_q^2}{\omega_1^2}+\frac{m_q^2}{\omega_2^2}\right) r^{(2)}_{\tilde{\mathcal{O}}}(x,L_\omega) + \dots\Bigg]\theta(\omega_1-m_q)\theta(\omega_2-m_q), \tag{5.2.13}$$

for $x=\omega_2/\omega_1$ and $L_\omega = \ln(\mu^2/(4\omega_1\omega_2))$.

The non-factorisable tree contributions for the colour singlet operators at order α_s have a vanishing color factor, yielding $r^{(j)}_{\tilde{Q}_i}=0$. In the massless limit it was found [55]

$$\begin{aligned} r^{(0)}_{\tilde{T}_1} &= -8+\frac{a_1}{8}+\frac{2\pi^2}{3}-\frac{3}{2}L_\omega-\frac{1}{4}\phi(x)\,,\\ r^{(0)}_{\tilde{T}_2} &= -\frac{29}{4}+\frac{a_2}{8}+\frac{2\pi^2}{3}-\frac{3}{2}L_\omega-\frac{1}{4}\phi(x)\,, \end{aligned} \tag{5.2.14}$$

and now we consider also

$$r^{(0)}_{\tilde{Q}_P} = \frac{1}{8N_c}\left[-30+\frac{8\pi^2}{3}-6L_\omega-\phi(x)\right], \tag{5.2.15}$$

for the penguin operator, where

$$\phi(x) = \begin{cases} x^2-8x+6\ln(x), & x\le 1,\\ \frac{1}{x^2}-\frac{8}{x}-6\ln(x), & x>1. \end{cases} \tag{5.2.16}$$

The linear terms in the strange quark mass read

$$\begin{aligned} r^{(1)}_{\tilde{T}_1} &= \frac{a_1}{8}+\frac{2\pi^2}{3}-\frac{3}{2}L_\omega-\begin{cases} \frac{2(36+9x+x^2)}{9(1+x)}+\frac{9+9x-2x^2}{6(1+x)}\ln(x), & x\le 1,\\ \frac{2(1+9x+36x^2)}{9x(1+x)}+\frac{2-9x-9x^2}{6x(1+x)}\ln(x), & x>1, \end{cases}\\ r^{(1)}_{\tilde{T}_2} &= \frac{a_2}{8}+\frac{2\pi^2}{3}-\frac{3}{2}L_\omega+\begin{cases} -\frac{29+11x-2x^2}{4(1+x)}-\frac{3}{2}\ln(x), & x\le 1,\\ \frac{2-11x-29x^2}{4x(1+x)}+\frac{3}{2}\ln(x), & x>1, \end{cases} \end{aligned} \tag{5.2.17}$$

$$r^{(1)}_{\tilde{Q}_P} = \frac{1}{36N_c}\Bigg[-12\pi^2 + 27L_\omega + \begin{cases} \frac{135+81x-22x^2}{1+x} + \frac{3(9+9x+2x^2)}{1+x}\ln(x), & x \le 1, \\ -\frac{22-81x-135x^2}{x(1+x)} - \frac{3(2+9x+9x^2)}{x(1+x)}\ln(x), & x > 1, \end{cases}\Bigg]$$

and for the corrections quadratic in m_s we find

$$r^{(2)}_{\tilde{T}_1} = \frac{1}{1+x^2}\Bigg[-\frac{(1-x)^2 a_1}{16} + \frac{3(1-x)^2}{4}L_\omega - \frac{x}{4}\psi(x)\left(1+\frac{3(1+x)}{1-x}\ln(x)\right)$$
$$+\begin{cases} \frac{\pi^2(1+8x-5x^2)}{12} + \frac{24-48x+16x^2+x^3}{6} + \frac{1+x^2}{2}\ln(x) & \\ +\frac{1-x^2}{2}\ln^2(x) + \frac{5(1-x^2)}{2}\mathrm{Li}_2\left(1-\frac{1}{x}\right), & x \le 1, \\ & \\ \frac{\pi^2(-5+8x+x^2)}{12} + \frac{1+16x-48x^2+24x^3}{6x} - \frac{1+x^2}{2}\ln(x) & \\ -\frac{1-x^2}{2}\ln^2(x) - \frac{5(1-x^2)}{2}\mathrm{Li}_2(1-x), & x > 1, \end{cases},$$

$$r^{(2)}_{\tilde{T}_2} = \frac{1}{1+x^2}\Bigg[-\frac{a_2(1-x)^2}{16} - \frac{\pi^2(1-4x+x^2)}{6} + \frac{3(1-x)^2}{4}L_\omega$$
$$+\frac{29-62x+29x^2}{8} - \frac{x}{2}\psi(x)\left(1+\frac{1+x}{1-x}\ln(x)\right)$$
$$+\begin{cases} \frac{(1-x)^2}{4}\ln(x) + (1-x^2)\mathrm{Li}_2\left(1-\frac{1}{x}\right), & x \le 1, \\ -\frac{(1-x)^2}{4}\ln(x) - (1-x^2)\mathrm{Li}_2\left(1-x\right), & x > 1, \end{cases}\Bigg], \tag{5.2.18}$$

$$r^{(2)}_{\tilde{Q}_P} = \frac{1}{24N_c(1+x^2)}\Bigg[9(1-x)^2 L_\omega - 9x\psi(x)\left(1+\frac{1+x}{3(1-x)}\ln(x)\right)$$
$$+\begin{cases} 45-102x+61x^2-2x^3-(5-8x-x^2)\pi^2 - 12x\ln(x) & \\ -6(1-x^2)\ln^2(x) - 6(1-x^2)\mathrm{Li}_2\left(1-\frac{1}{x}\right), & x \le 1, \\ & \\ -\frac{2-61x+102x-45x^3}{x} + (1+8x-5x^2)\pi^2 + 12x\ln(x) & \\ +6(1-x^2)\ln^2(x) + 6(1-x^2)\mathrm{Li}_2\left(1-x\right), & x > 1, \end{cases}\Bigg]$$

with

$$\psi(x) = \begin{cases} \frac{(1-x)^2}{x}\left[2\ln(1-x) - \ln(x)\right], & x \le 1, \\ \frac{(1-x)^2}{x}\left[2\ln(x-1) - \ln(x)\right], & x > 1. \end{cases} \tag{5.2.19}$$

The perturbative contribution to the double discontinuities of the eye-contractions, defined in Eq.(5.2.10), can be expressed in terms of their m_s (generally denoted as m_q and $m_{q'}$ below) expansion as

$$\begin{aligned}\Delta^{\text{pert}}_{\text{peng}}\rho^{q}_{\tilde{\mathcal{O}}^{q'}}(\omega_1,\omega_2) \equiv \frac{N_c C_F}{4}\frac{\omega_1^2\omega_2^2}{\pi^4}\frac{\alpha_s}{4\pi}\Bigg[& s^{(0)}_{\tilde{\mathcal{O}}}(x,L_\omega) + \left(\frac{m_q}{\omega_1}+\frac{m_q}{\omega_2}\right) s^{(1)}_{\tilde{\mathcal{O}}}(x,L_\omega) \\ &+ \left(\frac{1}{\omega_1^2}+\frac{1}{\omega_2^2}\right)\left[m_q^2 s^{(2)}_{\tilde{\mathcal{O}}}(x,L_\omega) + m_{q'}^2 t^{(2)}_{\tilde{\mathcal{O}}}(x,L_\omega)\right] + \dots\Bigg] \\ &\times \theta(\omega_1-m_q)\theta(\omega_2-m_q). \end{aligned} \tag{5.2.20}$$

For the non-valence expression Eq.(5.2.20), $s^{(i)}_{\tilde{\mathcal{O}}}$ corresponds to m_s corrections of order i stemming from a non-zero q quark mass (see Fig.5.1), whereas m_s corrections attributed to the q' quark are contained within the $t^{(2)}_{\tilde{\mathcal{O}}}$ term. It is also worth noting that there is no $t^{(1)}_{\tilde{\mathcal{O}}}$ in Eq.(5.2.20) since the double discontinuity evaluates to zero.

At the considered order the eye contributions for the color singlet and octet operators differ only by their color factors

$$s^{(j)}_{\tilde{T}_i} = \frac{-1}{2N_c}\, s^{(j)}_{\tilde{Q}_i}, \qquad t^{(2)}_{\tilde{T}_i} = \frac{-1}{2N_c}\, t^{(2)}_{\tilde{Q}_i}. \tag{5.2.21}$$

Our results for the singlet and penguin operators are in the massless case

$$\begin{aligned} s^{(0)}_{\tilde{Q}_1} &= \frac{20}{9}+\frac{2}{3}L_\omega+\frac{1}{9}\phi(x), \\ s^{(0)}_{\tilde{Q}_2} &= -\frac{13}{9}-\frac{1}{3}L_\omega-\frac{1}{18}\phi(x), \\ s^{(0)}_{\tilde{Q}_P} &= \frac{13}{9}+\frac{1}{3}L_\omega+\frac{1}{18}\phi(x). \end{aligned} \tag{5.2.22}$$

The corrections proportional to the strange quark mass read

$$s^{(1)}_{\tilde{Q}_1} = \frac{2}{3}L_\omega + \begin{cases} \frac{2(10+x-x^2)}{9(1+x)} + \frac{2}{3}\ln(x), & x\le 1, \\ -\frac{2(1-x-10x^2)}{9x(1+x)} - \frac{2}{3}\ln(x), & x>1, \end{cases},$$

$$s^{(1)}_{\tilde{Q}_2} = -\frac{1}{3}L_\omega + \begin{cases} -\frac{13+4x-x^2}{9(1+x)} - \frac{1}{3}\ln(x), & x\le 1, \\ \frac{1-4x-13x^2}{9x(1+x)} + \frac{1}{3}\ln(x), & x>1, \end{cases},$$

$$s^{(1)}_{\tilde{Q}_P} = -\frac{1}{3}L_\omega + \begin{cases} -\frac{13+4x-x^2}{9(1+x)} - \frac{1}{3}\ln(x), & x \leq 1, \\ \frac{1-4x-13x^2}{9x(1+x)} + \frac{1}{3}\ln(x), & x > 1, \end{cases} \tag{5.2.23}$$

while the corrections quadratic in m_s are given by

$$\begin{aligned}
s^{(2)}_{\tilde{Q}_1} &= \frac{1}{1+x^2}\left[-\frac{10(1-x)^2}{9} - \frac{(1-x)^2}{3}L_\omega + \frac{x}{3}\psi(x)\right], \\
s^{(2)}_{\tilde{Q}_2} &= \frac{1}{1+x^2}\left[\frac{13(1-x)^2}{18} + \frac{(1-x)^2}{6}L_\omega - \frac{x}{6}\psi(x)\right], \\
s^{(2)}_{\tilde{Q}_P} &= \frac{1}{1+x^2}\left[-\frac{13(1-x)^2}{18} - \frac{(1-x)^2}{6}L_\omega + \frac{x}{6}\psi(x)\right], \qquad (5.2.24) \\
t^{(2)}_{\tilde{Q}_1} &= \frac{1}{1+x^2}\left[\frac{2x^2}{(1-x)^2}\psi(x) - \begin{cases} 2x^2 - 2x\ln(x), & x \leq 1, \\ 2 + 2x\ln(x), & x > 1, \end{cases}\right], \\
t^{(2)}_{\tilde{Q}_2} &= \frac{1}{1+x^2}\left[-\frac{x^2}{(1-x)^2}\psi(x) + \begin{cases} x^2 - x\ln(x), & x \leq 1, \\ 1 + x\ln(x), & x > 1, \end{cases}\right], \\
t^{(2)}_{\tilde{Q}_P} &= \frac{1}{1+x^2}\left[\frac{x^2}{(1-x)^2}\psi(x) - \begin{cases} x^2 - x\ln(x), & x \leq 1, \\ 1 + x\ln(x), & x > 1, \end{cases}\right]. \qquad (5.2.25)
\end{aligned}$$

It can be clearly seen from Eq.(5.2.25) that the expressions for $t^{(2)}_{\mathcal{O}}$ logarithmically diverge at the point $x = 1$. For this reason, the weight function method is not applicable here since it requires the discontinuity $t^{(2)}_{\mathcal{O}}$ to be directly evaluated at the point $\omega_1 = \omega_2 = \overline{\Lambda}_s$. We briefly discuss the origin of this divergence in Appendix B.2. For the condensates, we find the following expressions up to contributions of dimension six:

$$\begin{aligned}
\Delta^{\text{cond}}_{\text{tree}}\rho^q_{\tilde{Q}^q_i}(\omega_1,\omega_2) &= 0 + \dots, \\
\Delta^{\text{cond}}_{\text{tree}}\rho^q_{\tilde{T}^q_1}(\omega_1,\omega_2) &= -\frac{\left\langle \frac{\alpha_s}{\pi}G^2\right\rangle}{64\pi^2}\left(1 + \frac{m_s}{\omega_1} + \frac{m_s}{\omega_2}\right)\theta(\omega_1 - m_s)\,\theta(\omega_2 - m_s) \\
&\quad + \frac{\left\langle g_s\bar{q}\sigma_{\mu\nu}G^{\mu\nu}q\right\rangle}{64\pi^2}\left[\delta(\omega_1)\,\theta(\omega_2 - m_s) + \delta(\omega_2)\,\theta(\omega_1 - m_s)\right] + \dots, \\
\Delta^{\text{cond}}_{\text{tree}}\rho^q_{\tilde{T}^q_2}(\omega_1,\omega_2) &= 0 + \dots,
\end{aligned} \tag{5.2.26}$$

$$\Delta^{\rm cond}_{\rm tree}\rho^{q}_{\tilde{Q}^{q}_{P}}(\omega_1,\omega_2) = \frac{\left\langle\frac{\alpha_s}{\pi}G^2\right\rangle}{384\pi^2}\left(1+\frac{m_s}{\omega_1}+\frac{m_s}{\omega_2}\right)\theta(\omega_1-m_s)\,\theta(\omega_2-m_s) - \frac{\left\langle g_s\bar{q}\sigma_{\mu\nu}G^{\mu\nu}q\right\rangle}{384\pi^2}\left[\delta(\omega_1)\,\theta(\omega_2-m_s)+\delta(\omega_2)\,\theta(\omega_1-m_s)\right]+\dots\,,$$

from which only the bag parameters ϵ_1 and B_P receive non-vanishing contributions, while

$$\Delta^{\rm cond}_{\rm peng}\rho^{q}_{\tilde{Q}^{q'}_{i}}(\omega_1,\omega_2) = 0+\dots\,, \tag{5.2.27}$$

as discussed above and therefore there are no condensate corrections to the δs at this order. Considering the case $m_s = 0$ we find perfect agreement with the results found in [202][1]. The analysis by [203] chooses instead an axial-vector interpolating current, $\overline{q}\gamma_\alpha\gamma^5 h$, and therefore their results differ from our own in addition to the inconsistency mentioned in Section 5.2.4. As pointed out in [202], this choice means that states of quantum number $J^P = 1^+$ are also being considered by the correlation function.

5.3 Results

For our numerical analysis, the continuum cut-off ω_c, and the Borel parameter t are fixed for the cases of the B_d (because of isospin in our analysis $B_u = B_d$) and B_s mesons separately through a sum rule analysis of their respective decay constants and mass differences. From this analysis we find,

$$B_d: \quad w_c = 0.90\,\text{GeV}, \quad t = 1\,\text{GeV}, \tag{5.3.1}$$

$$B_s: \quad w_c = 0.95\,\text{GeV}, \quad t = 1\,\text{GeV}. \tag{5.3.2}$$

We evaluate the sum rules for the HQET bag parameters at the scale $\mu = 1.5\,\text{GeV}$. For the strange quark mass, we use the $\overline{\rm MS}$ scheme value at the scale $\mu = 1.5\,\text{GeV}$ after running [204] from $\overline{m_s}(2\text{GeV}) = 95^{+9}_{-3}\,\text{MeV}$. As in the analysis of [1], we expand

[1] The additional factor of 4 appearing in Eq.(3.24) of [202] is accounted for by their choice of operator normalisation.

$\overline{m_s}(2\text{GeV})$	95^{+9}_{-3}	MeV	[206]
$\langle \frac{\alpha_s}{\pi} G^2 \rangle$	0.012 ± 0.006	GeV^4	[207]
$\langle \bar{d}d \rangle(2\text{GeV})$	$(-0.283 \pm 0.002)^3$	GeV^3	[154]
$\langle \bar{s}s \rangle(2\text{GeV})$	$(-0.296 \pm 0.002)^3$	GeV^3	[155]
$\overline{m_b}(\overline{m_b})$	$4.203^{+0.016}_{-0.034}$	GeV	[208, 209]
M_Z	91.1876	GeV	[169]
$\alpha_s(M_Z)$	0.1181 ± 0.0011		[169]

Table 5.2: Values of input parameter used in our numerical analysis.

the range of uncertainty to $95 \pm 30\,\text{MeV}$ in order to account for the missing terms after our truncation of the m_s expansion and scheme dependencies. After inspecting the range of stability in the HQET sum rules of $F_{d/s}$ and $\overline{\Lambda}$, we chose to vary t by ± 0.4 and to vary ω_c by ± 0.2 in our error analysis. The uncertainty associated with the sum rule scale is estimated by varying μ between 1-2 GeV, running back to the central value of 1.5 GeV and then scaling[1] the resulting uncertainty by a factor of 2. The inputs for the other parameters used in this analysis can be found listed in Table 5.2, which includes the numerical input of the condensates quoted at the scale 2 GeV.

We use the relation, $\left\langle g_s \bar{q} \sigma_{\mu\nu} G^{\mu\nu} q \right\rangle = m_0^2 \langle \bar{q} q \rangle$ at the scale 2 GeV with $m_0^2 = 0.8\,\text{GeV}^2$ [205] in order to determine the value of the mixed quark-gluon condensate. The renormalisation group equations describing the running of the condensates down to the sum rule scale can be found in Appendix B.3. In our analysis, a more conservative estimate for their individual uncertainties of $\pm 30\%$ was chosen over the values quoted in Table 5.2 in order to account for the accuracy in m_0^2.

Our numerical results for the bag parameters B_i, ϵ_i and B_P for the B^d and B^s systems can be found in Table 5.3 and Table 5.4 respectively, where the total estimated uncertainty is denoted by α. The contribution to the uncertainty associated

[1] We believe this treatment is justified given the usual procedure of varying between $[\mu/2, 2\mu]$ is not practical at such low scales, and so re-scale the uncertainty in order to compensate for this limitation.

B_i^d	TSR	α	$\mathcal{O}(m_d^0)$	$\mathcal{O}(m_d^1)$	$\mathcal{O}(m_d^2)$	α_μ	α_P
B_1^d	1.0026	$^{+0.0198}_{-0.0106}$	1.0026	–	–	$^{+0.0197}_{-0.0105}$	$^{+0.0005}_{-0.0007}$
B_2^d	0.9982	$^{+0.0052}_{-0.0066}$	0.9982	–	–	$^{+0.0051}_{-0.0066}$	$^{+0.0005}_{-0.0004}$
ϵ_1^d	−0.0165	$^{+0.0209}_{-0.0346}$	−0.0165	–	–	$^{+0.0191}_{-0.0310}$	$^{+0.0084}_{-0.0153}$
ϵ_2^d	−0.0004	$^{+0.0200}_{-0.0326}$	−0.0004	–	–	$^{+0.0200}_{-0.0326}$	$^{+0.0010}_{-0.0006}$
B_P^d	0.9807	$^{+0.0072}_{-0.0119}$	0.9807	–	–	$^{+0.0053}_{-0.0077}$	$^{+0.0049}_{-0.0091}$

Table 5.3: Bag parameter results for the B_d system using the traditional sum rule 'TSR'.

with variations of the sum rule scale is denoted by α_μ, whereas α_P represents the combined parametric uncertainty of m_s, the Borel parameter, the sum rule cut-off, and the condensates. We stress again that these parameters are taken in the strict HQET limit $m_b \to \infty$ and therefore we do not quote an uncertainty associated with $1/m_b$ corrections.

Evidently, the dominant source of uncertainty arises from scale variations. The parametric uncertainty seems negligible in comparison, with the exception of ϵ_1 and B_P. Unlike the other bag parameters, these receive non-vanishing condensate contributions (see Eq.(5.2.27)) and as a consequence are found to have a greater dependence on the cut-off ω_c and are sensitive to the numerical input of the condensates themselves. Additionally, we found dependence on the Borel parameter to be weak in our analysis[1].

We observe strong convergence of the m_s expansion which suggests that we can again be confident in the validity of the 'expansion by regions' method and it clearly indicates that working up to order m_s^2 is sufficient. Numerical differences between the $\mathcal{O}(m_s^0)$ term of the B^s bag parameters and those of B^d come from 3 sources: different input for the condensates, the lower cut of the sum rule integral (see Eq.(5.2.9) and Eq.(5.2.11)), and a different value of the decay constant in the denominator since

[1] As was also found to be the case in [202].

B_i^s	TSR	α	$\mathcal{O}(m_s^0)$	$\mathcal{O}(m_s^1)$	$\mathcal{O}(m_s^2)$	α_μ	α_P
B_1^s	1.0022	$^{+0.0185}_{-0.0099}$	1.0019	0.0006	−0.0003	$^{+0.0185}_{-0.0099}$	$^{+0.0004}_{-0.0005}$
B_2^s	0.9983	$^{+0.0052}_{-0.0067}$	0.9986	−0.0004	0.0001	$^{+0.0052}_{-0.0067}$	$^{+0.0004}_{-0.0003}$
ϵ_1^s	−0.0104	$^{+0.0202}_{-0.0330}$	−0.0097	−0.0008	0.0002	$^{+0.0195}_{-0.0319}$	$^{+0.0051}_{-0.0084}$
ϵ_2^s	0.0001	$^{+0.0199}_{-0.0324}$	−0.0001	0.0002	0.0001	$^{+0.0199}_{-0.0324}$	$^{+0.0010}_{-0.0008}$
B_P^s	0.9895	$^{+0.0053}_{-0.0077}$	0.9873	0.0016	0.0006	$^{+0.0043}_{-0.0059}$	$^{+0.0031}_{-0.0050}$

Table 5.4: Bag parameter results for the B_s system using the traditional sum rule 'TSR'.

δ_i^{ud}	TSR	α	$\mathcal{O}(m_d^0)$	$\mathcal{O}(m_d^1)$	$\mathcal{O}(m_d^2)$	α_μ	α_P
δ_1^{ud}	0.0026	$^{+0.0142}_{-0.0092}$	0.0026	–	–	$^{+0.0142}_{-0.0092}$	$^{+0.0005}_{-0.0007}$
δ_2^{ud}	−0.0018	$^{+0.0047}_{-0.0072}$	−0.0018	–	–	$^{+0.0046}_{-0.0071}$	$^{+0.0005}_{-0.0004}$
δ_3^{ud}	−0.0004	$^{+0.0015}_{-0.0024}$	−0.0004	–	–	$^{+0.0015}_{-0.0024}$	$^{+0.0001}_{-0.0001}$
δ_4^{ud}	0.0003	$^{+0.0012}_{-0.0008}$	0.0003	–	–	$^{+0.0012}_{-0.0008}$	$^{+0.0001}_{-0.0001}$
δ_P^{ud}	−0.0083	$^{+0.0209}_{-0.0322}$	−0.0083	–	–	$^{+0.0208}_{-0.0322}$	$^{+0.0025}_{-0.0017}$

Table 5.5: Non-valence bag parameters for the case $q = q' = u, d$ (note $\delta^{ud} = \delta^{du}$) using the traditional sum rule 'TSR'.

we do not expand the ratio in m_s.

At NLO in α_s, the only contribution to the bag parameters of the colour singlet operators comes from eye-contraction diagrams and therefore the deviation from their VSA value is suppressed in comparison to the bag parameters for the colour octet and penguin operators.

Our numerical findings for the non-valence bag parameters are presented in Tables 5.5-5.7. Again no significant shift away from the VSA values was found. Additionally, flavour breaking effects in the form of m_s corrections are small. The first non-vanishing corrections from the strange quark mass in the operator of an eye contraction diagram appear at $\mathcal{O}(m_s^2)$. This corresponds with the results for δ_i^{sd} shown in Table 5.7.

The plots in Fig. 5.4 show the dependence of the colour octet and penguin bag

δ_i^{ds}	TSR	α	$\mathcal{O}(m_s^0)$	$\mathcal{O}(m_s^1)$	$\mathcal{O}(m_s^2)$	α_μ	α_P
δ_1^{ds}	0.0025	$^{+0.0144}_{-0.0093}$	0.0019	0.0006	−0.0000	$^{+0.0144}_{-0.0093}$	$^{+0.0004}_{-0.0005}$
δ_2^{ds}	−0.0018	$^{+0.0047}_{-0.0072}$	−0.0014	−0.0004	0.0000	$^{+0.0047}_{-0.0072}$	$^{+0.0004}_{-0.0003}$
δ_3^{ds}	−0.0004	$^{+0.0015}_{-0.0024}$	−0.0003	−0.0001	0.0000	$^{+0.0015}_{-0.0024}$	$^{+0.0001}_{-0.0001}$
δ_4^{ds}	0.0003	$^{+0.0012}_{-0.0008}$	0.0002	0.0001	−0.0000	$^{+0.0012}_{-0.0008}$	$^{+0.0001}_{-0.0001}$
δ_P^{ds}	−0.0041	$^{+0.0217}_{-0.0338}$	−0.0062	0.0020	0.0001	$^{+0.0217}_{-0.0338}$	$^{+0.0018}_{-0.0015}$

Table 5.6: Non-valence bag parameters with a strange spectator quark using the traditional sum rule 'TSR'.

δ_i^{sd}	TSR	α	$\mathcal{O}(m_s^0)$	$\mathcal{O}(m_s^1)$	$\mathcal{O}(m_s^2)$	α_μ	α_P
δ_1^{sd}	0.0023	$^{+0.0140}_{-0.0091}$	0.0026	–	−0.0004	$^{+0.0140}_{-0.0090}$	$^{+0.0005}_{-0.0007}$
δ_2^{sd}	−0.0017	$^{+0.0046}_{-0.0070}$	−0.0018	–	0.0002	$^{+0.0046}_{-0.0070}$	$^{+0.0006}_{-0.0004}$
δ_3^{sd}	−0.0004	$^{+0.0015}_{-0.0023}$	−0.0004	–	0.0001	$^{+0.0015}_{-0.0023}$	$^{+0.0001}_{-0.0001}$
δ_4^{sd}	0.0003	$^{+0.0012}_{-0.0008}$	0.0003	–	−0.0000	$^{+0.0012}_{-0.0008}$	$^{+0.0001}_{-0.0001}$
δ_P^{sd}	−0.0074	$^{+0.0207}_{-0.0316}$	−0.0083	–	0.0008	$^{+0.0205}_{-0.0315}$	$^{+0.0025}_{-0.0017}$

Table 5.7: Non-valence bag parameters considering a strange light quark in the operator using the traditional sum rule 'TSR'.

parameters on the sum rule scale and the continuum cutoff for the B_d meson as calculated using the traditional sum rule method. Also indicated on the plots is an alternative result for which the perturbative tree contribution has been evaluated using the weight function analysis[1]. Comparing the two methods we observe that the predictions lie within the range of uncertainties of each other and therefore demonstrate a sound level of consistency which provides us with further confidence in the validity of the results presented in this chapter.

Finally we can compare our results with other sum rule analyses of the bag parameters that are available in the literature. The treatment in [202] shows several key differences compared to ours: in that study, the necessary tools to calculate the dominant perturbative 3-loop non-factorisable contributions shown in Fig. 5.1 were not yet available. However, additional non-factorisable effects do arise from their procedure for extracting the continuum cut-off, which in their case is not treated as common between the 3-point and 2-point correlators. The main result of that paper is quoted at the scale m_b, for which there is significant mixing between the bag parameters after running from the hadronic scale. It should also be noted that their results differ from our own by a factor of $F^2(m_b)/F^2(\mu)$ due to different conventions in our definition of the matrix elements, (see Eq.(5.2.3)).

The latest preliminary estimates of the lifetime bag parameters with lattice QCD were obtained 20 years ago in [194] and so an updated analysis would be greatly appreciated. Comparing those values to our own we find a similar degree of precision for the ϵ_i parameters, while our predictions for the B_i have a much smaller range of uncertainty and we disagree with the low value quoted for B_2.

[1] The corresponding plots for the colour singlet bag parameters have been omitted since they do not receive contributions from tree contraction terms.

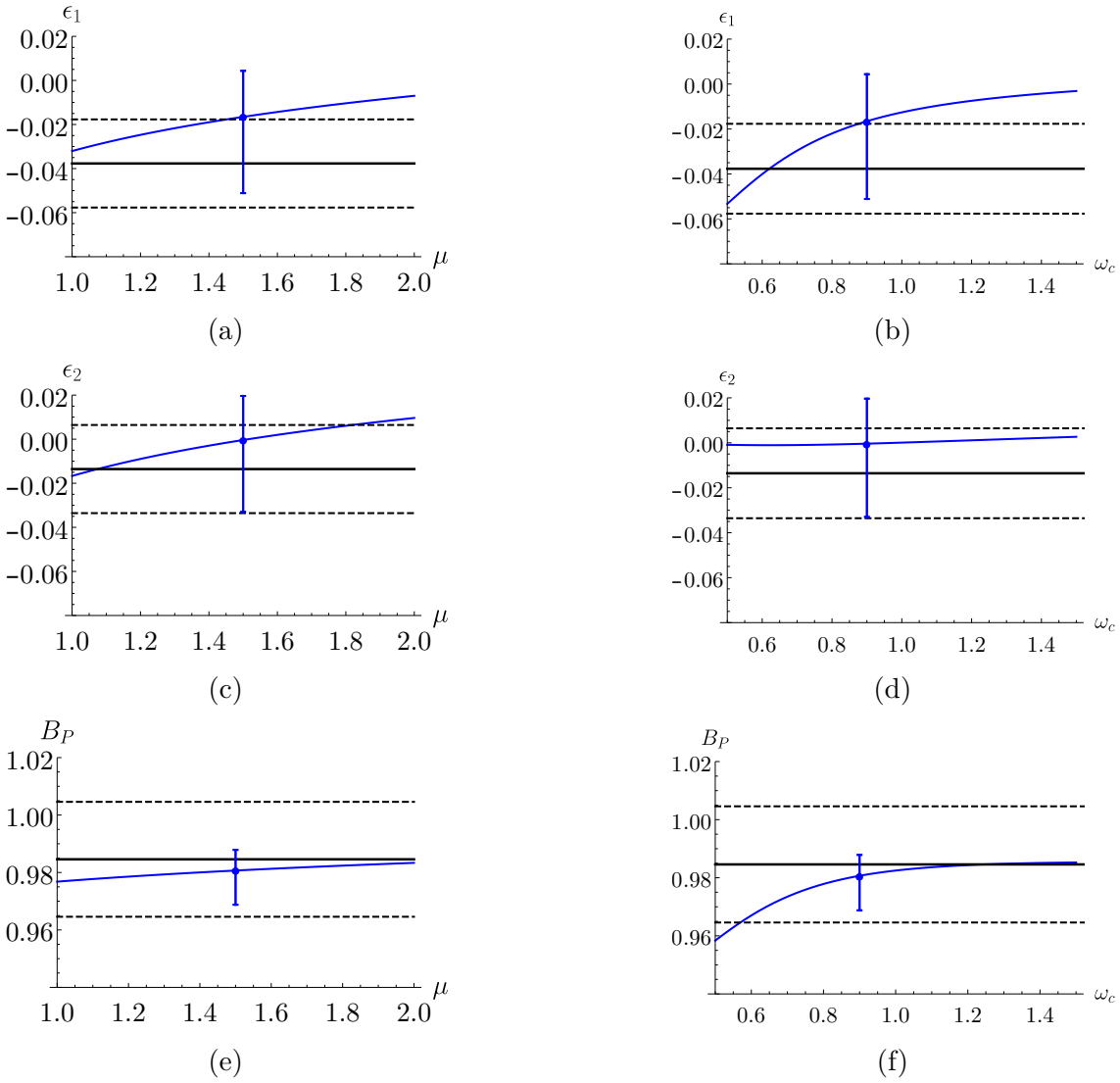

Figure 5.4: Comparison of the weight function method (shown in black) to the traditional sum rule approach (shown in blue) for the case of a B_d meson. The plots illustrate how the traditional result varies with respect to μ and ω_c on the left and right respectively. The dashed lines indicate the range of uncertainty in the weight function result, being set to ± 0.02. The blue vertical line indicates our final quoted error for the traditional sum rule method.

5.4 Summary

In this chapter, we have presented an updated sum rule analysis of the $\Delta B = 0$ bag parameters in the HQET limit which includes SU(3) flavour breaking effects for the first time, employing the expansion by regions approach. The presence of the eye-contraction diagrams and the mixing between operators of different dimensions in full QCD however poses an additional challenge. For this reason, we worked exclusively in HQET where no such mixing occurs. Consequently, the results presented here are also applicable to the $\Delta D = 0$ matrix elements and will be used in Chapter 6. Furthermore, taking this limit leads us to find relatively small uncertainties for the bag parameters themselves since all $1/m_Q$ corrections reside in $\tilde{\Gamma}_7$ of Eq.(5.1.1).

The eye contractions are first addressed in this work and also lead to a number of new effects. Firstly, their renormalization requires that the penguin operator Q_P be included in our operator basis. Additionally, since the light-quarks q' in the operators are not contracted with the light valence quarks q in the mesons, they generate non-valence matrix elements $\delta_i^{q'q}$ for $q \neq q'$. It was also found that the weight-function method we employed in our B-mixing analysis cannot be used with the non-valence matrix elements due to logarithmic divergences whose origin is discussed in Appendix B.2. Therefore, we adopted the traditional sum rule approach where the Borel parameter and the continuum cutoff are varied in our analysis. We note however that we obtain good consistency between the two methods when they are applied to the tree contractions as shown in Figure 5.4.

Numerically, we find that deviations from the VSA at the hadronic scale are generally small. The $\mathcal{O}(1)$ uncertainties in the sum rule for the deviations are therefore quite small in absolute terms and sufficient for a phenomenological analysis of the $\tau(B_s)/\tau(B_d)$ lifetime ratio.

Chapter 6

Charm Lifetime Analysis

6.1 Introduction

In the previous chapter we stressed that since our analysis of the bag parameters was done in the HQET limit that they are applicable to both the B and D systems. In the following we put these results to use by presenting an analysis of inclusive charm decays. The lifetimes of charm mesons are determined experimentally very precisely [169] [2] and show a pattern which is clearly less monotonous than in the b-sector, with values spreading over a rather large range. Moreover, inclusive semileptonic branching fractions have also been measured [169], and recently an update for the D_s^+-meson has been released by the BESIII Collaboration [210]. A summary of the current experimental status is presented in Table 6.1. While in the bottom sector, the approximation that the meson decay can be described in terms of the free b-quark decay is experimentally well accommodated, for the charm system this is poorly justified. A systematic way to study this assumption is provided by the HQE (see Section 2.1), according to which the inclusive decay width of a meson

[2] New results from Belle II have recently been published [199]: $\tau(D^0) = 410.5 \pm 1.1 \pm 0.8$ fs, $\tau(D^+) = 1030.4 \pm 4.7 \pm 3.1$ fs.

	D^0	D^+	D_s^+
τ [ps]	0.4101(15)	1.040(7)	0.504(4)
Γ [ps^{-1}]	2.44(1)	0.96(1)	1.98(2)
$\tau(D_q)/\tau(D^0)$	1	2.54(2)	1.20(1)
$\mathrm{Br}(D_q \to X e^+ \nu_e)$[%]	6.49(11)	16.07(30)	6.30(16)
$\frac{\Gamma(D_q \to X e^+ \nu_e)}{\Gamma(D^0 \to X e^+ \nu_e)}$	1	0.977(26)	0.790(26)

Table 6.1: Status of the experimental determinations of the lifetime and the semileptonic branching fractions of the lightest charmed mesons ($D_q \in \left\{D^0, D^+, D_s^+\right\}$). All values are taken from the PDG [169] apart from the semileptonic D_s^+-meson decays which were recently measured by the BESIII Collaboration [210].

containing a heavy charm quark can be written as

$$\Gamma(D) = \Gamma_3 + \Gamma_5 \frac{\langle \mathcal{O}_5 \rangle}{m_c^2} + \Gamma_6 \frac{\langle \mathcal{O}_6 \rangle}{m_c^3} + ... + 16\pi^2 \left(\tilde{\Gamma}_6 \frac{\langle \tilde{\mathcal{O}}_6 \rangle}{m_c^3} + \tilde{\Gamma}_7 \frac{\langle \tilde{\mathcal{O}}_7 \rangle}{m_c^4} + ... \right), \qquad (6.1.1)$$

with the matrix element of the $\Delta C = 0$ operators given by $\langle \mathcal{O}_Y \rangle = \langle D|\mathcal{O}_Y|D\rangle/(2m_D)$. Their numerical size is expected to be of the order of the hadronic scale $\Lambda_{\mathrm{QCD}} \leq 1$ GeV, but the actual value must be determined with a non-perturbative calculation. Note that in Eq. (6.1.1) quantities labelled by a tilde refer to the contribution of four-quark operators, while those without a tilde correspond to two-quark operators, cf. Figure 6.1. The Wilson coefficients Γ_i in Eq. (6.1.1) can be computed perturbatively and admit the following expansion in the strong coupling α_s, i.e.

$$\Gamma_i = \Gamma_i^{(0)} + \frac{\alpha_s(m_c)}{4\pi} \Gamma_i^{(1)} + \left[\frac{\alpha_s(m_c)}{4\pi} \right]^2 \Gamma_i^{(2)} + ... \,. \qquad (6.1.2)$$

In this chapter we will try to shed further light into whether the expansion parameters $\alpha_s(m_c)$ and $\Lambda_{\mathrm{QCD}}/m_c$ are small enough to ensure the viabilty of the HQE in the charm sector. The Particle Data Group [169] quotes, for the pole and $\overline{\mathrm{MS}}$ mass of the charm quark, the values

$$m_c^{\mathrm{Pole}} = (1.67 \pm 0.07) \text{ GeV} , \qquad \overline{m}_c(\overline{m}_c) = (1.27 \pm 0.02) \text{ GeV}, \qquad (6.1.3)$$

while the dependence of the strong coupling on both the charm scale and the loop order (obtained using the RunDec package [204]) is shown in Table 6.2. For our numerical analysis we use the 5-loop running of the strong coupling. While the

$\alpha_s(m_c)$	$m_c = 1.67\,\text{GeV}$	$m_c = 1.48\,\text{GeV}$	$m_c = 1.27\,\text{GeV}$
2-loop	0.322	0.346	0.373
5-loop	0.329	0.356	0.387

Table 6.2: Numerical values of the strong coupling α_s evaluated at different scales and loop order, obtained using the RunDec package [204].

determination of the $\overline{\text{MS}}$ mass is theoretically well founded, the pole mass appears to be affected by a potential breakdown of perturbation theory. On the other side, the pole mass is the natural expansion parameter of the HQE. The relation between the two mass schemes, up to third order in the strong coupling, reads [211–213]

$$\begin{aligned} m_c^{\text{Pole}} &= \overline{m}_c(\overline{m}_c)\left[1+\frac{4}{3}\frac{\alpha_s(\overline{m}_c)}{\pi}+10.43\left(\frac{\alpha_s(\overline{m}_c)}{\pi}\right)^2+116.5\left(\frac{\alpha_s(\overline{m}_c)}{\pi}\right)^3\right] \\ &= \overline{m}_c(\overline{m}_c)\left[1+0.1642+0.1582+0.2176\right], \end{aligned} \tag{6.1.4}$$

where we have used the 5-loop result for the strong coupling at the scale 1.27 GeV. Due to the fact that Γ_3 depends on the fifth power of the charm pole mass, see Section 6.2.2, one obtains quite different results according to how higher orders in Eq. (6.1.4) are treated. Specifically, by truncating the expansion in Eq. (6.1.4) at first order in α_s, from $\overline{m}_c(\overline{m}_c) = 1.27$ GeV, we obtain for the pole mass the value $m_c^{\text{Pole}} = 1.479$ GeV, which leads respectively to

$$\left(m_c^{\text{Pole}}\right)^5 = \overline{m}_c(\overline{m}_c)^5\left[1+0.1642\right]^5 = 2.14\,\overline{m}_c(\overline{m}_c)^5, \tag{6.1.5}$$

taking the fifth power of m_c^{Pole}, and

$$\left(m_c^{\text{Pole}}\right)^5 \approx \overline{m}_c(\overline{m}_c)^5\left[1+5\cdot 0.1642\right] = 1.82\,\overline{m}_c(\overline{m}_c)^5, \tag{6.1.6}$$

further expanding up to the first order in α_s. The result in Eq. (6.1.6) is about 15% smaller than the one in Eq. (6.1.5). Instead, by including also all the higher order

terms given in Eq. (6.1.4), we get

$$\left(m_c^{\rm Pole}\right)^5 \;=\; \overline{m}_c(\overline{m}_c)^5\,[1+0.1642+0.1582+0.2176]^5 = 8.66\,\overline{m}_c(\overline{m}_c)^5\,, \quad (6.1.7)$$

which is roughly a factor four larger than the value in Eq. (6.1.5).

In the following, we will thus consider four different quark mass schemes:

1. Use Eq. (6.1.4) to first order in α_s, since this is the order to which most of the Wilson coefficients are known. In this case we fix $m_c^{\rm Pole} = 1.48$ GeV and express everything in terms of the pole mass. A further possibility would be to consider the expansion in Eq. (6.1.4) to be an asymptotic one, whose smallest correction appears at order α_s^2, which is where we stop the expansion. In this case we get the pole mass value from PDG, $m_c^{\rm Pole} = 1.67$ GeV. We carried out numerical tests for this large value of the charm quark mass and found the decay rates to be roughly $70-90\%$ larger than those obtained using $m_c^{\rm Pole} = 1.48$ GeV. Since we expect this enhancement to be compensated by missing NNLO corrections to the non-leptonic decay rates, we will not present separate results for $m_c^{\rm Pole} = 1.67$ GeV.
2. Express the c-quark mass in terms of the $\overline{\rm MS}$ mass [214],

$$m_c^{\rm Pole} = \overline{m}_c(\overline{m}_c)\left[1+\frac{4}{3}\frac{\alpha_s(\overline{m}_c)}{\pi}\right], \quad (6.1.8)$$

   taking $\overline{m}_c(\overline{m}_c) = 1.27$ GeV [169], and expand consistently up to order α_s. Because of the dependence on the fifth power of the charm-quark mass, in this case Γ_3 is affected by a large correction $5\times(4/3)(\alpha_s/\pi)$.
3. Express the c-quark mass in terms of the kinetic mass [215, 216]. The kinetic scheme has been introduced in order to obtain a short distance definition of the heavy quark mass which allows a faster convergence of the perturbative series and is still valid at small scales $\mu \sim 1$ GeV. The relation between the kinetic scheme and the $\overline{\rm MS}$ and Pole schemes can be found, up to N^{3}LO corrections,

in [217]. At order α_s one has

$$m_c^{\rm Pole} = m_c^{\rm Kin}\left[1+\frac{4\alpha_s}{3\pi}\left(\frac{4}{3}\frac{\mu^{\rm cut}}{m_c^{\rm Kin}}+\frac{1}{2}\left(\frac{\mu^{\rm cut}}{m_c^{\rm Kin}}\right)^2\right)\right], \tag{6.1.9}$$

where $\mu^{\rm cut}$ is the Wilsonian cutoff separating the perturbative and non-perturbative regimes. Using $\overline{m}_c(\overline{m}_c)$ as an input, the authors of [217] obtain

$$m_c^{\rm Kin}(1{\rm GeV}) = 1.128\,{\rm GeV} \quad ({\rm N^3LO})\,, \tag{6.1.10}$$

$$m_c^{\rm Kin}(1{\rm GeV}) = 1.206\,{\rm GeV} \quad ({\rm NLO})\,. \tag{6.1.11}$$

Comparing with Eq. (6.1.8) it follows that the kinetic scheme might be preferred to the $\overline{\rm MS}$ scheme if the term in the round brackets of Eq. (6.1.9) would give a suppression factor. For $\mu^{\rm cut} = 1\,{\rm GeV}$ and $m_c^{\rm Kin} = 1.2$ GeV, this is not the case. Using lower values i.e. $\mu^{\rm cut} < 1$ GeV, the convergence of the series could be improved, however this would bring in an additional uncertainty due to the closeness to the non-perturbative scale $\Lambda_{\rm QCD}$. In our numerical analysis we will investigate the kinetic scheme with $\mu^{\rm cut} = 0.5$ GeV. From [217] we take the following value

$$m_c^{\rm kin}(0.5\,{\rm GeV}) = 1.363\,{\rm GeV}\,, \tag{6.1.12}$$

obtained for consistency at NLO in α_s and using as an input $\overline{m}_c(\overline{m}_c)$.

4. In addition, we will consider the $1S$-mass scheme defined as [218–220]:

$$m_c^{\rm Pole} = m_c^{1S}\left(1+\frac{(C_F\,\alpha_s)^2}{8}\right), \tag{6.1.13}$$

where $C_F = 4/3$, and the $1S$ mass $m_c^{1S} \approx 1.44$ GeV is obtained using the conversion from the $\overline{\rm MS}$-scheme (implemented in the RunDec package [204]) at one-loop level. Note that the correction within the $1S$ scheme in fact starts at order α_s^2 which however is still considered to be a NLO (not NNLO) effect [218].[1]

The above arguments clearly indicate the importance of including higher order

[1] Similarly, another possibility would be to study the potential subtracted mass [221].

perturbative QCD corrections to the decay rates.

With this work we present a study of the total decay rate of the D^0, D^+ and D_s^+ mesons, of their lifetime ratios $\tau(D^+)/\tau(D^0)$ and $\tau(D_s^+)/\tau(D^0)$ and of the semileptonic branching fractions $\mathrm{Br}(D_q \to X e^+ \nu_e)$ using state-of-the-art expressions for the $\Delta C = 0$ Wilson coefficients and for the non-perturbative parameters. Γ_3 is known at NLO-QCD [222–229] for non-leptonic decays. NNLO-QCD [230–239] and NNNLO-QCD [240, 241] corrections have been computed for semileptonic decays, while for non-leptonic decays NNLO corrections have been determined in the massless case and in full QCD (i.e. no effective Hamiltonian was used) in [242]. Γ_5 was determined at LO-QCD for both semileptonic and non-leptonic decays [59–61, 64]. For the semileptonic modes even NLO-QCD corrections are available [243–245]. In the b-system, Γ_6 was first computed at LO-QCD in [246] and recently the NLO-QCD corrections were determined in [247], both for the semileptonic case only. Very recently Γ_6 has been determined also for non-leptonic decays [124, 195, 248] and the coefficient was found to be large. For semileptonic D-meson decays, Γ_6 was determined in [249], see also the recent [250], while the corresponding results for the non-leptonic charm modes are presented for the first time in this work. $\tilde{\Gamma}_6$ is known at NLO-QCD for lifetimes of B-meson [190, 191] and of D-meson [200], while $\tilde{\Gamma}_7$ and $\tilde{\Gamma}_8$ have been estimated in LO-QCD in [251, 252].

On the non-perturbative side, at dimension-five, the matrix element of the chromomagnetic operator can be determined from spectroscopy, while for the kinetic operator there exist several heavy quark effective theory (HQET) determinations with lattice simulations [253–257] and using sum rules [215, 258, 259]. The matrix elements of the four-quark operators $\langle \tilde{\mathcal{O}}_6 \rangle$ have been computed using HQET sum rules [55]. In Chapters 3 and 5 we calculated $SU(3)_F$ violating effects and so far undetermined eye-contractions through HQET sum rules. Corresponding lattice results for the matrix elements of the four-quark operators would be highly desirable. We emphasise that the matrix element of the dimension-six Darwin operator, $\langle \mathcal{O}_6 \rangle$, can be expressed in terms of the above Bag parameters by taking into account the

equation of motion for the gluon field strength tensor.

The rest of this chapter is arranged as follows: In Section 6.2, after briefly introducing the effective Hamiltonian describing the c-quark decays, we analyse in detail the structure of the HQE, discussing each of the short-distance contributions in Eq. (6.1.1). In Section 6.3, we describe how the corresponding non-perturbative parameters are determined. Numerical results for the total D-meson decay widths, their ratios, as well as for the semileptonic branching fractions, are presented in Section 6.4. Finally, we conclude in Section 6.5 with an outlook on how to further improve the theoretical predictions in the charm sector. The numerical input used in the analysis are collected in Appendix C.1 and the complete expressions for the coefficients of the Darwin operator for non-leptonic c-quark decays are presented in Appendix C.2. We note here that unlike in Chapters 3 and 5, for the rest of this analysis the HQET states conform to relativistic normalisation. This change is reflected in our parameterisation of matrix elements and decay constants, for which we employ the conventions of [45] in the following. A summary of our parameterisation of the matrix elements of the four-quark operators used in this chapter can be found in Appendix C.3.

6.2 The Total Decay Rate

6.2.1 Effective Hamiltonian and HQE

The non-leptonic decay of a charm quark $c \to q_1 \bar{q}_2 u$ ($q_i = u, d, s$) is governed by the effective $\Delta C = 1$ Hamiltonian (see e.g. [67])

$$\begin{aligned}\mathcal{H}_{\text{eff}}^{\text{NL}} =& \frac{G_F}{\sqrt{2}} \left[\sum_{q_{1,2}=d,s} \lambda_{q_1 q_2} \left[C_1(\mu_1)\, Q_1^{q_1 q_2} + C_2(\mu_1)\, Q_2^{q_1 q_2} \right] - \lambda_b \sum_{j=3}^{6} C_j(\mu_1) Q_j \right] \\ &+ \text{h.c.}\,,\end{aligned} \tag{6.2.1}$$

where $\lambda_{q_1 q_2} = V_{cq_1}^* V_{uq_2}$ and $\lambda_b = V_{cb}^* V_{ub}$ are the CKM factors, $C_i(\mu_1)$ denote the Wilson coefficients at the renormalisation scale $\mu_1 \sim m_c$, $Q_{1,2}^{q_1 q_2}$ are tree-level $\Delta C = 1$

operators [1]

$$Q_1^{q_1q_2} = \left(\bar{q}_1^i\gamma_\rho(1-\gamma_5)c^i\right)\left(\bar{u}^j\gamma^\rho(1-\gamma_5)q_2^j\right), \quad (6.2.2)$$

$$Q_2^{q_1q_2} = \left(\bar{q}_1^i\gamma_\rho(1-\gamma_5)c^j\right)\left(\bar{u}^j\gamma^\rho(1-\gamma_5)q_2^i\right), \quad (6.2.3)$$

while Q_j, $j = 3...6$ are penguin operators, which can only arise in the singly Cabibbo suppressed decays $c \to s\bar{s}u$ and $c \to d\bar{d}u$ or in further suppressed pure penguin decays like $c \to u\bar{u}u$. Values of the Wilson coefficients at different scales are shown in Table 6.3 both at NLO-QCD and LO-QCD.

μ_1[GeV]	1	1.27	1.36	1.44	1.48	3
$C_1(\mu_1)$	1.25 (1.34)	1.20 (1.27)	1.19 (1.26)	1.18 (1.25)	1.18 (1.24)	1.10 (1.15)
$C_2(\mu_1)$	−0.48 (−0.62)	−0.39 (−0.50)	−0.40 (−0.53)	−0.37 (−0.49)	−0.37 (−0.48)	−0.24 (−0.32)
$C_3(\mu_1)$	0.03 (0.02)	0.02 (0.01)	0.02 (0.01)	0.01 (0.01)	0.01 (0.01)	0.00 (0.00)
$C_4(\mu_1)$	−0.06 (−0.04)	−0.05 (−0.03)	−0.04 (−0.03)	−0.04 (−0.02)	−0.04 (−0.02)	−0.01 (−0.01)
$C_5(\mu_1)$	0.01 (0.01)	0.01 (0.01)	0.01 (0.01)	0.01 (0.01)	0.01 (0.01)	0.00 (0.00)
$C_6(\mu_1)$	−0.08 (−0.05)	−0.05 (−0.03)	−0.05 (−0.03)	−0.04 (−0.03)	−0.04 (−0.03)	−0.01 (−0.01)

Table 6.3: Comparison of the Wilson coefficients at NLO-QCD (LO-QCD) for different values of μ_1.

From Table 6.3, we see that the Wilson coefficients of the penguin operators are considerably smaller than C_1 and C_2. Furthermore, their contributions are strongly CKM suppressed by the factor $\lambda_b \ll \lambda_{q_1q_2}$. We therefore exclude the effect of the penguin operators in our analysis, given the current limited theoretical accuracy in the charm sector.

The complete effective Hamiltonian describing all possible c-quark decays is a sum

[1] In our notation, $Q_1^{q_1q_2}$ is the colour-singlet operator.

of non-leptonic, semileptonic and radiative contributions, namely

$$\mathcal{H}_{\rm eff} \;=\; \mathcal{H}_{\rm eff}^{\rm NL} + \mathcal{H}_{\rm eff}^{\rm SL} + \mathcal{H}_{\rm eff}^{\rm rare}\,, \tag{6.2.4}$$

where $\mathcal{H}_{\rm eff}^{\rm NL}$ is given in Eq. (6.2.1),

$$\mathcal{H}_{\rm eff}^{\rm SL} = \frac{G_F}{\sqrt{2}} \sum_{q=d,s} \sum_{\ell=e,\mu} V_{cq}^*\, Q^{q\ell} + \text{h.c.}\,, \tag{6.2.5}$$

with the semileptonic operator $Q^{q\ell} = (\bar{q}\gamma^\mu(1-\gamma_5)c)\left(\bar{\nu}_\ell\gamma_\mu(1-\gamma_5)\ell\right)$, while $\mathcal{H}_{\rm eff}^{\rm rare}$ describes decays like $D \to \pi\ell^+\ell^-$, whose branching fraction is much smaller than those corresponding to tree-level transitions. For this reason, we will neglect rare decays and we do not show an explicit expression for $\mathcal{H}_{\rm eff}^{\rm rare}$.

In Section 2.1, we illustrated how the total decay width for the B meson could be expressed as a discontinuity of a forward scattering matrix element of the transition operator, consisting of a double insertion of the effective Hamiltonian (see Eqs.(2.1.2) and (2.1.3)). Therefore, for the total decay width of a heavy D meson with mass m_D and four-momentum p_D^μ we can write,

$$\Gamma(D) = \frac{1}{2m_D}\text{Im}\langle D|\mathcal{T}|D\rangle\,, \tag{6.2.6}$$

with the transition operator

$$\mathcal{T} = i\int d^4x\, T\left\{\mathcal{H}_{\rm eff}(x)\,, \mathcal{H}_{\rm eff}(0)\right\}\,. \tag{6.2.7}$$

Following the reasoning discussed in Section 2.2, we now reparameterise the four-momentum of the decaying c-quark, separating the "large" and "small" components as

$$p_c^\mu = m_c\, v^\mu + k^\mu, \tag{6.2.8}$$

where $v^\mu = p^\mu/m_D$ denotes the four-velocity of the D-meson. To account for the residual interaction of the c-quark with the light degrees of freedom inside the hadron (i.e soft gluons and quarks), we replace the residual momentum $k^\mu \to iD^\mu$, with D^μ being the covariant derivative with respect to the background gluon field.

Additionally, the heavy charm quark field is redefined as

$$c(x) = e^{-im_c v\cdot x} c_v(x)\,, \tag{6.2.9}$$

to remove the large fraction of the c-quark momentum. Using Eqs. (6.2.8) and (6.2.9), $\Gamma(D)$ in Eq. (6.2.6) can be expanded in the small quantity $D^\mu/m_c \sim \Lambda_{\rm QCD}/m_c$, leading to the series in Eq. (6.1.1). The result is schematically shown in Figure 6.1. The first diagram on the top line of Figure 6.1, corresponding to the limit $m_c \to \infty$, represents the decay of a free c-quark, while power corrections due to the interaction of the heavy quark with soft gluons and quarks are described respectively by the second and third diagrams on the top line of Figure 6.1. Finally, before discussing the individual terms in Eq. (6.1.1) separately, it is worth emphasizing that the field c_v is related to the effective heavy quark field h_v, introduced in the framework of the HQET (see Eq.(2.2.4), by

$$c_v(x) = h_v(x) + \frac{i\not{D}_\perp}{2m_c} h_v(x) + \mathcal{O}\left(\frac{1}{m_c^2}\right), \tag{6.2.10}$$

where $D_\perp^\mu = D^\mu - (v\cdot D)\, v^\mu$.

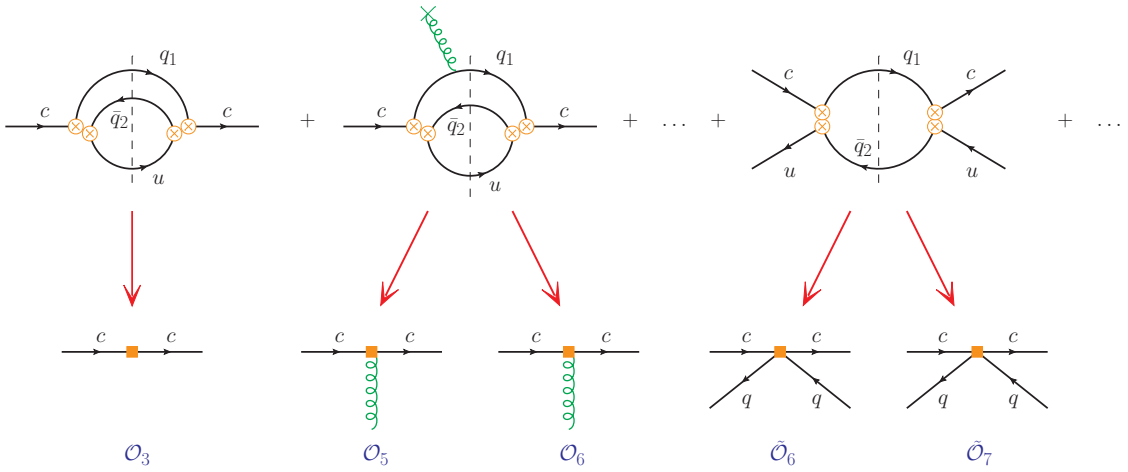

Figure 6.1: The diagrams describing contributions to the HQE in Eq. (6.1.1). The crossed circles denote the $\Delta C = 1$ operators Q_i of the effective Hamiltonian while the squares denote the local $\Delta C = 0$ operators $\mathcal{O}_i$ and $\tilde{\mathcal{O}}_i$. The two-loop and the phase space enhanced one-loop diagrams correspond respectively to the two-quark operators $\mathcal{O}_i$ and to the four-quark operators $\tilde{\mathcal{O}}_i$ in the HQE.

6.2.2 Dimension-three Contribution

The leading term in Eq. (6.1.1), $\Gamma_3^{(0)}$, can be schematically written as

$$\begin{aligned}\Gamma_3^{(0)} &= \Gamma_0\, c_3 \\ &= \Gamma_0 \left[f\left(z_s, z_e, z_{\nu_e}\right) + f\left(z_s, z_\mu, z_{\nu_\mu}\right) + |V_{ud}|^2 \mathcal{N}_a\, f\left(z_s, z_u, z_d\right) + \ldots \right] ,\end{aligned} \tag{6.2.11}$$

where we define

$$\Gamma_0 = \frac{G_F^2 m_c^5}{192\pi^3} |V_{cs}|^2 , \tag{6.2.12}$$

and we introduce the dimensionless mass parameter $z_q = m_q^2/m_c^2$. Note than we neglect the neutrino as well as the electron, the up and down quarks masses, i.e. $z_\nu = z_e = z_u = z_d = 0$, while $z_s \neq 0 \neq z_\mu$. The first two terms in c_3 in Eq. (6.2.11) correspond to the semileptonic modes $c \to s e^+ \nu_e$ and $c \to s \mu^+ \nu_\mu$, while the third term to the Cabibbo favoured decay $c \to s u \bar{d}$. The ellipsis stand for CKM suppressed contributions. The dependence on the $\Delta C = 1$ Wilson coefficients is absorbed in the combination $\mathcal{N}_a = 3\, C_1^2 + 3\, C_2^2 + 2\, C_1 C_2$. The behaviour of $\mathcal{N}_a$ as function of the renormalisation scale, both at LO- and NLO-QCD, is shown in Table 6.4 and in Figure 6.2, indicating a visible shift from LO to NLO and a moderate reduction of the scale uncertainty in the NLO result. Else there are no cancellations in $\mathcal{N}_a$ that might lead to numerical instability. The phase-space function $f(a, b, c)$ in Eq. (6.2.11) describes the effect of the final state masses. In the case of one massive particle, it reduces to the well-known expression

$$f(z, 0, 0) = 1 - 8z + 8z^3 - z^4 - 12 z^2 \ln z\,, \qquad f\left(z_s, 0, 0\right) \approx 1 - 0.03\,, \tag{6.2.13}$$

which shows that the contribution due to the finite s-quark mass is small. The analytic expression of $f(a, b, c)$ for two different masses in the final state, can be found e.g. in the Appendix of [260].

By including also NLO-QCD corrections, Γ_3 can be schematically presented as

$$\Gamma_3 = \Gamma_0 \left[3\, C_1^2\, \mathcal{C}_{3,11} + 2\, C_1 C_2\, \mathcal{C}_{3,12} + 3\, C_2^2\, \mathcal{C}_{3,22} + \mathcal{C}_{3,\mathrm{SL}} \right] , \tag{6.2.14}$$

where a summation over all the modes is implicitly assumed. At NLO, the expressions

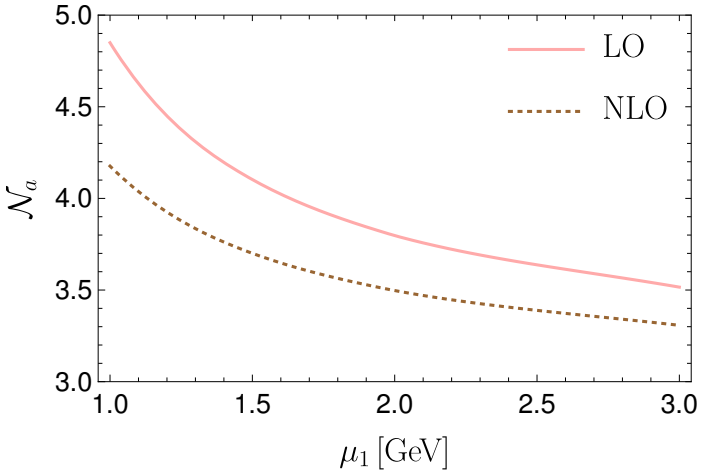

Figure 6.2: Scale dependence of the Wilson coefficient combination $\mathcal{N}_a = 3\,C_1^2 + 3\,C_2^2 + 2\,C_1 C_2$.

μ_1 [GeV]	1	1.27	1.36	1.44	1.48	3
$\mathcal{N}_a$(LO)	4.85	4.35	4.23	4.15	4.12	3.52
$\mathcal{N}_a$(NLO)	4.18	3.86	3.79	3.74	3.71	3.31

Table 6.4: Comparison of $\mathcal{N}_a$ at LO- and NLO-QCD, for different values of the renormalisation scale μ_1.

for $\mathcal{C}_{3,11}$, $\mathcal{C}_{3,22}$ and $\mathcal{C}_{3,\mathrm{SL}}$ are taken from [222], where the computation was done for three different final state masses, hence we can easily use these results for all c-quark decay modes. For the coefficient $\mathcal{C}_{3,12}$ we use [225] for the $c \to s\bar{d}u$, $c \to d\bar{s}u$ and $c \to d\bar{d}u$ decay channels, while the result of [229] is used in the case of final state with two massive s-quarks, $c \to s\bar{s}u$.

Neglecting final state masses and approximating $|V_{ud}|^2 \approx 1$ the following expression was determined in 1991 [223], i.e.

$$c_3^{\mathrm{NLO}} - c_3^{\mathrm{LO}} = 8\,\frac{\alpha_s}{4\pi}\left[\underbrace{\left(\frac{25}{4} - \pi^2\right)}_{<0} \underbrace{+(C_1^2 + C_2^2)\left(\frac{31}{4} - \pi^2\right)}_{<0} \underbrace{-\frac{2}{3}C_1 C_2\left(\frac{7}{4} + \pi^2\right)}_{\geq 0}\right]. \tag{6.2.15}$$

The first term on the r.h.s. of Eq. (6.2.15) stems from semileptonic decays and the next two terms from non-leptonic channels. For non-leptonic b-quark decays the NLO corrections are negative, while for charm quarks decays the third term will dominate over the second one and the correction becomes positive. Moreover, there

Mass scheme	$\Gamma_3^{\rm LO}$ [ps^{-1}]	$\Gamma_3^{\rm NLO}$ [ps^{-1}]
Pole ($m_c = 1.48$ GeV)	$1.45^{+0.17}_{-0.14}$	$1.52^{+0.20}_{-0.16}$
$\overline{\rm MS}$ (Eq. (6.1.8))	$0.69^{+0.06}_{-0.09}$	$1.32^{+0.06}_{-0.03}$
Kinetic (Eq. (6.1.9))	$0.97^{+0.10}_{-0.11}$	$1.47^{+0.27}_{-0.30}$
$1S$ (Eq. (6.1.13))	$1.25^{+0.14}_{-0.13}$	$1.50^{+0.31}_{-0.25}$

Table 6.5: Numerical values of $\Gamma_3^{\rm LO} = \Gamma_3^{(0)}$ and $\Gamma_3^{\rm NLO} = \Gamma_3^{(0)} + \alpha_s(m_c)/(4\pi)\,\Gamma_3^{(1)}$ using different schemes for the c-quark mass. The uncertainties are obtained by varying the renormalisation scale μ_1 between 1 GeV and 3 GeV.

is a sizable enhancement of the α_s-corrections in the non-leptonic b-quark decays due to finite charm quark mass effects [224–226, 229] - the corresponding increase in charm quark decays is much less pronounced as $m_c^2/m_b^2 \approx 0.1 \gg m_s^2/m_c^2 \approx 0.005$. The numerical values for Γ_3 both in LO- and NLO-QCD, for different c-quark mass schemes are shown in Table 6.5. The range of NLO-QCD values from $1.3\,\text{ps}^{-1}$ to $1.5\,\text{ps}^{-1}$ for the free charm-quark decay at NLO-QCD, is in good agreement with the experimental determinations in Table 6.1. Moreover we observe small ($< 5\%$) corrections because of a non-vanishing strange quark mass. Interestingly the NLO-QCD result is affected by strong cancellations. We observe a suppression of the non-leptonic contribution due to the opposing sign between the NLO corrections to the diagrams describing QCD corrections to the upper left diagram of Figure 6.1 and the QCD corrections intrinsic to the $\Delta C = 1$ Wilson coefficients. There is then a further cancellation between the semileptonic and the non-leptonic modes. This behaviour can be nicely read off from the result in the Pole scheme:

$$\Gamma_3 \;=\; \Gamma_3^{\rm LO}\left[1 + \left(\overbrace{\underbrace{1.84}_{\text{diag.}} - \underbrace{0.74}_{\text{WC}}}^{\text{NL}} - \overbrace{0.67}^{\text{SL}}\right)\frac{\alpha_s}{\pi} + \mathcal{O}\left(\frac{\alpha_s}{\pi}\right)^2\right]. \qquad (6.2.16)$$

Expressing the pole mass in terms of a short distance mass like the $\overline{\rm MS}$ scheme, an additional large NLO correction arises from the conversion factor of m_c^5, which is the origin of the large shift between the LO and the NLO values in the $\overline{\rm MS}$-, the

kinetic and the $1S$-schemes, see Table 6.5. We find e.g. in the $\overline{\text{MS}}$ scheme

$$\Gamma_3 = \Gamma_3^{\text{LO}} \left[1 + \left(\overbrace{\underbrace{2.10}_{\text{diag.}} - \underbrace{0.70}_{\text{WC}}}^{\text{NL}} - \overbrace{0.71}^{\text{SL}} + \overbrace{6.66}^{\text{conv.fac.}} \right) \frac{\alpha_s}{\pi} + \mathcal{O}\left(\frac{\alpha_s}{\pi}\right)^2 \right] \quad (6.2.17)$$

The corrections due to the mass conversion also make the overall semileptonic NLO term in the $\overline{\text{MS}}$ scheme positive.

To get a first indication of the behaviour of the QCD series for the decay rate at higher orders, we briefly discuss here the NNLO [238] and NNNLO [240] corrections for the semileptonic b-quark decay and the preliminary NNLO-QCD corrections for the non-leptonic b-quark decay [242]. In the Pole mass scheme [240]

$$\begin{aligned} \frac{\Gamma_3(B \to X_c \ell \bar{\nu}_\ell)}{\Gamma_3^{\text{LO}}(B \to X_c \ell \bar{\nu}_\ell)} &= 1 - 1.72 \frac{\alpha_s(\mu)}{\pi} - 13.09 \left(\frac{\alpha_s(\mu)}{\pi}\right)^2 - 163.3 \left(\frac{\alpha_s(\mu)}{\pi}\right)^3 \\ &= 1 - 0.12 - 0.06 - 0.05, \end{aligned} \quad (6.2.18)$$

the semileptonic decay rate gets large negative corrections, and in the $\overline{\text{MS}}$-scheme

$$\begin{aligned} \frac{\Gamma_3(B \to X_c \ell \bar{\nu}_\ell)}{\Gamma_3^{\text{LO}}(B \to X_c \ell \bar{\nu}_\ell)} &= 1 + 3.07 \frac{\alpha_s(\mu)}{\pi} + 13.36 \left(\frac{\alpha_s(\mu)}{\pi}\right)^2 + 62.7 \left(\frac{\alpha_s(\mu)}{\pi}\right)^3 \\ &= 1 + 0.21 + 0.06 + 0.02, \end{aligned} \quad (6.2.19)$$

one finds [240] sizable positive corrections - driven by the conversion of the quark mass from the Pole scheme to the $\overline{\text{MS}}$-scheme and indicating again the importance of higher order perturbative corrections. For the semileptonic charm quark decay one finds even larger corrections[1], e.g. in the Pole mass scheme

$$\begin{aligned} \frac{\Gamma_3(D \to X \ell^+ \nu_\ell)}{\Gamma_3^{\text{LO}}(D \to X \ell^+ \nu_\ell)} &= 1 - 2.41 \frac{\alpha_s(\mu)}{\pi} - 23.4 \left(\frac{\alpha_s(\mu)}{\pi}\right)^2 - 321.5 \left(\frac{\alpha_s(\mu)}{\pi}\right)^3 \\ &= 1 - 0.25 - 0.26 - 0.37, \end{aligned} \quad (6.2.20)$$

which clearly spoils the perturbative approach and makes the use of different quark mass schemes mandatory.

Regarding the NNLO-QCD corrections to the non-leptonic decay rates, [242] presents a partial result (not resumming the large logarithms, neglecting effects of the operator

[1] Results presented by Matteo Fael at CHARM 2020:
https://indico.nucleares.unam.mx/event/1488/session/12/contribution/56/material/slides/0.pdf

$Q_2^{q_1 q_2}$ and assuming a vanishing charm quark mass) for the b-quark. In the pole mass scheme the authors obtain

$$\frac{\Gamma(b \to c\bar{u}d)}{3\Gamma(b \to ce\bar{\nu})} = 1 + 1\,\frac{\alpha_s(\mu)}{\pi} + 67.1\left(\frac{\alpha_s(\mu)}{\pi}\right)^2 . \tag{6.2.21}$$

It is interesting to note that from the coefficient of the α_s^2 term, 67.1, a contribution of 54.7 stems from not summing large logarithms of the form $\ln(M_W/m_b)$ and $\ln^2(M_W/m_b)$. Using Eq. (6.2.18) and the fact that, in the approximations of [242] the ratio between non-leptonic and semileptonic rate is equal to 3 at LO-QCD, yields

$$\Gamma(b \to c\bar{u}d) = \Gamma^{\rm LO}(b \to c\bar{u}d)\left[1 - 0.7\,\frac{\alpha_s(\mu)}{\pi} + 52.3\left(\frac{\alpha_s(\mu)}{\pi}\right)^2\right] . \tag{6.2.22}$$

For non-leptonic charm-quark decays the logarithms become even larger and we find that the coefficient of the α_s^2 term increases from 52.3 to 91.2, which clearly indicates the necessity of summing the large logarithms. Neglecting final state masses seems to be well justified in the charm system. In order to further estimate the effect of neglecting the operator $Q_2^{q_1 q_2}$, we set in our code $C_1 = 1$ and $C_2 = 0$ and we get in the Pole scheme

$$\frac{\Gamma_3^{\rm NL}}{\Gamma_3^{\rm NL,LO}} \;=\; 1 - 1.4\,\frac{\alpha_s(\mu)}{\pi}, \tag{6.2.23}$$

while the result with the full inclusion of the effective Hamiltonian yields a very different value of the QCD corrections

$$\frac{\Gamma_3^{\rm NL}}{\Gamma_3^{\rm NL,LO}} = 1 + 1.6\,\frac{\alpha_s(\mu)}{\pi}. \tag{6.2.24}$$

All in all we conclude that, higher order corrections seem to be crucial for a reliable determination of Γ_3. Despite being conceptually very interesting, the result of [242] is not useful for phenomenological applications and a full NNLO determination of the non-leptonic decay rate using the effective Hamiltonian would be highly desirable.

6.2.3 Dimension-five Contribution

The first corrections to the free charm-quark decay arise at order $1/m_c^2$ and describe the effect of the kinetic and the chromomagnetic operators. Their matrix elements are parametrised by the two non-perturbative inputs μ_π^2 and μ_G^2, i.e.

$$2m_D\,\mu_\pi^2(D) = -\langle D(p)|\bar{c}_v(iD_\mu)(iD^\mu)c_v|D(p)\rangle\,, \tag{6.2.25}$$

$$2m_D\,\mu_G^2(D) = \langle D(p)|\bar{c}_v(iD_\mu)(iD_\nu)(-i\sigma^{\mu\nu})c_v|D(p)\rangle\,, \tag{6.2.26}$$

with $\sigma^{\mu\nu} = (i/2)[\gamma^\mu, \gamma^\nu]$. Both the operators receive a contribution from the expansion of the dimension-three matrix element $\langle D(p)|\bar{c}_v c_v|D(p)\rangle$ [261]. However, the chromomagnetic operator receives further contributions due to the expansion of the short distance coefficient c_3 and of the quark-propagator in the external gluon field [60, 61, 124] - see the second diagram on the top line of Figure 6.1. Therefore, at order $1/m_c^2$, we can schematically write

$$\Gamma_5\frac{\langle\mathcal{O}_5\rangle}{m_c^2} = \Gamma_0\left[c_{\mu_\pi}\frac{\mu_\pi^2}{m_c^2} + c_G\,\frac{\mu_G^2}{m_c^2}\right]. \tag{6.2.27}$$

The coefficient of the kinetic operator is related to the dimension-three contribution[1], $c_{\mu_\pi} = -c_3^{(0)}/2$, and the chromomagnetic coefficient c_G can be decomposed as

$$c_G = 3\,C_1^2\,\mathcal{C}_{G,11} + 2\,C_1C_2\,\mathcal{C}_{G,12} + 3\,C_2^2\,\mathcal{C}_{G,22} + \mathcal{C}_{G,SL}\,, \tag{6.2.28}$$

where again a summation over all the modes is assumed. The individual contributions $\mathcal{C}_{G,nm}$ for non-leptonic modes can be found e.g. in the Appendix of [124].
In the latter reference, the coefficients of the chromomagnetic operator were determined for the non-leptonic B-meson decays, however, since there are no IR-divergences at this order, it is straightforward to obtain the corresponding results for the charm-sector, namely by replacing $m_b \to m_c$, $m_c \to m_s$, etc. For the semileptonic decay $c \to s\mu^+\nu_\mu$, the expression for two different mass parameters $z_s \neq 0 \neq z_\mu$ can be

[1] Since the dimension-5 contribution for non-leptonic modes is known only at LO in QCD, we use the dimension-three coefficient c_3 just at LO-QCD for c_{μ_π}.

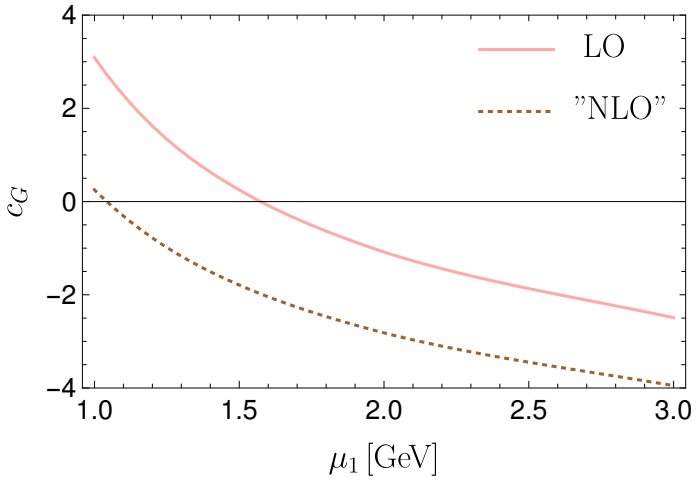

Figure 6.3: Scale dependence of the coefficient of the chromomagnetic operator.

found in the Appendix of [260].[1] By neglecting the strange and muon masses and by considering only the dominant CKM modes, the result for c_G becomes very compact, i.e.

$$c_G \approx -|V_{ud}|^2 \left[\frac{9}{2}\left(C_1^2 + C_2^2\right) + 19\, C_1 C_2\right] - 3. \tag{6.2.29}$$

Because of the large coefficient in front of $C_1 C_2$ and of its negative value, Eq. (6.2.29) can be affected by cancellations. In Figure 6.3 we plot c_G in Eq. (6.2.28), as a function of the renormalisation scale μ_1 while in Table 6.6 we list the numerical result for some reference values of μ_1. For c_G a change of sign occurs in the region between 1 and 2 GeV – leading to a large uncertainty due to scale variation. Note, that the "NLO" result shown in Figure 6.3 and Table 6.6 only includes QCD corrections due to the $\Delta C = 1$ Wilson coefficients. A complete calculation of the NLO-QCD corrections to c_G is still missing (these corrections are only known for the semileptonic case) and would be very desirable in order to reduce the huge scale dependence. The numerical values of the non-perturbative parameters μ_π^2 and μ_G^2 will be discussed in Sections 6.3.2 and 6.3.1.

[1] Since $m_s \approx m_\mu \approx 100\,\text{MeV} \ll m_c$, in principle one can safely set $z_s = z_\mu$ and use the non-leptonic expressions for the semileptonic modes, e.g. $c \to s\bar{s}u$ for $c \to s\mu\bar{\nu}_\mu$ by setting $N_c = 1$, $C_1 = 1$, $C_2 = 0$.

μ_1 [GeV]	1	1.27	1.36	1.44	1.48	3
$c_G^{\rm NL}$(LO)	6.20	4.34	3.91	3.58	3.43	0.62
$c_G^{\rm SL}$(LO)	-3.11	-3.11	-3.11	-3.11	-3.11	-3.11
c_G(LO)	3.09	1.23	0.80	0.47	0.32	-2.49
c_G("NLO")	0.25	-1.06	-1.37	-1.62	-1.74	-3.95

Table 6.6: Comparison of the coefficients $c_G^{\rm SL}$, $c_G^{\rm NL}$, and $c_G = c_G^{\rm SL} + c_G^{\rm NL}$ for different values of the renormalisation scale μ_1 at LO and "NLO", setting for reference $m_c = 1.5$ GeV.

6.2.4 Dimension-six Two-Quark Operator Contribution

By determining higher order $1/m_c$ corrections in the expansion, respectively, of the quark-propagator, of the matrix elements of mass dimension-three and mass dimension-five, and of the corresponding short-distance coefficients, see e.g. [60, 61, 122, 124] for details, one obtains the dimension-six contribution to $\Gamma(D)$, which can be compactly written as

$$\Gamma_6 \frac{\langle \mathcal{O}_6 \rangle}{m_c^3} = \Gamma_0 \, c_{\rho_D} \frac{\rho_D^3}{m_c^3} \,, \tag{6.2.30}$$

with the matrix element of the Darwin operator given by [1]

$$2 m_D \, \rho_D^3(D) \;\; = \;\; \langle D(p)| \bar{c}_v (iD_\mu)(iv \cdot D)(iD^\mu) c_v |D(p)\rangle \,. \tag{6.2.31}$$

The coefficient c_{ρ_D} can be decomposed into

$$c_{\rho_D} = 3\, C_1^2 \, \mathcal{C}_{\rho_D,11} + 2\, C_1 C_2 \, \mathcal{C}_{\rho_D,12} + 3\, C_2^2 \, \mathcal{C}_{\rho_D,22} + \mathcal{C}_{\rho_D,SL} \,, \tag{6.2.32}$$

including both non-leptonic and semileptonic contributions. For B-mesons decays, the non-leptonic coefficients were computed recently in [124, 195, 248]. In order to determine the corresponding expressions for the charm system, some subtleties have to be considered. In b-quark decays, one assumes $m_b \sim m_c \gg \Lambda_{\rm QCD}$, and the coefficient of the Darwin operator for the semileptonic $b \to c\ell\bar{\nu}_\ell$ decays is a finite function of $\rho = m_c^2/m_b^2$, which however diverges in the limit $\rho \to 0$, i.e.

[1] Note that with the given definition for the dimension-six two-quark operators, in terms of full covariant derivatives, the contribution of the spin-orbit operator to the decay width vanishes.

in correspondence of the $b \to u\ell\bar{\nu}_\ell$ transitions. This is due to the fact that, the radiation of a soft gluon off a massless quark-propagator leads to IR singularities at dimension-six. In non-leptonic b-quark decays, one has to further deal with the emission of a soft gluon from the internal light u-, d-, and s-quark lines. The corresponding IR divergences are of the form $\log(m_q/m_b)$, for $q = u, d, s$, and are removed by taking into account the mixing between the four-quark operators with external q quarks and the Darwin operator under renormalisation, for details see e.g. [124, 195, 262, 263]. Because of $m_c \gg m_s \sim \Lambda_{\rm QCD}$, it follows that one cannot trivially generalise the results from the b- to the c-sector, i.e. by only replacing $m_b \to m_c$, $m_c \to m_s$, etc., since there are further contributions due to the mixing of four-quark operators with external s-quarks which must be additionally included. Specifically, this leads to a modification of the coefficients proportional to C_1^2 and $C_1 C_2$. Using the same procedure as discussed in [124], we have recomputed the coefficients of the Darwin operator required for the study of D-meson decays. The analytic expressions for $\mathcal{C}_{\rho_D,nm}$, including the full s-quark mass dependence, however finite in the limit $m_s \to 0$, are presented in Appendix C.2 for all non-leptonic modes. To obtain the corresponding expression for $\mathcal{C}_{\rho_D,SL}$, it is sufficient to set in the results for the non-leptonic decays $N_c = 1$, $C_1 = 1$, $C_2 = 0$ and $z_s = z_\mu$ for the $c \to s\mu^+\nu_\mu$ mode. In particular, we confirm the results in [250].

Again, by neglecting the strange and muon masses and by considering only the dominant CKM modes, one finds

$$c_{\rho_D} \approx |V_{ud}|^2 \left(18\, C_1^2 - \frac{68}{3}\, C_1 C_2 + 18\, C_2^2\right) + 12\,. \tag{6.2.33}$$

Interestingly, in this combination all terms have the same sign and no cancellations arise. In Figure 6.4 we show the dependence of the function c_{ρ_D} in Eq. (6.2.32) on the renormalisation scale μ_1 and in Table 6.7 we quote the numerical result for some reference values of μ_1. The determination of the matrix element of the Darwin operator will be discussed in Section 6.3.3.

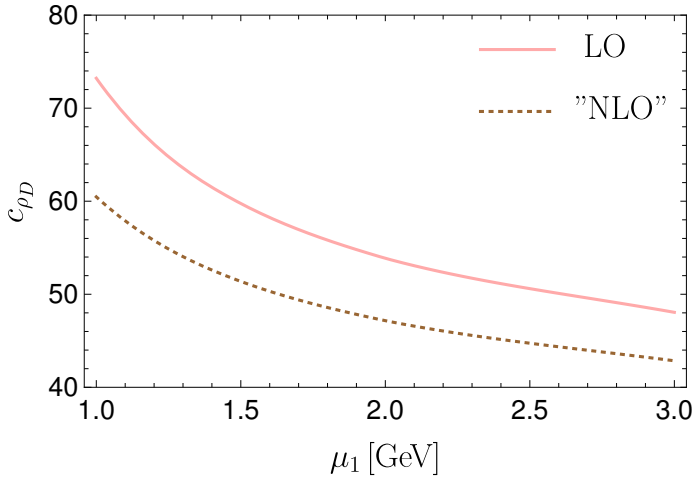

Figure 6.4: Scale dependence of the coefficient of the Darwin operator.

μ_1 [GeV]	1	1.27	1.36	1.44	1.48	3
$c_{\rho_D}^{\rm NL}$(LO)	60.6	51.7	49.6	48.1	47.5	35.4
$c_{\rho_D}^{\rm SL}$(LO)	12.6	12.6	12.6	12.6	12.6	12.6
c_{ρ_D}(LO)	73.2	64.3	62.3	60.8	60.1	48.1
c_{ρ_D}("NLO")	60.5	54.5	53.1	52.1	51.6	42.8

Table 6.7: Numerical values of $c_{\rho_D}^{\rm SL}$, $c_{\rho_D}^{\rm NL}$, and $c_{\rho_D} = c_{\rho_D}^{\rm SL} + c_{\rho_D}^{\rm NL}$ for different values of the renormalisation scale μ_1 at LO and "NLO" with $\mu_0 = m_c = 1.5$ GeV.

6.2.5 Dimension-six Four-Quark Operator Contribution

The perturbative coefficients in Eq. (6.1.1) considered so far are independent of the spectator quark in the D meson, in fact its effect appears only in the corresponding matrix elements of the dimension-five and dimension-six operators. Starting at order $1/m_c^3$, there are also one-loop contributions, cf. $\tilde{\Gamma}_6$ in Eq. (6.1.1), in which the spectator quark is directly involved. These correspond respectively to the weak exchange (WE), Pauli interference (PI) and weak annihilation (WA) diagrams, depicted in Figure 6.5 [1]. As discussed in Section 2.1, compared to the terms discussed above, these contributions are phase space enhanced by a factor of $16\pi^2$. The corresponding

[1] In the case of semileptonic decays, only the WA topology can contribute.

$\Delta C = 0$ four quark operators of dimension-six are [1]:

$$O_1^q = (\bar{c}\,\gamma_\mu(1-\gamma_5)q)\,(\bar{q}\,\gamma^\mu(1-\gamma_5)c), \tag{6.2.34}$$

$$O_2^q = (\bar{c}(1-\gamma_5)q)\,(\bar{q}(1+\gamma_5)c), \tag{6.2.35}$$

$$T_1^q = (\bar{c}\,\gamma_\mu(1-\gamma_5)T^A q)\,(\bar{q}\,\gamma^\mu(1-\gamma_5)T^A c), \tag{6.2.36}$$

$$T_2^q = (\bar{c}(1-\gamma_5)T^A q)\,(\bar{q}(1+\gamma_5)T^A c), \tag{6.2.37}$$

where T^A is a colour matrix and a summation over colour indices is implied. The parameterisation of the matrix elements of the operators in Eqs. (6.2.34) - (6.2.37) in QCD is given in Appendix C.3. Evaluating the matrix elements in the framework of the HQET, we obtain the set of operators defined in Eqs.(5.2.1), i.e. [2]

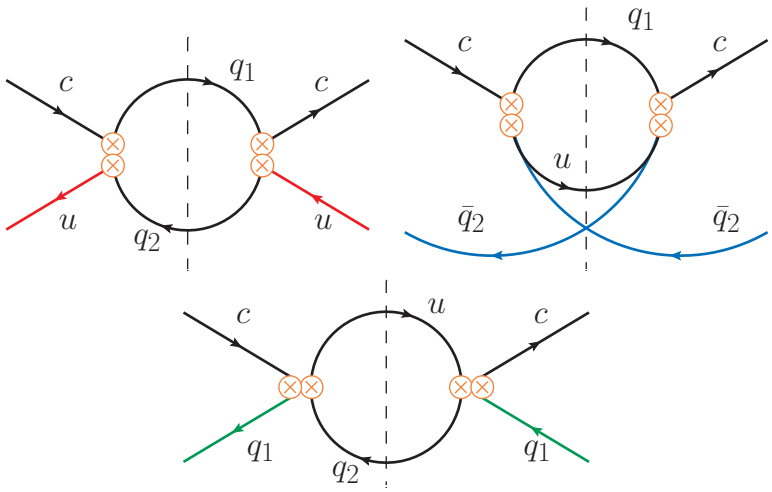

Figure 6.5: Spectator quark effects in the HQE expansion: WE (left), PI (middle) and WA (right).

$$\tilde{O}_1^q = (\bar{h}_v\,\gamma_\mu(1-\gamma_5)q)\,(\bar{q}\,\gamma^\mu(1-\gamma_5)h_v), \tag{6.2.38}$$

$$\tilde{O}_2^q = (\bar{h}_v(1-\gamma_5)q)\,(\bar{q}(1+\gamma_5)h_v), \tag{6.2.39}$$

$$\tilde{T}_1^q = (\bar{h}_v\,\gamma_\mu(1-\gamma_5)T^A q)\,(\bar{q}\,\gamma^\mu(1-\gamma_5)T^A h_v), \tag{6.2.40}$$

$$\tilde{T}_2^q = (\bar{h}_v(1-\gamma_5)T^A q)\,(\bar{q}(1+\gamma_5)T^A h_v), \tag{6.2.41}$$

[1] Sometimes, we will use the short-hand notation O_i^q, $i = 1, 2, 3, 4$ assuming $O_3^q \equiv T_1^q$, $O_4^q \equiv T_2^q$.
[2] Note that all quantities defined in HQET are labelled by a tilde, contrary to those in QCD.

here h_v denotes the HQET field defined by Eqs. (6.2.9), (6.2.10). The matrix elements of these operators are parameterised as

$$\langle D_q|\tilde{O}_i^q\,|D_q\rangle \;=\; F^2(\mu)\,m_{D_q}\,\tilde{B}_i^q, \tag{6.2.42}$$

$$\langle D_q|\tilde{O}_i^{q'}\,|D_q\rangle \;=\; F^2(\mu)\,m_{D_q}\,\tilde{\delta}_i^{q'q}, \qquad q\neq q'\,, \tag{6.2.43}$$

where $q, q' = u, d, s$, $\tilde{B}_i^q$ denote the Bag parameters in HQET, with $\tilde{B}_{1,2}^q$ corresponding to the colour-singlet operators, and $\tilde{B}_{3,4}^q \equiv \tilde{\epsilon}_{1,2}^q$ to the colour-octet ones, and $F(\mu)$ is the HQET decay constant, defined as

$$\langle 0|\bar{q}\gamma^\mu\gamma_5 h_v|D_q(v)\rangle_{\rm HQET} = i\,F(\mu)\,\sqrt{m_{D_q}}\,v^\mu. \tag{6.2.44}$$

where we have used relativistically normalised HQET states and hence the above definitions differ from those in previous chapters (see Eq.(3.2.10)). Additionally a factor of $\sqrt{2}$ has been absorbed into the definition of $F(\mu)$[1]. See Appendix C.3 for a summary of parameterisation used in this chapter of the 4-quark operator matrix elements.

Similarly, the QCD decay constant f_{D_q} is given by [2]

$$\langle 0|\bar{q}\gamma^\mu\gamma_5 c|D_q(p)\rangle_{\rm QCD} = i f_{D_q}\,p^\mu, \tag{6.2.45}$$

with $p = m_{D_q}v$. The relation between f_{D_q} and $F(\mu)$ up to α_s and $1/m_c$ corrections can be found e.g. in [264, 265]. At the scale $\mu = m_c$, it reads

$$f_{D_q} = \frac{F(m_c)}{\sqrt{m_{D_q}}}\left(1 - \frac{2}{3}\frac{\alpha_s(m_c)}{\pi} + \frac{G_1(m_c)}{m_c} + 6\,\frac{G_2(m_c)}{m_c} - \frac{1}{2}\frac{\bar{\Lambda}-m_q}{m_c}\right), \tag{6.2.46}$$

where $\bar{\Lambda} = m_{D_q} - m_c$, and the parameters G_1 and G_2 characterise matrix elements of non-local operators. Note that in our analysis we express the parameter $F(m_c)$ in Eqs. (6.2.42), (6.2.43), in terms of f_{D_q} using Eq. (6.2.46). This brings additional α_s corrections – which become part of NLO dimension-six contribution – as well

[1] This convention is normally chosen so that $F = m_{D_q} f_{D_q}$ when neglecting α_s corrections

[2] The subscript 'QCD' or 'HQET' on the states is usually omitted, however for clarity it is specified in the definition of the decay constant.

as $1/m_c$ ones. The latter, as it will be explained in detail in Section 6.2.6, can be partially absorbed in the contribution of some of the dimension-seven operators in HQET.

In vacuum insertion approximation (VIA), the Bag parameters of the colour-singlet operators are equal to one, $\tilde{B}^q_{1,2} = 1$, and the Bag parameters of the colour-octet operators vanish, $\tilde{\epsilon}^q_{1,2} = 0$. Note that throughout this work we assume isospin symmetry, i.e.

$$\tilde{B}^u_i = \tilde{B}^d_i . \tag{6.2.47}$$

The quantities $\tilde{\delta}^{q'q}_i$ in Eq. (6.2.43) describe the so-called eye-contractions, see Figure 6.6, and characterize "subleading" (compared to the large Bag parameters) effects in the non-perturbative matrix elements – in VIA all eye-contractions vanish i.e. $\tilde{\delta}^{q'q}_i = 0$. However, beyond VIA, the matrix elements of the four-quark operators with external q' quark differ from zero even when the spectator quark q in the D_q meson does not coincide with the quark q', as reflected by $\tilde{\delta}^{q'q}_i$ in Eq. (6.2.43). Note that in our notation the eye-contractions with $q = q'$, are in fact included in the Bag parameters $\tilde{B}^q_i$. And again, due to isospin symmetry we will use:

$$\tilde{\delta}^{uq'}_i = \tilde{\delta}^{dq'}_i , \qquad \tilde{\delta}^{q'u}_i = \tilde{\delta}^{q'd}_i , \qquad q' = u, d, s\,.$$

The Bag parameters $\tilde{B}^q_i$ and $\tilde{\delta}^{qq'}_i$ have been determined using HQET sum rules, specifically the Bag parameters $\tilde{B}^q_i$ for the $D^{+,0}$ mesons were calculated in [55], while corrections due to the strange quark mass as well as the contribution of the eye-contractions, see Figure 6.6, were computed in Chapter 5. The numerical values of the Bag parameters will be briefly discussed in Section 6.3.4 and they are summarised in Appendix C.1.

By considering only the dominant CKM modes and by neglecting the effect of the eye-contractions, at LO-QCD and at dimension-six, the contribution of four-quark operators to the D-mesons decay rate reads

$$\begin{aligned}
16\pi^2\,\tilde{\Gamma}_6^{D^0}\,\frac{\langle\tilde{O}_6\rangle^{D^0}}{m_c^3} &= \Gamma_0|V_{ud}^*|^2\,16\pi^2\frac{M_{D^0}f_{D^0}^2}{m_c^3}\,(1-z_s)^2 \\
&\quad\left\{\left(\frac{1}{3}C_1^2+2\,C_1C_2+3\,C_2^2\right)\left[(\tilde{B}_2^u-\tilde{B}_1^u)+z_s\left(2\tilde{B}_2^u-\frac{\tilde{B}_1^u}{2}\right)\right]\right. \\
&\quad\left.+2\,C_1^2\left[(\tilde{\epsilon}_2^u-\tilde{\epsilon}_1^u)+z_s\left(2\,\tilde{\epsilon}_2^u-\frac{\tilde{\epsilon}_1^u}{2}\right)\right]\right\}\,, \qquad (6.2.48)\\
16\pi^2\,\tilde{\Gamma}_6^{D^+}\,\frac{\langle\tilde{O}_6\rangle^{D^+}}{m_c^3} &= \Gamma_0|V_{ud}^*|^2\,16\pi^2\frac{M_{D^+}f_{D^+}^2}{m_c^3}(1-z_s)^2 \\
&\quad\left\{\left(C_1^2+6\,C_1C_2+C_2^2\right)\tilde{B}_1^d+6\left(C_1^2+C_2^2\right)\tilde{\epsilon}_1^d\right\}\,, \qquad (6.2.49)\\
16\pi^2\,\tilde{\Gamma}_6^{D_s^+}\,\frac{\langle\tilde{O}_6\rangle^{D_s^+}}{m_c^3} &= \Gamma_0|V_{ud}^*|^2\,16\pi^2\frac{M_{D_s^+}f_{D_s^+}^2}{m_c^3} \\
&\quad\left\{\left(3\,C_1^2+2\,C_1C_2+\frac{1}{3}C_2^2+\frac{2}{|V_{ud}^*|^2}\right)\left(\tilde{B}_2^s-\tilde{B}_1^s\right)\right. \\
&\quad\left.+2\,C_2^2\,(\tilde{\epsilon}_2^s-\tilde{\epsilon}_1^s)\right\}\,, \qquad (6.2.50)
\end{aligned}$$

respectively, for the WE, PI and WA topologies. Note that in the latter we have neglected the muon mass in the semileptonic decay $c\to s\mu^+\nu_\mu$. In Eqs. (6.2.48) - (6.2.50) some interesting numerical effects are arising. First, in the charm system, one expects that the contribution due to the spectator quark is of similar size compared to the leading term Γ_3 in the HQE, unless some additional cancellations are present. Using the pole mass $m_c^{\rm Pole}=1.48$ GeV and Lattice QCD values for the decay constants [157] we roughly obtain that

$$\begin{aligned}
16\pi^2\frac{M_{D^0}f_{D^0}^2}{m_c^3} &= 4.1\approx\mathcal{O}(c_3)\,, \qquad (6.2.51)\\
16\pi^2\frac{M_{D_s^+}f_{D_s^+}^2}{m_c^3} &= 6.0\approx\mathcal{O}(c_3)\,. \qquad (6.2.52)
\end{aligned}$$

This result has led the authors of [266] to propose a different ordering for the HQE series in the charm sector. However, to investigate further the size of four-quark contributions, we consider the combinations of Wilson coefficients that appear in

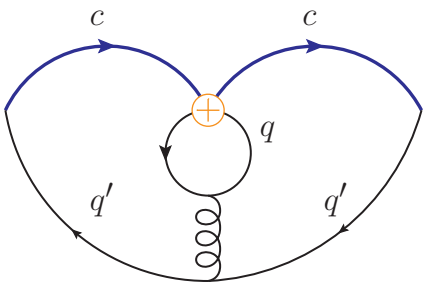

Figure 6.6: Diagram describing the eye-contractions.

Eqs. (6.2.48) - (6.2.50), i.e.

$$C^S_{\rm WE} = \frac{1}{3}C_1^2 + 2\,C_1C_2 + 3\,C_2^2, \qquad C^O_{\rm WE} = 2\,C_1^2, \tag{6.2.53}$$

$$C^S_{\rm PI} = C_1^2 + 6\,C_1C_2 + C_2^2, \qquad C^O_{\rm PI} = 6\,(C_1^2 + C_2^2)\,, \tag{6.2.54}$$

$$C^S_{\rm WA} = 3\,C_1^2 + 2\,C_1C_2 + \frac{1}{3}C_2^2, \qquad C^O_{\rm WA} = 2\,C_2^2\,, \tag{6.2.55}$$

where the superscripts S and O refer to coefficient in front of the colour-singlet and colour-octet Bag parameters, respectively. A comparison of these combinations for different values of the renormalisation scale μ_1 is shown in Table 6.8.

μ_1 [GeV]	1	1.27	1.36	1.44	1.48	3
$C^S_{\rm WE}$(LO)	0.09	0.03	0.02	0.02	0.01	0.01
$C^S_{\rm WE}$(NLO)	−0.03	−0.03	−0.03	−0.02	−0.02	0.04
$C^O_{\rm WE}$(LO)	3.57	3.24	3.16	3.11	3.08	2.63
$C^O_{\rm WE}$(NLO)	3.11	2.89	2.83	2.79	2.77	2.44
$C^S_{\rm PI}$(LO)	−2.80	−2.12	−1.96	−1.85	−1.79	−0.79
$C^S_{\rm PI}$(NLO)	−1.74	−1.28	−1.16	−1.08	−1.04	−0.27
$C^O_{\rm PI}$(LO)	13.0	11.4	11.0	10.7	10.6	8.50
$C^O_{\rm PI}$(NLO)	10.6	9.55	9.31	9.13	9.05	7.60
$C^S_{\rm WA}$(LO)	3.82	3.61	3.56	3.53	3.51	3.24
$C^S_{\rm WA}$(NLO)	3.57	3.42	3.38	3.36	3.35	3.16
$C^O_{\rm WA}$(LO)	0.77	0.55	0.51	0.47	0.46	0.21
$C^O_{\rm WA}$(NLO)	0.41	0.30	0.27	0.25	0.24	0.10

Table 6.8: Comparison of the combinations $C^{S,O}_{\rm WE,PI,WA}$, respectively at LO- and NLO-QCD, for different values of the renormalisation scale μ_1.

From this it is evident that the combination of Wilson coefficients multiplying the

colour-singlet Bag parameters of WE is strongly suppressed. Additionally, depending on whether we disregard α_s^2 corrections in these combinations of $\Delta C = 1$ Wilson coefficients – as we do – or not, we can get even different signs for $C_{\rm WE}^{\rm S}$ at NLO. Moreover, in Eq. (6.2.48) the Bag parameters of the colour singlet operators exactly cancel in VIA at leading order in $1/m_c$. On the other hand, the coefficient of the colour-octet operator is not suppressed for weak exchange. This indicates that, in this case, both singlet and octet operators may be of equal importance. For Pauli interference, the combinations of Wilson coefficients multiplying the colour-singlet operators are significantly enhanced compared to those in WE, the same holds for the colour-octet operators. Note that $C_{\rm PI}^{O}$ and $C_{\rm PI}^{S}$ get large modifications (and even a flip of sign) compared to the case $C_1 = 1$ and $C_2 = 0$ revealing the importance of gluon radiative corrections. Moreover $C_{\rm PI}^{O}$ is enhanced compared to $C_{\rm PI}^{S}$, indicating that both singlet and octet operators might be equally important for Pauli interference. For weak annihilation, the corresponding combination in front of the colour-singlet operators is large. On the other hand, the Bag parameters of the colour singlet operators exactly cancel in VIA at leading order in $1/m_c$.

The above arguments show that, by neglecting the effect of the colour-octet operators in VIA, one might be led to misleading conclusions, and therefore an accurate determination of the deviation of the Bag parameters from their VIA values, using non-perturbative methods like HQET sum rules or lattice simulations, is necessary.

Finally, by including all CKM modes as well as NLO-QCD corrections, the contribution of four-quark operators to the total decay width at order $1/m_c^3$ schematically reads

$$16\pi^2\,\tilde{\Gamma}_6^{D_q}\frac{\langle\tilde{\mathcal{O}}_6\rangle^{D_q}}{m_c^3} = \frac{\Gamma_0}{|V_{cs}|^2}\sum_{i=1}^{4}\Bigg\{\sum_{q_1,q_2=d,s}\left|\lambda_{q_1q_2}\right|^2\Bigg[A_{i,q_1q_2}^{\rm WE}\frac{\langle D_q|\tilde{O}_i^{u}|D_q\rangle}{m_c^3} + A_{i,q_1q_2}^{\rm PI}\frac{\langle D_q|\tilde{O}_i^{q_2}|D_q\rangle}{m_c^3} + A_{i,q_1q_2}^{\rm WA}\frac{\langle D_q|\tilde{O}_i^{q_1}|D_q\rangle}{m_c^3}\Bigg] + \sum_{q_1=d,s}|V_{cq_1}|^2\sum_{\ell=e,\mu}\left[A_{i,q_1\ell}^{\rm WA}\frac{\langle D_q|\tilde{O}_i^{q_1}|D_q\rangle}{m_c^3}\right]\Bigg\}, \tag{6.2.56}$$

where the matrix elements of the four-quark operators are given in Eqs. (6.2.42), (6.2.43), and the short-distance coefficients for the WE, PI and WA topologies, cf. Figure 6.5 are denoted by $A^{\rm WE}_{i,q_1q_2}$, $A^{\rm PI}_{i,q_1q_2}$ and $A^{\rm WA}_{i,q_1q_2}$, $A^{\rm WA}_{i,q_1\ell}$, respectively. NLO corrections to $A^{\rm WE}_{i,q_1q_2}$ and $A^{\rm PI}_{i,q_1q_2}$ have been computed for HQET operators in [191]. The corresponding results for $A^{\rm WA}_{i,q_1q_2}$ can be obtained by Fierz transforming the $\Delta C = 1$ operators given in Eqs. (6.2.2), (6.2.3). Since the Fierz symmetry is respected also at one-loop level, the functions $A^{\rm WA}_{i,q_1q_2}$ are derived from $A^{\rm WE}_{i,q_1q_2}$ by replacing $C_1 \leftrightarrow C_2$. For the semileptonic modes, the coefficients $A^{\rm WA}_{i,q_1\ell}$ have been determined in [200]. Note that in our analysis, we treat the contribution of the $\tilde{\delta}_i^{q'q}$ parameters as a subleading "NLO" effect, therefore their coefficients are included only at LO-QCD. To demonstrate the importance of the NLO-QCD corrections to the spectator effects, we show in Table 6.9 the dimension-six contributions to the D-meson decay widths (see Eq. (6.2.56)) splitting the LO and NLO parts, both in VIA and using HQET SR results for the Bag parameters. NLO-QCD corrections turn out to have an essential numerical effect for the four-quark contributions. In the case of the D^0 and D_s^+ mesons these corrections lift the helicity suppression of weak exchange and weak annihilation being present in LO-QCD when using VIA. For the D_s^+ meson, in addition to the CKM dominant WA contribution, there is a correction due to CKM suppressed but nevertheless large PI topology. In the case of the D^+ meson the overall contribution from Pauli interference turns out to be huge, of the order of $-2.5\ \text{ps}^{-1}$. In addition, the NLO correction to Pauli interference turn also out to be very large, $50\% - 100\%$ of the LO term depending on the mass scheme. Already in the B system this NLO-QCD corrections were found to be of the order of 30% for the ratio $\tau(B^+)/\tau(B_d)$, see e.g. [190] in the Pole scheme. Thus, neglecting these contributions for charm lifetime studies, as done in [267], is clearly not justified and a knowledge of NNLO-QCD corrections to the four-quark contributions would be highly desirable.

Scheme	D^0	D^+	D_s^+
VIA			
Pole	$\underbrace{-0.014}_{\text{NLO}} = \underbrace{0.000}_{\text{LO}} \underbrace{-0.014}_{\Delta\text{NLO}}$	$\underbrace{-2.64}_{\text{NLO}} = \underbrace{-1.68}_{\text{LO}} \underbrace{-0.97}_{\Delta\text{NLO}}$	$\underbrace{-0.20}_{\text{NLO}} = \underbrace{-0.12}_{\text{LO}} \underbrace{-0.08}_{\Delta\text{NLO}}$
$\overline{\text{MS}}$	$\underbrace{-0.010}_{\text{NLO}} = \underbrace{0.000}_{\text{LO}} \underbrace{-0.010}_{\Delta\text{NLO}}$	$\underbrace{-2.49}_{\text{NLO}} = \underbrace{-1.23}_{\text{LO}} \underbrace{-1.25}_{\Delta\text{NLO}}$	$\underbrace{-0.18}_{\text{NLO}} = \underbrace{-0.08}_{\text{LO}} \underbrace{-0.10}_{\Delta\text{NLO}}$
Kinetic	$\underbrace{-0.012}_{\text{NLO}} = \underbrace{0.000}_{\text{LO}} \underbrace{-0.012}_{\Delta\text{NLO}}$	$\underbrace{-2.53}_{\text{NLO}} = \underbrace{-1.42}_{\text{LO}} \underbrace{-1.11}_{\Delta\text{NLO}}$	$\underbrace{-0.19}_{\text{NLO}} = \underbrace{-0.10}_{\text{LO}} \underbrace{-0.09}_{\Delta\text{NLO}}$
$1S$	$\underbrace{-0.013}_{\text{NLO}} = \underbrace{0.000}_{\text{LO}} \underbrace{-0.013}_{\Delta\text{NLO}}$	$\underbrace{-2.60}_{\text{NLO}} = \underbrace{-1.58}_{\text{LO}} \underbrace{-1.02}_{\Delta\text{NLO}}$	$\underbrace{-0.19}_{\text{NLO}} = \underbrace{-0.11}_{\text{LO}} \underbrace{-0.08}_{\Delta\text{NLO}}$
HQET SR			
Pole	$\underbrace{0.007}_{\text{NLO}} = \underbrace{0.019}_{\text{LO}} \underbrace{-0.012}_{\Delta\text{NLO}}$	$\underbrace{-2.89}_{\text{NLO}} = \underbrace{-1.87}_{\text{LO}} \underbrace{-1.02}_{\Delta\text{NLO}}$	$\underbrace{-0.21}_{\text{NLO}} = \underbrace{-0.16}_{\text{LO}} \underbrace{-0.05}_{\Delta\text{NLO}}$
$\overline{\text{MS}}$	$\underbrace{0.020}_{\text{NLO}} = \underbrace{0.014}_{\text{LO}} \underbrace{+0.006}_{\Delta\text{NLO}}$	$\underbrace{-2.72}_{\text{NLO}} = \underbrace{-1.37}_{\text{LO}} \underbrace{-1.35}_{\Delta\text{NLO}}$	$\underbrace{-0.20}_{\text{NLO}} = \underbrace{-0.12}_{\text{LO}} \underbrace{-0.08}_{\Delta\text{NLO}}$
Kinetic	$\underbrace{0.014}_{\text{NLO}} = \underbrace{0.016}_{\text{LO}} \underbrace{-0.002}_{\Delta\text{NLO}}$	$\underbrace{-2.76}_{\text{NLO}} = \underbrace{-1.58}_{\text{LO}} \underbrace{-1.18}_{\Delta\text{NLO}}$	$\underbrace{-0.20}_{\text{NLO}} = \underbrace{-0.13}_{\text{LO}} \underbrace{-0.07}_{\Delta\text{NLO}}$
$1S$	$\underbrace{0.009}_{\text{NLO}} = \underbrace{0.018}_{\text{LO}} \underbrace{-0.008}_{\Delta\text{NLO}}$	$\underbrace{-2.84}_{\text{NLO}} = \underbrace{-1.76}_{\text{LO}} \underbrace{-1.08}_{\Delta\text{NLO}}$	$\underbrace{-0.21}_{\text{NLO}} = \underbrace{-0.15}_{\text{LO}} \underbrace{-0.06}_{\Delta\text{NLO}}$

Table 6.9: Dimension-six contributions to D-meson decay widths (see Eq. (6.2.56)) (in ps^{-1}) and split up into LO-QCD and NLO-QCD corrections within different mass schemes and both in VIA and using the HQET SR for Bag parameters.

6.2.6 Dimension-seven Four-Quark Operator Contribution

The dimension-six four-quark operator contribution discussed in the previous section, is obtained by neglecting in the expression of the incoming momentum $p^\mu = p_c^\mu + p_q^\mu$ the effect due to the small momentum of the light spectator quark $p_q \sim \Lambda_{\text{QCD}}$. Including also corrections linear in the quantity p_q/m_c, leads to the contribution of order $1/m_c^4$ to $\Gamma(D)$, which can be described in terms of the following basis of

dimension-seven operators, defined in full QCD, i.e. [1]

$$P_1^q = m_q\,(\bar{c}(1-\gamma_5)q)(\bar{q}(1-\gamma_5)c)\,, \tag{6.2.57}$$

$$P_2^q = \frac{1}{m_c}(\bar{c}\overleftarrow{D}_\nu\gamma_\mu(1-\gamma_5)D^\nu q)(\bar{q}\gamma^\mu(1-\gamma_5)c)\,, \tag{6.2.58}$$

$$P_3^q = \frac{1}{m_c}(\bar{c}\overleftarrow{D}_\nu(1-\gamma_5)D^\nu q)(\bar{q}(1+\gamma_5)c)\,, \tag{6.2.59}$$

together with the corresponding colour-octet operators S_1^q, S_2^q, S_3^q, containing the generators T^A, and again a summation over colour indices is implied. Due to the presence in Eqs. (6.2.58), (6.2.59) of a covariant derivative acting on the charm quark field, which scales as m_c at this order, there is no immediate power counting for these operators, cf. the HQET operators in Eqs. (6.2.61), (6.2.62). Moreover, note that this basis differs from the one used in [252] for the computation of dimension-seven and dimension-eight contributions.

In order to evaluate the matrix element of the dimension-seven four-quark operators using the framework of the HQET, one has to further expand the charm quark momentum, according to $p^\mu = m_c v^\mu + k^\mu + p_q^\mu$, see Eq. (6.2.8), as well as to include $1/m_c$ corrections to the effective heavy quark field and to the HQET Lagrangian, retaining only terms linear in k/m_c and p_q/m_c. The small residual momentum of the charm quark k^μ will result in a covariant derivative acting on h_v and the small momentum of the spectator quark p_q^μ will result in a covariant derivative acting on the light quark field q. In this case, one obtains the following basis, which includes the local operators

$$\tilde{P}_1^q = m_q\,(\bar{h}_v(1-\gamma_5)q)(\bar{q}(1-\gamma_5)h_v)\,, \tag{6.2.60}$$

$$\tilde{P}_2^q = (\bar{h}_v\gamma_\mu(1-\gamma_5)(iv\cdot D)q)(\bar{q}\gamma^\mu(1-\gamma_5)h_v)\,, \tag{6.2.61}$$

[1] Notice that in e.g. [200] it is used a redundant basis in which the operator denoted by P_2^q is related to P_1^q by hermitean conjugation, namely $P_2^q = m_q\,(\bar{c}(1+\gamma_5)q)(\bar{q}(1+\gamma_5)c) = (P_1^q)^\dagger$. Since these two operators lead to the same matrix element, we only include P_1^q in our basis. It then follows that the operators here denoted by P_2^q and P_3^q, correspond respectively to P_3^q and P_4^q in the notation of [200]. Furthermore, we point out that the matrix element of the operator P_4^q in Eqs. (C5) and (C6) of [200] should have the opposite sign.

$$\tilde{P}_3^q = (\bar{h}_v(1-\gamma_5)(iv\cdot D)q)(\bar{q}(1+\gamma_5)h_v)\,, \tag{6.2.62}$$

and

$$\tilde{R}_1^q = (\bar{h}_v\gamma_\mu(1-\gamma_5)q)(\bar{q}\gamma^\mu(1-\gamma_5)(i\not{D})h_v)\,, \tag{6.2.63}$$

$$\tilde{R}_2^q = (\bar{h}_v(1-\gamma_5)q)(\bar{q}(1+\gamma_5)(i\not{D})h_v)\,, \tag{6.2.64}$$

supplemented by the corresponding colour-octet operators $\tilde{S}^q_{1,2,3}$ and $\tilde{U}^q_{1,2}$, and the non-local operators

$$\tilde{M}^q_{1,\pi} = i\int d^4y\, T\left[\tilde{O}^q_1(0), (\bar{h}_v(iD)^2h_v)(y)\right], \tag{6.2.65}$$

$$\tilde{M}^q_{2,\pi} = i\int d^4y\, T\left[\tilde{O}^q_2(0), (\bar{h}_v(iD)^2h_v)(y)\right], \tag{6.2.66}$$

$$\tilde{M}^q_{1,G} = i\int d^4y\, T\left[\tilde{O}^q_1(0), \frac{1}{2}g_s\left(\bar{h}_v\sigma_{\alpha\beta}G^{\alpha\beta}h_v\right)(y)\right], \tag{6.2.67}$$

$$\tilde{M}^q_{2,G} = i\int d^4y\, T\left[\tilde{O}^q_2(0), \frac{1}{2}g_s\left(\bar{h}_v\sigma_{\alpha\beta}G^{\alpha\beta}h_v\right)(y)\right], \tag{6.2.68}$$

also supplemented by the corresponding colour-octet operators [1]. We see that, compared to the QCD basis, there are in addition the two local operators $\tilde{R}^q_1$ and $\tilde{R}^q_2$ (and also the corresponding colour-octet ones), which emerge from the expansion in Eq. (6.2.10), and the four non-local operators $\tilde{M}^q_{1,\pi}$, $\tilde{M}^q_{2,\pi}$, $\tilde{M}^q_{1,G}$ and $\tilde{M}^q_{2,G}$ (and the corresponding colour-octet ones) which are obtained by taking the time-ordered product of the dimension-six operators with the $1/m_c$ correction to the HQET Lagrangian, see e.g. [45] for details.

We parametrise the matrix elements of the operators in Eqs. (6.2.60) - (6.2.68) using VIA and account for deviations from it by including the corresponding Bag parameters, as it is explicitly shown in Appendix C.3. However, since for these matrix elements there is no non-perturbative evaluation available yet, in our analysis we have to rely only on VIA. It follows that, at LO-QCD the matrix element of the dimension-seven operators listed above, can be expressed in terms of the HQET non-perturbative parameters $F(\mu)$, $G_1(\mu)$, $G_2(\mu)$, and $\bar{\Lambda}$, so far determined only

[1] Operators which vanish due to the equation of motion $(iv\cdot D)h_v = 0$ are not shown.

with large uncertainties. For this reason, we prefer to use as an input the QCD decay constant f_D, which is computed very precisely using Lattice QCD [157]. In doing so, we obtain that in VIA and at the matching scale $\mu = m_c$, the contribution of the local operators $\tilde{R}^q_{1,2}$ as well as that of the non-local ones $\tilde{M}^q_{1,\pi}$, $\tilde{M}^q_{2,\pi}$, $\tilde{M}^q_{1,G}$ and $\tilde{M}^q_{2,G}$ can be entirely absorbed in the QCD decay constant f_D, cf. Eq. (6.2.46) (more precisely, in the matrix element of the dimension-six QCD operators in Eqs. (6.2.34), (6.2.35), which are proportional to f_D), so that we are left only with the $1/m_c$ contribution due to the operators $\tilde{P}^q_{1,2,3}$, analogously to the QCD case [1].

To make this point more clear, we consider as an example the contribution due to Pauli interference at LO-QCD and up to order $1/m_c^4$, in the case of $c \to s\bar{d}u$ transition, which constitutes the dominant correction to $\Gamma(D^+)$,

$$\begin{aligned}\mathrm{Im}\,\mathcal{T}^{\mathrm{PI}} \;=\; \Gamma_0\,|V_{ud}^*|^2\,\frac{32\pi^2}{m_c^3}(1-z_s)^2\Bigg[C_{\mathrm{PI}}^S\left(\tilde{O}_1^d+\frac{\tilde{R}_1^d}{m_c}+\frac{\tilde{M}_{1,\pi}^d}{m_c}+\frac{\tilde{M}_{1,G}^d}{m_c}+2\frac{1+z_s}{1-z_s}\frac{\tilde{P}_3^q}{m_c}\right)\\ +\,(\text{colour-octet part})\Bigg],\end{aligned} \tag{6.2.69}$$

with C_{PI}^S defined in Eq. (6.2.54). By evaluating the matrix element of $\mathrm{Im}\mathcal{T}^{\mathrm{PI}}$ in VIA, the contribution due to the colour-octet operators vanishes. Moreover, using the parametrisation for the matrix elements of the four-quark operators given in Eq. (6.2.42) and in Appendix C.3, we obtain in VIA and setting $\mu = m_c$, that

$$\begin{aligned}\langle D^+|\tilde{O}_1^d+\frac{\tilde{R}_1^d}{m_c}+\frac{\tilde{M}_{1,\pi}^d}{m_c}+\frac{\tilde{M}_{1,G}^d}{m_c}|D^+\rangle_{\mathrm{HQET}} &= F^2(m_c)\,m_{D^+}\left[1-\frac{\bar{\Lambda}}{m_c}\right.\\ &\quad\left.+\frac{2\,G_1(m_c)}{m_c}+\frac{12\,G_2(m_c)}{m_c}\right]\\ &= f_D^2\,m_{D^+}^2 = \langle D^+|O_1^d|D^+\rangle_{\mathrm{QCD}},\end{aligned} \tag{6.2.70}$$

where in the second line we have used the conversion between the QCD and HQET decay constants given in Eq. (6.2.46), showing that the contribution of the local operators $\tilde{R}_i^q$ and non-local operators $\tilde{M}_{i,\pi}^q$ and $\tilde{M}_{i,G}^q$ is entirely absorbed in the QCD

[1] In the matrix element of $\tilde{P}^q_{1,2,3}$ one can replace the HQET decay constant with the QCD one, up to higher order corrections.

decay constant. Note that, by neglecting the effect due to the strange quark mass and using VIA we reproduce the approximate result of Eq. (19) in [266].

The same argument applies also to the remaining topologies i.e. WE and WA. However, it is worth mentioning that in VIA and neglecting the strange quark mass, the contribution of WE and WA exactly vanishes at LO-QCD, due to the helicity suppression. This suppression is lifted once the s-quark mass or perturbative gluon corrections are included, and in this case it becomes again manifest that the contributions of $\tilde{R}_i^q$, $\tilde{\mathcal{M}}_{i,\pi}^q$ and $\tilde{\mathcal{M}}_{i,G}^q$ in HQET can be completely absorbed in f_D by evaluating the matrix elements in VIA [1]. We note that a detailed analysis of the dimension-seven contributions within the HQET has been performed in [265] for the case of $B-\bar{B}$-mixing. Specifically, it was found that in VIA, subleading power corrections due to non-local operators can be entirely absorbed in the definition of the QCD decay constant, and that the residual $1/m_b$ corrections, due to the running of the local dimension-seven operators from the scale m_b to $\mu \sim 1$ GeV, is numerically small ($\sim 5\%$ for [265]).[2]

Finally, by summing over all the CKM modes, at LO-QCD, the dimension-seven contribution can therefore be presented as (with $q = u, d, s$)

$$
\begin{aligned}
16\pi^2\,\tilde{\Gamma}_7^{D_q}\frac{\langle\tilde{\mathcal{O}}_7\rangle^{D_q}}{m_c^4} \;=\; & \frac{\Gamma_0}{|V_{cs}|^2}\sum_{i=1}^{3}\Bigg\{\sum_{q_1,q_2=d,s}\left|\lambda_{q_1q_2}\right|^2\Bigg[G^{\rm WE}_{i,q_1q_2}\frac{\langle D_q|\tilde{P}_i^{u}|D_q\rangle}{m_c^4} \\
& + G^{\rm PI}_{i,q_1q_2}\frac{\langle D_q|\tilde{P}_i^{q_2}|D_q\rangle}{m_c^4} + G^{\rm WA}_{i,q_1q_2}\frac{\langle D_q|\tilde{P}_i^{q_1}|D_q\rangle}{m_c^4}\Bigg] \\
& + \sum_{q_1=d,s}|V_{cq_1}|^2\sum_{\ell=e,\mu}\left[G^{\rm WA}_{i,q_1\ell}\frac{\langle D_q|\tilde{P}_i^{q_1}|D_q\rangle}{m_c^4}\right]\Bigg\} \\
& + (\text{colour-octet part})\,, \qquad (6.2.71)
\end{aligned}
$$

where the matrix elements of the dimension-seven operators are presented in Appendix C.3. We confirm the results for the short-distance coefficients $G^{\rm WE}_{i,q_1q_2}$, $G^{\rm PI}_{i,q_1q_2}$

[1] Note, that for the operator O_2^q the contribution of R_2^q is absorbed by the combination $(m_D\, f_D/m_c)^2 \approx (1 + 2\,\bar{\Lambda}/m_c)\, f_D^2$.

[2] By neglecting the effect of running down to a lower scale, from [265] one can see that in VIA the QCD decay constant entirely absorbs all the $1/m_b$ contributions.

and $G^{\rm WA}_{i,q_1q_2}$, $G^{\rm WA}_{i,q_1\ell}$ presented in [200]. Note that, due to the current accuracy of the analysis, at dimension-seven we include only the contribution of the valence-quark, therefore e.g. $\langle D^0|P_i^s|D^0\rangle = 0$. Numerical values of the dimension-seven contributions to the decay rates and the ratios will be presented in Section 6.4. In Table 6.10 we show the central values of the dimension-seven contributions in ps^{-1} in the kinetic mass scheme and we find for the D^+ meson a correction that is almost as large as the leading dimension three term, see Table 6.5.

	D^0	D^+	D_s^+
$16\pi^2\,\tilde{\Gamma}_7^{D_q}\dfrac{\langle\tilde{\mathcal{O}}_7\rangle^{D_q}}{m_c^4}\,[\mathrm{ps}^{-1}]$	4.6×10^{-7}	1.05	0.10

Table 6.10: Dimension-seven contributions to D-meson decay widths (see Eq. (6.2.71)) in ps^{-1} within VIA in the kinetic mass scheme.

6.3 Determination of the Non-perturbative Parameters

In the present section, we discuss the numerical determination for the matrix elements of the operators introduced in Sections 6.2.2 - 6.2.6. We start with the operators of the lowest mass dimension.

6.3.1 Parameters of the Chromomagnetic Operator

For the B system many of non-perturbative parameters have been determined by performing fits to the experimental data for inclusive semileptonic decays [197, 198]. In the case of the chromomagnetic operator, one finds [198]

$$\mu_G^2(B) \;=\; (0.306\pm0.050)\,\mathrm{GeV}^2\,. \tag{6.3.1}$$

Assuming heavy quark symmetry we expect the corresponding parameter in the D system to have a similar size. Another way of estimating the value of μ_G^2 is to use the well-known spectroscopy relation [268]

$$\mu_G^2(D_{(s)}) = \frac{3}{2} m_c \, (M_{D^*_{(s)}} - M_{D_{(s)}}) \,, \tag{6.3.2}$$

which holds up to power corrections. Using the value for the meson masses given in the PDG [169] and setting $m_c = 1.27\,\text{GeV}$, we obtain the following estimates:

$$\mu_G^2(D) = (0.268 \pm 0.107)\,\text{GeV}^2, \qquad \mu_G^2(D_s) = (0.274 \pm 0.110)\,\text{GeV}^2, \tag{6.3.3}$$

where we have conservatively added an uncertainty of 40% due to unknown power corrections of order $1/m_c$. The values in Eq. (6.3.3) are roughly 19% smaller than those obtained from experimental fits for semileptonic B-meson decays, see Eq. (6.3.1). Moreover, Eq. (6.3.2) leads to a tiny amount of $SU(3)_f$-symmetry breaking of $\approx 2\%$, which might, however, be enhanced by the neglected power corrections. In the literature many times instead of Eq. (6.3.2) the relation [45, 269]

$$\mu_G^2(D_{(s)}) \;=\; \frac{3}{4} \left(M^2_{D^*_{(s)}} - M^2_{D_{(s)}} \right) \tag{6.3.4}$$

is adopted, which coincides with Eq. (6.3.2) up to corrections of order $1/m_c$. Numerically we find that Eq. (6.3.4) yields

$$\mu_G^2(D) = 0.41\,\text{GeV}^2 \,, \qquad \mu_G^2(D_s^+) = 0.44\,\text{GeV}^2 \,, \tag{6.3.5}$$

which are roughly 23% higher than that in Eq. (6.3.1). In our numerical analysis, we will use the average value of the two determinations in Eq. (6.3.3) and Eq. (6.3.5). This gives

$$\mu_G^2(D) = (0.34 \pm 0.10)\,\text{GeV}^2, \qquad \mu_G^2(D_s^+) = (0.36 \pm 0.10)\,\text{GeV}^2 \,, \tag{6.3.6}$$

which agrees well with the one in Eq. (6.3.1).

Thus, from Eq. (6.2.27), we expect corrections to the total decay rate due to the chromomagnetic operator, $c_G\,\mu_G^2/(c_3\,m_c^2)$ ranging between -6% and $+8\%$ with respect

to the leading free-quark decay contribution. A large part of the sizable uncertainty derives from the cancellations in the coefficient c_G, shown in Table 6.6 and Figure 6.3, which could be reduced with a complete determination of the NLO-QCD corrections to c_G. For semileptonic rates the contribution of the chromomagnetic operator can be even of the order of 20%, see Section 6.4.3.

An experimental determination of $\mu_G^2(D)$ from inclusive semileptonic D-meson decays could further reduce the uncertainties and could in particular give some insight into the numerical size of $SU(3)_F$ breaking.

6.3.2 Parameters of the Kinetic Operator

For the matrix element of the kinetic operator no precise determination is available so far in the charm sector. Several predictions of μ_π^2 available in the literature for the B-meson cover a large range of values, see Table 6.11. Assuming heavy quark

Source	LQCD [270]	LQCD [254]	Exp. fit [197]	Exp. fit [198]	QCD SR [259]	QCD SR [258]
$\mu_\pi^2[\text{GeV}^2]$	0.05(22)	0.314(15)	0.465(68)	0.477(56)	0.10(5)	0.6(1)

Table 6.11: Different determinations of $\mu_\pi^2(B)$ available in the literature.

symmetry one can use the value obtained from the recent fit of the semileptonic B-meson decays [198]:

$$\mu_\pi^2(B) \;=\; (0.477 \pm 0.056)\,\text{GeV}^2\,, \tag{6.3.7}$$

to get the following estimate for the D-meson

$$\mu_\pi^2(D) \;=\; (0.48 \pm 0.20)\,\text{GeV}^2. \tag{6.3.8}$$

In the above, we have again added a conservative uncertainty of 40% to account for the breaking of the heavy quark symmetry. This value clearly fulfills the theoretical bound $\mu_\pi^2 \geq \mu_G^2$, see e.g. the review [271]. Thus we expect from Eq. (6.2.27)

corrections due to the kinetic operator of the order of -10%, which is also found in Section 6.4.3 – both for the total decay rate and the semileptonic one.

The $SU(3)_F$ breaking effects for the kinetic operator have been estimated in [200,272]

$$\mu_\pi^2(D_s^+) - \mu_\pi^2(D^0) \approx 0.09\,\mathrm{GeV}^2\,, \tag{6.3.9}$$

leading to the following estimate we use for the D_s meson:

$$\mu_\pi^2(D_s^+) = (0.57 \pm 0.23)\,\mathrm{GeV}^2. \tag{6.3.10}$$

Again a more precise experimental determination of μ_π^2 from fits to semileptonic D^+, D^0 and D_s^+ meson decays – as it was done for the B^+ and B^0 decays – would be very desirable.

6.3.3 Parameters of the Darwin Operator

For the matrix element of the Darwin operator no theoretical determination for the charm sector is available. We again could assume heavy quark symmetry and use the corresponding value in the B-system, obtained from recent fits of the semileptonic decays [198]:

$$\rho_D^3(B) = (0.185 \pm 0.031)\,\mathrm{GeV}^3\,, \tag{6.3.11}$$

and add quadratically an uncertainty of 40% for the transition from the B to the D system, leading to a first estimate of

$$\rho_D^3(D)^I = (0.185 \pm 0.080)\,\mathrm{GeV}^3\,. \tag{6.3.12}$$

Alternatively the Darwin parameter can be related to the matrix elements of the dimension-six four-quark operators through the equation of motion for the gluon

field. At leading order in $1/m_Q$ one obtains:

$$\rho_D^3(H) = \frac{g_s^2}{18} f_H^2\, m_H \left[2\,\tilde{B}_2^{q'} - \tilde{B}_1^{q'} + \frac{3}{4}\tilde{\epsilon}_1^{q'} - \frac{3}{2}\tilde{\epsilon}_2^{q'} + \sum_{q=u,d,s} \left(2\tilde{\delta}_2^{qq'} - \tilde{\delta}_1^{qq'} + \frac{3}{4}\tilde{\delta}_3^{qq'} - \frac{3}{2}\tilde{\delta}_4^{qq'} \right) \right] + \mathcal{O}\left(\frac{1}{m_Q}\right), \tag{6.3.13}$$

where H is a heavy hadron with the mass m_H and the decay constant f_H, $q' = u, d, s$ is the light valence quark in the H-hadron, and the Bag parameters $\tilde{B}_1^q$, $\tilde{B}_2^q$, $\tilde{\epsilon}_1^q$, $\tilde{\epsilon}_2^q$, $\tilde{\delta}_1^{qq'}$ $\tilde{\delta}_2^{qq'}$ $\tilde{\delta}_3^{qq'}$ and $\tilde{\delta}_4^{qq'}$ were introduced in Section 6.2.5. Their numerical values are summarised in Table C.2 in Appendix C.3. The strong coupling g_s has its origin in the non-perturbative regimes – e.g. [273] suggests to set $\alpha_s = 1$.

Using the input from the Appendix C.1 and applying Eq. (6.3.13) we derive estimates of ρ_D^3 for B- and D-mesons both in VIA and using the HQET SR results for the Bag parameters. The values are summarised in Table 6.12 for the three different choices, $\alpha_s(\mu = 1.5\,\text{GeV})$, $\alpha_s(\mu = 1\,\text{GeV})$ and $\alpha_s = 1$.

	$\mu = 1.5$ GeV		$\mu = 1.0$ GeV		$\alpha_s = 1$	
$\rho_D^3[\text{GeV}^3]$	VIA	HQET	VIA	HQET	VIA	HQET
B^+, B_d	0.048	0.047	0.066	0.064	0.133	0.129
B_s	0.072	0.070	0.098	0.095	0.199	0.193
D^+, D^0	0.021	0.020	0.027	0.026	0.059	0.056
D_s^+	0.030	0.029	0.040	0.038	0.086	0.082

Table 6.12: Values of $\rho_D^3(H)$ for B- and D-mesons in VIA and using HQET SR for Bag parameters for three different choices of α_s in Eq. (6.3.13).

Setting $\alpha_s = 1$ in Eq. (6.3.13) yields values for ρ_D^3 that are close to the one determined from the fit of semileptonic B meson decays, Eq. (6.3.11), indicating $1/m_b$-corrections in Eq. (6.3.13) of the order of +30%. Moreover, we find that VIA gives in Eq. (6.3.13) values which are very close to the HQET sum rule ones. We emphasise that due to the sizeable $SU(3)_F$ breaking in the decay constants, Eq. (6.3.13) leads also to

a sizable $SU(3)_F$ breaking for the non-perturbative parameters $\rho_D^3(D)$, $\rho_D^3(D_s^+)$. Taking the values corresponding to $\alpha_s = 1$ and using HQET SR results for the bag parameters we get the second estimate (last column in Table 6.12)

$$\rho_D^3(D)^{II} = (0.056 \pm 0.022)\,\text{GeV}^3\,, \qquad \rho_D^3(D_s^+)^{II} = (0.082 \pm 0.033)\,\text{GeV}^3\,, \quad (6.3.14)$$

where we have again added a 40% uncertainty. Finally, another possibility to extract $\rho_D^3(D)$ is to substitute in Eq. (6.3.13) the values of the Bag parameters in VIA, which gives

$$\rho_D^3(H) \approx \frac{g_s^2}{18} f_H^2\, m_H. \quad (6.3.15)$$

Assuming a similar size for the strong coupling in both the B- and D-meson matrix elements, from Eq. (6.3.15) one obtains:

$$\rho_D^3(D) \approx \frac{f_D^2\, m_D}{f_B^2\, m_B}\, \rho_D^3(B)\,, \qquad \rho_D^3(D_s) \approx \frac{f_{D_s}^2 m_{D_s}}{f_B^2\, m_B}\, \rho_D^3(B)\,. \quad (6.3.16)$$

Using the most precise determination of the decay constants from Lattice QCD [157], and of the meson masses from PDG [169] and taking into account the value of $\rho_D^3(B)$ in Eq. (6.3.11), leads to the following estimates:

$$\rho_D^3(D)^{III} = (0.082 \pm 0.035)\,\text{GeV}^3\,, \qquad \rho_D^3(D_s)^{III} = (0.119 \pm 0.052)\,\text{GeV}^3\,, \quad (6.3.17)$$

where we again assign in addition a conservative 40% uncertainty due to missing power corrections. These values are consistent with the numbers shown in Table 6.12 for $\alpha_s = 1$. Contrary to the case of the dimension-five non-perturbative parameters, in Eq. (6.3.17) one observes a large $SU(3)_f$ -symmetry breaking of $\approx 46\%$, similar to the $\approx 49\%$ that one obtains for the $B_{(s)}$-mesons, mostly stemming from the ratios f_{B_s}/f_{B_d} and $f_{D_s^+}/f_{D^0}$. In our numerical analysis we use the values shown in Eq. (6.3.17), which lies between the estimates obtained in Eq. (6.3.12) and Eq. (6.3.14).

Again, here a more precise experimental determination of ρ_D^3 from fits to semileptonic D^+, D^0 and D_s^+ meson decays – as it was done for the B^+ and B^0 decays – would be very desirable and could have a significant effect on the phenomenology of inclusive

charm decays.

6.3.4 Bag parameters of Dimension-six and Dimension-seven

The dimension-six Bag parameters of the D^+ and D^0 mesons have been determined using HQET Sum Rules [55]; strange quark mass corrections, relevant for the Bag parameter of the D_s^+ meson, as well as eye-contractions have been computed for the first time in Chapter 5. The results are collected in Table C.2 and the HQET sum rules suggest values for the Bag parameter that are very close to VIA.

For the dimension-seven Bag parameters (defined in HQET), we apply VIA. As one can see from Appendix C.3, the matrix elements of dimension-seven operators in HQET depend also on the parameters $\bar{\Lambda}_{(s)} = m_{D_{(s)}} - m_c$, for which we use the following ranges [3]

$$\begin{aligned} \bar{\Lambda} &= (0.5 \pm 0.1)\,\text{GeV}, \\ \bar{\Lambda}_s &= (0.6 \pm 0.1)\,\text{GeV}. \end{aligned} \tag{6.3.18}$$

6.4 Numerical Results

In this section, using all the ingredients described above, we present the theoretical prediction for the total and semileptonic decay rates, and for their ratios. All the input used in our numerical analysis are collected in Appendix C.1. For each observable, we investigate several quark mass schemes (with the kinetic scheme as default) and compare the corresponding results using both VIA and HQET SR values for the Bag parameters. The uncertainties quoted below are obtained by varying all the input parameters within their intervals. For the renormalisation scales, we fix the central values to $\mu_1 = \mu_0 = 1.5\,\text{GeV}$ and vary both of them independently between 1 and 3 GeV. Moreover we add an estimated uncertainty due to missing

VIA					
Observable	Pole	$\overline{\text{MS}}$	Kinetic	$1S$	Exp. value
$\Gamma(D^0)[\text{ps}^{-1}]$	1.71	1.49	1.58	1.66	2.44
$\Gamma(D^+)[\text{ps}^{-1}]$	0.22	-0.01	0.11	0.18	0.96
$\bar{\Gamma}(D_s^+)[\text{ps}^{-1}]$	1.76	1.51	1.61	1.71	1.88
$\tau(D^+)/\tau(D^0)$	2.55	2.56	2.53	2.54	2.54
$\bar{\tau}(D_s^+)/\tau(D^0)$	0.97	0.99	0.98	0.98	1.30
$B_{sl}^{D^0}[\%]$	5.43	6.55	6.14	5.75	6.49
$B_{sl}^{D^+}[\%]$	13.8	16.6	15.6	14.6	16.07
$B_{sl}^{D_s^+}[\%]$	7.12	8.42	7.95	7.50	6.30
$\Gamma_{sl}^{D^+}/\Gamma_{sl}^{D^0}$	1.00	1.00	1.00	1.00	0.985
$\Gamma_{sl}^{D_s^+}/\Gamma_{sl}^{D^0}$	1.06	1.05	1.05	1.05	0.790

Table 6.13: Central values of the charm observables in different quark mass schemes using VIA for the matrix elements of the 4-quark operators compared to the corresponding experimental values (last column).

higher power corrections. The results are discussed in the following subsections and they are summarised in Tables 6.13, 6.14, 6.15 and in Figure 6.7.

6.4.1 The Total Decay Rates

We start by investigating the theory prediction of the total decay rates, which are expected to have sizable uncertainties due to the dependence of the free quark decay on the fifth power of the charm quark mass and due to large perturbative and power corrections. The central values for the HQE prediction of the decay widths in different mass schemes, are shown in the three first rows of Table 6.13, using VIA for the Bag parameters and of Table 6.14 using the HQET sum rules results. In Table 6.15 we show the theoretical prediction including the corresponding

HQET SR					
Observable	Pole	$\overline{\text{MS}}$	Kinetic	$1S$	Exp. value
$\Gamma(D^0)[\text{ps}^{-1}]$	1.73	1.52	1.61	1.68	2.44
$\Gamma(D^+)[\text{ps}^{-1}]$	-0.03	-0.24	-0.12	-0.06	0.96
$\bar{\Gamma}(D_s^+)[\text{ps}^{-1}]$	1.75	1.50	1.60	1.69	1.88
$\tau(D^+)/\tau(D^0)$	2.83	2.83	2.80	2.82	2.54
$\bar{\tau}(D_s^+)/\tau(D^0)$	0.99	1.01	1.00	1.00	1.30
$B_{sl}^{D^0}[\%]$	5.26	6.42	6.00	5.59	6.49
$B_{sl}^{D^+}[\%]$	13.4	16.3	15.2	14.2	16.07
$B_{sl}^{D_s^+}[\%]$	7.10	8.36	7.91	7.48	6.30
$\Gamma_{sl}^{D^+}/\Gamma_{sl}^{D^0}$	1.002	1.001	1.001	1.002	0.985
$\Gamma_{sl}^{D_s^+}/\Gamma_{sl}^{D^0}$	1.08	1.06	1.07	1.08	0.790

Table 6.14: Central values of the charm observables in different quark mass schemes using HQET sum rule results [3,55] for the matrix elements of the 4-quark operators compared to the corresponding experimental values (last column).

uncertainties within the kinetic mass scheme and using the HQET SR values for the dimension-six Bag parameters – the same result is visualised in Figure 6.7. In each table, the corresponding experimental determinations are listed in the last column. For the D_s^+ meson an additional subtlety is arising due to the large branching fraction of the leptonic decay $D_s^+ \to \tau^+\nu_\tau$, which is not included in the HQE, since the tau lepton is more massive than the charm quark. Using the experimental value of the leptonic branching ratio [169] (online update)

$$\text{Br}(D_s^+ \to \tau^+\nu_\tau) \;=\; (5.48 \pm 0.23)\%\,, \tag{6.4.1}$$

we therefore define a reduced decay rate $\bar{\Gamma}(D_s^+)$:

$$\bar{\Gamma}(D_s^+) \equiv \Gamma(D_s^+) - \Gamma(D_s^+ \to \tau^+\nu_\tau) \;=\; (1.88 \pm 0.02)\,\text{ps}^{-1}\,, \tag{6.4.2}$$

Observable	HQE prediction	Exp. value
$\Gamma(D^0)[\text{ps}^{-1}]$	$1.61 \pm 0.37^{+0.46\,+0.01}_{-0.37\,-0.01}$	2.44 ± 0.01
$\Gamma(D^+)[\text{ps}^{-1}]$	$-0.12 \pm 0.77^{+0.59\,+0.25}_{-0.28\,-0.10}$	0.96 ± 0.01
$\bar{\Gamma}(D_s^+)[\text{ps}^{-1}]$	$1.60 \pm 0.44^{+0.52\,+0.02}_{-0.41\,-0.01}$	1.88 ± 0.02
$\tau(D^+)/\tau(D^0)$	$2.80 \pm 0.85^{+0.01\,+0.11}_{-0.14\,-0.26}$	2.54 ± 0.02
$\bar{\tau}(D_s^+)/\tau(D^0)$	$1.00 \pm 0.16^{+0.02\,+0.01}_{-0.03\,-0.01}$	1.30 ± 0.01
$B_{sl}^{D^0}[\%]$	$6.00 \pm 1.57^{+0.33}_{-0.28}$	6.49 ± 0.11
$B_{sl}^{D^+}[\%]$	$15.23 \pm 4.07^{+0.83}_{-0.72}$	16.07 ± 0.30
$B_{sl}^{D_s^+}[\%]$	$7.91 \pm 2.64^{+0.43}_{-0.38}$	6.30 ± 0.16
$\Gamma_{sl}^{D^+}/\Gamma_{sl}^{D^0}$	$1.001 \pm 0.008 \pm 0.001$	0.985 ± 0.028
$\Gamma_{sl}^{D_s^+}/\Gamma_{sl}^{D^0}$	$1.07 \pm 0.24 \pm 0.01$	0.790 ± 0.026

Table 6.15: HQE predictions for all the ten observables in the kinetic scheme (second column), using HQET SR results for the Bag parameters. The first uncertainty is parametric, the second and third uncertainties are due to μ_1- and μ_0-scales variation, respectively. The results are compared with the corresponding experimental measurements (third column).

leading also to a reduced lifetime ratio

$$\frac{\bar{\tau}(D_s^+)}{\tau(D^0)} \;=\; 1.30 \pm 0.01\,. \tag{6.4.3}$$

The first and main result we deduce from Table 6.15 and Figure 6.7, is that the HQE gives values of $\Gamma(D^0)$, $\Gamma(D^+)$ and $\Gamma(D_s^+)$ which lie in the ballpark of the experimental numbers. Looking closer we find that our prediction for $\Gamma(D_s)$ is in good agreement with experiment (within large uncertainties), while the total decay rates of the D^0 and D^+ mesons are underestimated. As a reason for that we suspect missing NNLO-QCD corrections to the free charm quark decay.

Second, using different mass schemes yields similar results, and further higher order correction will reduce the differences between these schemes. Due to the fact that the values of the HQET Bag parameters [3, 55] listed in Table C.2 are close to the

corresponding ones in VIA, the predictions shown in Table 6.13 and in Table 6.14 do not differ much. A peculiar role is played by the D^+ meson, where we get a huge theoretical uncertainty stemming from the large negative value of the Pauli interference contribution at dimension-six. This term actually dominates the total decay rate. Moreover, the large negative value is further enhanced by NLO-QCD corrections, but partly compensated by the dimension-seven contribution. Here further studies of the Bag parameters, e.g. via an independent confirmation of the HQET sum rule results with lattice QCD, as well as calculation of higher order QCD corrections to dimension-six and dimension-seven might yield deeper insights.

In order to further analyse the size of the individual contributions to the total decay rate, we show below the numerical coefficients of each non-perturbative parameter in the HQE, using the central values for the input in Appendix C.1 and (as an example) the kinetic scheme for the charm mass with $\mu^{\rm cut} = 0.5$ GeV, namely[1]

$$\begin{aligned}
\Gamma(D^0) &= \Gamma_0 \Bigg[\underbrace{6.15}_{c_3^{\rm LO}} + \underbrace{2.95}_{\Delta c_3^{\rm NLO}} - 1.66\,\frac{\mu_\pi^2(D)}{\rm GeV^2} + 0.13\,\frac{\mu_G^2(D)}{\rm GeV^2} + 23.6\,\frac{\rho_D^3(D)}{\rm GeV^3} \\
&\quad - 1.60\,\tilde{B}_1^q + 1.53\,\tilde{B}_2^q - 21.0\,\tilde{\epsilon}_1^q + 19.2\,\tilde{\epsilon}_2^q + \underbrace{0.00}_{\rm dim-7,VIA} \\
&\quad - 10.7\,\tilde{\delta}_1^{qq} + 1.53\,\tilde{\delta}_2^{qq} + 54.6\,\tilde{\delta}_3^{qq} + 0.13\,\tilde{\delta}_4^{qq} \\
&\quad - 29.2\,\tilde{\delta}_1^{sq} + 28.8\,\tilde{\delta}_2^{sq} + 0.56\,\tilde{\delta}_3^{sq} + 2.36\,\tilde{\delta}_4^{sq} \Bigg] \\
&= 6.15\,\Gamma_0 \Bigg[1 + 0.48 - 0.13\,\frac{\mu_\pi^2(D)}{0.48\,\rm GeV^2} + 0.01\,\frac{\mu_G^2(D)}{0.34\,\rm GeV^2} + 0.31\,\frac{\rho_D^3(D)}{0.082\,\rm GeV^3} \\
&\quad - \underbrace{0.01}_{\rm dim-6,VIA} - 0.005\,\frac{\delta\tilde{B}_1^q}{0.02} + 0.005\,\frac{\delta\tilde{B}_2^q}{0.02} + 0.137\,\frac{\tilde{\epsilon}_1^q}{-0.04} - 0.125\,\frac{\tilde{\epsilon}_2^q}{-0.04} \\
&\quad + \underbrace{0.00}_{\rm dim-7,VIA} \\
&\quad - 0.0045\,r_1^{qq} - 0.0004\,r_2^{qq} - 0.0035\,r_3^{qq} + 0.0000\,r_4^{qq} \\
&\quad - 0.0109\,r_1^{sq} - 0.0079\,r_2^{sq} - 0.0000\,r_3^{sq} + 0.0001\,r_4^{sq} \Bigg] . \qquad (6.4.4)
\end{aligned}$$

[1] Here and hereafter, in the Bag parameters we use the same label q both for u or d-quarks, reflecting the isospin symmetry, namely $\tilde{B}_i^u = \tilde{B}_i^d \equiv \tilde{B}_i^q$ and $\tilde{\delta}_i^{ud} = \tilde{\delta}_i^{du} \equiv \tilde{\delta}_i^{qq}$, $\tilde{\delta}_i^{us} = \tilde{\delta}_i^{ds} \equiv \tilde{\delta}_i^{qs}$, $\tilde{\delta}_i^{su} = \tilde{\delta}_i^{sd} \equiv \tilde{\delta}_i^{sq}$.

In the second equality in Eq. (6.4.4) we have normalised the HQE parameters $\mu_\pi^2(D)$, $\mu_G^2(D)$ and $\rho_D^3(D)$ to their central values. Moreover, we introduce

$$\tilde{B}_i^q = 1 + \delta\tilde{B}_i^q \,, \tag{6.4.5}$$

to indicate deviations from VIA and we conservatively normalise $\delta\tilde{B}_i^q$ to 0.02. The matrix elements of the colour-octet operators are normalised to -0.04 – here using the central value of the HQET determination for $\tilde{\epsilon}_2^q$ might underestimate its effect due to the quoted HQET uncertainties. Furthermore, we introduce also the ratios $r_i^{qq'} \equiv \tilde{\delta}_i^{qq'}/\langle\tilde{\delta}_i^{qq'}\rangle$, with $\langle\tilde{\delta}_i^{qq'}\rangle$ being the central values listed in Table C.2.

For the neutral D meson we find a convergent series, with the largest correction due to the QCD corrections to the free quark decay and the contribution of the Darwin operator. Here a calculation of the NNLO-QCD corrections to the free-quark decay would be very desirable, as well as a more profound determination of the value of the matrix element of the Darwin operator. Note that since we take as a central value $\mu_1 = 1.5$ GeV, the coefficient of the chromomagnetic operator in Eq. (6.4.4) turns out accidentally to be very small, see Figure 6.3. In fact, varying the renormalisation scale μ_1 between 1 and 3 GeV one finds quite sizable contribution of $\sim 5 - 10\%$ due to $\mu_G^2(D)$.

Because of the helicity suppression, we get only small contributions from the weak exchange diagrams. In LO-QCD and VIA these corrections actually vanish, the small value ≈ -0.01 stems from NLO-QCD corrections, which break the helicity suppression. Nevertheless, depending on the size of the $\tilde{\epsilon}_i^q$, the colour-octet operator could give contributions of a similar size as the kinetic operator. Finally, according to the HQET SR determination, the numerical effect of the eye-contractions does not seem to be pronounced.

Similarly, we get for the D^+-meson decay width:

$$\begin{aligned}
\Gamma(D^+) &= \Gamma_0\Bigg[\underbrace{6.15}_{c_3^{\rm LO}}+\underbrace{2.95}_{\Delta c_3^{\rm NLO}} -1.66\,\frac{\mu_\pi^2(D)}{\rm GeV^2}+0.13\,\frac{\mu_G^2(D)}{\rm GeV^2}+23.6\,\frac{\rho_D^3(D)}{\rm GeV^3}\\
&\quad -16.9\,\tilde{B}_1^q+0.56\,\tilde{B}_2^q+84.0\,\tilde{\epsilon}_1^q-1.34\,\tilde{\epsilon}_2^q+\underbrace{6.76}_{\rm dim-7}\\
&\quad -0.06\,\tilde{\delta}_1^{qq}+0.06\,\tilde{\delta}_2^{qq}-16.8\,\tilde{\delta}_3^{qq}+16.9\,\tilde{\delta}_4^{qq}\\
&\quad -29.3\,\tilde{\delta}_1^{sq}+28.8\,\tilde{\delta}_2^{sq}+0.56\,\tilde{\delta}_3^{sq}+2.36\,\tilde{\delta}_4^{sq}\Bigg]\\
&= 6.15\,\Gamma_0\Bigg[1+0.48-0.13\,\frac{\mu_\pi^2(D)}{0.48\,\rm GeV^2}+0.01\,\frac{\mu_G^2(D)}{0.34\,\rm GeV^2}+0.31\,\frac{\rho_D^3(D)}{0.082\,\rm GeV^3}\\
&\quad -\underbrace{2.66}_{\rm dim-6,VIA}-0.055\,\frac{\delta\tilde{B}_1^q}{0.02}+0.002\,\frac{\delta\tilde{B}_2^q}{0.02}-0.546\,\frac{\tilde{\epsilon}_1^q}{-0.04}+0.009\,\frac{\tilde{\epsilon}_2^q}{-0.04}\\
&\quad +\underbrace{1.10}_{\rm dim-7,VIA}\\
&\quad -0.0000\,r_1^{qq}-0.0000\,r_2^{qq}+0.0011\,r_3^{qq}+0.0008\,r_4^{qq}\\
&\quad -0.0109\,r_1^{sq}-0.0080\,r_2^{sq}-0.0000\,r_3^{sq}+0.0001\,r_4^{sq}\Bigg], \qquad (6.4.6)
\end{aligned}$$

where we observe huge negative corrections due to Pauli interference. In VIA we get from dimension-six (summing LO and NLO-QCD) a $\approx -270\%$ correction to the LO-free-quark decay. Dimension-seven yields a large positive correction of $+110\%$. Because of the almost perfect cancellation between the three dominant terms, $16\pi^2\left(\tilde{\Gamma}_6^{(0)}+\alpha_s/\pi\tilde{\Gamma}_6^{(1)}\right)\langle\tilde{\mathcal{O}}_6\rangle^{\rm VIA}/m_c^3$, Γ_3 and $16\pi^2\tilde{\Gamma}_7^{(0)}\langle\tilde{\mathcal{O}}_7\rangle^{\rm VIA}/m_c^4$, the HQE series for $\Gamma(D^+)$ becomes very sensitive to sub-dominant terms, e.g. higher order QCD corrections to $\tilde{\Gamma}_6$, $\tilde{\Gamma}_7$, Γ_3, Γ_5 and Γ_6, and to deviations of the Bag parameter from VIA. In this case it might also be interesting to further study estimates of higher orders in the HQE, see e.g. [251,252]. Else, we get for the two-quark $\Delta C=0$ contributions the same (due to isospin) size of corrections as in the D^0 case and we find, based on the HQET sum rules estimates, again that the eye-contractions give only tiny corrections.

Finally, we have for the D_s^+-meson decay width:

$$\begin{aligned}
\Gamma(D_s^+) &= \Gamma_0\Bigg[\underbrace{6.15}_{c_3^{\rm LO}} + \underbrace{2.95}_{\Delta c_3^{\rm NLO}} - 1.66\,\frac{\mu_\pi^2(D_s)}{\rm GeV^2} + 0.13\,\frac{\mu_G^2(D_s)}{\rm GeV^2} + 23.6\,\frac{\rho_D^3(D_s)}{\rm GeV^3} \\
&\quad - 49.6\,\tilde{B}_1^s + 48.4\,\tilde{B}_2^s - 13.7\,\tilde{\epsilon}_1^s + 18.8\,\tilde{\epsilon}_2^s + \underbrace{0.63}_{\rm dim-7} \\
&\quad - 15.8\,\tilde{\delta}_1^{qs} + 2.34\,\tilde{\delta}_2^{qs} + 55.4\,\tilde{\delta}_3^{qs} + 25.0\,\tilde{\delta}_4^{qs}\Bigg] \\
&= 6.15\,\Gamma_0\Bigg[1 + 0.48 - 0.15\,\frac{\mu_\pi^2(D_s)}{0.57\,\rm GeV^2} + 0.01\,\frac{\mu_G^2(D_s)}{0.36\,\rm GeV^2} + 0.46\,\frac{\rho_D^3(D_s)}{0.119\,\rm GeV^3} \\
&\quad - \underbrace{0.20}_{\rm dim-6,VIA} - 0.161\,\frac{\delta\tilde{B}_1^s}{0.02} + 0.157\,\frac{\tilde{B}_2^s}{0.02} + 0.089\,\frac{\tilde{\epsilon}_1^s}{-0.04} + 0.122\,\frac{\tilde{\epsilon}_2^s}{0.04} \\
&\quad + \underbrace{0.10}_{\rm dim-7,VIA} \\
&\quad - 0.0064\,r_1^{qs} - 0.0007\,r_2^{qs} - 0.0036\,r_3^{qs} + 0.0012\,r_4^{qs}\Bigg]\,, \qquad (6.4.7)
\end{aligned}$$

where we find again a converging series with the dominant contribution coming from the NLO-QCD corrections to the free quark decay and the Darwin term. For the latter a more reliable determination of the corresponding non-perturbative matrix elements would be highly desirable. In VIA, the four-quark operators show again a pronounced cancellation between dimension-six and dimension-seven contributions.

6.4.2 The Lifetime Ratios

In order to eliminate the contribution of the free-quark decay, we calculate the lifetime ratios as

$$\frac{\tau(D_{(s)}^+)}{\tau(D^0)} = 1 + \left[\Gamma^{\rm HQE}(D^0) - \Gamma^{\rm HQE}(D_{(s)}^+)\right]\tau^{\rm exp}(D_{(s)}^+)\,, \qquad (6.4.8)$$

where $\Gamma^{\rm HQE}(D^0)$ and $\Gamma^{\rm HQE}(D_{(s)}^+)$ are given in Eqs. (6.4.4) and (6.4.6), (6.4.7), respectively. In these ratios, Γ_3 cancels exactly and Γ_5 and Γ_6 cancel up to isospin or $SU(3)_F$ breaking corrections in the corresponding non-perturbative matrix elements. The lifetime ratios should then be dominated by the contribution of four-quark

operators.

The central values for the HQE prediction of the lifetime ratios in several mass schemes are shown in the fourth and fifth rows of Table 6.13, Table 6.14, Table 6.15 and in Figure 6.7 and it turns out that the large lifetime ratio $\tau(D^+)/\tau(D^0)$ is well reproduced in all schemes, while in the case of $\tau(D_s^+)/\tau(D^0)$ the HQE predictions lie closer to one compared to the experimental values. The latter theory result is dominated by $SU(3)_F$ breaking differences of the non-perturbative matrix elements μ_π^2, μ_G^2 and ρ_D^3, which are only very roughly known, see Section 6.3. With future, more precise determinations of these parameters our conclusion might significantly change for this lifetime ratio.

The large lifetime ratio $\tau(D^+)/\tau(D^0)$ can be expressed as

$$\begin{aligned}
\frac{\tau(D^+)}{\tau(D^0)} &= 1 + 2.46\,\tilde{B}_1^q + 0.16\,\tilde{B}_2^q - 16.9\,\tilde{\epsilon}_1^q + 3.31\,\tilde{\epsilon}_2^q \underbrace{-\,1.09}_{\text{dim}-7,\text{VIA}} \\
&\quad - 1.71\,\tilde{\delta}_1^{qq} + 0.24\,\tilde{\delta}_2^{qq} + 1.15\,\tilde{\delta}_3^{qq} - 2.71\,\tilde{\delta}_4^{qq} \\
&\quad + 0.01\,\tilde{\delta}_1^{sq} - 0.01\,\tilde{\delta}_2^{sq} + 0.00\,\tilde{\delta}_3^{sq} + 0.00\,\tilde{\delta}_4^{sq} \\
&= 1 \underbrace{+\,2.62}_{\text{dim}-6,\text{VIA}} \underbrace{-\,1.09}_{\text{dim}-7,\text{VIA}} \\
&\quad + 0.049\,\frac{\delta\tilde{B}_1^q}{0.02} + 0.003\,\frac{\delta\tilde{B}_2^q}{0.02} + 0.676\,\frac{\tilde{\epsilon}_1^q}{-0.04} - 0.132\,\frac{\tilde{\epsilon}_2^q}{-0.04} \\
&\quad - 0.004\,r_1^{qq} - 0.000\,r_2^{qq} - 0.005\,r_3^{qq} - 0.001\,r_4^{qq}\,. \qquad (6.4.9)
\end{aligned}$$

In VIA, we predict a lifetime ratio of 2.5, which is already quite close to the experimental value. Again, we observe here a sizable cancellation between dimension-six and dimension-seven contributions. In order to improve the theoretical prediction, a more precise determination of the Bag parameters of the colour-octet operators is mandatory, as well as of the perturbative higher order QCD corrections in $\tilde{\Gamma}_6$ and $\tilde{\Gamma}_7$.

And finally we get for the lifetime ratio $\tau(D_s^+)/\tau(D^0)$:

$$\begin{aligned}
\frac{\tau(D_s^+)}{\tau(D^0)} &= 1 + 0.14\,\frac{\mu_\pi^2(D_s) - \mu_\pi^2(D)}{\text{GeV}^2} - 0.01\,\frac{\mu_G^2(D_s) - \mu_G^2(D)}{\text{GeV}^2} \\
&\quad -1.93\,\frac{\rho_D^3(D_s) - \rho_D^3(D)}{\text{GeV}^3}\;\underbrace{-0.05}_{\text{dim}-7,\text{VIA}} \\
&\quad - 0.13\,\tilde{B}_1^q + 0.13\,\tilde{B}_2^q + 4.06\,\tilde{B}_1^s - 3.96\,\tilde{B}_2^s \\
&\quad -1.72\,\tilde{\epsilon}_1^q + 1.57\,\tilde{\epsilon}_2^q + 1.12\,\tilde{\epsilon}_1^s - 1.54\,\tilde{\epsilon}_2^s \\
&\quad - 0.88\,\tilde{\delta}_1^{qq} + 0.13\,\tilde{\delta}_2^{qq} + 4.47\,\tilde{\delta}_3^{qq} + 0.01\,\tilde{\delta}_4^{qq} \\
&\quad -2.39\,\tilde{\delta}_1^{qs} + 2.36\,\tilde{\delta}_2^{qs} + 0.05\,\tilde{\delta}_3^{qs} + 0.19\,\tilde{\delta}_4^{qs} \\
&\quad + 1.29\,\tilde{\delta}_1^{sq} - 0.19\,\tilde{\delta}_2^{sq} - 4.54\,\tilde{\delta}_3^{sq} - 2.04\,\tilde{\delta}_4^{sq} \\
&= 1 + 0.012\,\frac{\mu_\pi^2(D_s) - \mu_\pi^2(D)}{0.09\,\text{GeV}^2} - 0.0002\,\frac{\mu_G^2(D_s) - \mu_G^2(D)}{0.02\,\text{GeV}^2} \\
&\quad -0.071\,\frac{\rho_D^3(D_s) - \rho_D^3(D)}{0.037\,\text{GeV}^3} \\
&\quad \underbrace{+0.10}_{\text{dim}-6,\text{VIA}}\;\underbrace{-0.05}_{\text{dim}-7,\text{VIA}} - 0.003\,\frac{\delta\tilde{B}_1^q}{0.02} + 0.003\,\frac{\delta\tilde{B}_2^q}{0.02} + 0.081\,\frac{\delta\tilde{B}_1^s}{0.02} - 0.079\,\frac{\delta\tilde{B}_2^s}{0.02} \\
&\quad + 0.069\,\frac{\tilde{\epsilon}_1^q}{-0.04} - 0.063\,\frac{\tilde{\epsilon}_2^q}{-0.04} - 0.045\,\frac{\tilde{\epsilon}_1^s}{-0.04} - 0.062\,\frac{\tilde{\epsilon}_2^s}{0.04} \\
&\quad - 0.0023\,r_1^{qq} - 0.0002\,r_2^{qq} - 0.0018\,r_3^{qq} + 0.0000\,r_4^{qq} \\
&\quad - 0.0055\,r_1^{qs} - 0.0040\,r_2^{qs} - 0.0000\,r_3^{qs} + 0.0001\,r_4^{qs} \\
&\quad + 0.0032\,r_1^{sq} + 0.0003\,r_2^{sq} + 0.0018\,r_3^{sq} - 0.0006\,r_4^{sq}\,. \qquad (6.4.10)
\end{aligned}$$

With the estimates of μ_π^2, μ_G^2 and ρ_D^3 from Section 6.3 we find that the largest individual $SU(3)_F$ breaking effect ($\approx -7\%$) comes from the Darwin term. Using VIA we obtain a correction of $+5\%$ due to the four-quark contributions of dimension-six and dimension-seven – finite values of the matrix elements of the colour-octet operators as well as of $\delta\tilde{B}_{1,2}^s$ might lead to numerically similar effects. Else we have a large number of smaller $SU(3)_F$ breaking effects, which can be both positive and negative.

6.4.3 The Semileptonic Decay Widths and Their Ratios

For discussing the inclusive semileptonic decays of D mesons, we introduce the shorthand notations $\Gamma_{sl}^D \equiv \Gamma(D \to Xe^+\nu_e)$ and $B_{sl}^D \equiv \mathrm{Br}(D \to Xe^+\nu_e)$. We determine the theory value of the semileptonic branching ratio as

$$B_{sl}^{D,\mathrm{HQE}} = \Gamma_{sl}^{D,\mathrm{HQE}} \cdot \tau(D)^{\mathrm{exp}} \,. \tag{6.4.11}$$

The central values for the HQE prediction of the lifetime ratios in several mass schemes are shown in the sixth, seventh and eighth row of Table 6.13, Table 6.14 and Table 6.15 and in Figure 6.7.

The semileptonic decay rate of the D^0 meson can be written (in the kinetic scheme) as

$$\begin{aligned}
\Gamma_{sl}^{D^0} &= \Gamma_0 \Bigg[\underbrace{1.02}_{c_3^{\mathrm{LO}}} + \underbrace{0.16}_{\Delta c_3^{\mathrm{NLO}}} - 0.27\,\frac{\mu_\pi^2(D)}{\mathrm{GeV}^2} - 0.84\,\frac{\mu_G^2(D)}{\mathrm{GeV}^2} + 2.48\,\frac{\rho_D^3(D)}{\mathrm{GeV}^3} \\
&\qquad - 0.28\,\tilde{\delta}_1^{qq} + 0.28\,\tilde{\delta}_2^{qq} - 5.23\,\tilde{\delta}_1^{sq} + 5.23\,\tilde{\delta}_2^{sq} \Bigg] \\
&= 1.02\,\Gamma_0 \Bigg[1 + 0.16 - 0.13\,\frac{\mu_\pi^2(D)}{0.48\,\mathrm{GeV}^2} - 0.28\,\frac{\mu_G^2(D)}{0.34\,\mathrm{GeV}^2} + 0.20\,\frac{\rho_D^3(D)}{0.082\,\mathrm{GeV}^3} \\
&\qquad - 0.0007\,r_1^{qq} - 0.0005\,r_2^{qq} - 0.0118\,r_1^{sq} - 0.0087\,r_2^{sq} \Bigg] \,,
\end{aligned} \tag{6.4.12}$$

where as for the total D^0-meson decay width we find a converging series, with the largest correction due to the dimension-five operators, followed by the Darwin operator contribution and the NLO-QCD corrections to the free quark decay. Note that only the non-valence four-quark operator contributions (eye-contractions) are present here.

For the semileptonic D^+-meson decay we obtain

$$\begin{aligned}
\Gamma_{sl}^{D^+} &= \Gamma_0\Bigg[\underbrace{1.02}_{c_3^{\rm LO}} + \underbrace{0.16}_{\Delta c_3^{\rm NLO}} - 0.27\,\frac{\mu_\pi^2(D)}{\rm GeV^2} - 0.84\,\frac{\mu_G^2(D)}{\rm GeV^2} + 2.48\,\frac{\rho_D^3(D)}{\rm GeV^3} + \underbrace{0.00}_{\rm dim-7,VIA} \\
&\quad - 0.28\,\tilde{B}_1^q + 0.28\,\tilde{B}_2^q - 0.09\,\tilde{\epsilon}_1^q + 0.09\,\tilde{\epsilon}_2^q - 5.24\,\tilde{\delta}_1^{sq} + 5.24\,\tilde{\delta}_2^{sq}\Bigg] \\
&= 1.02\,\Gamma_0\Bigg[1 + 0.16 - 0.13\,\frac{\mu_\pi^2(D)}{0.48\,\rm GeV^2} - 0.28\,\frac{\mu_G^2(D)}{0.34\,\rm GeV^2} + 0.20\,\frac{\rho_D^3(D)}{0.082\,\rm GeV^3} \\
&\quad - \underbrace{0.00}_{\rm dim-6,7,VIA} - 0.005\,\frac{\delta\tilde{B}_1^q}{0.02} + 0.005\,\frac{\delta\tilde{B}_2^q}{0.02} + 0.004\,\frac{\tilde{\epsilon}_1^q}{-0.04} - 0.004\,\frac{\tilde{\epsilon}_2^q}{-0.04} \\
&\quad - 0.0118\,r_1^{sq} - 0.0088\,r_2^{sq}\Bigg], \qquad (6.4.13)
\end{aligned}$$

where we find the same series as for the neutral D-meson supplemented by contributions from CKM suppressed weak annihilation, which vanish in VIA both at dimension-six and dimension-seven. Deviations from VIA give very small corrections.

For the D_s^+-meson we obtain

$$\begin{aligned}
\Gamma_{sl}^{D_s^+} &= \Gamma_0\Bigg[\underbrace{1.02}_{c_3^{\rm LO}} + \underbrace{0.16}_{\Delta c_3^{\rm NLO}} - 0.27\,\frac{\mu_\pi^2(D_s)}{\rm GeV^2} - 0.84\,\frac{\mu_G^2(D_s)}{\rm GeV^2} + 2.48\,\frac{\rho_D^3(D_s)}{\rm GeV^3} + \underbrace{0.00}_{\rm dim-7,VIA} \\
&\quad - 7.63\,\tilde{B}_1^s + 7.63\,\tilde{B}_2^s - 2.55\,\tilde{\epsilon}_1^s + 2.37\,\tilde{\epsilon}_2^s - 0.41\,\tilde{\delta}_1^{qs} + 0.41\,\tilde{\delta}_2^{qs}\Bigg] \\
&= 1.02\,\Gamma_0\Bigg[1 + 0.16 - 0.15\,\frac{\mu_\pi^2(D_s)}{0.57\,\rm GeV^2} - 0.30\,\frac{\mu_G^2(D_s)}{0.36\,\rm GeV^2} + 0.29\,\frac{\rho_D^3(D_s)}{0.119\,\rm GeV^3} \\
&\quad - \underbrace{0.00}_{\rm dim-6,VIA} - 0.15\,\frac{\delta\tilde{B}_1^s}{0.02} + 0.15\,\frac{\delta\tilde{B}_2^s}{0.02} + 0.10\,\frac{\tilde{\epsilon}_1^s}{-0.04} + 0.09\,\frac{\tilde{\epsilon}_2^s}{0.04} \\
&\quad - 0.0010\,r_1^{qs} - 0.0007\,r_2^{qs}\Bigg], \qquad (6.4.14)
\end{aligned}$$

where we have a larger contribution due to CKM dominant weak annihilation as well as $SU(3)_F$ breaking corrections. Again, in VIA the four-quark contributions vanish both at dimension-six and dimension-seven, but now deviations from VIA might give sizable corrections.

Using the experimental values for the D^0 lifetime and semileptonic branching fraction,

we determine the semileptonic ratios in the following way

$$\frac{\Gamma_{sl}^{D^+}}{\Gamma_{sl}^{D^0}} = 1 + \left[\Gamma_{sl}^{D^+} - \Gamma_{sl}^{D^0}\right]^{\rm HQE} \left[\frac{\tau(D^0)}{B_{sl}^{D^0}}\right]^{\rm exp} , \tag{6.4.15}$$

$$\frac{\Gamma_{sl}^{D_s^+}}{\Gamma_{sl}^{D^0}} = 1 + \left[\Gamma_{sl}^{D_s^+} - \Gamma_{sl}^{D^0}\right]^{\rm HQE} \left[\frac{\tau(D^0)}{B_{sl}^{D^0}}\right]^{\rm exp} , \tag{6.4.16}$$

where $\left[\Gamma_{sl}^{D^0}\right]^{\rm HQE}$, $\left[\Gamma_{sl}^{D^+}\right]^{\rm HQE}$ and $\left[\Gamma_{sl}^{D_s^+}\right]^{\rm HQE}$ are given in Eqs. (6.4.12), (6.4.13) and (6.4.14), respectively.

The HQE values of these ratios are shown in the ninth and tenth rows of Tables 6.13, 6.14 and 6.15 and in Figure 6.7. In agreement with experiment HQE predicts values for $\Gamma_{sl}^{D^+}/\Gamma_{sl}^{D^0}$ very close to one. Using the inputs from Appendix C.1 the HQE prefers also for $\Gamma_{sl}^{D_s^+}/\Gamma_{sl}^{D^0}$ values close to one, while experiment find a value as low as 0.79 – again a more profound determination of μ_G^2, μ_π^2 and ρ_D^3 as well as an inclusion of dimension-seven contributions with two-quarks operators for D mesons might change this conclusion.

We expand $\Gamma_{sl}^{D^+}/\Gamma_{sl}^{D^0}$ as

$$\begin{aligned}
\frac{\Gamma_{sl}^{D^+}}{\Gamma_{sl}^{D^0}} &= 1 - 0.27\,\tilde{B}_1^q + 0.27\,\tilde{B}_2^q - 0.09\,\tilde{\epsilon}_1^q + 0.08\,\tilde{\epsilon}_2^q \underbrace{+\,0.00}_{\rm dim-7,VIA} \\
&\quad + 0.27\,\tilde{\delta}_1^{qq} - 0.27\,\tilde{\delta}_2^{qq} - 0.01\,\tilde{\delta}_1^{sq} + 0.01\,\tilde{\delta}_2^{sq} \\
&= 1 + \underbrace{0.00}_{\rm dim-6,7,VIA} \\
&= -0.005\,\frac{\delta\tilde{B}_1^q}{0.02} + 0.005\,\frac{\delta\tilde{B}_2^q}{0.02} + 0.004\,\frac{\tilde{\epsilon}_1^q}{-0.04} - 0.003\,\frac{\tilde{\epsilon}_2^q}{-0.04}\,.
\end{aligned} \tag{6.4.17}$$

Due to isospin symmetry, in Eq. (6.4.17) the contributions of the kinetic, chromomagnetic and the Darwin operators vanish. Moreover, in VIA there is also no correction due to the spectator quark effects. Thus this ratio, within the framework of the HQE, is predicted to be very close to one. Additionally, the effects of isospin symmetry and cancellation of spectator terms in the VIA also results in a much smaller estimate of the uncertainty, which is notable from Figure 6.7, when compared to the rest of the observables.

Finally, we obtain for the ratio $\Gamma_{sl}^{D_s^+}/\Gamma_{sl}^{D^0}$ [1]

$$\begin{aligned}
\frac{\Gamma_{sl}^{D_s^+}}{\Gamma_{sl}^{D^0}} &= 1 - 0.27\,\frac{\mu_\pi^2(D_s)-\mu_\pi^2(D)}{\mathrm{GeV}^2} - 0.82\,\frac{\mu_G^2(D_s)-\mu_G^2(D)}{\mathrm{GeV}^2} + 2.42\,\frac{\rho_D^3(D_s)-\rho_D^3(D)}{\mathrm{GeV}^3} \\
&\quad - 7.47\,\tilde{B}_1^s + 7.47\,\tilde{B}_2^s - 2.50\,\tilde{\epsilon}_1^s + 2.32\,\tilde{\epsilon}_2^s \underbrace{+0.00}_{\mathrm{dim-7,VIA}} \\
&\quad + 0.27\,\tilde{\delta}_1^{qq} - 0.27\,\tilde{\delta}_2^{qq} + 5.11\,\tilde{\delta}_1^{sq} - 5.11\,\tilde{\delta}_2^{sq} - 0.40\,\tilde{\delta}_1^{qs} + 0.40\,\tilde{\delta}_2^{qs} \\
&= 1 - 0.024\,\frac{\mu_\pi^2(D_s)-\mu_\pi^2(D)}{0.09\,\mathrm{GeV}^2} - 0.016\,\frac{\mu_G^2(D_s)-\mu_G^2(D)}{0.02\,\mathrm{GeV}^2} \\
&\quad + 0.090\,\frac{\rho_D^3(D_s)-\rho_D^3(D)}{0.037\,\mathrm{GeV}^3} + \underbrace{0.00}_{\mathrm{dim-6,7,VIA}} \\
&\quad - 0.15\,\frac{\delta\tilde{B}_1^s}{0.02} + 0.15\,\frac{\delta\tilde{B}_2^s}{0.02} + 0.10\,\frac{\tilde{\epsilon}_1^s}{-0.04} + 0.09\,\frac{\tilde{\epsilon}_2^s}{0.04} \\
&\quad + 0.0007\,r_1^{qq} + 0.0005\,r_2^{qq} + 0.0118\,r_1^{sq} + 0.0087\,r_2^{sq} - 0.0001\,r_1^{qs} \\
&\quad - 0.0007\,r_2^{qs}\,, \qquad (6.4.18)
\end{aligned}$$

which is dominated by $SU(3)_F$-symmetry breaking corrections. The Darwin operator gives a sizable positive contribution to the ratio, which is partly compensated by the kinetic and the chromomagnetic terms. The spectator effects give in VIA a vanishing contribution, but deviations from VIA could sizably affect the ratio and also eye-contractions could yield a visible effect – here again a more precise determination of the non-perturbative parameters is necessary in order to make more profound statements.

6.5 Summary

We have performed a comprehensive study of charmed mesons lifetimes, of their ratios and of the inclusive semileptonic decay rates. Compared to previous studies we have included for the first time the sizeable contribution due to the Darwin term in the charm sector (with new expressions shown in Appendix C.2), non-perturbative

[1] We note here a typo in the corresponding expression of this ratio in [200]. In Eq. (40) of [200], the sign in front of the contribution of the kinetic operator has to be changed.

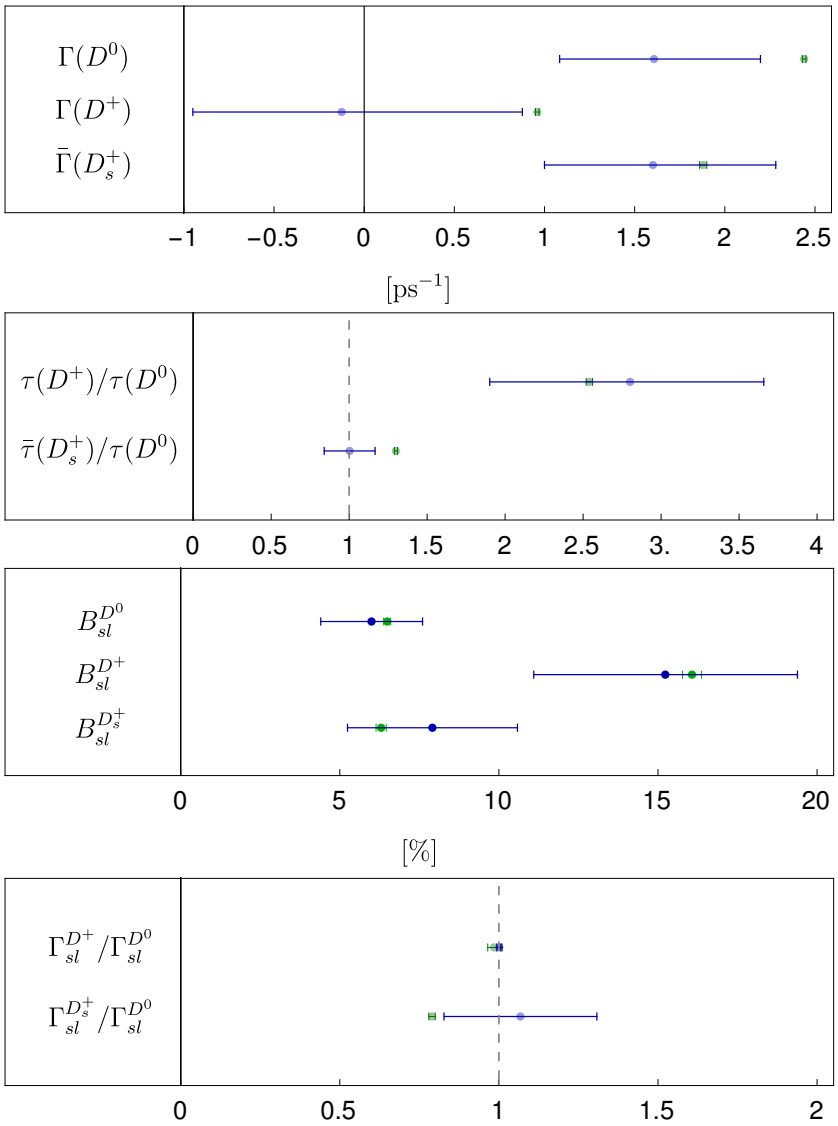

Figure 6.7: A comparison of the HQE prediction for the charm observables in the kinetic scheme (blue) with the corresponding experimental data (green).

estimates of the eye-contractions [3] and strange quark mass corrections to the Bag parameters of the D_s^+ meson [3]. Moreover we have studied different mass schemes for the charm quark.

In particular our new study supersedes the one done by some of us in [55] and we could clarify in the present work that the dimension-seven operators $\tilde{R}_{1,2}^q$ (introduced in [55] as $P_{5,6}^q$) can be absorbed in the definition of the QCD decay constant. In contrast to the present work, [55] could describe the experimental number for $\tau(D_s^+)/\tau(D^0)$ by fitting the Bag parameters in order to accommodate the experimental value of

$\Gamma_{sl}^{D_s^+}/\Gamma_{sl}^{D^0}$ – this can be achieved by demanding e.g. for the difference $\tilde{B}_1^s - \tilde{B}_2^s \approx 0.032$, which is in slight tension with the HQET sum rule result $\tilde{B}_1^s - \tilde{B}_2^s = 0.004^{+0.019}_{-0.012}$ we are using here.

[267] also studies charm mesons, albeit restricting exclusively to a LO-QCD analysis. Different quark mass schemes can only be distinguished starting from NLO-QCD onwards – working at leading order in QCD only, the different quark mass schemes used in our work would induce a relative uncertainty to the free-quark decay of $(1.48/1.27)^5 \approx 2.15$, which is clearly not acceptable. Moreover, as can be nicely read from Table 6.9, NLO-QCD corrections to the four-quark operators can dominate over the LO contribution. Using exclusively LO-QCD expressions is thus a far too crude and unnecessary assumption in the charm sector. Furthermore, [267] considers only the $\overline{\text{MS}}$ scheme for the charm quark mass and obviously the recently determined Darwin term and the eye-contractions could not have been included, since they were not known at that point of time.

Finally, there is also some overlap with two recent studies of the B_c lifetime [274,275]. The first paper [274] considers also the free charm quark decay Γ_3 and the second one [275] the total D-meson decay rate without the free charm quark decay, i.e. $\Gamma(D) - \Gamma_3$. For Γ_3 the authors of [274] consider three quark mass schemes: $\overline{\text{MS}}$, $1S$ and the meson mass scheme. They find in Table 3 and 4 of their paper values in the $\overline{\text{MS}}/1S$ scheme which are slightly smaller/slightly larger than our values in Table 6.5: $1.0\,\text{ps}^{-1}$ vs $1.3\,\text{ps}^{-1}$ and $1.7\,\text{ps}^{-1}$ vs $1.5\,\text{ps}^{-1}$. Since they in principle use the same NLO-QCD expressions as we do, we expect the slight difference to be rooted in a different treatment of higher orders in α_s and some differences in the values of the input parameters. As in our study, they also find a relatively small effect due to a non-vanishing strange quark mass. In [275] the authors determine the D-meson decay rate without the free charm quark decay. In that respect they consider all the corrections we also take into account, except contributions of dimension-seven and eye-contractions. In the end, when considering the D^+ meson they obtain values for the B_c-meson decay rate of around $3.3\,\text{ps}^{-1}$ (see Table III of [275]), compared

to the experimental value of $1.961(35)\,\mathrm{ps}^{-1}$. We naively estimate that an inclusion of the dimension-seven contribution to the D^+ meson decay rate would decrease their result by about $1.1\,\mathrm{ps}^{-1}$, see Table 6.10, and bring it in nice agreement with the measurement. On the other hand, these missing dimension-seven contributions might be partially compensated by the corresponding contributions to the B_c-meson decay rate. Here a further investigation might be necessary to clarify this point.

Our main numerical results are presented in Tables 6.13, 6.14 and 6.15 and in Figure 6.7. At a first glance all considered observables lie in the ballpark of the experimental results. In particular, we find good agreement with experiment for the ratio $\tau(D^+)/\tau(D^0)$, for the total D_s^+-meson decay rate, for the semileptonic rates of all three mesons D^0, D^+ and D_s^+, and for the semileptonic ratio $\Gamma_{sl}^{D^+}/\Gamma_{sl}^{D^0}$. The values obtained with different mass schemes for the charm quark overlap and the exclusive use of only one scheme might underestimate the uncertainties. Including higher orders in the perturbative QCD expansion will further alleviate the differences among the mass schemes. Looking, as a starting point, at the structure of the contributions to the total decay rates and neglecting spectator effects, we find that the NLO-QCD corrections to the free quark decay give the dominant correction (of the order of 50% of LO-QCD free quark decay), followed by the Darwin term (of the order of 30% of LO-QCD free quark decay). In the case of semileptonic decay rates the chromomagnetic term provides the dominant contribution (of the order of 30%), followed by the Darwin term and NLO-QCD corrections to the free quark decay. Turning now to the spectator effects, we find them to be tiny for $\Gamma(D^0)$, $\Gamma_{sl}^{D^0}$ and $\Gamma_{sl}^{D^+}$, but they provide visible corrections to $\Gamma_{sl}^{D_s^+}$ and $\Gamma(D_s^+)$ – in the latter case we find also sizable cancellations between dimension-six and dimension-seven contributions. For the D^+ meson we find, however, a huge negative Pauli interference contribution – with a substantial part stemming from the NLO-QCD corrections. Moreover, one observes here a significant cancellation between dimension-six and dimension-seven terms related to Pauli interference. The values of the HQET Bag parameters entering the spectator effects are close to the VIA values, deviations

from the latter can, however, lead to sizable effects in $\Gamma(D^+)$ and to visible effects in $\Gamma(D^0)$, $\Gamma(D_s^+)$ and $\Gamma_{sl}^{D_s^+}$. Based on the HQET sum rule results [3] we find that eye-contractions constitute only subleading corrections, they might, however, turn out to be relevant for $\Gamma_{sl}^{D_s^+}/\Gamma_{sl}^{D^0}$ and $\tau(D_s^+)/\tau(D^0)$, when more precise non-perturbative estimates will become available. In the end, the total decay rates of the D^0 and D^+ mesons stay underestimated in our HQE approach and we suspect that this is due to missing higher-order QCD corrections to the free charm quark decay and the Pauli interference contribution. For the $SU(3)_F$ breaking ratios $\tau(D_s^+)/\tau(D^0)$ and $\Gamma_{sl}^{D_s^+}/\Gamma_{sl}^{D^0}$ our predictions lie closer to one than experiment. This might originate from the poor knowledge of the non-perturbative parameters μ_G^2, μ_π^2 and ρ_D^3 in the D^0 and D_s^+ systems, as discussed in Section 6.3.

Our numerical analysis shows that there are many possibilities for future improvements of the HQE predictions in the charm sector:

- $\Gamma_3^{(2)}$: NNLO-QCD [230–241] contributions to the semileptonic decays have been found to be large and NLO-QCD corrections to the non-leptonic decay rates represent one of the dominant corrections. Moreover we observe that at NLO-QCD there is pronounced cancellation - see Eq. (6.2.16) and Eq. (6.2.17) - which might not be necessarily present at NNLO-QCD. Thus a first determination of the NNLO-QCD corrections to the non-leptonic decays might have some sizable impact on the numerical studies of the total decay rates.

- $\Gamma_5^{(1)}$: Cancellations in the coefficient c_G for the total decay rate, shown in Eq. (6.6) and Figure 6.3 lead to large uncertainties, even the sign of these corrections is ambiguous. Here a determination of the QCD-corrections to the coefficient c_G for the non-leptonic case might considerably improve the situation.

- $\Gamma_6^{(1)}$: The Wilson oefficients of the Darwin operator are large, therefore QCD corrections for the non-leptonic case might be important.

- $\Gamma_{7,8}^{(0)}$: Since the dimension-six contribution is sizable, the LO-QCD determination of the dimension-seven and dimension-eight contributions with two-quark operators for the non-leptonic case might bring some additional insights on the convergence of the HQE in the charm sector.

- $\tilde{\Gamma}_6^{(2)}$, $\tilde{\Gamma}_7^{(1)}$: Pauli interference dominates the total decay rate of the D^+ meson. Currently $\tilde{\Gamma}_6^{(0)}$, $\tilde{\Gamma}_6^{(1)}$ and $\tilde{\Gamma}_7^{(0)}$ are known and their numerical values were found to be huge, see e.g. Table 6.9. Thus further QCD corrections will turn out to be very important.

- $\tilde{\Gamma}_8^{(0)}$: since the four-quark dimension-six contribution can dominate the total decay rate and $\tilde{\Gamma}_7^{(0)}$ is also very sizable, a further study of the dimension-eight contributions might bring further insights on the convergence of the HQE in the charm sector, see [251, 252].

- More precise determinations for the parameters μ_G^2, μ_π^2 and ρ_D^3 – both for the D^0 and the D_s^+ mesons: the Darwin term and the chromomagnetic term provide large corrections to the decay rates and they are poorly known – in particular the size of $SU(3)_F$ breaking effects is largely unknown. An experimental determination of μ_G^2, μ_π^2 and ρ_D^3 from fits to semileptonic D^+-, D^0- and D_s^+-meson decays - as done in the B system, see e.g. [197] – would be very desirable. This might be doable at BESIII, Belle II and a future tau-charm factory. Moreover, new theoretical determinations, e.g. via lattice simulations or sum rules could be undertaken.

- Independent lattice determination of the matrix elements of the four-quark operators of dimension-six: here we have currently only HQET sum rule determinations [3, 55] or outdated lattice results [194, 276].

- A first non-perturbative determination of the matrix elements of the dimension-seven four-quark operators in order to test the validity of VIA. A similar endeavour has already been performed for B_s mixing [80].

Overall, we find that the HQE can describe inclusive charm observables, in which no pronounced GIM cancellation arises[1], albeit with very large uncertainties. We therefore do not observe a clear signal for a breakdown of the HQE in the charm sector or of violations of quark hadron duality, see e.g. [277] and we presented a long list of potential theoretical improvements, which might shed further light into the convergence properties of the HQE in the charm sector.

[1] See e.g. [78] for a recent discussion of the extreme GIM cancellations in mixing of neutral D mesons.

Chapter 7

Conclusions

In this work we have highlighted a sample of recent technical developments in the theory of heavy quark physics. For some of the methods employed in multiloop calculations, we discussed their application via elementary examples and we have pointed the readers attention towards the pioneering papers and reviews.

Building on this introduction, we applied these concepts in a complete HQET sum rule determination of the bag parameter for all five dimension-6 $\Delta B = 2$ operators relevant for the SM and BSM predictions of B_s mixing. This involved a NLO 3-loop calculation of the 3-point correlator including $SU(3)$ flavour breaking corrections up to m_s^2. Our analysis achieved a highly competitive level of precision and offers an independent alternative to lattice determinations for which there is currently a slight tension between the results found by the FNAL/MILC collaboration and the more recent HPQCD findings. This situation hopes to be resolved in future, with work ongoing by the RBC/UKQCD and JLQCD collaborations.

Using weighted averages of the bag parameter from the results presented here and results from the most recent lattice determinations, we then discussed the current status of SM predictions for ΔM_q and $\Delta\Gamma_q$. These values are currently used by HFLAV as the SM benchmark values. An accurate prediction of these observables is highly desirable due to their relevance for tests of the SM, for the determination of SM parameters and for NP searches. Moreover, growing evidence from $b \to s l^+ l^-$

transitions supports extensions to the SM that also introduce additional contributions to ΔM_s. As a result, B-mixing is extremely well positioned to place stringent bounds on such models and a precise determination of the bag parameter is crucial in this respect since it is by far the largest source of uncertainty in the theory prediction of the mass difference.

With this aim in mind, we have demonstrated in this work the effectiveness of the sum rule approach. Furthermore, there is potential still for a further improved precision of the HQET sum rule via the inclusion of NNLO matching to QCD and the inclusion of $1/m_b$ corrections.

Expanding on this work, we calculated the HQET bag parameters of the $\Delta Q = 0$ operators relevant for an analysis of the B_s and D_s^+ inclusive decay widths and the $SU(3)$ flavour violating lifetime ratios. We calculated for the first time the bag parameter of the penguin operator and also the non-valence contributions of so called eye contractions, along with m_s corrections to the condensates. In contrast to mixing, there has been little progress by the lattice community in this area and the most recent lattice determination of these bag parameters for B mesons are already over 20 years old with a corresponding result for the charm sector completely absent. Therefore our findings represent the only state of the art determinations and in the case of charm lifetimes are the only values at all currently available.

Furthermore, we studied the phenomenological implications of our findings, using our results to extract values of the CKM parameters $|V_{tb}V_{ts}|$, $|V_{td}/V_{ts}|$, V_{cb} and γ. Predictions of the top quark $\overline{\text{MS}}$ mass where made and, using the experimental value of $\Delta M_{d/s}$ and only the bag parameter as a non-perturbative input, extracted values for the leptonic branching ratios $\mathcal{B}(B_{s/d} \to l^+l^-)$.

Finally a thorough analysis of inclusive decay widths of charmed mesons was presented. This was done in an effort to study the validity of the HQE in the charm sector. It also brought together for the first time 2 recent technical developments: the calculation of 4-quark operator matrix elements, and the non-leptonic contribution to the coefficient of the Darwin operator. From our findings, we saw no clear sign of a

breakdown of the HQE in inclusive charm decays and observe that the semileptonic decay rates $\Gamma_{sl}^{D^0}$, $\Gamma_{sl}^{D^+}$ and $\Gamma_{sl}^{D_s^+}$ the semileptonic ratio $\Gamma_{sl}^{D^+}/\Gamma_{sl}^{D^0}$, the total decay rate $\Gamma(D_s^+)$, and the lifetime ratio $\tau(D^+)/\tau(D^0)$ are all consistent with experimental results. As a result of this work we were also able to offer a comprehensive list of the key theoretical and experimental measures that are required to further improve the precision of the HQE in the D system.

The breadth of flavour physics observables provides ample opportunity for physicists to further test the robustness of the SM and the potential structure of possible extensions. Equipped with an arsenal of advanced theoretical tools and presented with a generous selection of precision data, the flavour physicist today is well positioned to probe our current understanding of the universe for weaknesses and deduce a more accurate description.

Appendix A

Additional material for "Mixing Bag parameter"

A.1 Inputs and uncertainties

	$\overline{\Lambda}$	intrinsic SR	condensates	μ_ρ	m_s	$1/m_b$	μ_m	a_i
$\overline{B}^s_{Q_1}$	$^{+0.002}_{-0.003}$	± 0.018	± 0.004	$^{+0.013}_{-0.027}$	$^{+0.003}_{-0.002}$	± 0.010	$^{+0.044}_{-0.038}$	$^{+0.007}_{-0.008}$
$\overline{B}^s_{Q_2}$	$^{+0.012}_{-0.014}$	± 0.020	± 0.004	$^{+0.010}_{-0.015}$	$^{+0.004}_{-0.004}$	± 0.010	$^{+0.072}_{-0.063}$	$^{+0.015}_{-0.015}$
$\overline{B}^s_{Q_3}$	$^{+0.047}_{-0.055}$	± 0.107	± 0.023	$^{+0.026}_{-0.001}$	$^{+0.024}_{-0.026}$	± 0.010	$^{+0.091}_{-0.073}$	$^{+0.054}_{-0.053}$
$\overline{B}^s_{Q_4}$	$^{+0.006}_{-0.005}$	± 0.021	± 0.011	$^{+0.000}_{-0.002}$	$^{+0.003}_{-0.002}$	± 0.010	$^{+0.088}_{-0.079}$	$^{+0.006}_{-0.006}$
$\overline{B}^s_{Q_5}$	$^{+0.014}_{-0.012}$	± 0.018	± 0.009	$^{+0.000}_{-0.007}$	$^{+0.007}_{-0.006}$	± 0.010	$^{+0.075}_{-0.067}$	$^{+0.012}_{-0.012}$

Table A.1: Individual errors for the Bag parameters in the B_s system.

	$\overline{\Lambda}$	intrinsic SR	condensates	μ_ρ	m_s	$1/m_b$	μ_m	a_i
$\overline{B}^{s/d}_{Q_1}$	$^{+0.001}_{-0.002}$	± 0.005	± 0.002	$^{+0.002}_{-0.006}$	$^{+0.003}_{-0.002}$	± 0.002	$^{+0.000}_{-0.000}$	$^{+0.000}_{-0.000}$
$\overline{B}^{s/d}_{Q_2}$	$^{+0.004}_{-0.003}$	± 0.005	± 0.002	$^{+0.005}_{-0.002}$	$^{+0.005}_{-0.004}$	± 0.002	$^{+0.000}_{-0.000}$	$^{+0.000}_{-0.000}$
$\overline{B}^{s/d}_{Q_3}$	$^{+0.036}_{-0.023}$	± 0.025	± 0.010	$^{+0.042}_{-0.019}$	$^{+0.029}_{-0.031}$	± 0.002	$^{+0.004}_{-0.005}$	$^{+0.005}_{-0.005}$
$\overline{B}^{s/d}_{Q_4}$	$^{+0.001}_{-0.002}$	± 0.005	± 0.002	$^{+0.002}_{-0.005}$	$^{+0.003}_{-0.002}$	± 0.002	$^{+0.000}_{-0.000}$	$^{+0.000}_{-0.000}$
$\overline{B}^{s/d}_{Q_5}$	$^{+0.003}_{-0.004}$	± 0.005	± 0.002	$^{+0.004}_{-0.010}$	$^{+0.006}_{-0.006}$	± 0.002	$^{+0.000}_{-0.000}$	$^{+0.000}_{-0.000}$

Table A.2: Individual errors for the ratio of Bag parameters in the B_s and B_d system.

Parameter	Value	Source
$\overline{m}_b(\overline{m}_b)$	$(4.203^{+0.016}_{-0.034})$ GeV	[208, 209]
$m_b^{\rm PS}(2\ {\rm GeV})$	$(4.532^{+0.013}_{-0.039})$ GeV	[208, 209]
$\overline{m}_c(\overline{m}_c)$	(1.279 ± 0.013) GeV	[278]
$m_t^{\rm pole}$	(173.0 ± 0.4) GeV	[151]
$\alpha_s(M_Z)$	0.1181 ± 0.0011	[151]
V_{us}	$0.224745^{+0.000254}_{-0.000059}$	[182]
V_{ub}	$0.003746^{+0.000090}_{-0.000062}$	[182]
V_{cb}	$0.04240^{+0.00030}_{-0.00115}$	[182]
γ	$(65.81^{+0.99}_{-1.66})^\circ$	[182]
f_B	(190.0 ± 1.3) MeV	[157]
f_{B_s}	(230.3 ± 1.3) MeV	[157]
f_{B_s}/f_B	1.209 ± 0.005	[157]
$\tau(B_s^{0,{\rm H}})$	$(1.615 \pm 0.009)\ {\rm ps}^{-1}$	[151]
$\tau(B_d^0)$	$(1.520 \pm 0.004)\ {\rm ps}^{-1}$	[151]

Table A.3: Input values for parameters.

Appendix B

Additional material for "Lifetime Bag Parameter"

B.1 Renormalisation Group Equations

To determine the counterterm contribution to the three-point correlator (5.2.5) we require the one-loop renormalisation of the operators (5.2.1). We obtain the structure

$$\gamma_{\tilde{O}^{q'}\tilde{O}^{q}} = \delta_{qq'}\gamma_{\tilde{O}\tilde{O}} + \gamma_{\tilde{O}'\tilde{O}} \tag{B.1.1}$$

with

$$\tilde{\gamma}^{(0)}_{\tilde{O}\tilde{O}} = \begin{pmatrix} \frac{3}{N_c} - 3N_c & 0 & 6 & 0 & 0 \\ 0 & \frac{3}{N_c} - 3N_c & 0 & 6 & 0 \\ \frac{3}{2} - \frac{3}{2N_c^2} & 0 & -\frac{3}{N_c} & 0 & 0 \\ 0 & \frac{3}{2} - \frac{3}{2N_c^2} & 0 & -\frac{3}{N_c} & 0 \\ 0 & 0 & 0 & 0 & -3N_c \end{pmatrix}, \tag{B.1.2}$$

and

$$\tilde{\gamma}^{(0)}_{\tilde{O}'\tilde{O}} = \begin{pmatrix} 0 & 0 & 0 & 0 & \frac{8}{3} \\ 0 & 0 & 0 & 0 & -\frac{4}{3} \\ 0 & 0 & 0 & 0 & -\frac{4}{3N_c} \\ 0 & 0 & 0 & 0 & \frac{2}{3N_c} \\ 0 & 0 & 0 & 0 & \frac{4}{3} \end{pmatrix}, \tag{B.1.3}$$

The renormalised correlator then takes the form

$$K^{q,(1)}_{\tilde{Q}_i^{q'}} = K^{q,(1),\text{bare}}_{\tilde{Q}_i^{q'}} + \frac{1}{2\epsilon}\left[\left(2\tilde{\gamma}^{(0)}_{\tilde{j}}\delta_{ij} + \tilde{\gamma}^{(0)}_{\tilde{Q}_i\tilde{Q}_j}\right) K^{q,(0)}_{\tilde{Q}_j^{q'}} + \tilde{\gamma}^{(0)}_{\tilde{Q}_i\tilde{E}_j} K^{q,(0)}_{\tilde{E}_j^{q'}}\right] + \frac{1}{2\epsilon}\tilde{\gamma}^{(0)}_{\tilde{Q}_i'\tilde{Q}_P} K^{q,(0)}_{\tilde{Q}_P^{q}}, \tag{B.1.4}$$

where the second term is the counterterm for the tree-level contractions and the third term is the counterterm for the eye contractions.

Now, we consider the RGE for the Bag parameters. We have

$$\frac{d\tilde{\mathbf{O}}^{q'}}{d\ln\mu} = -\sum_q \tilde{\gamma}_{\tilde{O}^{q'}\tilde{O}^q}\tilde{\mathbf{O}}^q\,, \qquad \frac{dF_q(\mu)}{d\ln\mu} = -\tilde{\gamma}_{\tilde{j}}F_q(\mu)\,, \tag{B.1.5}$$

and thus obtain the following RGE for the Bag parameters in the case with two light-quark flavors q and s:

$$\frac{d}{d\ln\mu}\begin{pmatrix} \tilde{\mathcal{B}}_i^q \\ \tilde{\delta}_i^{qs} \end{pmatrix} = -\frac{\tilde{A}_j}{\tilde{A}_i}\begin{pmatrix} \tilde{\gamma}_{\tilde{O}_i\tilde{O}_j} + \tilde{\gamma}_{\tilde{O}_i'\tilde{O}_j} - 2\tilde{\gamma}_{\tilde{j}}\delta_{ij} & \tilde{\gamma}_{\tilde{O}_i'\tilde{O}_j} \\ \tilde{\gamma}_{\tilde{O}_i'\tilde{O}_j} & \tilde{\gamma}_{\tilde{O}_i'\tilde{O}_j} - 2\tilde{\gamma}_{\tilde{j}}\delta_{ij} \end{pmatrix}\begin{pmatrix} \tilde{\mathcal{B}}_j^q \\ \tilde{\delta}_j^{qs} \end{pmatrix}, \tag{B.1.6}$$

which can be easily generalised to more than two quark flavours.

B.2 On the logarithmic divergence at $x = 1$

To investigate the origin of the logarithmic divergences in the results (5.2.25) for the eye contractions, we study the cuts of the relevant diagram which are contributing to

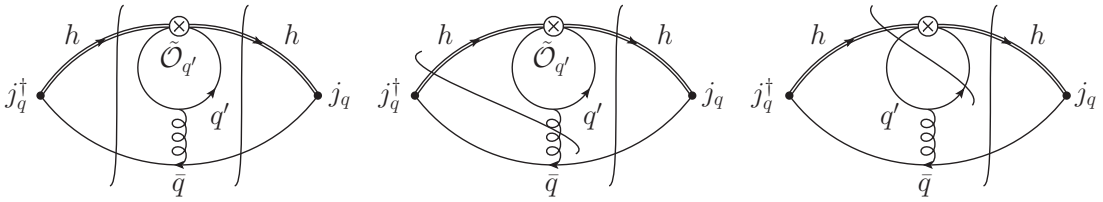

Figure B.1: Cuts which yield contributions to the double discontinuity. Symmetric diagrams are not shown.

the double discontinuity (see Figure B.1). To simplify the discussion in this appendix we only consider the scalar diagram and only work to the first order in ϵ where such a logarithm appears, but we retain the full strange-quark mass dependence in the penguin loop. Our results for the cuts (assuming $\omega_2 > \omega_1$, denoted by S_l, S_m and S_r in this order for the three diagrams) are

$$\begin{aligned} S_l &= \prod_{j=1}^{3}\left(\int \frac{d^dk_j}{i\pi^{d/2}}\right) \frac{(-2\pi i)^4\delta(2\omega_1 - 2v\cdot k_1)\delta(2\omega_2 - 2v\cdot k_2)\delta_+(k_1^2)\delta_+(k_2^2)}{(k_1-k_2)^2[k_3^2-m_s^2][(k_3+k_2-k_1)^2-m_s^2]} \\ &= \frac{2\pi^3\Gamma(\epsilon)\Gamma(-\epsilon)}{\Gamma(1/2-\epsilon)\Gamma(1-\epsilon)\Gamma(3/2-\epsilon)\omega_1^{2\epsilon}\omega_2^{2\epsilon}m_s^{2\epsilon}} + \mathcal{O}(\epsilon^0)\,, \end{aligned} \tag{B.2.1}$$

$$\begin{aligned} S_m &= \prod_{j=1}^{3}\left(\int \frac{d^dk_j}{i\pi^{d/2}}\right) \frac{(-2\pi i)^4\delta(2\omega_1 - 2v\cdot k_1)\delta(2\omega_2 - 2v\cdot (k_1+k_2))\delta_+(k_1^2)\delta_+(k_2^2)}{(k_1+k_2)^2[k_3^2-m_s^2][(k_3+k_2)^2-m_s^2]} \\ &= -\frac{2\pi^3\Gamma(\epsilon)\Gamma(-\epsilon)}{\Gamma(1/2-\epsilon)\Gamma(1-\epsilon)\Gamma(3/2-\epsilon)\omega_1^{2\epsilon}(\omega_2-\omega_1)^{2\epsilon}m_s^{2\epsilon}}\,, \end{aligned} \tag{B.2.2}$$

$$\begin{aligned} S_r &= \prod_{j=1}^{3}\left(\int \frac{d^dk_j}{i\pi^{d/2}}\right) \frac{(-2\pi i)^5\delta(2\omega_1 - 2v\cdot k_1)\delta(2\omega_2 - 2v\cdot (k_1+k_2))}{k_2^2(k_1+k_2)^2} \\ &\quad \times \delta_+(k_1^2)\delta_+(k_3^2-m_s^2)\delta_+((k_2+k_3)^2-m_s^2) \\ &= \mathcal{O}(\epsilon^0)\,. \end{aligned} \tag{B.2.3}$$

Summing up these contributions, we find at the first non-vanishing order

$$S_l + S_m + S_r|_{\omega_2>\omega_1} = -\frac{8\pi^2}{\epsilon}\ln\left(1-\frac{\omega_1}{\omega_2}\right) + \mathcal{O}(\epsilon^0)\,, \tag{B.2.4}$$

which diverges logarithmically as $\omega_1 \to \omega_2$. We reproduced this result by using our setup described in Section 5.2.3 to first compute the scalar diagram and then taking its double discontinuity. To understand this behaviour, we first note that the external momentum $p_2 - p_1$ at the four-quark operator is assumed to be light-like and thus vanishes when $\omega_1 = \omega_2$. Thus, in this limit the process between the two

cuts in the diagram in the middle of Figure B.1 therefore reduces to the amplitude with two external eikonal lines and one massless line which are all on-shell and is not kinematically allowed. On the other hand the processes between the two cuts of the other diagrams reduce to amplitudes with four external on-shell legs, which are kinematically possible. We further note that both the left and middle diagrams contain collinear divergences which cancel between the leading poles of both contributions, but generate the logarithms at sub-leading orders. Examining the diagrams in the 'tree' contributions, we find that there are no double-cuts which yield processes that are kinematically forbidden in the limit $\omega_1 \to \omega_2$, which explains why the logarithmic divergences are only found in the 'eye' contributions. This behaviour is reminiscent of large threshold logarithms that e.g. arise in Higgs production, where infrared $1/\epsilon$ poles cancel in the sum of real and virtual corrections, but large logarithms appear because the real corrections are phase-space suppressed near the threshold. Interestingly though, the logarithms we observe here appear to be of collinear rather than soft origin.

B.3 F_q and $\overline{\Lambda}_q$ analysis

For the discontinuity $\rho_\Pi(\omega)$ needed to form the sum rule of the HQET decay constant, we use the NLO result computed in Ref. [94] along with the m_s expanded result computed in Ref. [1],

$$\rho_\Pi(\omega) \equiv \frac{\Pi(\omega+i0)-\Pi(\omega-i0)}{2\pi i} \tag{B.3.1}$$

$$\begin{aligned}
&= \frac{N_c\omega^2}{2\pi^2}\,\theta(\omega-m_s)\Bigg\{1+\frac{m_s}{\omega}-\frac{1}{2}\left(\frac{m_s}{\omega}\right)^2+\dots \\
&\quad+\frac{\alpha_s C_F}{4\pi}\left[17+\frac{4\pi^2}{3}+3\ln\frac{\mu_\rho^2}{4\omega^2}+\left(20+\frac{4\pi^2}{3}+6\ln\frac{\mu_\rho^2}{4\omega^2}-3\ln\frac{\mu_\rho^2}{m_s^2}\right)\frac{m_s}{\omega}\right. \\
&\quad\left.+\left(1-\frac{9}{2}\ln\frac{\mu_\rho^2}{4\omega^2}+3\ln\frac{\mu_\rho^2}{m_s^2}\right)\left(\frac{m_s}{\omega}\right)^2+\dots\right]+\mathcal{O}(\alpha_s^2)\Bigg\} \qquad \text{(B.3.2)} \\
&\quad-\frac{\langle\bar{s}s\rangle}{2}\delta(\omega)\left[1+6\frac{\alpha_s C_F}{4\pi}+\mathcal{O}(\alpha_s^2)\right]+\frac{\langle\bar{s}i\sigma_{\mu\nu}G^{\mu\nu}s\rangle}{32}\delta''(\omega)\left[1+\mathcal{O}(\alpha_s)\right]+\mathcal{O}(\Lambda^6).
\end{aligned}$$

After plugging Eq.(B.3.3) into Eq.(2.4.14), logarithmic terms of the form $\log(\mu^2/m_s^2)$ can be resummed by switching to the $\overline{\text{MS}}$ scheme,

$$m_s = \bar{m}_s(\mu_\rho)\left[1 + \frac{\alpha_s(\mu_\rho)C_F}{4\pi}\left(4 + 3\log\left(\frac{\mu_\rho^2}{\bar{m}_s^2(\mu_\rho)}\right)\right) + \dots\right]. \tag{B.3.3}$$

We also note that m_s terms arising from the lower integration cut in Eq.(2.4.14) were not expanded in m_s.

The running of the quark condensates takes the form [see Ref. [95]]

$$\begin{aligned}\langle\bar{s}s\rangle(\mu_\rho) &= \langle\bar{s}s\rangle(\mu_0)\left[\frac{\alpha_s(\mu_\rho)}{\alpha_s(\mu_0)}\right]^{\frac{\gamma_0^{(3)}}{2\beta_0}} \times \left[1 + \frac{\alpha_s(\mu_\rho)-\alpha_s(\mu_0)}{4\pi}\frac{\gamma_0^{(3)}}{2\beta_0}\left(\frac{\gamma_1^{(3)}}{\gamma_0^{(3)}} - \frac{\beta_1}{\beta_0}\right)\right], \\ \langle\bar{s}i\sigma_{\mu\nu}G^{\mu\nu}s\rangle(\mu_\rho) &= \langle\bar{s}i\sigma_{\mu\nu}G^{\mu\nu}s\rangle(\mu_0)\left[\frac{\alpha_s(\mu_\rho)}{\alpha_s(\mu_0)}\right]^{\frac{\gamma_0^{(5)}}{2\beta_0}},\end{aligned} \tag{B.3.4}$$

with $\gamma_0^{(3)} = -8$, $\gamma_0^{(5)} = -4/3$, $\gamma_1^{(3)} = -404/3 + 40n_f/9$, $\beta_0 = 11 - 2n_f/3$ and $\beta_1 = 102 - 38n_f/3$. The logarithmic derivative of Eq.(2.4.14) furthermore gives us a sum rule for the mass difference $\overline{\Lambda}_s$ in the form [see Ref. [95]]

$$\overline{\Lambda} = t^2\frac{\frac{d}{dt}\int_0^{\omega_c} d\omega\, e^{-\frac{\omega}{t}}\rho_\Pi(\omega)}{\int_0^{\omega_c} d\omega\, e^{-\frac{\omega}{t}}\rho_\Pi(\omega)} = \frac{\int_0^{\omega_c} d\omega\,\omega\, e^{-\frac{\omega}{t}}\rho_\Pi(\omega)}{\int_0^{\omega_c} d\omega\, e^{-\frac{\omega}{t}}\rho_\Pi(\omega)}. \tag{B.3.5}$$

To determine the appropriate ranges for the Borel parameters t_i and the continuum cutoff ω_c in our bag parameter analysis, we consider the sum rules for the meson-heavy quark mass difference $\overline{\Lambda}_q$ and the HQET decay constant F and compare with the values found in the literature. The values of the HQET decay constants,

$$F(1.5\,\text{GeV}) = (0.29 \pm 0.01)\,\text{GeV}, \qquad F_s(1.5\,\text{GeV}) = (0.35 \pm 0.02)\,\text{GeV}, \tag{B.3.6}$$

are determined from the static results of the ALPHA collaboration from Ref. [279]

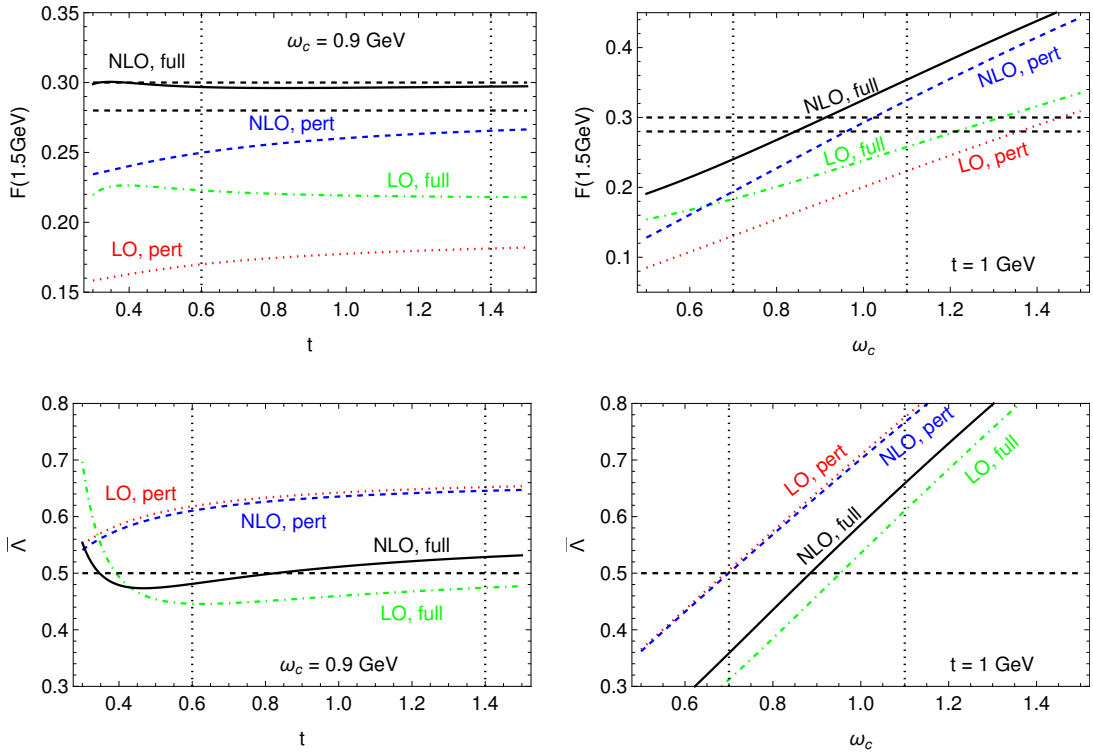

Figure B.2: Dependence of the sum rule results for $F(\mu)$ (top) and $\overline{\Lambda}$ (bottom) on the Borel parameter t (left) and the continuum cutoff ω_c (right) in the B_q system.

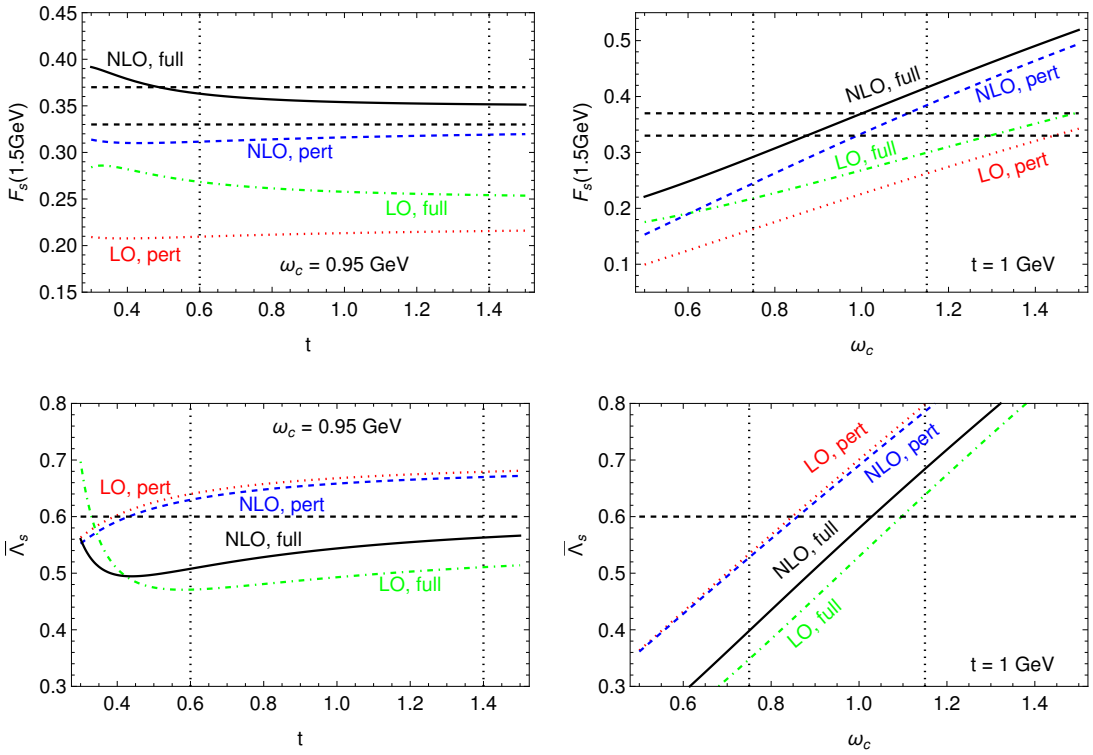

Figure B.3: Dependence of the sum rule results for $F_s(\mu)$ (top) and $\overline{\Lambda}_s$ (bottom) on the Borel parameter t (left) and the continuum cutoff ω_c (right) in the B_s system.

by matching at the scale $\bar{m}_b(\bar{m}_b)$ and evolving the HQET decay constants down to the scale 1.5GeV. For the mass differences we use, $\overline{\Lambda}_q = 0.5$ and $\overline{\Lambda}_s = 0.6$ for the B_q and B_s mesons respectively. We find the behaviour shown in Figures B.2 and B.3 from which we determine the following intervals:

$$\begin{aligned} B_q: &\qquad t = (1.0 \pm 0.4)\,\mathrm{GeV}\,, \quad \omega_c = (0.90 \pm 0.2)\,\mathrm{GeV}\,, \\ B_s: &\qquad t = (1.0 \pm 0.4)\,\mathrm{GeV}\,, \quad \omega_c = (0.95 \pm 0.2)\,\mathrm{GeV}\,. \end{aligned} \tag{B.3.7}$$

Appendix C

Additional material for "Charm Lifetime Analysis"

C.1 Numerical input for Charm Analysis

We use five-loop running for $\alpha_s(\mu)$ [204] with four active flavours at the scale $\mu \sim m_c$, and the most recent value [169]

$$\alpha_s(M_Z) \;=\; 0.1179 \pm 0.0010. \tag{C.1.1}$$

For the CKM matrix elements we apply the standard parametrisation in terms of $\theta_{12}, \theta_{13}, \theta_{22}, \delta$ and use as an input [182] (online update)

$$|V_{us}| \;=\; 0.224834^{+0.000252}_{-0.000059}\,, \tag{C.1.2}$$

$$\frac{|V_{ub}|}{|V_{cb}|} \;=\; 0.088496^{+0.001885}_{-0.002244}\,, \tag{C.1.3}$$

$$|V_{cb}| \;=\; 0.04162^{+0.00026}_{-0.00080}\,, \tag{C.1.4}$$

$$\delta \;=\; \left(65.80^{+0.94}_{-1.29}\right)^{\circ}. \tag{C.1.5}$$

For the c-quark mass, we use different values depending of the scheme. In the $\overline{\rm MS}$-scheme we take [169]:

$$\overline{m}_c(\overline{m}_c) = (1.27 \pm 0.02)\,\text{GeV}, \tag{C.1.6}$$

in the kinetic scheme we employ (at NLO) [217]:

$$m_c^{\rm kin}(0.5\,{\rm GeV}) = (1.363 \pm 0.02)\,{\rm GeV}, \tag{C.1.7}$$

and in the $1S$-scheme (see Eq. (6.1.13)) we use $m_c^{1S} = 1.44$ GeV [204].

For the s-quark mass we take the value [169]

$$m_s = \left(93^{+11}_{-5}\right)\ {\rm MeV}. \tag{C.1.8}$$

The masses of D-mesons are known very precisely [169]:

$$M_{D^0} = 1.86493\,{\rm GeV}, \qquad M_{D^+} = 1.86965\,{\rm GeV}, \qquad M_{D_s^+} = 1.96834\,{\rm GeV}.$$

The values of the non-perturbative parameters used in the analysis are shown in Tables C.1 and C.2.

Parameter	$D^{+,0}$	Source	D_s^+	Source
f_D [GeV]	0.2120 ± 0.0007	Lattice QCD [157]	0.2499 ± 0.0005	Lattice QCD [157]
$\mu_\pi^2(D)$ [GeV^2]	0.48 ± 0.20	Exp. fit [198] and HQ symmetry	0.57 ± 0.23	Exp. fit [243], $SU(3)_f$-breaking [272] and HQ symmetry
$\mu_G^2(D)$ [GeV^2]	0.34 ± 0.10	Spectroscopy relations [268]	0.36 ± 0.10	Spectroscopy relations [268]
$\rho_D^3(D)$ [GeV^3]	0.082 ± 0.035	Exp. fit [198] and E.O.M relation	0.119 ± 0.052	Exp. fit [198] and E.O.M relation

Table C.1: Numerical values of the non-perturbative parameters used in our analysis.

HQET, $\mu_0 = 1.5\,\text{GeV}$	$\tilde{B}_1$	$\tilde{B}_2$	$\tilde{\epsilon}_1$	$\tilde{\epsilon}_2$
$D^{+,0}$	$1.0026^{+0.0198}_{-0.0106}$	$0.9982^{+0.0052}_{-0.0066}$	$-0.0165^{+0.0209}_{-0.0346}$	$-0.0004^{+0.0200}_{-0.0326}$
D_s^+	$1.0022^{+0.0185}_{-0.0099}$	$0.9983^{+0.0052}_{-0.0067}$	$-0.0104^{+0.0202}_{-0.0330}$	$0.0001^{+0.0199}_{-0.0324}$
HQET, $\mu_0 = 1.5\,\text{GeV}$	$\tilde{\delta}_1$	$\tilde{\delta}_2$	$\tilde{\delta}_3$	$\tilde{\delta}_4$
$\langle D_q\|\tilde{O}^q\|D_q\rangle$	$0.0026^{+0.0142}_{-0.0092}$	$-0.0018^{+0.0047}_{-0.0072}$	$-0.0004^{+0.0015}_{-0.0024}$	$0.0003^{+0.0012}_{-0.0008}$
$\langle D_s\|\tilde{O}^q\|D_s\rangle$	$0.0025^{+0.0144}_{-0.0093}$	$-0.0018^{+0.0047}_{-0.0072}$	$-0.0004^{+0.0015}_{-0.0024}$	$0.0003^{+0.0012}_{-0.0008}$
$\langle D_q\|\tilde{O}^s\|D_q\rangle$	$0.0023^{+0.0140}_{-0.0091}$	$-0.0017^{+0.0046}_{-0.0070}$	$-0.0004^{+0.0015}_{-0.0023}$	$0.0003^{+0.0012}_{-0.0008}$

Table C.2: Numerical values of the HQET Bag parameters [3, 55] evaluated through a traditional HQET sum rule.

C.2 Expressions for the Darwin Coefficients

The coefficients $C^{(q_1q_2)}_{\rho_D,mn}(\rho,\mu_0)$ including full $\rho = m_s^2/m_c^2$ dependence are given by the expressions:

$$\mathcal{C}^{(d\bar{d})}_{\rho_D,11} = 6 + 8\,\log\left(\frac{\mu_0^2}{m_c^2}\right), \tag{C.2.1}$$

$$\mathcal{C}^{(d\bar{d})}_{\rho_D,12} = -\frac{34}{3}, \tag{C.2.2}$$

$$\mathcal{C}^{(d\bar{d})}_{\rho_D,22} = 6 + 8\,\log\left(\frac{\mu_0^2}{m_c^2}\right), \tag{C.2.3}$$

$$\begin{aligned}\mathcal{C}^{(d\bar{s})}_{\rho_D,11} &= \frac{2}{3}(1-\rho)\Big[9 + 11\rho - 12\rho^2\log(\rho) - 24\left(1-\rho^2\right)\log(1-\rho) - 25\rho^2 + 5\rho^3\Big] \\ &\quad + 8\,(1-\rho)(1-\rho^2)\log\left(\frac{\mu_0^2}{m_c^2}\right),\end{aligned} \tag{C.2.4}$$

$$\begin{aligned}\mathcal{C}^{(d\bar{s})}_{\rho_D,12} &= -\frac{2}{3}\Big[17 + 12\rho\left(5 + 2\rho - 2\rho^2\right)\log(\rho) + 48(1-\rho)(1-\rho^2)\log(1-\rho) \\ &\quad -26\rho + 18\rho^2 - 38\rho^3 + 5\rho^4 + 24\,\rho\,(1+\rho-\rho^2)\log\left(\frac{\mu_0^2}{m_c^2}\right)\Big],\end{aligned} \tag{C.2.5}$$

$$\begin{aligned}\mathcal{C}^{(d\bar{s})}_{\rho_D,22} &= \frac{2}{3}(1-\rho)\Big[9 + 11\rho - 12\rho^2\log(\rho) - 24\left(1-\rho^2\right)\log(1-\rho) - 25\rho^2 + 5\rho^3\Big], \\ &\quad + 8\,(1-\rho)(1-\rho^2)\log\left(\frac{\mu_0^2}{m_c^2}\right),\end{aligned} \tag{C.2.6}$$

$$\mathcal{C}^{(s\bar{d})}_{\rho_D,11} = \frac{2}{3}\Big[9 - 16\rho - 12\rho^2 + 16\rho^3 - 5\rho^4 + 12\log\left(\frac{\mu_0^2}{m_c^2}\right)\Big], \tag{C.2.7}$$

$$\begin{aligned}\mathcal{C}^{(s\bar{d})}_{\rho_D,12} &= -\frac{2}{3}\Big[17 + 12\,\rho^2\,(3-\rho)\log(\rho) - 24(1-\rho)^3\log(1-\rho) \\ &\quad -50\rho + 90\rho^2 - 54\rho^3 + 5\rho^4 - 12\rho\,(3 - 3\rho + \rho^2)\log\left(\frac{\mu_0^2}{m_c^2}\right)\Big],\end{aligned} \tag{C.2.8}$$

$$\begin{aligned}\mathcal{C}^{(s\bar{d})}_{\rho_D,22} &= \frac{2}{3}(1-\rho)\Big[9 + 11\rho - 12\rho^2\log(\rho) - 24\left(1-\rho^2\right)\log(1-\rho) \\ &\quad -25\rho^2 + 5\rho^3 + 12\,(1-\rho^2)\log\left(\frac{\mu_0^2}{m_c^2}\right)\Big],\end{aligned} \tag{C.2.9}$$

$$\mathcal{C}^{(s\bar{s})}_{\rho_D,11} = \frac{2}{3}\Big[\sqrt{1-4\rho}\left(17 + 8\rho - 22\rho^2 - 60\rho^3\right) - 4\left(2 - 3\rho + \rho^3\right) +$$

$$
\begin{aligned}
&- 12\left(1-\rho-2\rho^2+2\rho^3+10\rho^4\right)\log\left(\frac{1+\sqrt{1-4\rho}}{1-\sqrt{1-4\rho}}\right)\\
&- 12\,(1-\rho)(1-\rho^2)\left(\log(\rho)-\log\left(\frac{\mu_0^2}{m_c^2}\right)\right)\Bigg], \qquad \text{(C.2.10)}
\end{aligned}
$$

$$
\begin{aligned}
\mathcal{C}^{(s\bar{s})}_{\rho_D,12} \;=\; \frac{2}{3}\Bigg[&\sqrt{1-4\rho}\left(-33+24\,\log(\rho)-24\,\log(1-4\rho)+46\rho-106\rho^2-60\rho^3\right)\\
&+12\left(3-2\rho+4\rho^2-16\rho^3-10\rho^4\right)\log\left(\frac{1+\sqrt{1-4\rho}}{1-\sqrt{1-4\rho}}\right)\\
&+4\,(1-\rho)^2\,(4+3(1-\rho)\log(\rho)-\rho)\\
&-12\,\left(1-\sqrt{1-4\rho}-3\rho+3\rho^2-\rho^3\right)\,\log\left(\frac{\mu_0^2}{m_c^2}\right)\Bigg], \qquad \text{(C.2.11)}
\end{aligned}
$$

$$
\begin{aligned}
\mathcal{C}^{(s\bar{s})}_{\rho_D,22} \;=\; \frac{2}{3}\Bigg[&\sqrt{1-4\rho}\left(9+24\,\log(\rho)-24\,\log(1-4\rho)+22\rho-34\rho^2-60\rho^3\right)\\
&+24\left(1-2\rho-\rho^2-2\rho^3-5\rho^4\right)\log\left(\frac{1+\sqrt{1-4\rho}}{1-\sqrt{1-4\rho}}\right)\\
&+12\,\sqrt{1-4\rho}\,\log\left(\frac{\mu_0^2}{m_c^2}\right)\Bigg]. \qquad \text{(C.2.12)}
\end{aligned}
$$

The numerical values of the above coefficients for $\rho = 0.006$ are shown in Table C.3.

	$3\,C_1^2$	$2\,C_1C_2$	$3\,C_2^2$
$c \to d\bar{d}u$	6	-11.33	6
$c \to d\bar{s}u$	6.10	-9.81	6.10
$c \to s\bar{d}u$	5.94	-11.23	6.10
$c \to s\bar{s}u$	6.04	-9.70	6.21

Table C.3: Numerical values of $C^{(q_1q_2)}_{\rho_D,nm}$ for $\rho = 0.006$ and $\mu_0 = m_c$.

C.3 Parametrisation of the Matrix Element of Four-Quark Operators

The matrix elements of the dimension-six operators in QCD are parametrised in the following way

$$\langle D_q|O_i^q\,|D_q\rangle \;=\; A_i\, f_{D_q}^2 m_{D_q}^2\, B_i^q, \tag{C.3.1}$$

$$\langle D_q|O_i^{q'}\,|D_q\rangle \;=\; A_i\, f_{D_q}^2 m_{D_q}^2\, \delta_i^{qq'}, \qquad q \neq q'\,, \tag{C.3.2}$$

where

$$A_1^q = A_3^q = 1, \qquad A_2^q = A_4^q = \frac{m_D^2}{(m_c + m_q)^2}.$$

In VIA the Bag parameters reduce to $B_1^q = B_2^q = 1$ and $B_3^q = \epsilon_1^q = 0$, $B_4^q = \epsilon_2^q = 0$ and all $\delta_i^{qq'} = 0$.

The matrix elements of the dimension-seven four-quark operators in Eqs. (6.2.60) - (6.2.68) in HQET are parametrised in the following way:

$$\langle D_q|\tilde{P}_1^q|D_q\rangle \;=\; -m_q F^2(\mu_0)\, m_D\, \tilde{B}_{P,1}^q\,, \tag{C.3.3}$$

$$\langle D_q|\tilde{P}_2^q|D_q\rangle \;=\; -F^2(\mu_0)\, m_D\, \bar{\Lambda}\, \tilde{B}_{P,2}^q\,, \tag{C.3.4}$$

$$\langle D_q|\tilde{P}_3^q|D_q\rangle \;=\; -F^2(\mu_0)\, m_D\, \bar{\Lambda}\, \tilde{B}_{P,3}^q\,, \tag{C.3.5}$$

$$\langle D_q|\tilde{R}_1^q|D_q\rangle \;=\; -F^2(\mu_0)\, m_D\, (\bar{\Lambda} - m_q)\, \tilde{B}_{R,1}^q\,, \tag{C.3.6}$$

$$\langle D_q|\tilde{R}_2^q|D_q\rangle \;=\; F^2(\mu_0)\, m_D\, (\bar{\Lambda} - m_q)\, \tilde{B}_{R,1}^q\,, \tag{C.3.7}$$

with $\bar{\Lambda} = m_D - m_c$, and

$$\langle D_q|\tilde{M}_{1,\pi}^q|D_q\rangle \;=\; 2\, F^2(\mu_0)\, m_D\, G_1(\mu_0)\, \tilde{L}_{1,\pi}^q\,, \tag{C.3.8}$$

$$\langle D_q|\tilde{M}_{2,\pi}^q|D_q\rangle \;=\; 2\, F^2(\mu_0)\, m_D\, G_1(\mu_0)\, \tilde{L}_{2,\pi}^q\,, \tag{C.3.9}$$

$$\langle D_q|\tilde{M}_{1,G}^q|D_q\rangle \;=\; 12\, F^2(\mu_0)\, m_D\, G_2(\mu_0)\, \tilde{L}_{1,G}^q\,, \tag{C.3.10}$$

$$\langle D_q|\tilde{M}_{2,G}^q|D_q\rangle \;=\; 12\, F^2(\mu_0)\, m_D\, G_2(\mu_0)\, \tilde{L}_{2,G}^q\,, \tag{C.3.11}$$

and similar expressions for the colour-octet operators. Again, in VIA, the dimension-seven Bag parameters are $\tilde{B}^q_{P,i} = 1$, $\tilde{B}^q_{R,i} = 1$, and $\tilde{L}^q_{1,\pi} = 1$, $\tilde{L}^q_{1,G} = 1$ and the corresponding colour-octet Bag parameters vanish.

The expressions in Eqs. (C.3.3) - (C.3.7) can be obtained using a general parametrisation of matrix elements of the HQET quark currents with a heavy pseudo-scalar meson $\mathcal{M}$ (see e.g. [45]):

$$\langle 0|\bar{q}\,\Gamma\,h_v|M(v)\rangle = \frac{i}{2}F(\mu)\,\mathrm{Tr}[\Gamma\mathcal{M}(v)]\,, \tag{C.3.12}$$

$$\langle 0|\bar{q}\,\Gamma\,iD_\alpha h_v|M(v)\rangle = -\frac{i}{6}(\bar{\Lambda}-m_q)F(\mu)\,\mathrm{Tr}[(v_\alpha+\gamma_\alpha)\Gamma\mathcal{M}(v)]\,, \tag{C.3.13}$$

$$\langle 0|\bar{q}(-i\overleftarrow{D}_\alpha)\,\Gamma\,h_v|M(v)\rangle = -\frac{i}{6}F(\mu)\,\mathrm{Tr}[((4\bar{\Lambda}-m_q)v_\alpha + (\bar{\Lambda}-m_q)\gamma_\alpha)\Gamma\mathcal{M}(v)], \tag{C.3.14}$$

and for the non-local operators:

$$\langle 0|i\int d^4y\,T\left[(\bar{q}\,\Gamma\,h_v)(0),(\bar{h}_v(iD)^2h_v)(y)\right]|\mathcal{M}(v)\rangle = F(\mu)\,G_1(\mu)\,\mathrm{Tr}[\Gamma\mathcal{M}(v)], \tag{C.3.15}$$

and

$$\langle 0|i\int d^4y\,T\left[(\bar{q}\,\Gamma\,h_v)(0),\frac{1}{2}g_s\left(\bar{h}_v\sigma_{\alpha\beta}G^{\alpha\beta}h_v\right)(y)\right]|\mathcal{M}(v)\rangle = 6\,F(\mu)\,G_2(\mu)\,\mathrm{Tr}[\Gamma\mathcal{M}(v)], \tag{C.3.16}$$

where Γ is a generic Dirac structure, and

$$\mathcal{M}(v) = -\sqrt{m_D}\,\frac{(1+\not{v})}{2}\gamma_5\,. \tag{C.3.17}$$

Since we are limited to LO-QCD for the dimension-seven contribution, we can just replace the HQET decay constant $F(\mu)$ by the full QCD one f_D, using $F(\mu) = f_D\,\sqrt{m_D}$.

Bibliography

[1] D. King, A. Lenz and T. Rauh, *B_s mixing observables and $|V_{td}/V_{ts}|$ from sum rules*, *JHEP* **05** (2019) 034, [1904.00940].

[2] D. King, M. Kirk, A. Lenz and T. Rauh, *$|V_{cb}|$ and γ from B-mixing - Addendum to "B_s mixing observables and $|V_{td}/V_{ts}|$ from sum rules"*, *JHEP* **03** (2019) 112, [1911.07856].

[3] D. King, A. Lenz and T. Rauh, *$SU(3)$ breaking effects in B and D meson lifetimes*, 2112.03691.

[4] D. King, A. Lenz, M. L. Piscopo, T. Rauh, A. V. Rusov and C. Vlahos, *Revisiting Inclusive Decay Widths of Charmed Mesons*, 2109.13219.

[5] ATLAS collaboration, G. Aad et al., *Observation of a new particle in the search for the Standard Model Higgs boson with the ATLAS detector at the LHC*, *Phys. Lett. B* **716** (2012) 1–29, [1207.7214].

[6] CMS collaboration, S. Chatrchyan et al., *Observation of a New Boson at a Mass of 125 GeV with the CMS Experiment at the LHC*, *Phys. Lett. B* **716** (2012) 30–61, [1207.7235].

[7] P. W. Higgs, *Broken Symmetries and the Masses of Gauge Bosons*, *Phys. Rev. Lett.* **13** (1964) 508–509.

[8] F. Englert and R. Brout, *Broken Symmetry and the Mass of Gauge Vector Mesons*, *Phys. Rev. Lett.* **13** (1964) 321–323.

[9] G. S. Guralnik, C. R. Hagen and T. W. B. Kibble, *Global Conservation Laws and Massless Particles*, *Phys. Rev. Lett.* **13** (1964) 585–587.

[10] FCC collaboration, A. Abada et al., *FCC Physics Opportunities: Future Circular Collider Conceptual Design Report Volume 1*, *Eur. Phys. J. C* **79** (2019) 474.

[11] FCC collaboration, A. Abada et al., *FCC-ee: The Lepton Collider: Future Circular Collider Conceptual Design Report Volume 2*, *Eur. Phys. J. ST* **228** (2019) 261–623.

[12] FCC collaboration, A. Abada et al., *FCC-hh: The Hadron Collider: Future Circular Collider Conceptual Design Report Volume 3*, *Eur. Phys. J. ST* **228** (2019) 755–1107.

[13] A. D. Sakharov, *Violation of CP Invariance, C asymmetry, and baryon asymmetry of the universe*, *Pisma Zh. Eksp. Teor. Fiz.* **5** (1967) 32–35.

[14] F. R. Klinkhamer and N. S. Manton, *A Saddle Point Solution in the Weinberg-Salam Theory*, *Phys. Rev. D* **30** (1984) 2212.

[15] M. B. Gavela, P. Hernandez, J. Orloff and O. Pene, *Standard model CP violation and baryon asymmetry*, *Mod. Phys. Lett. A* **9** (1994) 795–810, [hep-ph/9312215].

[16] P. Huet and E. Sather, *Electroweak baryogenesis and standard model CP violation*, *Phys. Rev. D* **51** (1995) 379–394, [hep-ph/9404302].

[17] F. Zwicky, *Die Rotverschiebung von extragalaktischen Nebeln*, *Helv. Phys. Acta* **6** (1933) 110–127.

[18] S. Smith, *The Mass of the Virgo Cluster*, *Astrophys. J.* **83** (1936) 23–30.

[19] J. H. Oort, *The force exerted by the stellar system in the direction perpendicular to the galactic plane and some related problems*, *Bull. Astron. Inst. Netherlands* **6** (1932) 249–287.

[20] H. W. Babcock, *The rotation of the Andromeda Nebula*, *Lick Observatory Bulletin* **498** (Jan., 1939) 41–51.

[21] M. Schumann, *Direct Detection of WIMP Dark Matter: Concepts and Status*, *J. Phys. G* **46** (2019) 103003, [1903.03026].

[22] Super-Kamiokande collaboration, Y. Fukuda et al., *Evidence for oscillation of atmospheric neutrinos*, *Phys. Rev. Lett.* **81** (1998) 1562–1567, [hep-ex/9807003].

[23] SNO collaboration, Q. R. Ahmad et al., *Direct evidence for neutrino flavor transformation from neutral current interactions in the Sudbury Neutrino Observatory*, *Phys. Rev. Lett.* **89** (2002) 011301, [nucl-ex/0204008].

[24] S. L. Glashow, J. Iliopoulos and L. Maiani, *Weak Interactions with Lepton-Hadron Symmetry*, *Phys. Rev. D* **2** (1970) 1285–1292.

[25] ARGUS collaboration, H. Albrecht et al., *Observation of $B^0 - \overline{B}^0$ Mixing*, *Phys. Lett. B* **192** (1987) 245–252.

[26] UA1 collaboration, G. Arnison et al., *Associated Production of an Isolated Large Transverse Momentum Lepton (electron or Muon), and Two Jets at the CERN p anti-p Collider*, *Phys. Lett. B* **147** (1984) 493.

[27] E. Boos, O. Brandt, D. Denisov, S. Denisov and P. Grannis, *The top quark (20 years after its discovery)*, *Phys. Usp.* **58** (2015) 1133–1158, [1509.03325].

[28] L. Di Luzio, M. Kirk, A. Lenz and T. Rauh, *ΔM_s theory precision confronts flavour anomalies*, *JHEP* **12** (2019) 009, [1909.11087].

[29] M. Bordone, G. Isidori and A. Pattori, *On the Standard Model predictions for R_K and R_{K^*}*, *Eur. Phys. J. C* **76** (2016) 440, [1605.07633].

[30] LHCb collaboration, R. Aaij et al., *Test of lepton universality with $B^0 \to K^{*0}\ell^+\ell^-$ decays*, *JHEP* **08** (2017) 055, [1705.05802].

[31] LHCb collaboration, R. Aaij et al., *Test of lepton universality in beauty-quark decays*, 2103.11769.

[32] Y. Aoki et al., *FLAG Review 2021*, 2111.09849.

[33] LHCb collaboration, R. Aaij et al., *Measurement of the $B_s^0 \to \mu^+\mu^-$ decay properties and search for the $B^0 \to \mu^+\mu^-$ and $B_s^0 \to \mu^+\mu^-\gamma$ decays*, 2108.09283.

[34] ATLAS collaboration, M. Aaboud et al., *Study of the rare decays of B_s^0 and B^0 mesons into muon pairs using data collected during 2015 and 2016 with the ATLAS detector*, *JHEP* **04** (2019) 098, [1812.03017].

[35] CMS collaboration, A. M. Sirunyan et al., *Measurement of properties of $B_s^0 \to \mu^+\mu^-$ decays and search for $B^0 \to \mu^+\mu^-$ with the CMS experiment*, *JHEP* **04** (2020) 188, [1910.12127].

[36] W. Altmannshofer and P. Stangl, *New physics in rare B decays after Moriond 2021*, *Eur. Phys. J. C* **81** (2021) 952, [2103.13370].

[37] L.-S. Geng, B. Grinstein, S. Jäger, S.-Y. Li, J. Martin Camalich and R.-X. Shi, *Implications of new evidence for lepton-universality violation in $b \to s l^+ l^-$ decays*, *Phys. Rev. D* **104** (2021) 035029, [2103.12738].

[38] Muon g-2 collaboration, B. Abi et al., *Measurement of the Positive Muon Anomalous Magnetic Moment to 0.46 ppm*, *Phys. Rev. Lett.* **126** (2021) 141801, [2104.03281].

[39] Muon g-2 collaboration, G. W. Bennett et al., *Final Report of the Muon E821 Anomalous Magnetic Moment Measurement at BNL*, *Phys. Rev. D* **73** (2006) 072003, [hep-ex/0602035].

[40] T. Aoyama et al., *The anomalous magnetic moment of the muon in the Standard Model*, *Phys. Rept.* **887** (2020) 1–166, [2006.04822].

[41] R. H. Parker, C. Yu, W. Zhong, B. Estey and H. Müller, *Measurement of the fine-structure constant as a test of the Standard Model*, *Science* **360** (2018) 191, [1812.04130].

[42] D. Hanneke, S. F. Hoogerheide and G. Gabrielse, *Cavity Control of a Single-Electron Quantum Cyclotron: Measuring the Electron Magnetic Moment*, *Phys. Rev. A* **83** (2011) 052122, [1009.4831].

[43] T. Aoyama, T. Kinoshita and M. Nio, *Revised and Improved Value of the QED Tenth-Order Electron Anomalous Magnetic Moment*, *Phys. Rev. D* **97** (2018) 036001, [1712.06060].

[44] A. Lenz, *Lifetimes and heavy quark expansion*, *Int. J. Mod. Phys. A* **30** (2015) 1543005, [1405.3601].

[45] M. Neubert, *Heavy quark symmetry*, *Phys. Rept.* **245** (1994) 259–396, [hep-ph/9306320].

[46] M. A. Shifman, A. I. Vainshtein and V. I. Zakharov, *QCD and Resonance Physics. Theoretical Foundations*, *Nucl. Phys. B* **147** (1979) 385–447.

[47] K. G. Wilson, *Confinement of Quarks*, *Phys. Rev. D* **10** (1974) 2445–2459.

[48] I. I. Balitsky, V. M. Braun and A. V. Kolesnichenko, *Radiative Decay $\sigma^+ \to p\gamma$ in Quantum Chromodynamics*, *Nucl. Phys. B* **312** (1989) 509–550.

[49] A. Khodjamirian and A. V. Rusov, *$B_s \to K\ell\nu_\ell$ and $B_{(s)} \to \pi(K)\ell^+\ell^-$ decays at large recoil and CKM matrix elements*, *JHEP* **08** (2017) 112, [1703.04765].

[50] A. Khodjamirian, T. Mannel and Y. M. Wang, *$B \to K\ell^+\ell^-$ decay at large hadronic recoil*, *JHEP* **02** (2013) 010, [1211.0234].

[51] C. Bourrely, I. Caprini and L. Lellouch, *Model-independent description of $B \to \pi l\nu$ decays and a determination of $|V_{ub}|$*, *Phys. Rev. D* **79** (2009) 013008, [0807.2722].

[52] A. Bharucha, D. M. Straub and R. Zwicky, *$B \to V\ell^+\ell^-$ in the Standard Model from light-cone sum rules*, *JHEP* **08** (2016) 098, [1503.05534].

[53] J. A. Bailey et al., *$B \to Kl^+l^-$ Decay Form Factors from Three-Flavor Lattice QCD*, *Phys. Rev. D* **93** (2016) 025026, [1509.06235].

[54] A. G. Grozin, R. Klein, T. Mannel and A. A. Pivovarov, *$B^0 - \bar{B}^0$ mixing at next-to-leading order*, *Phys. Rev. D* **94** (2016) 034024, [1606.06054].

[55] M. Kirk, A. Lenz and T. Rauh, *Dimension-six matrix elements for meson mixing and lifetimes from sum rules*, *JHEP* **12** (2017) 068, [1711.02100].

[56] V. A. Khoze and M. A. Shifman, *Heavy Quarks*, *Sov. Phys. Usp.* **26** (1983) 387.

[57] M. A. Shifman and M. B. Voloshin, *Preasymptotic Effects in Inclusive Weak Decays of Charmed Particles*, *Sov. J. Nucl. Phys.* **41** (1985) 120.

[58] I. I. Y. Bigi and N. G. Uraltsev, *Gluonic enhancements in non-spectator beauty decays: An Inclusive mirage though an exclusive possibility*, *Phys. Lett. B* **280** (1992) 271–280.

[59] I. I. Y. Bigi, N. G. Uraltsev and A. I. Vainshtein, *Nonperturbative corrections to inclusive beauty and charm decays: QCD versus phenomenological models*, *Phys. Lett.* **B293** (1992) 430–436, [hep-ph/9207214].

[60] B. Blok and M. A. Shifman, *The Rule of discarding $1/N_c$ in inclusive weak decays. 1.*, *Nucl. Phys.* **B399** (1993) 441–458, [hep-ph/9207236].

[61] B. Blok and M. A. Shifman, *The Rule of discarding $1/N_c$ in inclusive weak decays. 2.*, *Nucl. Phys.* **B399** (1993) 459–476, [hep-ph/9209289].

[62] J. Chay, H. Georgi and B. Grinstein, *Lepton energy distributions in heavy meson decays from QCD*, *Phys. Lett. B* **247** (1990) 399–405.

[63] M. E. Luke, *Effects of subleading operators in the heavy quark effective theory*, *Phys. Lett. B* **252** (1990) 447–455.

[64] I. I. Y. Bigi, B. Blok, M. A. Shifman, N. G. Uraltsev and A. I. Vainshtein, *A QCD 'manifesto' on inclusive decays of beauty and charm*, in *The Fermilab Meeting DPF 92. Proceedings, 7th Meeting of the American Physical Society, Division of Particles and Fields, Batavia, USA, November 10-14, 1992. Vol. 1, 2*, pp. 610–613, 1992, hep-ph/9212227.

[65] A. J. Buras, M. Jamin and P. H. Weisz, *Leading and Next-to-leading QCD Corrections to ϵ Parameter and $B^0 - \bar{B}^0$ Mixing in the Presence of a Heavy Top Quark*, *Nucl. Phys. B* **347** (1990) 491–536.

[66] M. D. Schwartz, *Quantum Field Theory and the Standard Model*. Cambridge University Press, 3, 2014.

[67] G. Buchalla, A. J. Buras and M. E. Lautenbacher, *Weak decays beyond leading logarithms*, *Rev. Mod. Phys.* **68** (1996) 1125–1144, [hep-ph/9512380].

[68] A. J. Buras, *Weak Hamiltonian, CP violation and rare decays*, in *Les Houches Summer School in Theoretical Physics, Session 68: Probing the Standard Model of Particle Interactions*, pp. 281–539, 6, 1998, hep-ph/9806471.

[69] M. Neubert, *Heavy quark effective theory*, *Subnucl. Ser.* **34** (1997) 98–165, [hep-ph/9610266].

[70] N. Isgur and M. B. Wise, *Weak Decays of Heavy Mesons in the Static Quark Approximation*, *Phys. Lett. B* **232** (1989) 113–117.

[71] N. Isgur and M. B. Wise, *Weak Transition Form-Factors Between Heavy Mesons*, *Phys. Lett. B* **237** (1990) 527–530.

[72] H. Georgi, *An Effective Field Theory for Heavy Quarks at Low-energies*, *Phys. Lett. B* **240** (1990) 447–450.

[73] A. F. Falk, *Hadrons of arbitrary spin in the heavy quark effective theory*, *Nucl. Phys. B* **378** (1992) 79–94.

[74] *B physics at the Tevatron: Run II and beyond*, 12, 2001.

[75] A. Lenz and U. Nierste, *Theoretical update of $B_s - \bar{B}_s$ mixing*, *JHEP* **06** (2007) 072, [hep-ph/0612167].

[76] M. Artuso, G. Borissov and A. Lenz, *CP violation in the B_s^0 system*, *Rev. Mod. Phys.* **88** (2016) 045002, [1511.09466].

[77] A. Lenz, U. Nierste, J. Charles, S. Descotes-Genon, A. Jantsch, C. Kaufhold et al., *Anatomy of New Physics in $B - \bar{B}$ mixing*, *Phys. Rev. D* **83** (2011) 036004, [1008.1593].

[78] A. Lenz, M. L. Piscopo and C. Vlahos, *Renormalization scale setting for D-meson mixing*, *Phys. Rev. D* **102** (2020) 093002, [2007.03022].

[79] T. Inami and C. S. Lim, *Effects of Superheavy Quarks and Leptons in Low-Energy Weak Processes $K_L \to \mu\overline{\mu}$, $K^+ \to \pi^+\nu\overline{\nu}$ and $K^0 - \overline{K}^0$*, *Prog. Theor. Phys.* **65** (1981) 297.

[80] HPQCD collaboration, C. T. H. Davies, J. Harrison, G. P. Lepage, C. J. Monahan, J. Shigemitsu and M. Wingate, *Lattice QCD matrix elements for the $B_s^0 - \bar{B}_s^0$ width difference beyond leading order*, *Phys. Rev. Lett.* **124** (2020) 082001, [1910.00970].

[81] P. Colangelo and A. Khodjamirian, *QCD sum rules, a modern perspective*, hep-ph/0010175.

[82] E. de Rafael, *An Introduction to sum rules in QCD: Course*, in *Les Houches Summer School in Theoretical Physics, Session 68: Probing the Standard Model of Particle Interactions*, pp. 1171–1218, 7, 1997, hep-ph/9802448.

[83] S. Narison, *QCD spectral sum rules for heavy flavors*, *Acta Phys. Polon. B* **26** (1995) 687–710, [hep-ph/9503234].

[84] E. V. Shuryak, *Correlation functions in the QCD vacuum*, *Rev. Mod. Phys.* **65** (1993) 1–46.

[85] L. J. Reinders, H. Rubinstein and S. Yazaki, *Hadron Properties from QCD Sum Rules*, *Phys. Rept.* **127** (1985) 1.

[86] B. L. Ioffe, *Calculation of Baryon Masses in Quantum Chromodynamics*, *Nucl. Phys. B* **188** (1981) 317–341.

[87] A. F. Falk, M. Neubert and M. E. Luke, *The Residual mass term in the heavy quark effective theory*, *Nucl. Phys. B* **388** (1992) 363–375, [hep-ph/9204229].

[88] T. Schäfer and E. V. Shuryak, *Instantons in QCD*, *Rev. Mod. Phys.* **70** (1998) 323–426, [hep-ph/9610451].

[89] E. V. Shuryak, *The Role of Instantons in Quantum Chromodynamics. 1. Physical Vacuum*, *Nucl. Phys. B* **203** (1982) 93.

[90] M. A. Shifman, A. I. Vainshtein and V. I. Zakharov, *QCD and Resonance Physics: Applications*, *Nucl. Phys. B* **147** (1979) 448–518.

[91] M. A. Shifman, *Quark hadron duality*, in *8th International Symposium on Heavy Flavor Physics*, vol. 3, (Singapore), pp. 1447–1494, World Scientific, 7, 2000, hep-ph/0009131, DOI.

[92] B. Blok, M. A. Shifman and D.-X. Zhang, *An Illustrative example of how quark hadron duality might work*, *Phys. Rev. D* **57** (1998) 2691–2700, [hep-ph/9709333].

[93] B. Chibisov, R. D. Dikeman, M. A. Shifman and N. Uraltsev, *Operator product expansion, heavy quarks, QCD duality and its violations*, *Int. J. Mod. Phys. A* **12** (1997) 2075–2133, [hep-ph/9605465].

[94] D. J. Broadhurst and A. G. Grozin, *Operator product expansion in static quark effective field theory: Large perturbative correction*, *Phys. Lett. B* **274** (1992) 421–427, [hep-ph/9908363].

[95] E. Bagan, P. Ball, V. M. Braun and H. G. Dosch, *QCD sum rules in the effective heavy quark theory*, *Phys. Lett. B* **278** (1992) 457–464.

[96] M. Neubert, *Heavy meson form-factors from QCD sum rules*, *Phys. Rev. D* **45** (1992) 2451–2466.

[97] K. G. Chetyrkin and F. V. Tkachov, *Integration by Parts: The Algorithm to Calculate beta Functions in 4 Loops*, *Nucl. Phys. B* **192** (1981) 159–204.

[98] V. A. Smirnov, *Analytic tools for Feynman integrals*, vol. 250. 2012, 10.1007/978-3-642-34886-0.

[99] A. V. Smirnov and A. V. Petukhov, *The Number of Master Integrals is Finite*, *Lett. Math. Phys.* **97** (2011) 37–44, [1004.4199].

[100] J. M. Henn, *Multiloop integrals in dimensional regularization made simple*, *Phys. Rev. Lett.* **110** (2013) 251601, [1304.1806].

[101] J. M. Henn, *Lectures on differential equations for Feynman integrals*, *J. Phys. A* **48** (2015) 153001, [1412.2296].

[102] S. Laporta, *High precision calculation of multiloop Feynman integrals by difference equations*, *Int. J. Mod. Phys. A* **15** (2000) 5087–5159, [hep-ph/0102033].

[103] T. Gehrmann and E. Remiddi, *Differential equations for two loop four point functions*, *Nucl. Phys. B* **580** (2000) 485–518, [hep-ph/9912329].

[104] R. N. Lee, *Group structure of the integration-by-part identities and its application to the reduction of multiloop integrals*, *JHEP* **07** (2008) 031, [0804.3008].

[105] A. V. Smirnov, *FIRE5: a C++ implementation of Feynman Integral REduction*, *Comput. Phys. Commun.* **189** (2015) 182–191, [1408.2372].

[106] P. Maierhöfer, J. Usovitsch and P. Uwer, *Kira—A Feynman integral reduction program*, *Comput. Phys. Commun.* **230** (2018) 99–112, [1705.05610].

[107] C. Anastasiou and A. Lazopoulos, *Automatic integral reduction for higher order perturbative calculations*, *JHEP* **07** (2004) 046, [hep-ph/0404258].

[108] A. von Manteuffel and C. Studerus, *Reduze 2 - Distributed Feynman Integral Reduction*, 1201.4330.

[109] V. A. Smirnov, *Evaluating Feynman integrals*, *Springer Tracts Mod. Phys.* **211** (2004) 1–244.

[110] E. E. Boos and A. I. Davydychev, *A Method of evaluating massive Feynman integrals*, *Theor. Math. Phys.* **89** (1991) 1052–1063.

[111] J. B. Tausk, *Nonplanar massless two loop Feynman diagrams with four on-shell legs*, *Phys. Lett. B* **469** (1999) 225–234, [hep-ph/9909506].

[112] V. A. Smirnov, *Analytical result for dimensionally regularized massless on shell double box*, *Phys. Lett. B* **460** (1999) 397–404, [hep-ph/9905323].

[113] M. Beneke and V. A. Smirnov, *Asymptotic expansion of Feynman integrals near threshold*, *Nucl. Phys. B* **522** (1998) 321–344, [hep-ph/9711391].

[114] B. Jantzen, *Foundation and generalization of the expansion by regions*, *JHEP* **12** (2011) 076, [1111.2589].

[115] J. S. Schwinger, *On gauge invariance and vacuum polarization*, *Phys. Rev.* **82** (1951) 664–679.

[116] M. S. Dubovikov and A. V. Smilga, *Analytical Properties of the Quark Polarization Operator in an External Selfdual Field*, *Nucl. Phys. B* **185** (1981) 109–132.

[117] M. A. Shifman, *Wilson Loop in Vacuum Fields*, *Nucl. Phys. B* **173** (1980) 13–31.

[118] A. V. Smilga, *Calculation of the Degree Corrections in Fixed Point Gauge. (In Russian)*, *Sov. J. Nucl. Phys.* **35** (1982) 271–277.

[119] E. V. Shuryak, *Hadrons Containing a Heavy Quark and QCD Sum Rules*, *Nucl. Phys. B* **198** (1982) 83–101.

[120] V. Fock, *Proper time in classical and quantum mechanics*, *Phys. Z. Sowjetunion* **12** (1937) 404–425.

[121] J. S. Schwinger, *Particles, Sources, and Fields*. CRC Press, 1998, 10.1201/9780429498480.

[122] V. A. Novikov, M. A. Shifman, A. I. Vainshtein and V. I. Zakharov, *Calculations in External Fields in Quantum Chromodynamics. Technical Review*, *Fortsch. Phys.* **32** (1984) 585.

[123] P. Pascual and R. Tarrach, *QCD: Renormalisation for the Practitioner*, vol. 194. 1984.

[124] A. Lenz, M. L. Piscopo and A. V. Rusov, *Contribution of the Darwin operator to non-leptonic decays of heavy quarks*, *JHEP* **12** (2020) 199, [2004.09527].

[125] M. L. Piscopo, *Higher Order Corrections To The Lifetime Of Heavy Hadrons*, Ph.D. thesis, Siegen U., 2021. 2112.03137. 10.25819/ubsi/10024.

[126] W. Hubschmid and S. Mallik, *Operator expansion at short distance in QCD*, *Nucl. Phys. B* **207** (1982) 29–42.

[127] HFLAV collaboration, Y. S. Amhis et al., *Averages of b-hadron, c-hadron, and τ-lepton properties as of 2018 and online update at https://hflav.web.cern.ch*, 1909.12524.

[128] CDF collaboration, A. Abulencia et al., *Observation of $B_s^0 - \bar{B}_s^0$ Oscillations*, *Phys. Rev. Lett.* **97** (2006) 242003, [hep-ex/0609040].

[129] LHCb collaboration, R. Aaij et al., *Measurement of the $B_s^0 - \bar{B}_s^0$ oscillation frequency Δm_s in $B_s^0 \to D_s^-(3)\pi$ decays*, *Phys. Lett. B* **709** (2012) 177–184, [1112.4311].

[130] LHCb collaboration, R. Aaij et al., *Precision measurement of the B_s^0-$\bar{B}_s^0$ oscillation frequency with the decay $B_s^0 \to D_s^-\pi^+$*, *New J. Phys.* **15** (2013) 053021, [1304.4741].

[131] LHCb collaboration, R. Aaij et al., *Observation of B_s^0-$\bar{B}_s^0$ mixing and measurement of mixing frequencies using semileptonic B decays*, *Eur. Phys. J. C* **73** (2013) 2655, [1308.1302].

[132] LHCb collaboration, R. Aaij et al., *Updated measurement of time-dependent CP-violating observables in $B_s^0 \to J/\psi K^+K^-$ decays*, *Eur. Phys. J. C* **79** (2019) 706, [1906.08356].

[133] CMS collaboration, A. M. Sirunyan et al., *Measurement of the CP-violating phase ϕ_s in the $B_s^0 \to J/\psi\,\phi(1020) \to \mu^+\mu^-K^+K^-$ channel in proton-proton collisions at $\sqrt{s} = 13$ TeV*, *Phys. Lett. B* **816** (2021) 136188, [2007.02434].

[134] LHCb collaboration, R. Aaij et al., *Precise determination of the B_s^0-$\overline{B}_s^0$ oscillation frequency*, 2104.04421.

[135] E. Dalgic, A. Gray, E. Gamiz, C. T. H. Davies, G. P. Lepage, J. Shigemitsu et al., *$B_s^0 - \bar{B}_s^0$ mixing parameters from unquenched lattice QCD*, *Phys. Rev. D* **76** (2007) 011501, [hep-lat/0610104].

[136] ETM collaboration, N. Carrasco et al., *B-physics from $N_f = 2$ tmQCD: the Standard Model and beyond*, *JHEP* **03** (2014) 016, [1308.1851].

[137] Fermilab Lattice, MILC collaboration, A. Bazavov et al., *$B^0_{(s)}$-mixing matrix elements from lattice QCD for the Standard Model and beyond*, *Phys. Rev. D* **93** (2016) 113016, [1602.03560].

[138] P. Boyle, L. Del Debbio, F. Erben, A. Jüttner, T. Kaneko, M. Marshall et al., *BSM $B - \bar{B}$ mixing on JLQCD and RBC/UKQCD $N_f = 2 + 1$ DWF ensembles*, in *38th International Symposium on Lattice Field Theory*, 11, 2021, 2111.11287.

[139] A. G. Grozin, T. Mannel and A. A. Pivovarov, *Towards a Next-to-Next-to-Leading Order analysis of matching in B^0-$\bar{B}^0$ mixing*, *Phys. Rev. D* **96** (2017) 074032, [1706.05910].

[140] A. G. Grozin, T. Mannel and A. A. Pivovarov, *B^0-$\bar{B}^0$ mixing: Matching to HQET at NNLO*, *Phys. Rev. D* **98** (2018) 054020, [1806.00253].

[141] RBC/UKQCD collaboration, P. A. Boyle, L. Del Debbio, N. Garron, A. Juttner, A. Soni, J. T. Tsang et al., *SU(3)-breaking ratios for $D_{(s)}$ and $B_{(s)}$ mesons*, 1812.08791.

[142] F. Gabbiani, E. Gabrielli, A. Masiero and L. Silvestrini, *A Complete analysis of FCNC and CP constraints in general SUSY extensions of the standard model*, *Nucl. Phys. B* **477** (1996) 321–352, [hep-ph/9604387].

[143] E. Eichten and B. R. Hill, *An Effective Field Theory for the Calculation of Matrix Elements Involving Heavy Quarks*, *Phys. Lett. B* **234** (1990) 511–516.

[144] S. C. Generalis, *Improved two loop quark mass corrections*, *J. Phys. G* **15** (1989) L225–L229.

[145] K. G. Chetyrkin, A. L. Kataev, A. B. Krasulin and A. A. Pivovarov, *Calculation of the $K^0 - \overline{K}^0$ mixing parameter via the QCD sum rules at finite energies*, *Phys. Lett. B* **174** (1986) 104, [hep-ph/0103230].

[146] J. G. Korner, A. I. Onishchenko, A. A. Petrov and A. A. Pivovarov, *$B^0 - overline B^0$ mixing beyond factorization*, *Phys. Rev. Lett.* **91** (2003) 192002, [hep-ph/0306032].

[147] P. Nogueira, *Automatic Feynman graph generation*, *J. Comput. Phys.* **105** (1993) 279–289.

[148] M. Jamin and M. E. Lautenbacher, *TRACER: Version 1.1: A Mathematica package for gamma algebra in arbitrary dimensions*, *Comput. Phys. Commun.* **74** (1993) 265–288.

[149] A. G. Grozin and R. N. Lee, *Three-loop HQET vertex diagrams for B0 - anti-B0 mixing*, *JHEP* **02** (2009) 047, [0812.4522].

[150] T. Huber and D. Maitre, *HypExp 2, Expanding Hypergeometric Functions about Half-Integer Parameters*, *Comput. Phys. Commun.* **178** (2008) 755–776, [0708.2443].

[151] Particle Data Group collaboration, M. Tanabashi et al., *Review of Particle Physics*, *Phys. Rev. D* **98** (2018) 030001.

[152] T. Mannel, B. Pecjak and A. Pivovarov, *Analyzing $B_s - \overline{B}_s$ Mixing: Non-perturbative Contributions to Bag Parameters from Sum Rules.*, *Red Report (2007),* (04, 2007) .

[153] T. Mannel, B. D. Pecjak and A. A. Pivovarov, *Sum rule estimate of the subleading non-perturbative contributions to $B_s - \bar{B}_s$ mixing*, *Eur. Phys. J. C* **71** (2011) 1607, [hep-ph/0703244].

[154] C. McNeile, A. Bazavov, C. T. H. Davies, R. J. Dowdall, K. Hornbostel, G. P. Lepage et al., *Direct determination of the strange and light quark condensates from full lattice QCD*, *Phys. Rev. D* **87** (2013) 034503, [1211.6577].

[155] HPQCD collaboration, C. T. H. Davies, K. Hornbostel, J. Komijani, J. Koponen, G. P. Lepage, A. T. Lytle et al., *Determination of the quark condensate from heavy-light current-current correlators in full lattice QCD*, *Phys. Rev. D* **100** (2019) 034506, [1811.04305].

[156] R. J. Dowdall, C. T. H. Davies, R. R. Horgan, G. P. Lepage, C. J. Monahan, J. Shigemitsu et al., *Neutral B-meson mixing from full lattice QCD at the physical point*, 1907.01025.

[157] Flavour Lattice Averaging Group collaboration, S. Aoki et al., *FLAG Review 2019: Flavour Lattice Averaging Group (FLAG)*, *Eur. Phys. J. C* **80** (2020) 113, [1902.08191].

[158] P. Boyle, N. Garron, J. Kettle, A. Khamseh and J. T. Tsang, *BSM Kaon Mixing at the Physical Point*, *EPJ Web Conf.* **175** (2018) 13010, [1710.09176].

[159] C. Hughes, C. T. H. Davies and C. J. Monahan, *New methods for B meson decay constants and form factors from lattice NRQCD*, *Phys. Rev. D* **97** (2018) 054509, [1711.09981].

[160] A. Bazavov et al., *B- and D-meson leptonic decay constants from four-flavor lattice QCD*, *Phys. Rev. D* **98** (2018) 074512, [1712.09262].

[161] A. Lenz and G. Tetlalmatzi-Xolocotzi, *Model-independent bounds on new physics effects in non-leptonic tree-level decays of B-mesons*, *JHEP* **07** (2020) 177, [1912.07621].

[162] M. Beneke, G. Buchalla, C. Greub, A. Lenz and U. Nierste, *Next-to-leading order QCD corrections to the lifetime difference of B(s) mesons*, *Phys. Lett. B* **459** (1999) 631–640, [hep-ph/9808385].

[163] M. Beneke, G. Buchalla, A. Lenz and U. Nierste, *CP asymmetry in flavor specific B decays beyond leading logarithms*, *Phys. Lett. B* **576** (2003) 173–183, [hep-ph/0307344].

[164] M. Ciuchini, E. Franco, V. Lubicz, F. Mescia and C. Tarantino, *Lifetime differences and CP violation parameters of neutral B mesons at the next-to-leading order in QCD*, *JHEP* **08** (2003) 031, [hep-ph/0308029].

[165] M. Beneke, G. Buchalla and I. Dunietz, *Width Difference in the $B_s - \bar{B}_s$ System*, *Phys. Rev. D* **54** (1996) 4419–4431, [hep-ph/9605259].

[166] A. S. Dighe, T. Hurth, C. S. Kim and T. Yoshikawa, *Measurement of the lifetime difference of B(d) mesons: Possible and worthwhile?*, *Nucl. Phys. B* **624** (2002) 377–404, [hep-ph/0109088].

[167] H. M. Asatrian, A. Hovhannisyan, U. Nierste and A. Yeghiazaryan, *Towards next-to-next-to-leading-log accuracy for the width difference in the $B_s - \bar{B}_s$ system: fermionic contributions to order $(m_c/m_b)^0$ and $(m_c/m_b)^1$*, *JHEP* **10** (2017) 191, [1709.02160].

[168] A. V. Bednyakov, B. A. Kniehl, A. F. Pikelner and O. L. Veretin, *Stability of the Electroweak Vacuum: Gauge Independence and Advanced Precision*, *Phys. Rev. Lett.* **115** (2015) 201802, [1507.08833].

[169] Particle Data Group collaboration, P. Zyla et al., *Review of Particle Physics*, *PTEP* **2020** (2020) 083C01.

[170] A. H. Hoang, S. Plätzer and D. Samitz, *On the Cutoff Dependence of the Quark Mass Parameter in Angular Ordered Parton Showers*, *JHEP* **10** (2018) 200, [1807.06617].

[171] M. Beneke, Y. Kiyo, P. Marquard, A. Penin, J. Piclum and M. Steinhauser, *Next-to-Next-to-Next-to-Leading Order QCD Prediction for the Top Antitop S-Wave Pair Production Cross Section Near Threshold in e^+e^- Annihilation*, *Phys. Rev. Lett.* **115** (2015) 192001, [1506.06864].

[172] M. Beneke, A. Maier, T. Rauh and P. Ruiz-Femenia, *Non-resonant and electroweak NNLO correction to the e^+e^- top anti-top threshold*, *JHEP* **02** (2018) 125, [1711.10429].

[173] F. Simon, *Impact of Theory Uncertainties on the Precision of the Top Quark Mass in a Threshold Scan at Future e^+e^- Colliders*, *PoS* **ICHEP2016** (2017) 872, [1611.03399].

[174] C. Bobeth, M. Gorbahn, T. Hermann, M. Misiak, E. Stamou and M. Steinhauser, *$B_{s,d} \to l^+l^-$ in the Standard Model with Reduced Theoretical Uncertainty*, *Phys. Rev. Lett.* **112** (2014) 101801, [1311.0903].

[175] A. J. Buras, *Relations between $\Delta M_{(s,d)}$ and $B_{(s,d)} \to \mu\bar{\mu}$ in models with minimal flavor violation*, *Phys. Lett. B* **566** (2003) 115–119, [hep-ph/0303060].

[176] M. Beneke, C. Bobeth and R. Szafron, *Enhanced electromagnetic correction to the rare B-meson decay $B_{s,d} \to \mu^+\mu^-$*, *Phys. Rev. Lett.* **120** (2018) 011801, [1708.09152].

[177] P. Gambino, M. Jung and S. Schacht, *The V_{cb} puzzle: An update*, *Phys. Lett.* **B795** (2019) 386–390, [1905.08209].

[178] LHCb collaboration, M. W. Kenzie and M. P. Whitehead, *Update of the LHCb combination of the CKM angle γ*, .

[179] M. Blanke and A. J. Buras, *Emerging ΔM_d -anomaly from tree-level determinations of $|V_{cb}|$ and the angle γ*, *Eur. Phys. J. C* **79** (2019) 159, [1812.06963].

[180] LHCb collaboration, *Updated LHCb combination of the CKM angle γ*, .

[181] BaBar collaboration, J. P. Lees et al., *Observation of direct CP violation in the measurement of the Cabibbo-Kobayashi-Maskawa angle gamma with $B^\pm \to D^{(*)}K^{(*)\pm}$ decays*, *Phys. Rev. D* **87** (2013) 052015, [1301.1029].

[182] CKMfitter Group collaboration, J. Charles, A. Hocker, H. Lacker, S. Laplace, F. R. Le Diberder, J. Malcles et al., *CP violation and the CKM*

matrix: Assessing the impact of the asymmetric B factories, *Eur. Phys. J. C* **41** (2005) 1–131, [hep-ph/0406184].

[183] UTfit collaboration, M. Bona et al., *The Unitarity Triangle Fit in the Standard Model and Hadronic Parameters from Lattice QCD: A Reappraisal after the Measurements of ΔM_s and $\mathcal{B}(B \to \tau\nu_\tau)$*, *JHEP* **10** (2006) 081, [hep-ph/0606167].

[184] M. Bordone, M. Jung and D. van Dyk, *Theory determination of $\bar{B} \to D^{(*)}\ell^-\bar{\nu}$ form factors at $\mathcal{O}(1/m_c^2)$*, 1908.09398.

[185] LHCb collaboration, R. Aaij et al., *Measurement of the CP-violating phase ϕ_s from $B_s^0 \to J/\psi\pi^+\pi^-$ decays in 13 TeV pp collisions*, *Phys. Lett. B* **797** (2019) 134789, [1903.05530].

[186] ATLAS collaboration, G. Aad et al., *Measurement of the CP-violating phase ϕ_s in $B_s^0 \to J/\psi\phi$ decays in ATLAS at 13 TeV*, 2001.07115.

[187] A. Lenz, *Theory Motivation: What measurements are needed?*, in *15th International Conference on Heavy Quarks and Leptons*, 10, 2021, 2110.01662.

[188] N. G. Uraltsev, *On the problem of boosting nonleptonic b baryon decays*, *Phys. Lett.* **B376** (1996) 303–308, [hep-ph/9602324].

[189] M. Neubert and C. T. Sachrajda, *Spectator effects in inclusive decays of beauty hadrons*, *Nucl. Phys.* **B483** (1997) 339–370, [hep-ph/9603202].

[190] M. Beneke, G. Buchalla, C. Greub, A. Lenz and U. Nierste, *The $B^+ - B_d^0$ Lifetime Difference Beyond Leading Logarithms*, *Nucl. Phys. B* **639** (2002) 389–407, [hep-ph/0202106].

[191] E. Franco, V. Lubicz, F. Mescia and C. Tarantino, *Lifetime ratios of beauty hadrons at the next-to-leading order in QCD*, *Nucl. Phys.* **B633** (2002) 212–236, [hep-ph/0203089].

[192] M. Ciuchini, E. Franco, V. Lubicz and F. Mescia, *Next-to-leading order QCD corrections to spectator effects in lifetimes of beauty hadrons*, *Nucl. Phys. B* **625** (2002) 211–238, [hep-ph/0110375].

[193] Y.-Y. Keum and U. Nierste, *Probing penguin coefficients with the lifetime ratio $\tau(B_s)/\tau(B_d)$*, *Phys. Rev. D* **57** (1998) 4282–4289, [hep-ph/9710512].

[194] D. Becirevic, *Theoretical progress in describing the B meson lifetimes*, *PoS* **HEP2001** (2001) 098, [hep-ph/0110124].

[195] T. Mannel, D. Moreno and A. Pivovarov, *Heavy quark expansion for heavy hadron lifetimes: completing the $1/m_b^3$ corrections*, *JHEP* **08** (2020) 089, [2004.09485].

[196] D. Moreno Torres, *Completing $1/m_b^3$ corrections to non-leptonic bottom-to-up-quark decays*, *JHEP* **01** (2021) 051, [2009.08756].

[197] A. Alberti, P. Gambino, K. J. Healey and S. Nandi, *Precision Determination of the Cabibbo-Kobayashi-Maskawa Element V_{cb}*, *Phys. Rev. Lett.* **114** (2015) 061802, [1411.6560].

[198] M. Bordone, B. Capdevila and P. Gambino, *Three loop calculations and inclusive Vcb*, *Phys. Lett. B* **822** (2021) 136679, [2107.00604].

[199] Belle-II collaboration, F. Abudinén et al., *Precise measurement of the D^0 and D^+ lifetimes at Belle II*, *Phys. Rev. Lett.* **127** (2021) 211801, [2108.03216].

[200] A. Lenz and T. Rauh, *D-meson lifetimes within the heavy quark expansion*, *Phys. Rev. D* **88** (2013) 034004, [1305.3588].

[201] S. A. Larin, *The Renormalization of the axial anomaly in dimensional regularization*, *Phys. Lett. B* **303** (1993) 113–118, [hep-ph/9302240].

[202] H.-Y. Cheng and K.-C. Yang, *Nonspectator effects and B meson lifetimes from a field theoretic calculation*, *Phys. Rev. D* **59** (1999) 014011, [hep-ph/9805222].

[203] M. S. Baek, J. Lee, C. Liu and H. S. Song, *Four quark operators relevant to B meson lifetimes from QCD sum rules*, *Phys. Rev. D* **57** (1998) 4091–4096, [hep-ph/9709386].

[204] F. Herren and M. Steinhauser, *Version 3 of RunDec and CRunDec*, *Comput. Phys. Commun.* **224** (2018) 333–345, [1703.03751].

[205] V. M. Belyaev and B. L. Ioffe, *Determination of Baryon and Baryonic Resonance Masses from QCD Sum Rules. 1. Nonstrange Baryons*, *Sov. Phys. JETP* **56** (1982) 493–501.

[206] Particle Data Group collaboration, M. Tanabashi et al., *Review of Particle Physics*, *Phys. Rev. D* **98** (2018) 030001.

[207] P. Ball, V. M. Braun and A. Lenz, *Higher-twist distribution amplitudes of the K meson in QCD*, *JHEP* **05** (2006) 004, [hep-ph/0603063].

[208] M. Beneke, A. Maier, J. Piclum and T. Rauh, *The bottom-quark mass from non-relativistic sum rules at NNNLO*, *Nucl. Phys. B* **891** (2015) 42–72, [1411.3132].

[209] M. Beneke, A. Maier, J. Piclum and T. Rauh, *NNNLO determination of the bottom-quark mass from non-relativistic sum rules*, *PoS* **RADCOR2015** (2016) 035, [1601.02949].

[210] BESIII collaboration, M. Ablikim et al., *Measurement of the absolute branching fraction of inclusive semielectronic D_s^+ decays*, 2104.07311.

[211] K. Chetyrkin and M. Steinhauser, *The Relation between the MS-bar and the on-shell quark mass at order α_s^3*, *Nucl. Phys. B* **573** (2000) 617–651, [hep-ph/9911434].

[212] K. Chetyrkin and M. Steinhauser, *Short distance mass of a heavy quark at order α_s^3*, *Phys. Rev. Lett.* **83** (1999) 4001–4004, [hep-ph/9907509].

[213] K. Melnikov and T. v. Ritbergen, *The Three loop relation between the MS-bar and the pole quark masses*, *Phys. Lett. B* **482** (2000) 99–108, [hep-ph/9912391].

[214] W. A. Bardeen, A. J. Buras, D. W. Duke and T. Muta, *Deep Inelastic Scattering Beyond the Leading Order in Asymptotically Free Gauge Theories*, *Phys. Rev. D* **18** (1978) 3998.

[215] I. I. Y. Bigi, M. A. Shifman, N. G. Uraltsev and A. I. Vainshtein, *Sum rules for heavy flavor transitions in the SV limit*, *Phys. Rev.* **D52** (1995) 196–235, [hep-ph/9405410].

[216] I. I. Y. Bigi, M. A. Shifman, N. Uraltsev and A. I. Vainshtein, *High power n of m_b in beauty widths and $n = 5 \to \infty$ limit*, *Phys. Rev. D* **56** (1997) 4017–4030, [hep-ph/9704245].

[217] M. Fael, K. Schönwald and M. Steinhauser, *Relation between the $\overline{\text{MS}}$ and the kinetic mass of heavy quarks*, *Phys. Rev. D* **103** (2021) 014005, [2011.11655].

[218] A. H. Hoang, Z. Ligeti and A. V. Manohar, *B decay and the Upsilon mass*, *Phys. Rev. Lett.* **82** (1999) 277–280, [hep-ph/9809423].

[219] A. H. Hoang, Z. Ligeti and A. V. Manohar, *B decays in the upsilon expansion*, *Phys. Rev. D* **59** (1999) 074017, [hep-ph/9811239].

[220] A. H. Hoang and T. Teubner, *Top quark pair production close to threshold: Top mass, width and momentum distribution*, *Phys. Rev. D* **60** (1999) 114027, [hep-ph/9904468].

[221] M. Beneke, *A Quark mass definition adequate for threshold problems*, *Phys. Lett. B* **434** (1998) 115–125, [hep-ph/9804241].

[222] Q. Ho-kim and X.-Y. Pham, *Exact One Gluon Corrections for Inclusive Weak Processes*, *Annals Phys.* **155** (1984) 202.

[223] G. Altarelli and S. Petrarca, *Inclusive beauty decays and the spectator model*, *Phys. Lett.* **B261** (1991) 303–310.

[224] M. B. Voloshin, *QCD radiative enhancement of the decay $b \to c\bar{c}s$*, *Phys. Rev.* **D51** (1995) 3948–3951, [hep-ph/9409391].

[225] E. Bagan, P. Ball, V. M. Braun and P. Gosdzinsky, *Charm quark mass dependence of QCD corrections to nonleptonic inclusive B decays*, *Nucl. Phys.* **B432** (1994) 3–38, [hep-ph/9408306].

[226] E. Bagan, P. Ball, B. Fiol and P. Gosdzinsky, *Next-to-leading order radiative corrections to the decay $b \to c\bar{c}s$*, *Phys. Lett.* **B351** (1995) 546–554, [hep-ph/9502338].

[227] A. Lenz, U. Nierste and G. Ostermaier, *Penguin diagrams, charmless B decays and the missing charm puzzle*, *Phys. Rev.* **D56** (1997) 7228–7239, [hep-ph/9706501].

[228] A. Lenz, U. Nierste and G. Ostermaier, *Determination of the CKM angle gamma and $|V_{ub}/V_{cb}|$ from inclusive direct CP asymmetries and branching ratios in charmless B decays*, *Phys. Rev.* **D59** (1999) 034008, [hep-ph/9802202].

[229] F. Krinner, A. Lenz and T. Rauh, *The inclusive decay $b \to c\bar{c}s$ revisited*, *Nucl. Phys.* **B876** (2013) 31–54, [1305.5390].

[230] A. Czarnecki and K. Melnikov, *Two loop QCD corrections to semileptonic b decays at maximal recoil*, *Phys. Rev. Lett.* **78** (1997) 3630–3633, [hep-ph/9703291].

[231] A. Czarnecki and K. Melnikov, *Two - loop QCD corrections to semileptonic b decays at an intermediate recoil*, *Phys. Rev.* **D59** (1999) 014036, [hep-ph/9804215].

[232] T. van Ritbergen, *The Second order QCD contribution to the semileptonic $b \to u$ decay rate*, *Phys. Lett.* **B454** (1999) 353–358, [hep-ph/9903226].

[233] K. Melnikov, *$\mathcal{O}(\alpha_s^2)$ corrections to semileptonic decay $b \to c l \bar{\nu}_l$*, *Phys. Lett.* **B666** (2008) 336–339, [0803.0951].

[234] A. Pak and A. Czarnecki, *Heavy-to-heavy quark decays at NNLO*, *Phys. Rev.* **D78** (2008) 114015, [0808.3509].

[235] A. Pak and A. Czarnecki, *Mass effects in muon and semileptonic $b \to c$ decays*, *Phys. Rev. Lett.* **100** (2008) 241807, [0803.0960].

[236] M. Dowling, A. Pak and A. Czarnecki, *Semi-Leptonic b-decay at Intermediate Recoil*, *Phys. Rev.* **D78** (2008) 074029, [0809.0491].

[237] R. Bonciani and A. Ferroglia, *Two-Loop QCD Corrections to the Heavy-to-Light Quark Decay*, *JHEP* **11** (2008) 065, [0809.4687].

[238] S. Biswas and K. Melnikov, *Second order QCD corrections to inclusive semileptonic $b \to X_c \ell \bar{\nu}_l$ decays with massless and massive lepton*, *JHEP* **02** (2010) 089, [0911.4142].

[239] M. Brucherseifer, F. Caola and K. Melnikov, *On the $O(\alpha_s^2)$ corrections to $b \to X_u e \bar{\nu}$ inclusive decays*, *Phys. Lett.* **B721** (2013) 107–110, [1302.0444].

[240] M. Fael, K. Schönwald and M. Steinhauser, *Third order corrections to the semi-leptonic $b \to c$ and the muon decays*, 2011.13654.

[241] M. Czakon, A. Czarnecki and M. Dowling, *Three-loop corrections to the muon and heavy quark decay rates*, *Phys. Rev. D* **103** (2021) L111301, [2104.05804].

[242] A. Czarnecki, M. Slusarczyk and F. V. Tkachov, *Enhancement of the hadronic b quark decays*, *Phys. Rev. Lett.* **96** (2006) 171803, [hep-ph/0511004].

[243] A. Alberti, P. Gambino and S. Nandi, *Perturbative corrections to power suppressed effects in semileptonic B decays*, *JHEP* **01** (2014) 147, [1311.7381].

[244] T. Mannel, A. A. Pivovarov and D. Rosenthal, *Inclusive semileptonic B decays from QCD with NLO accuracy for power suppressed terms*, *Phys. Lett.* **B741** (2015) 290–294, [1405.5072].

[245] T. Mannel, A. A. Pivovarov and D. Rosenthal, *Inclusive weak decays of heavy hadrons with power suppressed terms at NLO*, *Phys. Rev.* **D92** (2015) 054025, [1506.08167].

[246] M. Gremm and A. Kapustin, *Order $1/m_b^3$ corrections to $B \to X(c)$ lepton anti-neutrino decay and their implication for the measurement of $\bar{\Lambda}$ and λ_1*, *Phys. Rev.* **D55** (1997) 6924–6932, [hep-ph/9603448].

[247] T. Mannel and A. A. Pivovarov, *QCD corrections to inclusive heavy hadron weak decays at $\Lambda_{\rm QCD}^3/m_Q^3$*, *Phys. Rev.* **D100** (2019) 093001, [1907.09187].

[248] D. Moreno, *Completing $1/m_b^3$ corrections to non-leptonic bottom-to-up-quark decays*, *JHEP* **01** (2021) 051, [2009.08756].

[249] P. Gambino and J. F. Kamenik, *Lepton energy moments in semileptonic charm decays*, *Nucl. Phys. B* **840** (2010) 424–437, [1004.0114].

[250] M. Fael, T. Mannel and K. K. Vos, *The Heavy Quark Expansion for Inclusive Semileptonic Charm Decays Revisited*, 1910.05234.

[251] F. Gabbiani, A. I. Onishchenko and A. A. Petrov, *Λ_b lifetime puzzle in heavy quark expansion*, *Phys. Rev. D* **68** (2003) 114006, [hep-ph/0303235].

[252] F. Gabbiani, A. I. Onishchenko and A. A. Petrov, *Spectator effects and lifetimes of heavy hadrons*, *Phys. Rev.* **D70** (2004) 094031, [hep-ph/0407004].

[253] Fermilab Lattice, MILC, TUMQCD collaboration, A. Bazavov et al., *Up-, down-, strange-, charm-, and bottom-quark masses from four-flavor lattice QCD*, *Phys. Rev.* **D98** (2018) 054517, [1802.04248].

[254] P. Gambino, A. Melis and S. Simula, *Extraction of heavy-quark-expansion parameters from unquenched lattice data on pseudoscalar and vector heavy-light meson masses*, *Phys. Rev.* **D96** (2017) 014511, [1704.06105].

[255] JLQCD collaboration, S. Aoki et al., *Heavy quark expansion parameters from lattice NRQCD*, *Phys. Rev.* **D69** (2004) 094512, [hep-lat/0305024].

[256] A. S. Kronfeld and J. N. Simone, *Computation of Lambda-bar and lambda(1) with lattice QCD*, *Phys. Lett.* **B490** (2000) 228–235, [hep-ph/0006345].

[257] V. Gimenez, G. Martinelli and C. T. Sachrajda, *A High statistics lattice calculation of λ_1 and λ_2 in the B meson*, *Nucl. Phys.* **B486** (1997) 227–244, [hep-lat/9607055].

[258] P. Ball and V. M. Braun, *Next-to-leading order corrections to meson masses in the heavy quark effective theory*, *Phys. Rev.* **D49** (1994) 2472–2489, [hep-ph/9307291].

[259] M. Neubert, *QCD sum rule calculation of the kinetic energy and chromo interaction of heavy quarks inside mesons*, *Phys. Lett.* **B389** (1996) 727–736, [hep-ph/9608211].

[260] T. Mannel, A. V. Rusov and F. Shahriaran, *Inclusive semitauonic B decays to order $\mathcal{O}(\Lambda_{QCD}^3/m_b^3)$*, *Nucl. Phys.* **B921** (2017) 211–224, [1702.01089].

[261] B. M. Dassinger, T. Mannel and S. Turczyk, *Inclusive semi-leptonic B decays to order $1/m_b^4$*, *JHEP* **03** (2007) 087, [hep-ph/0611168].

[262] C. Breidenbach, T. Feldmann, T. Mannel and S. Turczyk, *On the Role of 'Intrinsic Charm' in Semi-Leptonic B-Meson Decays*, *Phys. Rev.* **D78** (2008) 014022, [0805.0971].

[263] I. Bigi, T. Mannel, S. Turczyk and N. Uraltsev, *The Two Roads to 'Intrinsic Charm' in B Decays*, *JHEP* **04** (2010) 073, [0911.3322].

[264] M. Neubert, *Symmetry breaking corrections to meson decay constants in the heavy quark effective theory*, *Phys. Rev. D* **46** (1992) 1076–1087.

[265] W. Kilian and T. Mannel, *QCD corrected $1/m_b$ contributions to $B - \bar{B}$ mixing*, *Phys. Lett. B* **301** (1993) 382–392, [hep-ph/9211333].

[266] T. Mannel, D. Moreno and A. A. Pivovarov, *The Heavy Quark Expansion for the Charm Quark*, 2103.02058.

[267] H.-Y. Cheng, *Phenomenological Study of Heavy Hadron Lifetimes*, *JHEP* **11** (2018) 014, [1807.00916].

[268] N. Uraltsev, *On the chromomagnetic expectation value μ_G^2 and higher power corrections in heavy flavor mesons*, *Phys. Lett. B* **545** (2002) 337–344, [hep-ph/0111166].

[269] A. F. Falk and M. Neubert, *Second order power corrections in the heavy quark effective theory. 1. Formalism and meson form-factors*, *Phys. Rev. D* **47** (1993) 2965–2981, [hep-ph/9209268].

[270] Fermilab Lattice, MILC, TUMQCD collaboration, A. Bazavov et al., *Up-, down-, strange-, charm-, and bottom-quark masses from four-flavor lattice QCD*, *Phys. Rev. D* **98** (2018) 054517, [1802.04248].

[271] I. I. Y. Bigi, M. A. Shifman and N. Uraltsev, *Aspects of heavy quark theory*, *Ann. Rev. Nucl. Part. Sci.* **47** (1997) 591–661, [hep-ph/9703290].

[272] I. I. Bigi, T. Mannel and N. Uraltsev, *Semileptonic width ratios among beauty hadrons*, *JHEP* **09** (2011) 012, [1105.4574].

[273] I. I. Y. Bigi, M. A. Shifman, N. G. Uraltsev and A. I. Vainshtein, *On the motion of heavy quarks inside hadrons: Universal distributions and inclusive decays*, *Int. J. Mod. Phys. A* **9** (1994) 2467–2504, [hep-ph/9312359].

[274] J. Aebischer and B. Grinstein, *Standard Model prediction of the B_c lifetime*, 2105.02988.

[275] J. Aebischer and B. Grinstein, *A novel determination of the B_c lifetime*, 2108.10285.

[276] UKQCD collaboration, M. Di Pierro and C. T. Sachrajda, *A Lattice study of spectator effects in inclusive decays of B mesons*, *Nucl. Phys. B* **534** (1998) 373–391, [hep-lat/9805028].

[277] T. Jubb, M. Kirk, A. Lenz and G. Tetlalmatzi-Xolocotzi, *On the ultimate precision of meson mixing observables*, *Nucl. Phys.* **B915** (2017) 431–453, [1603.07770].

[278] K. G. Chetyrkin, J. H. Kuhn, A. Maier, P. Maierhofer, P. Marquard, M. Steinhauser et al., *Charm and Bottom Quark Masses: An Update*, *Phys. Rev. D* **80** (2009) 074010, [0907.2110].

[279] ALPHA collaboration, F. Bernardoni et al., *Decay constants of B-mesons from non-perturbative HQET with two light dynamical quarks*, *Phys. Lett. B* **735** (2014) 349–356, [1404.3590].